

2-13-2014

# ENHANCEMENT OF SATURATION BOILING OF PF-5060 DIELECTRIC LIQUID ON MICROPOROUS SURFACES

Ali Amir

Follow this and additional works at: [https://digitalrepository.unm.edu/me\\_etds](https://digitalrepository.unm.edu/me_etds)

---

## Recommended Citation

Amir, Ali. "ENHANCEMENT OF SATURATION BOILING OF PF-5060 DIELECTRIC LIQUID ON MICROPOROUS SURFACES." (2014). [https://digitalrepository.unm.edu/me\\_etds/20](https://digitalrepository.unm.edu/me_etds/20)

This Dissertation is brought to you for free and open access by the Engineering ETDs at UNM Digital Repository. It has been accepted for inclusion in Mechanical Engineering ETDs by an authorized administrator of UNM Digital Repository. For more information, please contact [disc@unm.edu](mailto:disc@unm.edu).

Amir Faris Ali

*Candidate*

Mechanical Engineering

*Department*

This dissertation is approved, and it is acceptable in quality and form for publication:

*Approved by the Dissertation Committee:*

Prof. Mohamed S. El-Genk, Chairperson

Prof. Timothy L. Ward

Prof. Juan C. Heinrich

Prof. Zayd Leseman

**ENHANCEMENT OF SATURATION BOILING OF PF-5060  
DIELECTRIC LIQUID ON MICROPOROUS SURFACES**

**by**

**AMIR FARIS ALI**

B.S., Mechanical Engineering, Benha High Institute of Technology, Egypt, 1996  
M. S., Mechanical Engineering, Benha University, Egypt, 2004

DISSERTATION

Submitted in Partial Fulfillment of the  
Requirements for the Degree of

**Doctor of Philosophy**

**Engineering**

The University of New Mexico  
Albuquerque, New Mexico

**December 2013**

## DEDICATION

*To the soul of my Dad; the first teacher in  
my life*

## ACKNOWLEDGMENT

I wish to acknowledge the **University of New Mexico's Institute for Space and Nuclear Power Studies in the School of Engineering** for funding this research and providing the means by which I was able to complete my education at UNM. I would also like to acknowledge my research and academic advisor and the chair of the Dissertation committee, Dr. Mohamed S. El-Genk, Regents' Professor of Chemical, Nuclear and Mechanical Engineering and the Founding Director of the Institute for Space and Nuclear Power Studies for his help and insight during the course of this research. Many thanks are due to other members of the committee, Dr. Timothy L. Ward, Professor and Chair Department of Chemical and Nuclear Engineering, Dr. Juan C. Heinrich, Professor of Mechanical Engineering, and Dr. Zayd Leseman, Associate Professor of Mechanical Engineering for their helpful suggestions and valuable feedback and comments.

I appreciate the help I have received by former graduate students, Dr. Jack L. Parker, Dr. In-Hwan Yang, and to Arthur Suszko, graduate student who is working on a related topic.

Special thanks are due to the members of my family, my wife Wesam, and my children Eslam, Saher, and my beautiful angel Malak. I could not have done this achievement without their patience, support, understanding and hopes for better things to come.

# **Enhancement of Saturation Boiling of PF-5060 Dielectric Liquid on MicroPorous Surfaces**

by

**Amir Faris Ali**

**B.S., Mechanical Engineering, Benha High Institute of Technology, Egypt, 1996**

**M. S., Mechanical Engineering, Benha University, Egypt, 2004**

**Ph.D. Engineering, University of New Mexico, USA, 2013**

## **ABSTRACT**

This research experimentally investigated microporous Copper (MPC) surfaces for enhancing nucleate boiling and increasing the Critical Heat Flux (CHF) of PF-5060 dielectric liquid and the potential application of the results to immersion cooling of high power computer chips. MPC surfaces of different thicknesses (80–230  $\mu\text{m}$ ), fabricated using conventional electrochemical deposition at high current density, have different morphology and microstructure. The PF-5060 liquid is chemically inert, environmentally friendly, and has low enough saturation temperature ( $\sim 54^\circ\text{C}$  at 0.10 MPa). This helps maintain the chip junction's temperature below that recommended by the chip manufacturer (85-120  $^\circ\text{C}$ , depending on the application).

To ensure consistency of the results, all saturation pool boiling experiments reported in this Dissertations are for degassed PF-5060 dielectric liquid and uniformly heated and conditioned 10 x 10 mm MPC surfaces (80, 95, 115, 140, 171, 197, 230  $\mu\text{m}$  thick) at different inclination angles. These are  $0^\circ$  (upward facing),  $30^\circ$ ,  $60^\circ$ ,  $90^\circ$  (vertical),  $120^\circ$ ,  $150^\circ$ , and  $180^\circ$  (downward facing). The MPC surfaces are conditioned, by performing several experiments at the same conditions separated by at least 2 hours and someone a couple of days. The experiments demonstrated the reproducibility of the measurements and the absence of boiling hysteresis. Thus, confirming that nucleate boiling in the present experiments is not influenced by the thermal inertia of the heated surface but solely depends on the thermophysical properties of the PF-5060 and morphology and microstructure of the MPC surfaces.

In order quantify the effects of MPC surface thickness and orientation on the enhancements of the nucleate boiling heat transfer coefficient and CHF; the results are

compared to those on smooth polished Cu of the same dimensions at the same experimental conditions. Results are also compared to those reported in the literature for other micro-structured surfaces and microporous coatings. In addition, high speed video movies are recorded of the transient growth of nucleating vapor bubbles on MPC surfaces in the upward facing orientation. The results are used to determine the detachment diameter and the frequency of the ebullition cycle of the bubbles, as well as estimate the surface density of active sites for bubble nucleation.

The values of the saturation nucleate boiling heat transfer coefficient,  $h_{NB}$ , in the upward facing orientation are correlated as a function of the surface heat flux. The exponent of the heat flux depends on the MPC thickness, increasing from 0.52 to 0.7. The corresponding values of the maximum heat transfer coefficient,  $h_{MNB}$ , occurring at the end of the fully developed nucleate boiling,  $h_{MNB}$ , are also presented at different orientation angle on the same PC surface. The recorded still photographs of the boiling process on these surfaces at different inclinations helped the interpretation of the results and experimental measurements.

In addition to reducing ( $< 5$  K) or eliminating the temperature excursion prior to nucleate boiling, the experimental measurements demonstrated large enhancements in both  $h_{NB}$  and CHF. In upward facing orientation, the present values of  $h_{MNB}$  ( $7.8 \text{ W/cm}^2 \text{ K}$ ) is the highest representing a 10 folds increase compared to those on smooth polished Copper ( $\sim 0.78 \text{ W/cm}^2 \text{ K}$ ). The developed correlation for  $h_{NB}$  in the upward facing orientation as function of the MPC surface thickness is within  $\pm 10\%$  of the present experimental measurements. The correlated CHF values account for the effect of MPC thickness as well as the surface inclination angle. The developed correlation is in good agreement with the present experimental data to within  $\pm 8\%$ . CHF on MPC surfaces not only increases with increased thickness, but also the corresponding surface superheat decreases. CHF increases from 22 to  $26 \text{ W/cm}^2$  as the MPC surface thickness increases from  $80 \text{ }\mu\text{m}$  to  $230 \text{ }\mu\text{m}$ , while the corresponding surface superheat decreases from 15 to 5 K. Present CHF values on MPC surfaces are 39% to 59% higher than on a smooth Cu. The reported values for PF-5060 liquid on nano-finned, micro-wired, nano-structured and microporous coated surfaces are 38%- 91% of the present values on MPC surfaces, and the corresponding surface superheats are much higher, varying from 17- 42

K, compared to  $< 15$  K on present MPC surfaces. Increasing surface inclination decreases CHF and the corresponding surface superheat. However, CHF increases with increased thickness of MPC surfaces. Regardless of the thickness, CHF in the downward facing is  $\sim 28\%$  of its value in the upward facing orientation.

Transient growth of vapor bubbles on MPC surfaces (80, 95, 115, 125, and 140  $\mu\text{m}$  thick) are recorded for a several ebullition cycles. The growth is proportional to the square root of time, confirming that the bubbles are in the thermal growth stage. The developed correlation for the transient growth of the bubbles is in a good agreement with the measurements to within  $\pm 5\%$ . Determined bubble departure diameter,  $D_d$ , and detachment frequency,  $f_d$ , for saturation boiling of PF-5060 dielectric liquid in the upward facing orientation are independent of surface morphology. The determined values of  $D_d = 431 \pm 7 \mu\text{m}$  and  $f_d = 36 \pm 2 \text{ Hz}$  are used to calculate the surface average density of active nucleation site. It ranges from 1000-10000 sites/ $\text{cm}^2$  compared to 300-1000 sites/ $\text{cm}^2$  for FC-77 on rough Copper surfaces.

The present results are incorporated in a numerical thermal analysis investigating the performance of Cu spreaders with MPC surfaces for cooling a 10 x 10 mm underlying high power chip with a central hot-spot (CHS). Analysis varied the dimensions of the CHS from 1 x 1 mm to 2 x 2 mm and increased the heat flux at the CHS up to 6 times that of the chip surface average outside the hot spot. The analysis also varied the thermal conductance of the thermal interface materials (TIM) between the spreaders Cu substrate and the underling chip from 0.19 to 0.02  $^\circ\text{C}\cdot\text{cm}^2/\text{W}$ . The spreaders are cooled by saturation boiling of PF-5060 dielectric liquid.

Numerical results confirmed the effectiveness of MPC spreaders for immersion cooling of high power chips, removing  $> 85 \text{ W}$  at junctions' temperature  $< 100^\circ\text{C}$ . With a TIM impedance of 0.19  $^\circ\text{C}\cdot\text{cm}^2/\text{W}$ , a MPC spreader with a 3.2 mm-thick Cu substrate removes 90.1 W and 87.85 W for the chip with a 1 and 4  $\text{mm}^2$  CHS and heat flux ratio (HFR) at CHSs = 6. The corresponding chip maximum surface temperatures at the CHSs are  $90.16^\circ\text{C}$  and  $96.6^\circ\text{C}$ , respectively. Decreasing TIM impedance to 0.02 $^\circ\text{C}\cdot\text{cm}^2/\text{W}$  decreases the chip's maximum surface temperature to  $73.4$  and  $76.1^\circ\text{C}$ , but slightly changes the removed thermal power to 90.3 W and 86.24W, respectively.



For industrial applications involving nucleate boiling heat transfer, such as boilers, steam generators nuclear reactors, and immersion cooling of electronics, this research proposed correlations for CHF and the fully developed nucleate boiling heat transfer coefficient,  $h_{NB}$ . These correlations are useful tools for thermal engineers to protect the heat transfer device from severe damage by avoiding CHF and determine the design and operational conditions for the best performance of the heat transfer devices. MPC spreaders are a promising option for cooling high power computer chips.

# Table of Contents

<b>DEDICATION</b> .....	iii
<b>ACKNOWLEDGMENT</b> .....	iv
<b>ABSTRACT</b> .....	v
<b>Table of Contents</b> .....	ix
<b>List of Figures</b> .....	xii
<b>List of Tables</b> .....	xv
<b>Nomenclature</b> .....	xvi
<b>1. Introduction</b> .....	1
1.1 Surface morphology and microstructure.....	6
1.2 Effect of surface orientation.....	12
1.3 Objectives .....	13
<b>2. Background and Review of Prior Work</b> .....	15
2.1 Methods for Cooling High Power Electronics Chips .....	15
2.2 Fundamentals of Pool Boiling and Bubble Nucleation .....	18
2.2.1 Nucleate Pool Boiling Heat Transfer.....	18
2.2.2 Ebullition Cycle .....	21
2.3 Nucleate Boiling of Dielectric Liquids .....	23
2.3.1 Boiling regimes of dielectric liquids.....	23
2.3.2 Critical heat flux .....	26
2.4 Nucleate Boiling Enhancements .....	28
2.4.1 Effect of liquid thermophysical properties .....	30
2.4.2 Effect of Surface Condition .....	32
2.4.3 Effect of Surface Orientation.....	37
2.5 Bubble departure diameter and frequency .....	40
2.6 Active nucleation site density .....	42
<b>3. Deposition of MicroPorous Copper Surfaces</b> .....	45
3.1 Review of prior work .....	45
3.1.1 Surface preparation .....	49
3.1.2 Setup and procedures .....	51

3.1.3 Surface morphology and SEM.....	54
4. Pool Boiling Experiments .....	63
4.1 Test Section.....	63
4.2 Experimental setup.....	65
4.3 Experimental Procedures .....	71
5. Saturation Nucleate Boiling.....	75
5.1 Conditioning of MPC Surfaces .....	75
5.2 Boiling Hysteresis .....	77
5.3 Nucleate Boiling Results.....	77
5.4 Natural Convection .....	80
5.5 Nucleate Boiling and Heat Transfer Coefficient .....	83
5.5.1 Effect of MPC surface thickness.....	83
5.5.2 Effect of surface orientation.....	84
5.5.3 Nucleate boiling heat transfer correlation.....	87
5.6 Transient Bubble Growth.....	93
5.7 Summary and Conclusion .....	99
6. Saturation Boiling Critical Heat Flux .....	102
6.1 Effect of MPC thickness .....	102
6.2 Effect of inclination angle.....	102
6.3 Critical heat flux correlation .....	107
7. Composite Spreaders for Immersion Cooling of Computer Chips with Central Hot Spots.....	116
7.1 Prior work .....	116
7.2 Problem Statement.....	119
7.3 Approach and methodology .....	123
7.4 Numerical analysis and meshing grid .....	125
7.5 Results and Discussion .....	125
7.5.1 Total thermal power removed and footprint area without TIM .....	126
7.5.2 Chip Maximum temperature at hot spot .....	128
7.5.3 Effect of MPC surface thickness.....	132
7.5.4 Effects of TIM and HFR at CHS .....	134
7.5.5 Spreader's thermal resistance .....	136
7.5.6 Chip Surface Temperature .....	139

7.6 Summary and closing marks .....	143
8. Summary and Conclusions .....	145
9. Recommendations for Future Work.....	149
10. References.....	150
Appendix A: Uncertainty Analysis .....	162
Appendix B: List of Publications Related to Work .....	166

## List of Figures

Figure 1.1 Increases in clock speed and dissipated power of high performance computer chips (Courtesy of Kunle Olukotun, Lance Hammond, Herb Sutter, and Burton Smith).....	2
Figure 1.2 Hot spot effect on the local surface temperature of a computer chip surface (Wei, 2008). ....	2
Figure 1.3 Schematics of different methods of liquid-based cooling of electronics. ....	3
Figure 2.1 Range of capability of different electronic cooling methods. ....	17
Figure 2.2 Gas entrapment in a cavity for poorly and highly wetting liquids (Carey, 1992). ....	20
Figure 2.3 Growth of entrapped gas to bubble nucleation.....	22
Figure 2.4 Range of cavity sizes for active nucleation of different dielectric liquids. ....	22
Figure 2.5 Illustration of bubble Ebullition cycle in nucleate boiling. ....	24
Figure 2.6 Typical nucleate boiling curves of dielectric liquids (El-Genk and Ali, 2010). ....	27
Figure 2.7 Vapor dynamic for triggering the critical heat flux (CHF). ....	29
Figure 2.8 Selected surfaces for nucleate boiling enhancement of dielectric liquids. ....	31
Figure 3.1 SEM images on the effect of deposition time on structure pore size for the same concentration and current density of 3 A/cm <sup>2</sup> for (a) 5 Seconds (b) 10 Seconds (c) 15 Seconds .....	47
Figure 3.2 SEM images of the deposited MPC structure at different current densities (Kim, 2006).....	48
Figure 3.3 SEM images of deposited MPC structure before (top) and after (Lower) annealing at 600 °C for 5 hours (Furberg, 2006). ....	50
Figure 3.4 Microscopic images of plane Copper substrate after treatment using emery of 400 and 1500 grit emery paper and polishing.....	52
Figure 3.5 A Schematic of the electrochemical deposition setup at high current density. ....	53
Figure 3.6 SEM images of layer # 1 after 1st and 2nd stage of deposition (Thickness $80 \pm 1.81 \mu\text{m}$ ).....	57
Figure 3.7 SEM images of layer # 2 after 1st and 2nd stage of deposition (Thickness $95.1 \pm 1.81 \mu\text{m}$ ).....	58
Figure 3.8 SEM images of layer # 4 after 1st and 2nd stage of deposition (Thickness $139.4 \pm 2.64 \mu\text{m}$ ).....	59
Figure 3.9 SEM images of layer # 5 after 1st and 2nd stage of deposition (Thickness $171.1 \pm 3.13 \mu\text{m}$ ).....	60

Figure 3.10 SEM images of layer # 6 after 1st and 2nd stage of deposition (Thickness $197.4 \pm 3.61 \mu\text{m}$ ).....	61
Figure 3.11 SEM images of layer # 7 after 1st and 2nd stage of deposition (Thickness $230.3 \pm 4.2 \mu\text{m}$ ).....	62
Figure 4.1 Test section assembly.....	64
Figure 4.2. Cross sectional views of the fully assembled test section with MicroPorous Copper.....	66
Figure 4.3 Line diagram of the pool boiling test facility (El-Genk and Parker, 2005).....	67
Figure 4.4 Photograph of the pool boiling facility (Parker, 2008). ....	69
Figure 4.5 Fully assembled test section support (Parker, 2008). ....	69
Figure 4.6 Photographs of rotation assembly and fully assembled rotation mechanism (Parker, 2008). ....	70
Figure 4.7 Photographs of pool boiling test vessel and assembly (Parker, 2008). ....	72
Figure 4.8 Saturation boiling curves on smooth Copper and MPC surfaces based on the readings of two thermocouples (Fig. 4.2c). ....	74
Figure 5.1 Conditioning of saturation boiling curves of PF-5060 on MPC surfaces. ....	76
Figure 5.2 Reproducibility of saturation pool boiling curves. ....	78
Figure 5.3 Hysteresis of saturation boiling curves of PF-5060 on MPC surfaces.....	79
Figure 5.4 Saturation boiling curve of PF-5060 on 230 $\mu\text{m}$ -thick MPC surfaces in the upward facing orientation. ....	81
Figure 5.5 Natural convection data of dielectric liquids on smooth, porous, micro-structured, and MPC surfaces. ....	82
Figure 5.6 Effect of $\delta_{\text{MPC}}$ on saturation boiling of PF-5060 in the upward facing orientation. ....	85
Figure 5.7 Effect of inclination angle on saturation boiling of PF-5060 on MPC surfaces. ....	86
Figure 5.8 Developed correlation of saturation boiling $h_{\text{NB}}$ on of PF-5060 on MPC surfaces of different thicknesses. ....	88
Figure 5.9 Coefficients for fully developed nucleate boiling heat transfer correlation on MPC surfaces. ....	89
Figure 5.10 Comparison of predicted and measured $h_{\text{NB}}$ values for saturation boiling of PF-5060 on MPC surfaces. ....	89
Figure 5.11 Comparison of present values for $h_{\text{NB}}$ of PF-5060 on MPC with those reported for PF-5060 and other dielectric liquids on micro- structured, microporous coated, and other MPC surfaces. ....	91
Figure 5.12 Present values of $h_{\text{MNB}}$ for saturation boiling of PF-5060 on MPC surfaces at different inclinations. ....	92

Figure 5.13 Photographs growing bubbles at discrete sites on 80 $\mu\text{m}$ -thick MPC during saturation boiling of PF-5060. ....	93
Figure 5.14 Transient Growth Images of discrete bubble in saturation boiling of PF-5060 on MPC surfaces in the upward facing orientation. ....	94
Figure 5.15 Bubbles diameter during transient growth in saturation boiling of PF-5060 on Upward Facing on MPC surfaces in the upward facing orientation. ....	96
Figure 5.16 Bubbles transient growth diameter in saturation boiling of PF-5060 on MPC surfaces in the upward facing orientation. ....	97
Figure 5.17 Bubble departure diameter and detachment frequency in saturation boiling of PF-5060 on MPC surfaces in the upward facing orientation. ....	98
Figure 5.18 Comparison of the surface average density of active nucleation sites in saturation boiling of PF-5060 on MPC, FC-77 on Aluminum, and FC-72 on Silicon surfaces. ....	100
Figure 6.1 Effect of inclination on saturation boiling CHF on MPC surfaces of different thickness at different inclination angles. ....	103
Figure 6.2 Dependence of saturation boiling CHF, and $\Delta T_{\text{sat}}@CHF$ on the thickness of MPC surfaces in the upward facing orientation. ....	104
Figure 6.3 Effect of inclination angle on saturation boiling CHF of PF-5060 on different thickness MPC surfaces. ....	106
Figure 6.4 Comparison of saturation boiling CHF of PF-5060 dielectric liquid and the $\Delta T_{\text{sat}}$ on MPC surfaces with reported values on other surfaces. ....	108
Figure 6.5 Still photographs of saturation boiling of PF-5060 near CHF on smooth and MPC surfaces in the upward facing orientation (* applied heat flux, $\dagger$ corresponding $\Delta T_{\text{sat}}$ ). ....	109
Figure 6.6 CHF coefficient for Saturation boiling of PF-5060 dielectric liquid on MPC surfaces in the upward facing orientation. ....	111
Figure 6.7 Normalized saturation boiling CHF of PF-5060 on smooth Copper and MPC surfaces. ....	113
Figure 6.8 Comparison of experimental versus correlated values of saturation boiling CHF of PF-5060 on MPC surfaces at different inclination angle. ....	114
Figure 7.1 A schematic of a composite spreader for immersion cooling nucleate boiling of PF-5060 dielectric liquid of high power computer chips. ....	117
Figure 7.2 A schematic and cross sectional views of a spreader comprised of a Cu substrate and a MPC surface layer. ....	120
Figure 7.3 Experimental saturation pool boiling and nucleate boiling heat transfer coefficient curves of PF-5060 dielectric liquid on plane Cu and MPC surfaces. ....	122
Figure 7.4 Numerical mesh grid used in the present numerical thermal Analysis of composite spreaders. ....	124

Figure 7.5 Thermal power dissipation by underlying chip and removed from spreader surface assuming no thermal interface material.....	127
Figure 7.6 Temperature distributions at the surface of the chips with and without a central hot spot.....	130
Figure 7.7 Comparison of composite spreaders performance for immersion cooling of 10 x 10 mm underlying chip with 2 x 2 mm CHS having HFR=3. ....	131
Figure 7.8 Surface temperature contours and footprints of composite spreaders with 3.2 mm-thick Cu substrate and MPC surfaces of different thicknesses. ....	133
Figure 7.9 Effect of CHS area and HFR on the performance of the composite and plane Cu spreaders.....	135
Figure 7.10 Comparison of the thermal resistances for composite and plane Cu spreaders. ....	138
Figure 7.11 Comparison of the calculated chip maximum surface temperatures and the removed total thermal power: (a) plane Cu (b) MPC spreaders [HFR=6, $t_{Cu}=2.4\text{mm}$ , $TI_{TIM}=0.19\text{ }^{\circ}\text{C-cm}^2/\text{W}$ and CHS= 1 and 4 $\text{mm}^2$ ].....	141
Figure 7.12 Comparison of the calculated chip maximum surface temperatures and the removed total thermal power: (a) $TI_{TIM} = 0.19\text{ }^{\circ}\text{C-cm}^2/\text{W}$ (b) $TI_{TIM} = 0.02\text{ }^{\circ}\text{C-cm}^2/\text{W}$ [HFR=6, $t_{Cu}=3.2\text{mm}$ , and CHS= 1 and 4 $\text{mm}^2$ ].....	141



## **List of Tables**

Table 1.1 Comparison of Thermo physical properties of dielectric liquids PF-5060, HFE-7100, FC-72, and Water (3M, 2013).....	5
Table 1.2 Other properties of dielectric liquids PF-5060, FC-72, and HFE-7100 (3M, 2013). .....	5
Table 1.3 Selected investigations on enhanced saturation nucleate boiling of dielectric liquids on various surfaces.....	7
Table 3.1 Deposition conditions and characteristics of deposited MPC surfaces. ....	55
Table 7.1 Properties of electrochemical deposited MPC surfaces.....	123
Table A.1 Selected values and associated uncertainties for test measurements. ....	165

## Nomenclature

$A$	Area, Footprint area ( $\text{cm}^2$ ), Correlation coefficient
$B$	Correlation coefficient
$C$	Correlation coefficient
$CHF$	Critical Heat Flux ( $\text{W}/\text{cm}^2$ )
$CHS$	Central hot spot
$CNT$	Carbon Nanotubes
$c_p$	Heat capacity at constant pressure ( $\text{J}/\text{kg K}$ )
$Cu$	Copper
$D, d$	Diameter ( $\mu\text{m}$ )
$DC$	Direct current
$f$	frequency ( $\text{s}^{-1}$ )
$G$	General function
$g$	Gravitational acceleration ( $\text{m}/\text{s}^2$ )
$h$	Heat transfer coefficient ( $\text{W}/\text{m}^2 \text{K}$ , $\text{kW}/\text{m}^2 \text{K}$ )
$h_{fg}$	Latent heat of vaporization ( $\text{J}/\text{kg}$ )
$HFR$	Heat flux ratio
$Hs$	Hot spot
$I$	Current (A)
$Ja$	Jakob number
$k$	Thermal conductivity ( $\text{W}/\text{m K}$ )
$L$	Length (m)
$M$	General measurement of independent variable
$MPC$	Microporous copper
$N$	Active nucleation site density ( $\text{cm}^{-2}$ )
$P$	Power (W), Pressure (Pa)
$PG$	Porous Graphite
$P_l$	Ambient liquid pressure (Pa)
$Q$	Total heat or power (W, KW)
$q$	Heat flux ( $\text{W}/\text{cm}^2$ , $\text{kW}/\text{m}^2$ )
$r$	Radius of a cavity opening (m)

$R$	Thermal resistance ( $^{\circ}\text{C}/\text{W}$ ), Angular dependent CHF coefficient
$Ra$	Average surface roughness ( $\mu\text{m}$ )
$r_c$	Critical radius (m)
$SEM$	Scanning Electron Microscope
$\bar{T}$	Average surface temperature (K)
$T$	Temperature (K)
$t$	Time (s), Thickness ( $\mu\text{m}$ , mm)
$t_o$	Arbitrary initial time (s)
$t_b$	Bubble growth time, ( $t - t_o$ ) (s)
$TI$	Thermal impedance ( $^{\circ}\text{C}\text{-cm}^2/\text{W}$ )
$TIM$	Thermal interface material
$V$	Voltage measurement (V)
$w$	General variable
$x, y, z$	Cartesian coordinates

### **Greek Symbols**

$\beta$	Cavity angle
$\varepsilon$	Volume porosity (%)
$\delta_{MPC}$	Microporous copper layer thickness ( $\mu\text{m}$ )
$\Theta$	Temperature rise ( $^{\circ}\text{C}$ , K)
$\Delta$	Uncertainty estimate
$\Delta T$	Temperature difference (K)
$\delta_t$	Thermal boundary layer thickness (m)
$\mu$	Viscosity ( $\text{kg}/\text{m s}$ )
$\theta$	Inclination angle, Contact angle, Cavity angle ( $^{\circ}$ )
$\rho$	Density ( $\text{kg}/\text{m}^3$ )
$\sigma$	Surface tension (N/m)

### **Subscripts**

$b$	Bulk or pool, Bubble
$Boil$	Saturation nucleate boiling

<i>cav</i>	Cavity
<i>CHF</i>	Critical Heat Flux
<i>Chip</i>	Computer chip, chip surface
<i>Cu</i>	Copper
<i>eff</i>	Effective
<i>l</i>	Liquid
<i>loss</i>	Refers to estimated heat losses
<i>max</i>	Maximum
<i>min</i>	Minimum
<i>MNB</i>	Maximum nucleate boiling
<i>MPC</i>	Microporous Copper
<i>NB</i>	Nucleate boiling
<i>NC</i>	Natural convection
<i>s</i>	Surface
<i>sat</i>	At saturation conditions
<i>sp</i>	Spreader, Cu substrate
<i>TIM</i>	Thermal interface material
<i>TOT</i>	Total
<i>v</i>	Vapor
<i>w</i>	Wall or surface

# 1. Introduction

The continuous increase in transistor density and/or processing speed and the miniaturization of the computer chip size presented many challenges to thermal management, including high rate of heat dissipation, and the development of hot spots. Over the past few decades, the transistor density and clock speed of chips have doubled about every two years (Figure 1.1). In addition, the total thermal power dissipation by a chip could exceed 100 W and the surface heat flux is  $> 100 \text{ W/cm}^2$  (ITRS, 2011; Refai-Ahmed, 2007; El-Genk, 2012). The local heat flux at hot spots could be three to six times that of the chip's surface average (Yang et al, 2007; Wei, J., 2008). The high local temperature at the hot spots and temperature differential across the chip surface could induce thermal stresses, markedly decreasing the service life of the chip (Figure 1.2) (Lin and Banjeree, 2008; J. Wei, 2008). Thus, an effective cooling method of computer chips is that capable of removing the high thermal power dissipated by the chips, while keeping the junctions' temperature at or below the recommended value by the manufacturers ( $< 85^\circ\text{C} - 115^\circ\text{C}$ , depending on the application) (ITRS, 2011). In addition, it is desirable to mitigate the effect of hot spots by increasing the uniformity of the chip surface temperature. Unlike forced air convection, liquid methods based cooling offer many advantages. These methods include, forced convection in microchannel, spray and impinging jets, and immersion nucleate boiling (Estes and Mudawar, 1995; Katsuta, 1977; Monde, 1978; Bar-Cohen and Wang, 2009; Mudawar, 1992; Hall and Mudawar, 1999; Rainey and You, 2000; Khan et al, 2008; Arik and Bar-Cohen, 2001; Anandan and Ramalingam, 2008; El-Genk and Ali, 2009, 2010a,b ; Ali and El-Genk, 2012a).

Micro-channels heat sinks, spray cooling, and impinging jets are methods essentially require circulating pumps and special arrangement to supply, distribute, and recollect the cooling liquid (Figure 1.3) jet impingement cooling offers high cooling capability for extremely high local heat flux. However, it has inherent limitations including induced thermal stress due to non-uniform surface and temporal distribution. Spray cooling provides uniform cooling with less impact on the integrity of the chip surface. In addition to the high pressure required to break up the liquid into a spray or stream of very small liquid droplets, a specially designed nozzle is required to ensure a repeatable cooling

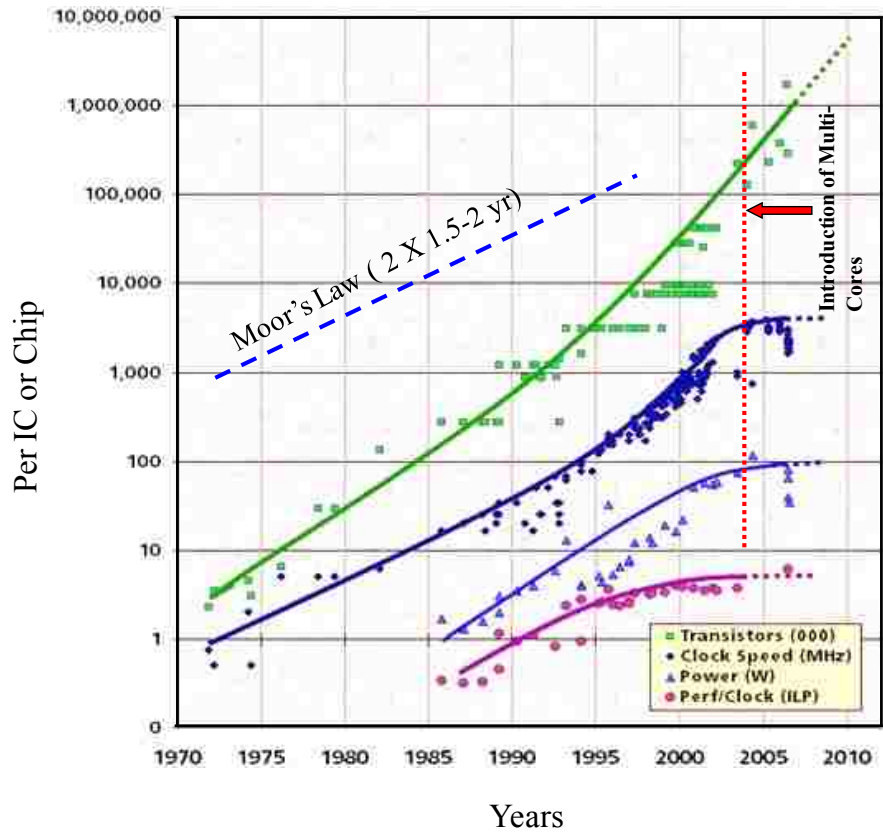


Figure 1.1 Increases in clock speed and dissipated power of high performance computer chips (Ben Yoo, 2011).

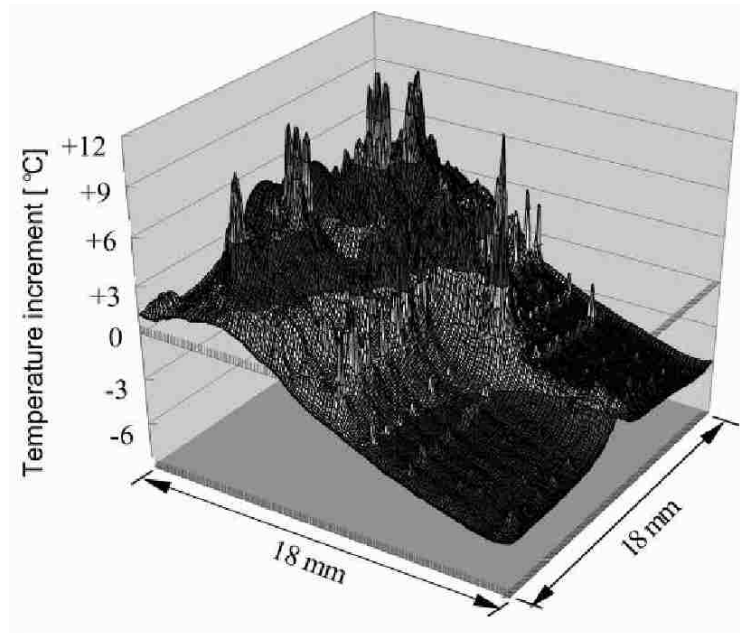
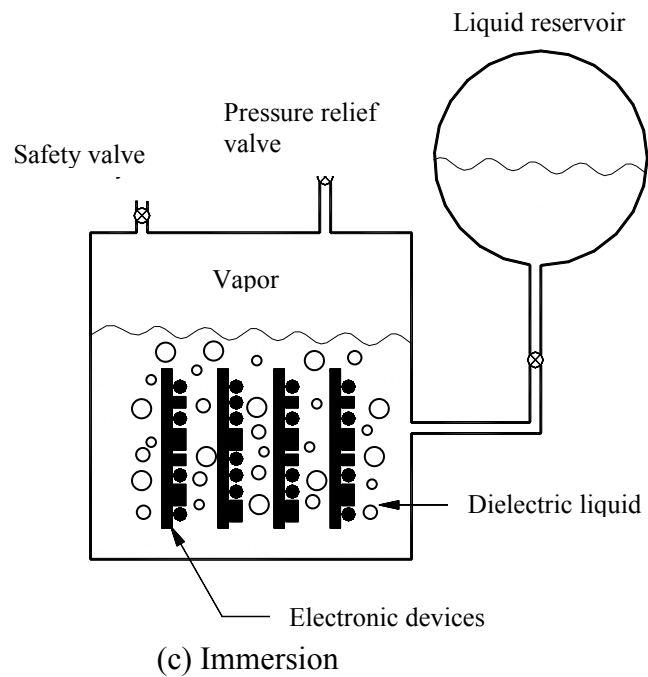
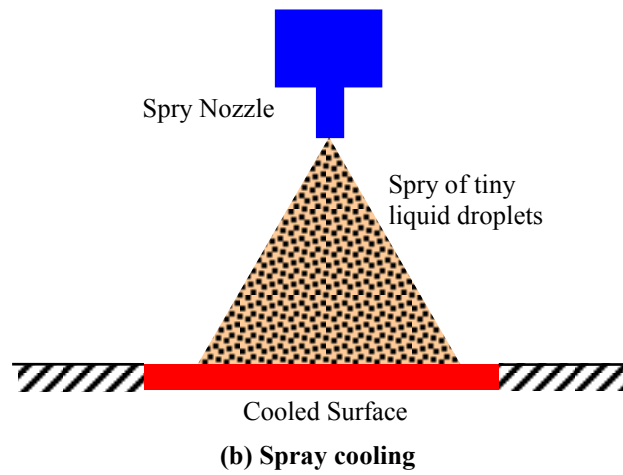
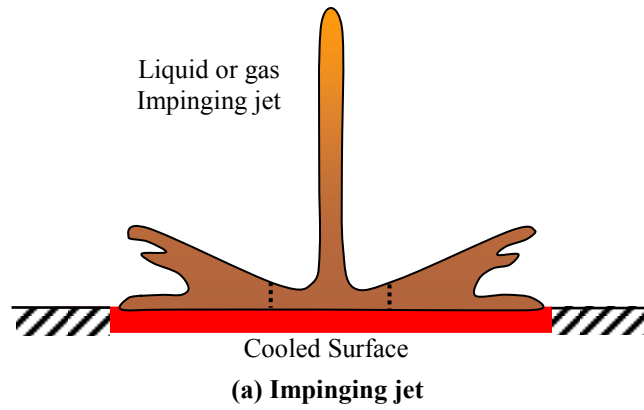


Figure 1.2 Hot spot effect on the local surface temperature of a computer chip surface (Wei, 2008).



**Figure 1.3 Schematics of different methods of liquid-based cooling of electronics.**

pattern and avoid clogging (Figure 1.3b)( Hall and Mudawar, 1999; Tilton and Tilton 1993; Estes and Mudawar, 1995).

In immersion cooling nucleate boiling, the entire mother or circuit board is fully immersed in a pool of dielectric liquid and the dissipated heat is removed from the chip surface by nucleate pool boiling (Figure 1.3c). The most promising dielectric liquids for immersion cooling applications are those with low saturation temperatures ( $< 85\text{ }^{\circ}\text{C}$ ) such as the Fluorinert FC-72, Novec HFE-7100 and the Performance Fluid PF-5060 (3M Inc, 2013). The low saturation temperatures of these liquids at atmospheric pressure, keep the junctions' temperature of the chip below that recommended by the chip manufacturers. Tables 1.1 and 1.2 compare the thermophysical properties of these liquids to those of water as well as list some of the favorable environmental and dielectrical properties. These dielectric liquids are environmentally friendly, and chemically combatable with most of the standard electronic materials with no handling concern.

The highly wetting liquids (Table 1.1) tend to flood surface crevices, reducing the amount of trapped air and delaying boiling incipience till reaching a high surface temperature. The temperature excursion prior to boiling incipience of dielectric liquids has been reported in the literature to exceed 25 K on plane Copper and Silicon surfaces (Rainey and You, 2000; b; El-Genk and Bostanci, 2003a, b; McNiel, 1992; Chang, You, and Haji-Sheikh, 1998). Such temperature excursion is a concern in electronic cooling because it increases the chip junctions' temperature at very low power level.

Methods to improve nucleate boiling of dielectric liquids and reduce or eliminate temperature excursion prior to boiling incipience have been employed. Many studies have performed pool boiling experiments of dielectric liquids on micro- and macro-structured or porous surfaces, surfaces with reentrant cavities, fabricated pores or micro-fins, rough and micro-structured surfaces, surfaces with micro-porous coatings or metal foam (Table 1.3) (e.g., Nakayama et al.1980; Anderson and Mudawa, 1989; Ramilison, Sadasivan, and Lienhard, 1992; Misale et al. 1999; Kim et al., 2007; El-Genk and Parker, 2008; Li et al., 2008; Nimkar et al., 2006; Rainey and You, 2000; Vemuri and Kim, 2005; Yu et al., 2006; El-Genk and Bostanci, 2003; Kim, 2006; Xu et al., 2004; Albertson, 1977; Launay et al., 2006; Wei and Honda, 2003; Ghiu, 2005; Ramaswamy et al., 2003; Mchall et al, 2010; Arik et al., 2007; El-Genk and Ali, 2009, 2010).



**Table 1.1 Comparison of Thermo physical properties of dielectric liquids PF-5060, HFE-7100, FC-72, and Water (3M, 2013).**

Saturation Physical Properties	FC-72 (0.1 MPa)	PF-5060 (0.1 MPa)	HFE-7100 (0.1 MPa)	Water (0.1 MPa)
Boiling point (°C)	56.8	56.8	60	100
Freeze point (°C)	-90	-90	-135	0
Ave. molecular weight (g/mole)	338	338	250	18
Liquid density (kg/m <sup>3</sup> )	1601	1601	1372	958
Vapor density (kg/m <sup>3</sup> )	13.127	13.127	9.7	0.6
Liquid viscosity (kg/m.s)	4.6x10 <sup>-4</sup>	4.6x10 <sup>-4</sup>	3.7x10 <sup>-4</sup>	2.8x10 <sup>-4</sup>
Liquid specific heat (J/kg.K)	1102	1102	1253	4220
Latent heat of Vaporization (kJ/kg)	95.03	95.03	111.5	2256.7
Liquid thermal conductivity (W/m.K)	0.0537	0.0537	0.062	0.68
Liquid surface tension (mN/m)	8.3	7.931	0.010	59

**Table 1.2 Other properties of dielectric liquids PF-5060, FC-72, and HFE-7100 (3M, 2013).**

	FC-72	PF-5060	HFE-7100
<b>Environmental Properties</b>			
Ozon Depletion Potential (CFC-11=1.0)	0	0	0
Global Warming Potential (100 y integrated time horizon)	7400	7400	320
Atmospheric life time (y)	3200	3200	4.1
<b>Electric Properties</b>			
Dielectric strength (kV in 0.1” gap @ 25 °C)	28	28	38
Dielectric constant ( @ 25 °C)	1.75 (1 kHz)	1.75 (1 kHz)	7.39 (100-10 <sup>7</sup> Hz)
Volume Resistivity (Ωcm @ 25 °C)	1 x 10 <sup>15</sup>	1 x 10 <sup>15</sup>	3.3 x 10 <sup>9</sup>

The summary in Table 1.3 is not exhaustive, but representative of previous research on enhancing nucleate boiling of dielectric liquids. The surfaces used have been fabricated using different methods. These include, chemical etching, painting and brushing, particles sintering, electrochemical deposition. Surfaces partially and fully covered with carbon nano-tubes or nano-wires have also been investigated. These surfaces enhanced nucleate boiling, including the maximum heat transfer coefficient,  $h_{MNB}$ , and increase the critical heat flux (CHF) by varying amount. The  $h_{MNB}$ , occurs near the end of the fully developed nucleate boiling region of the pool boiling curve, and is often used to quantify the enhancement in heat transfer. In addition, some of these surfaces reduced or eliminated the temperature excursion prior to boiling incipience of dielectric liquids (Figure 1.4).

Other parameters that affect nucleate boiling and CHF include liquid subcooling, and the orientation of the boiling surface (Rainey and You 2000; Wei and Honda 2003; Ghiu and Joshi 2005; Geisler and Bar-Cohen 2005; El-Genk and Parker, 2004; Parker and El-Genk, 2008; El-Genk and Ali, 2010; Ali and El-Genk 2012,2013). Investigating these effects is important in the industrial applications to immersion cooling of electronics packing, where the circuit board might be mounted in the vertical or the downward facing orientation. The next section briefly reviews some of the reported work on enhancing nucleate boiling of dielectric liquids; more review is given in the next background chapter.

## ***1.1 Surface morphology and microstructure***

The effect of surface roughness on enhancing nucleate has been investigated by many researchers (Ramilison, Sadasivan, and Lienhard, 1992; Ferjančič and Golobič, 2002; Oktay, 1982; Change, J. Y., 1997; Chang and You, 1997; Kahn, Toh, and Pinjala, 2008; El-Genk et al., 2013; Honda, Takamatsu, and Wei, 2002; Rainey and You, 2000). Pool boiling experiments have been performed using different liquids (water, acetone, n-hexane, carbon tetrachloride, and carbon disulfide) on flat rough surfaces to quantify the average surface density of active nucleation sites, and nucleate boiling heat transfer (Kurihara and Myers, 1960). They have shown that the nucleate boiling heat transfer coefficient is proportional to the active nucleation site density, and the later is directly related to the surface roughness. CHF has been shown to increase with surface roughness

**Table 1.3 Selected investigations on enhanced saturation nucleate boiling of dielectric liquids on various surfaces.**

Reference	Dielectric liquid	Surface	CHF (W/cm <sup>2</sup> )	$h_{MNB}$ (W/cm <sup>2</sup> K)
Rainey and You (2001)	FC-72	Microporous coating (DOM)	26.8	< 2.0
Ferjančič and Golobič (2002)	FC-72	steel 1010, smooth, sanded, and chemically etched	8-12	NA
Wei and Honda (2003)	FC-72	Silicon etched micro pins	25-33	Up to 2.3
El-Genk and Parker (2004) and Parker and El-Genk (2005)	FC-72, HFE-7100	Porous Graphite	27.2 – 31.6	3.0 – 2.8
Ghiu and Joshi (2005)	PF-5060	Copper microstructure , Micro- machined channels	16	0.5-0.6
Kim, J. H. (2006)	FC-72	Copper microporous coating using electrochemical deposition	22-27	1.2-4.9
Launay et al. (2006)	PF-5060	Si bare, Pin-fin array covered with carbon nanotubes,	27	0.93
Richard Furberg (2006)	FC-72	Microporous Copper using electrochemical deposition	NA	4.0
Sriraman and Banerjee (2007)	PF-5060	Micro pillars using Lithography	13	0.7-0.8
Arik et al. (2007)	FC-72	Diamond and silver flakes using (DOA and SOA)	18-22	1.6-1.8
Ujereh, Fisher, and Mudawar (2007)	FC-72	carbon nanotubes	19.5	17.1-17.5
Kim et al.,(2008)	PF-5060	Plain, etched and microporous coating surfaces (DOM)	12-20	0.5-1.5
Mchall et al. (2010)	HFE-7300	Sintered Copper particles and Copper with carbon nano-tubes	24-27	0.8 – 1.5
Jeon at al. (2011)	PF-5060	BEC, commercial boiling enhancement coating by 3M	8	< 0.6

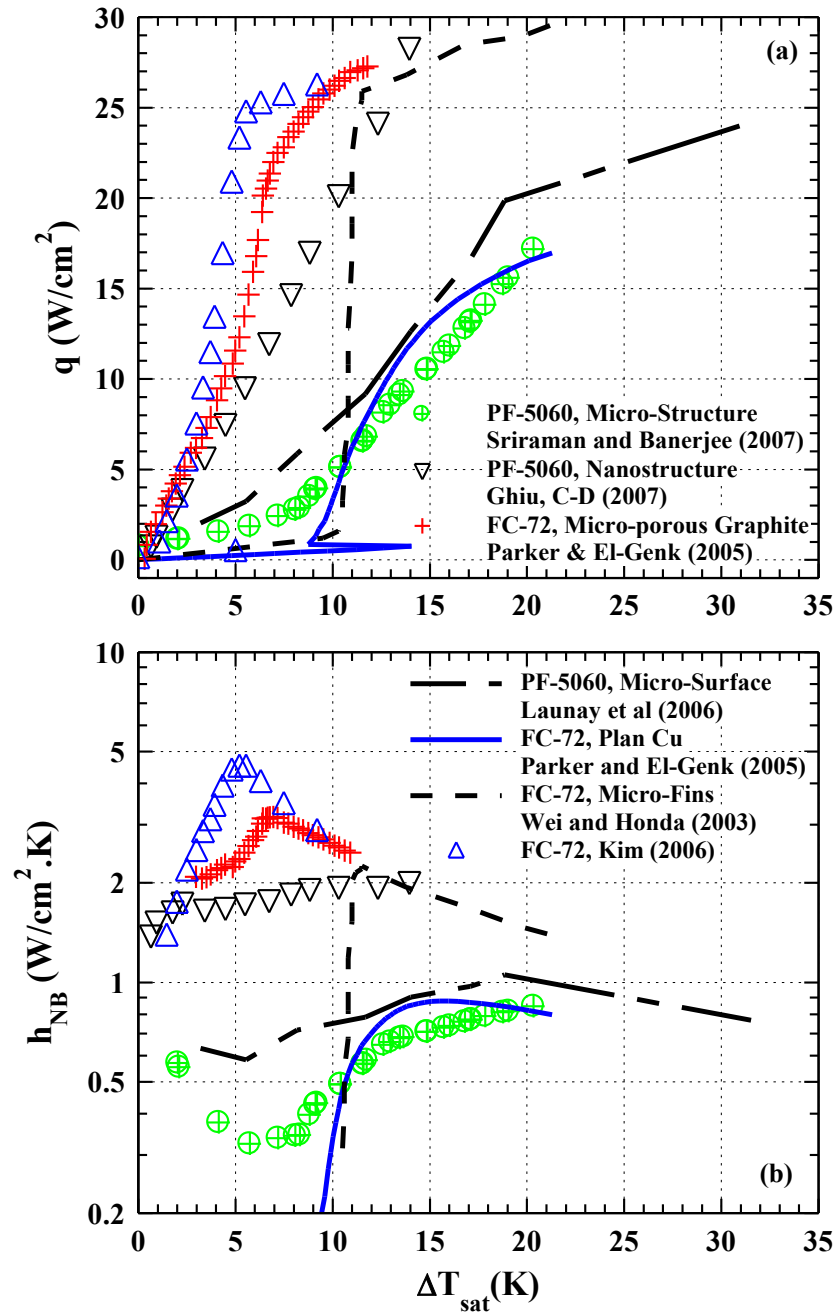


Figure 1.4 Nucleate boiling and heat transfer coefficient curves of dielectric liquids on boiling enhancement surfaces.

to the power 0.125 (Ramilison et al., 1992; Ferjančič and Golobič, 2002). Enhancement in nucleate boiling of FC-72 on a rough Copper surface has been reported by Rainey and You (2000). They reported lower temperature excursion at boiling incipience and ~ 40% higher CHF than that on polished Copper surface was reported. CHF was ~18.8 and 13.2 W/cm<sup>2</sup> on the rough and smooth Cu surfaces, respectively.

Similar results have been reported for sputtered and chemically etched silicon to a RMS roughness of 25-32 nm surfaces (Honda, Takamatsu, and Wei 2002). Results showed only ~ 10 K temperature excursion prior to boiling incipience compared to ~ 18 K on smooth silicon and 40% increase in the CHF. McHale and Garimella (2011) have investigated experimentally the effect of surface roughness on saturation boiling of FC-77 on polished surfaces with average roughness from 0.027  $\mu$ m and 0.038  $\mu$ m and on 1.08  $\mu$ m to 10.0  $\mu$ m rough electrical discharge machined (EDM) surfaces. Results showed that the rough surfaces increase the nucleate boiling heat transfer coefficient by up to ~ 210% of those on polished surfaces.

Rainey and You (2000, 2001) and Rainey, You, and Lee (2003) have investigated surfaces with microporous coatings for enhancing nucleate boiling. The tiny pores in the micro-porous coatings are believed to range in size from 0.1-1  $\mu$ m. However, these coatings made with 1-20  $\mu$ m particles bonded with epoxy, have low effective thermal conductivity of ~ 0.95 W/m K (O'Connor and You, 1995). Thin layers of the coating (~50  $\mu$ m) is applied to flat surfaces and wires> these surfaces resulted in significant enhancements in nucleate boiling of FC-72 liquid at lower surface superheat. They also decreased the temperature excursion prior to boiling incipience (Rainey and You, 2000; Chang and You, 1997a, b; Rainey, You, and Lee, 2003; O'Connor, You, and Chang, 1996; Kim et al, 2007). They attributed the results to the increase in the nucleation sites density as well as the ability to entrap air in the micro-pores of the coatings. Similar results have been reported by You et al. (1995) using an Aluminum oxide particles coating. CHF for saturation boiling for FC-72 increased by 39% at 46% at lower superheat compared to that on a non-treated surface. However, the coating structure was delicate and easily to remove with a swipe of a finger. The structure was improved by adding glue material to increase the adhesion of the particles to the base surface. The boiling on the modified structure gave the same CHF value, but at 4-9 K higher

superheat. In saturation boiling of FC-72 on surfaces with micro-porous coating, O'Connor, You, and Chang (1996) reported ~ 330% increase in the nucleate boiling heat flux and ~100% increase in CHF, compared to untreated Copper surfaces (Chang and You, 1997b).

Porous graphite (PG) have been shown to enhance nucleate boiling of FC-72 and HFE-7100 dielectric liquids (El-Genk and Parker 2004a,b, 2005; Parker and El-Genk, 2006a and b, 2007). Saturation and subcooled boiling experiments on porous graphite and smooth Copper surfaces have been reported. Porous graphite, with a high volume porosity of 60% and 95% of enclosed pores and interconnected re-entrant cavities with mouth sizes ranging from a few to hundreds of microns, effectively increases the active nucleation sites density, thereby enhancing nucleate boiling. There was not temperature excursion prior to boiling incipience compared to 24 K on plane Copper. CHF was 61.5 % higher than on plane Copper (El-Genk and Parker, 2004a, b, 2007).

Studies of nucleate boiling of dielectric liquids enhancement on surfaces partially or fully covered with carbon nano-tubes have shown promising results for saturation boiling of FC-72 and PF-5060. The carbon nano-tubes increased the nucleate boiling heat transfer rate and reduced or eliminated the temperature overshoot at boiling incipience (Ujereh, Fisher, and Mudawar, 2007). Results showed that CHF for FC-72 on a silicon surface fully coated with carbon nano-tubes increased by 6 - 44% over that of an uncoated silicon surface. Similar results for saturation boiling of PF-5060 dielectric liquid on carbon nano-tubes coated pin fins have been reported (Launay et al, 2006). McHale et al. (2011) have experimentally investigated pool boiling of HFE-7300 on smooth Copper, Copper with sintered Copper particles, smooth Copper with Copper-coated carbon nano-tubes (CNT), and Copper with sintered Copper particles and Copper-coated carbon nano-tubes. Results showed that the hybrid (with sintered Cu particles and CNTs) showed the lowest wall superheat at the highest heat flux with no temperature excursion prior to boiling incipience. CHF increased by more than 45% for the hybrid surface relative to the smooth Copper.

Saturation boiling of FC-72 has also been investigated on surfaces with pyramidal-shaped re-entrant cavities having different center-to center spacing (Baldwin, Bahavani, and Jeager, 1998). Results showed increased nucleate boiling heat transfer rate and CHF

on the surface with pyramidal-shaped re-entrant cavities compared to smooth surfaces and surfaces with bulb shaped cavities. Similarly, Si with re-entrant cavities for enhancing nucleate boiling of subcooled FC-72 liquid has been investigated. Results showed higher nucleate boiling heat transfer coefficient and CHF compared to a smooth Si (Kubo, Takamatsu, and Honda, 1999). Sriraman and Banerjee (2007) have used a lithography technique to fabricate a nano-structure on silicon for enhancing nucleate boiling of the dielectric performance fluid PF-5060. Results showed a 41% increase in CHF compared to the reference silicon surface. No significant decrease in the surface superheat at CHF has been reported in saturation and subcooled boiling. Liquid subcooling 10 and 20 K increased CHF by 19% and 27%, respectively.

Recent results of nucleate boiling enhancement of dielectric liquids on MicroPorous Copper (MPC) have been investigated with very promising results (Kim, 2006; Furberg, 2006; Kim et al., 2007; Li et al., 2008; Furberg et al., 2006, 2008, 2009; Furberg and Palm, 2011). These surfaces are fabricated using electrochemical processes at high current density (0.3 to 3 A/cm<sup>2</sup>). Results showed nearly 600% increase in the nucleate boiling heat transfer coefficient and nearly 40% in CHF compared to plane Copper surfaces. Electrochemically deposited MPC surfaces have been investigated for enhancing nucleate boiling of R134a liquid (Furberg, 2006; Li et al, 2008). The boiling experiments were carried out at 4 bar and applied heat flux from 0.1~10 W/cm<sup>2</sup>. Results showed significant increase in the nucleate boiling heat transfer coefficient on 220  $\mu$ m thick MPC surface by up to 7 times that on plane Copper (Furberg et al., 2006). For boiling of R134a on MPC at 6.5 bar, results showed that the nucleate boiling heat transfer coefficient was 4.8 times that on plane surface (Furberg et al, 2008, 2009).

In brief, many surfaces have been investigated experimentally for enhancing nucleate boiling of dielectric liquids. These include rough, partially and fully covered with carbon nano-tubes, porous and surfaces with microporous coating. Some of these surfaces reduced or completely eliminated the temperature excursion prior to boiling incipience. Most reported work with these surfaces is for saturation boiling in the upward facing orientation. Little work has been reported on the effect of surface inclination angle on nucleate boiling and CHF. Investigating the effect of inclination is useful to electronic

cooling application where the chip or the circuit board might not be in an upward facing orientation. Next section summarizes some of the reported work for the effect of surface orientation on nucleate boiling of dielectric liquids.

## **1.2 Effect of surface orientation**

Since electronic packaging may necessitate different orientations of the CPU or computer chips, several investigations have been reported on the effect of the surface inclination angle on nucleate boiling and CHF of dielectric liquids (Chang and You, 1996; El-Genk and Bostanci 2003a, b; Honda and Wei, 2003; Rainey and You, 2001; Priarone, 2005). Earlier work has also been reported for water, liquid nitrogen, and liquid helium (El-Genk and Guo, 1993; Nishikawa et al. 1984). The reported results for dielectric and non-dielectric liquids have been consistent, confirming that: (a) At low surface superheats, the nucleate boiling heat transfer coefficient increases as the inclination angle of the surface increases from  $0^\circ$ - $180^\circ$ . Conversely, at high surface superheats, the nucleate boiling heat transfer coefficient decreases with increased inclination angle. (b) CHF decreases slightly as the inclination angle increases from  $0^\circ$  to  $90^\circ$  then decreases rapidly to its lowest value in the downward facing orientation ( $180^\circ$ ). CHF values for saturation boiling of dielectric liquids FC-72 and HFE-7100 in the downward-facing orientation ( $180^\circ$ ) on smooth Copper and micro-porous coatings are  $\sim 7\%$  to  $28\%$  of those in the upward facing position ( $0^\circ$ ) (Chang and You, 1996; El-Genk and Bostanci, 2003a,b; Priarone, 2005; Parker and El-Genk 2006). Saturation CHF correlations incorporating the effect of surface characteristics and orientation have been developed for dielectric and non-dielectric liquids (Chang and You 1996; El-Genk and Bostanci 2003a, b; El-Genk and Guo 1993).

Recently, MPC surfaces have been investigated experimentally for enhancing nucleate boiling of dielectric liquids, with promising results. The morphology and microstructure of MPC surfaces varied with the thickness and so are the enhancements in nucleate boiling and CHF. A systematic study of the effects of MPC surfaces' morphology on enhancing nucleate boiling of dielectric liquids is needed. In addition, nucleate boiling results of dielectric liquids such as PF-5060 on MPC surfaces for immersion cooling of high power chips are limited. The effects of inclination angle on



nucleate boiling of dielectric liquids on MPC surfaces has not been investigated. Thus, there is a need for investigating these effects, which is the main motivation of this work.

### **1.3 Objectives**

The Objectives of this research are to experimentally investigate MicroPorous Copper (MPC) surfaces for enhancing saturation nucleate boiling and increasing CHF of PF-5060 dielectric liquid and their potential application to immersion cooling of high power computer chips. Saturation boiling experiments are performed using degassed PF-5060 dielectric liquid on conditioned MPC surfaces (80, 95, 115, 140, 171, 197, 230  $\mu\text{m}$  thick) are conducted at different inclination angles. These are  $0^\circ$  (upward facing),  $30^\circ$ ,  $60^\circ$ ,  $90^\circ$  (vertical),  $120^\circ$ ,  $150^\circ$ , and  $180^\circ$  (downward facing). The effects of MPC thickness and surface orientation on enhancing nucleate boiling and CHF are correlated and compared to those on smooth polished Cu of the same dimensions. Results are also compared to those reported in the literature for other micro-structured surfaces and surfaces with microporous coatings. In addition, high speed video movies are recorded of the transient growth of vapor bubbles on MPC surfaces in the upward facing orientation. Results are used to determine the detachment diameter and the frequency of the bubbles, as well as estimate the surface density of active sites for bubble nucleation.

A numerical analysis is carried out to investigate the potential use of MPC on Cu spreaders to increase the total thermal power removed from a underlying 10 x 10 mm chip and mitigates the effect of hot spots. The chip has a central hot spot (CHS) of either 1 or 4  $\text{mm}^2$ . The effects of hot spot area, heat flux ratio, and the thermal interface material (TIM) between the underlying chip and the spreaders on the total thermal power removed, spreader footprint area, and maximum chip temperature are investigated.

Chapter 2 reviews prior Work and provides details on the fundamentals of nucleate boiling curve of dielectric liquids and bubble nucleation. This chapter also reviews the published work on the effectiveness of porous, micro and macro-structured surfaces for enhance nucleate boiling of dielectric liquids and the effect of liquid thermophysical properties and surface orientation on nucleate boiling heat transfer and CHF. The reported work on estimating the bubble departure diameter and detachment frequency is also reviewed. Chapter 3, provides details on the fabrication process of the MPC surfaces

used in this research, including, surface preparation, and electrochemical deposition. Scanning Electron Microscope (SEM) images of the deposited MPC surfaces are presented to show the morphology of the deposited structure.

Chapter 4, describes the experimental pool boiling facility, the design and assembly of the test section, and the experimental procedures. Chapter 5 reports the obtained results of nucleate boiling of PF-5060 on different thickness MPC surfaces at different inclination angles. A developed correlation for the fully developed nucleate boiling heat transfer coefficient,  $h_{NB}$ , at upward facing orientation ( $\theta = 0^\circ$ ) is also introduced. In addition, this chapter introduces the results of the bubble departure diameter and detachment frequency, and the estimate of the active nucleation site density on MPC surfaces in upward facing orientation. Chapter 6 presents and discusses the obtained results for CHF on MPC surfaces of different thickness at different inclination angles. Developed is CHF correlation that accounts for the MPC surface thickness and inclination angles. Chapter 7 presents and discusses the numerical analysis performed to quantify the potential of using Cu spreaders with thin layer of MPC to increase the total thermal power removed from underlying chip and mitigate the effect of hot spots. Also presented and discussed are the results of the spreader performance including the total thermal power removed, footprint area, and the maximum temperature of the underlying computer chip. This chapter investigated the effect of thermal interface material on the spreader performance Chapter 8 gives a summary and conclusions, and chapter 9 gives recommendations for future work

## **2. Background and Review of Prior Work**

This chapter briefly summarizes the capabilities of different methods for cooling high power computer chips with the focus on immersion cooling nucleate boiling. Review of prior work and details on the fundamentals of nucleate boiling curve of dielectric liquids and bubble nucleation are provided. This chapter also reviews the published work on the effectiveness of porous, micro and macro-structured surfaces for enhance nucleate boiling of dielectric liquids and the effect of liquid thermophysical properties and surface orientation on nucleate boiling heat transfer and CHF. In addition, the reported work on bubble departure diameter and frequency, and active nucleation site density is presented.

### ***2.1 Methods for Cooling High Power Electronics Chips***

Methods of cooling electronics could be categorized into active and passive. Active cooling depends on mechanical devices such as fans and pumps to drive and circulate the working fluid. It includes, jet impingement, spray cooling, and forced convection in microchannel heat sinks. When the mechanical element is eliminated, the cooling method is passive. This category includes natural convection cooled heat sinks and heat spreaders, and immersion cooling. Both active and passive cooling methods could use gases or liquids as working fluids. Figure 2.1 compares the applicable ranges of the different cooling methods for electronics. Natural convection cooling, a simple and passive method for cooling power electronics dissipating up to 5 W (Cengel, 2002), is free supply, with no maintenance cost. Owing to the low heat transfer coefficient provided by natural convection (Figure 2.1) heat spreaders/sinks with large surface areas are needed to increase the total thermal power removal. When natural convection is not adequate, forced air convection, by means of fans provides higher heat transfer coefficient, requiring heat sinks/spreaders with much less surface area compared to those for natural convection. Forced convection cooling methods require proper selection of parameters such as operating pressure, and coolant flow rate (Anandan and Ramalingam, 2008). Gases or liquids are used as cooling media for both natural and forced convection. Liquids provide higher heat transfer coefficient than gases (Figure 2.1), thus liquid cooling methods have been favored over gaseous for cooling high power electronic. Liquid cooling methods include, jet impingement, spray cooling, forced convection in

microchannel, and immersion cooling nucleate boiling. In general, jet impingement, spray cooling and microchannel heat sinks require special arrangements to supply, distribute, and recollect the cooling liquid.

Jet impingement has been the subject of extensive studies for electronic cooling applications. Studied parameter includes liquid conditions (e.g. inlet velocity and temperature) and configuration and arrangement (e.g. single or multiple). While jet impingement cooling offers the highest cooling capability for extremely high local heat flux, it has practical limitations of induced thermal stress due to non-uniform surface cooling and temporal distribution (Estes and Mudawar, 1995). Spray cooling can be implemented by means of liquid jets or stream of liquid droplets. The injected liquid or droplets form a thin liquid film on the cooled surface. The heat dissipated from the surface by boiling or vaporization provides uniform cooling of the target surface. In addition to the high pressure required to break up the liquid into tiny droplets, a specially designed nozzle with a periodic testing is required to ensure a repeatable cooling pattern with no clogging (Hall and Mudawar, 1999).

Microchannel heat sinks have been used and tested for cooling high heat flux surfaces. The mass flow rate, channel size, type of cooling liquid and liquid subcooling have been major study parameters. Flow boiling in microchannel is capable of removing high heat flux, while maintaining a uniform surface temperature. The high driving pressure and the surge in surface local temperature at dry out spots are main challenges for using such cooling technique (Hall and Mudawar, 1999; I. Mudawar, 2001). In immersion cooling, the thermal power dissipated by the immersed electronic device in a stagnant liquid pool is removed by nucleate boiling of dielectric liquid in contact with the heated surface. Such method has the advantage of a high heat transfer coefficient (Figure 2.1) for moderate to high rate of thermal power removal. The relatively uniform surface temperature associated with the pool, help mitigates the effect of surface hot spots, reducing the induced stress and increasing the performance and life time of the computer chip.

In immersion cooling, the dielectric liquids used have high dielectric constant, chemically compatible with components and have low boiling temperature to maintain chip junction's temperature below 85 °C as recommended by the manufacturer. Novec

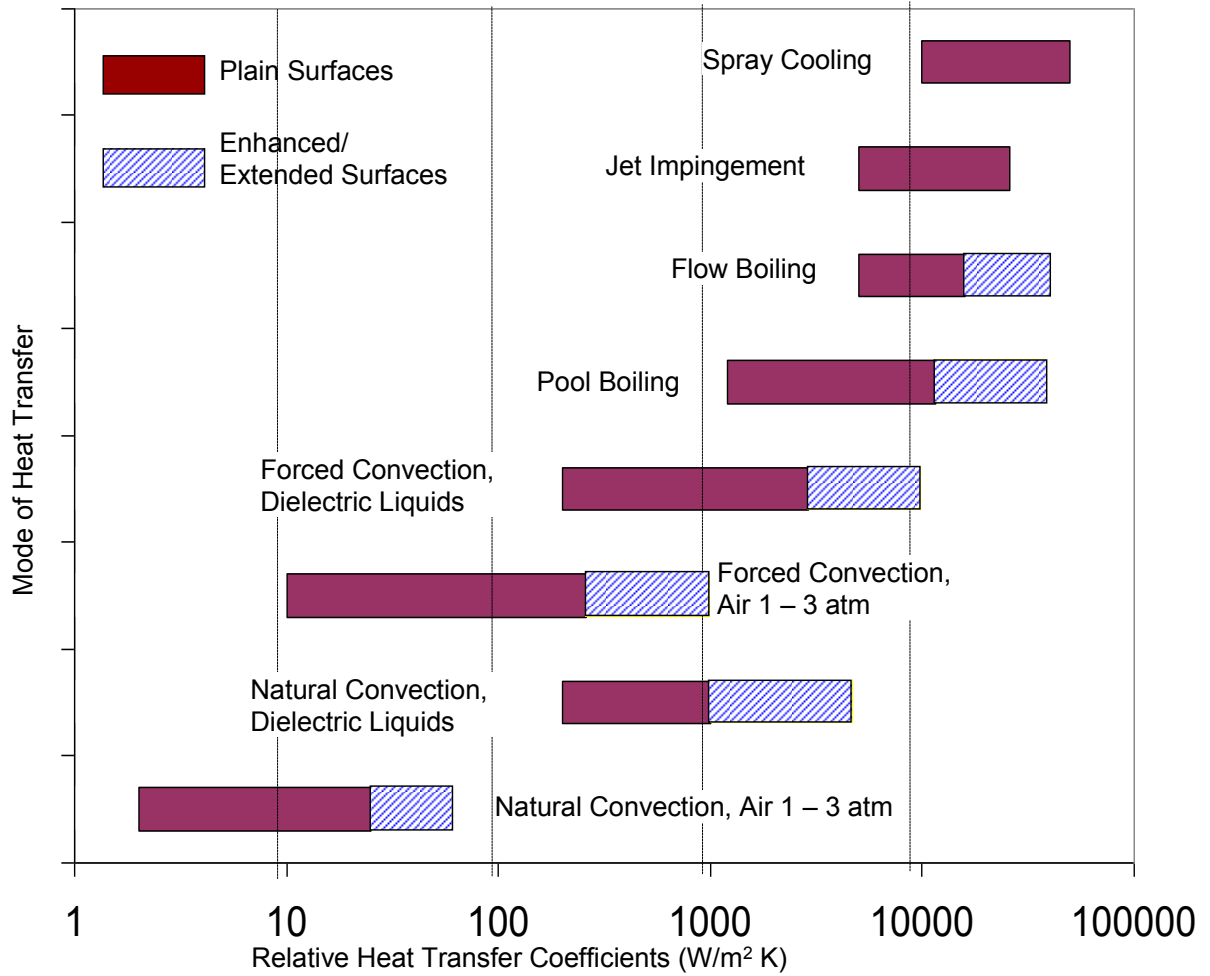


**Figure 2.1 Range of capability of different electronic cooling methods.**

and Fluorinert liquids developed by 3M are used. Tables 1.1 and 1.2 list some of the thermal and physical properties of PF-5060, FC-72 and HFE-7100 liquids as compared to water. These liquids are environmentally friendly with no handling concerns and the saturation temperatures at atmospheric pressure are  $< 65\text{ }^{\circ}\text{C}$ . These highly wetting liquids, however delay of boiling incipience until reaching high surface temperature;. When used in conjunction with structured surfaces and surfaces with microporous coatings, such a concern is effectively reduced or eliminated. In general, immersion cooling nucleate boiling with dielectric liquids is a viable option for thermal management of high power electronics.

## **2.2 Fundamentals of Pool Boiling and Bubble Nucleation**

In pool boiling prior to boiling incipience, heat transfer by natural convection usually occurs. It is a heat transfer process associate with circulation of the liquid near the heated surface under the effect of gravity. The temperature difference between the surface and bulk liquid causes a density gradient in the liquid film adjacent to the surface. The resulting buoyant force replaces the worm liquid rising near the surface by a cold fluid from the bulk. The total heat transfer flux removed by natural convection from uniformly heated surface is proportional to the temperature difference between the surface and bulk liquid to the power 1.2 (Chang and You, 1996; Rainey and You, 2001; El-Genk, 2012).

$$q'' \propto (T_w - T_{sat})^{1.2} \quad (2.1)$$

While natural convection occurs anytime that the surface temperature exceeds the liquid bulk temperature, higher wall temperature in excess of saturation is required to initiate and maintain nucleate boiling.

### **2.2.1 Nucleate Pool Boiling Heat Transfer**

In nucleate boiling, tiny vapor bubbles or embryos grow from specific surface sites that trap air, which initiate nucleate boiling at relatively low surface temperature. The amount of entrapped gas in surface cavities is a strongly function of the shape of the cavity and liquid surface tension or wettability. As the liquid penetrates into the cavity, it keeps the dynamic contact angle with the cavity wall unchanged, if the contact angle,  $\theta$ , larger than the effective angle of the cavity,  $\beta$  (Van P. Cary, 1978; Bar-Cohen et al.,

1992). Figure 2.2 shows the gas entrapment in surface cavity by advancing poorly and highly wetting liquids. For poor wetting liquid (large contact angle) the advancing liquid front strikes the opposite wall of the cavity before the contact line reach the bottom of the cavity (Figure 2.2a), and vice versa for the highly wetting liquids (Figure 2.2b). Thus in surface grooves or crevices more air is trapped by poorly wetting than highly wetting liquids, initiating nucleate boiling at lower surface temperature.

Because dielectric liquids such as PF-5060 and FC-72 have low surface tension and highly wetting contact angle  $< 5^\circ$  (Reed and Mudawar, 1996, 1997), they liquid trap very little amount of air in the surface crevices. As the applied heat flux increases, the surface temperature increases, and the volume of trapped gas in surface cavities grows by thermal expansion, eventually initiate nucleate boiling (Figure 2.3). The increase in wall temperature before boiling incipience is referred to as temperature excursion. On smooth surfaces, such temperature excursion may exceed 35 K (Chang You, and Haji-Sheikh, 1998; El-Genk and Bostanci, 2003a, b).

For bubble nucleation to ensue at a given site, the radius of the cavity mouth,  $r$ , must be greater than a critical value,  $r_c$ , which depends on the liquid's thermophysical properties and the wall superheat (or applied heat flux), given by (Carey, 1992)

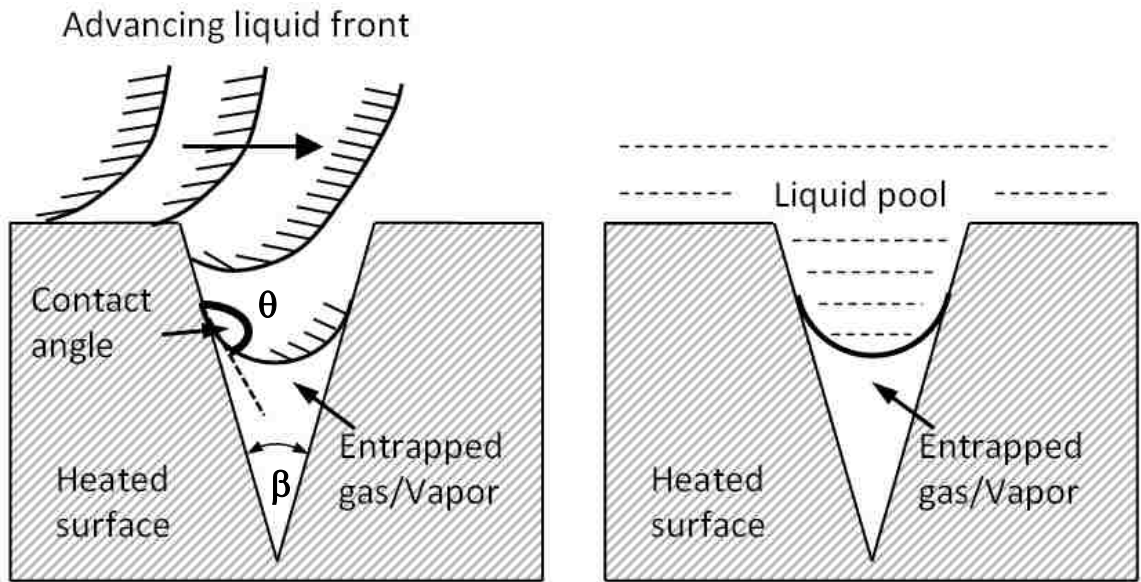
$$r_c = \frac{2\sigma T_{sat}(P_l)\left(\frac{1}{\rho_v} - \frac{1}{\rho_l}\right)}{h_{fg}(T_w - T_{sat}(P_l))} \quad (2.2)$$

Hsu (1962) proposed a semi-theoretical model outlining the size range of active nucleation sites in nucleate boiling. Assuming conical cavities, the model indicates that:

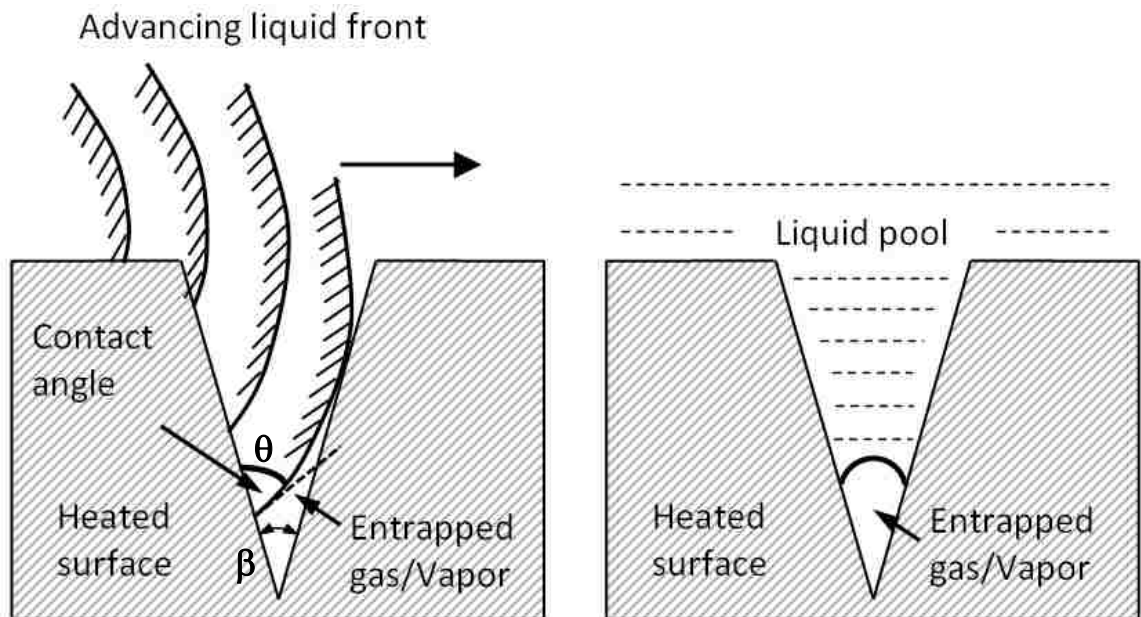
(a) A certain wall superheat is necessary to activate potential nucleation sites, and (b) only a finite range of cavity sizes become active boiling sites. The relationship describing the range of radii of active cavity is given by (Carey, 1992) as

$$\left\{ \begin{matrix} r_{c,max} \\ r_{c,min} \end{matrix} \right\} = \frac{\delta_t}{4} \left[ 1 - \left( \frac{T_w - T_b}{T_w - T_b} \right) \{ \pm \} \sqrt{1 - \left( \frac{T_w - T_b}{T_w - T_b} \right)^2 - \frac{12.8\sigma T_{sat}}{\rho_v h_{fg} \delta_t (T_w - T_b)}} \right] \quad (2.3)$$

As can be seen in Figure 2.4, for the same applied heat flux for boiling incipience and system pressure there is a range of active cavity sizes inside the envelope for each dielectric liquid for bubbles nucleation. As the applied heat flux or surface superheat



**(a) Penetration of poorly wetting liquids into surface cavity**



**(b) Penetration of highly wetting liquids into surface cavity**

Figure 2.2 Gas entrapment in a cavity for poorly and highly wetting liquids (Carey, 1992).



increases, the range of active cavities increases. The cavity sizes outside the envelope are inactive, the larger lose the entrapped air and the smaller do not entrap enough air to initiate boiling. According to the Hsu (1962), there is also a minimum wall temperature above saturation at which cavities may active (Solid squares, Figure 2.4). Figure 2.4 also shows the dependence of the size range of active nucleation sites on liquid properties and surface characteristics. According to Hsu's (1962), saturation boiling of FC-72 on porous graphite (El-Genk and Parker 2004; Parker, 2008) provide the widest ranges of cavity sizes for bubble nucleation respectively, while FC-772 on plane rough Copper ( $Ra = 5.89 \mu m$ ) surface provides the narrowest range of active cavity size.

### **2.2.2 Ebullition Cycle**

Once boiling starts, bubbles forming on the surface grow, and detach when the buoyant force overcomes the surface tension force holding the bubble to the mouth of the surface cavity. The cyclic formation and release of vapor bubbles at an active nucleation site is called the ebullition cycle (Figure 2.5). The cycle consists of four stages: the waiting period, nucleation, bubble growth, and bubble departure. The waiting period starts immediately after a bubble detaches. Liquid from the pool tends to fill the void left by the detached vapor bubble whose departure destroys the thermal boundary layer (Figure 2.5a). A waiting period is necessary to re-establish the thermal boundary layer for subsequent bubble nucleation at the same site (Figure 2.5b).

At the end of the waiting period, the embryonic bubble reaches a critical size and begins to grow (Figure 2.5b). Energy supplied by the heated surface at the vapor-liquid-solid triple point evaporates the liquid to sustain the bubble growth. Initially, bubble growth is rapid and is driven by the inertia of the generated vapor in the liquid microlayer at the heated surface (Figure 2.5c). Heat transfer from the heated wall is very fast and the bubble growth is driven by inertia of the generated vapor pushing back the surrounding liquid at the triple point. As the bubble grows a thin liquid micro-layer of liquid is left between the heated wall and bubble. Heat transfer across this liquid micro-layer directly vaporizes the liquid at the interface. As the bubble grows, the rate of growth increases driven by evaporation at liquid vapor interface. This is known as thermal driven bubble growth (Figure 2.5d). The bubble continues to grow until the buoyant force pulling the bubble upward overcomes the surface tension holding the bubble down to the surface cavity

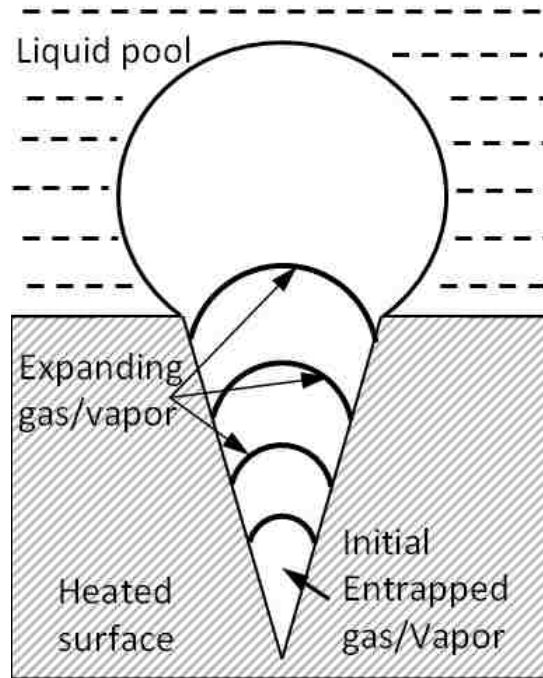


Figure 2.3 Growth of entrapped gas to bubble nucleation.

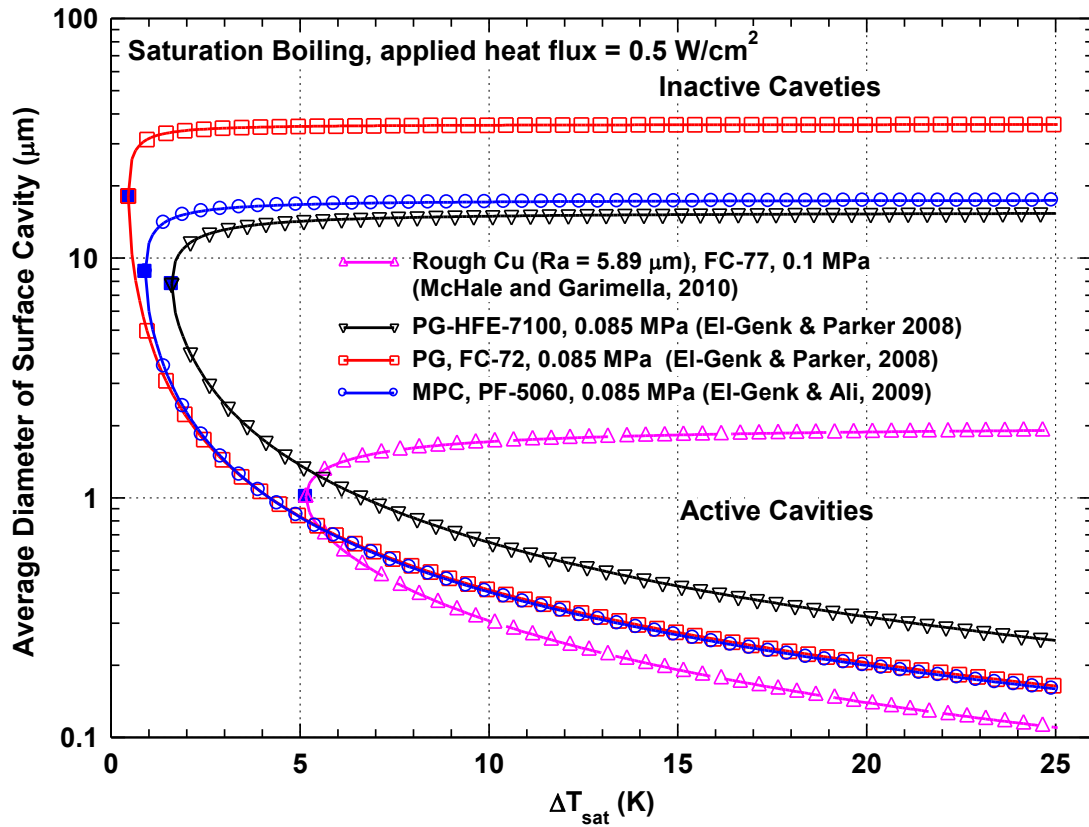


Figure 2.4 Range of cavity sizes for active nucleation of different dielectric liquids.

mouth. As the bubble starts to pull away from the surface, liquid pinches and breaks off the bubble from the nucleation site (Figure 2.5e and f). When the bubble detach, liquid from the pool rushes to fill the space previously occupied by the growing bubble and the ebullition cycle starts over.

The frequency of this cycle is the inverse of the sum of the waiting time (time necessary for re-establishing the thermal boundary layer) and the growth period (time between bubble nucleation and detachment) (Carey, 1992):

$$f = \frac{1}{t_{wait} + t_{growth}}. \quad (2.4)$$

The ebullition frequency and the detached bubble diameter are inversely proportional. Zuber (1963) had proposed the following relationship between the two as:

$$fd_d = 0.59 \left[ \frac{\sigma g (\rho_l - \rho_v)}{\rho_l^2} \right]^{1/4} \quad (2.5)$$

The work reported in the literature on bubble departure diameter and frequency, and active nucleation site density will be summarized later in this chapter

## **2.3 Nucleate Boiling of Dielectric Liquids**

Because of their low surface tension and high wetting, dielectric liquids tend to flood the grooves and crevices of the boiling surfaces, trapping less amount of air. As a result, boiling incipience of dielectric liquids on commercial surfaces such as Copper and silicon is delayed until reaching high superheats (Rainey and You, 2000; El-Genk and Bostanci, 2003a, b) also referred to as temperature excursion. Such high temperature excursion is undesirable because of concern that junction's temperature might exceed the limit of safe operation. Consequently, the lifetime of the chip could be reduced and failure frequency increased (Peterson, 1994). In an attempt to enhance nucleate boiling, increase CHF, and reduces or eliminate temperature excursion prior to boiling incipience many surfaces have been investigated (Chang and You, 1996, Rainey and You, 2001; Sriraman and Banerjee, 2007, Im et al., 2012; El-Genk and Parker, 2008; El-Genk and Ali, 2010; )

### **2.3.1 Boiling regimes of dielectric liquids**

Prior to boiling incipience, increasing the applied heat flux increases the wall temperature ( $T_w$ ) over the liquid's bulk temperature ( $T_b$ ) causing density gradient near the surface. The density gradient results buoyant force that circulates the liquid from the bulk

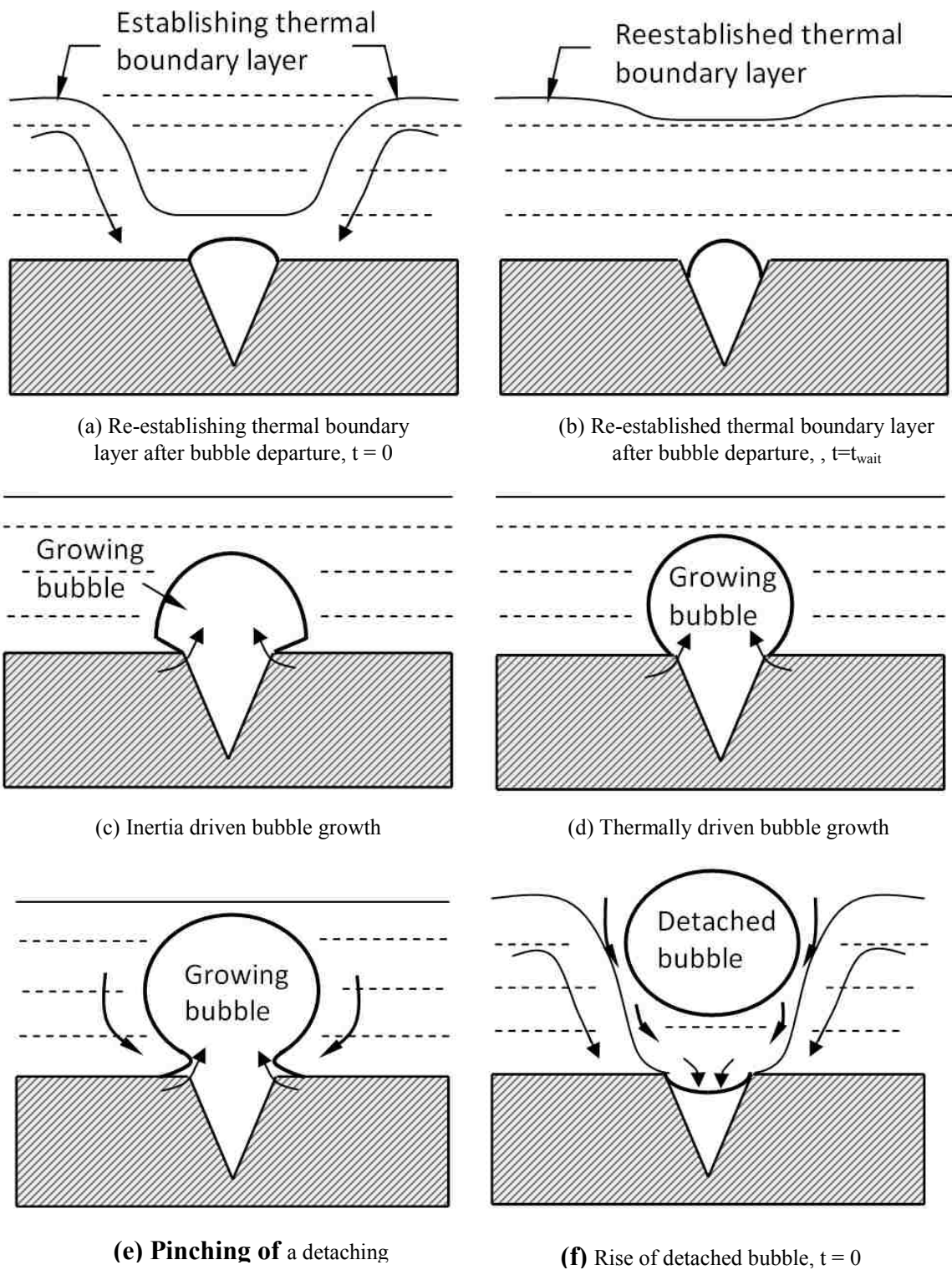


Figure 2.5 Illustration of bubble Ebullition cycle in nucleate boiling.

near the surface. Natural convection cooling continues until nucleate boiling ensues. To initiate and sustain nucleate boiling, the wall temperature has to exceed the liquid saturation temperature. The surface superheat prior to boiling incipience is known as "temperature excursion". It depends on the amount of trapped air in the surface crevices which depends on the surface morphology and microstructure and the liquid properties. The highly wetting dielectric liquids trap less air in the surface crevices compared to non-dielectric liquids. As the applied heat flux and the corresponding surface temperature increase, the trapped volume of air grows by thermal expansion, eventually initiating nucleate boiling. Thus, a high value of surface superheat is typically required to initiate boiling of dielectric liquids. The temperature excursion on smooth surface such as Copper and silicon is reported to be 30 K (Rainey and You, 2000; El-Genk and Parker, 2004a, b; El-Genk and Bostanci, 2003a, b).

A typical pool boiling curve of dielectric liquids with increasing thermal power is shown in Figure 2.6. The curve plots the applied heat flux,  $q$ , versus the surface superheat ( $T_w - T_{sat}$ ). Natural convection extends from very low heat flux to nucleate boiling incipience (A-B, Fig. 2.6). The nucleate boiling portion of the pool boiling curve can be divided into three regions (El-Genk and Parker, 2008; El-Genk and Ali, 2011). The discrete bubbles region (I), the fully developed nucleate boiling region (II), and bubble coalescence region (III). The discrete bubble extends from boiling incipience to some intermediate heat flux (C-D). The fully developed nucleate boiling region (II) extends from point D to the location of the maximum nucleate boiling heat transfer coefficient,  $h_{MNB}$  (Figure 2.6). The heat flux at this region is much higher but the surface superheat slightly higher than in the discrete bubble region. The bubble coalescence region (III) is characterized by much lower slope and higher surface superheat than the previous two regions. It extends to the critical heat flux, where a surge in the surface temperature due to local dryout transitions the curve to film boiling region.

In the discrete bubble region (I), not all nucleation sites become active. As the heat flux and hence, surface superheat increases, the number of active sites increases, increasing the slope of the boiling curve and hence the heat transfer coefficient. In the fully developed nucleate boiling region (II), the density of active nucleation sites and the heat transfer coefficient are the highest, as indicated by the steepest slope of the boiling

curve. The maximum heat transfer coefficient,  $h_{MNB}$  occurs near the end of this region before transitioning to region (III), where all the potential sites of nucleation are active.

In region (III) the heat transfer coefficient decreases with a small increase in the input power results in large increase in the surface temperature. This is caused by the added heat transfer resistance by the coalescence of the growing and rising bubbles at and near the surface (El-Genk and Bostanci, 2003; Parker and El-Genk 2005). At the end of this region, failure to sufficiently replenish the surface with liquid, triggers critical heat flux (CHF), and surface dryout. CHF is associated with local dryout and large jump in the surface temperature, which can leads to physical burnout or melting of the surface. CHF is a critical limit not to exceed for electronic cooling application; which it is preferable to operate at or near,  $h_{MNB}$ , on the low superheat side of the boiling curve occurring at the end of fully developed nucleate boiling region(El-Genk et al. 2013). The  $h_{MNB}$  is much higher than that at CHF and the corresponding superheat is much lower.

### 2.3.2 Critical heat flux

Different models describing the mechanism responsible for CHF have been proposed (Kutateladze, 1952; Griffith, 1957; Zuber, 1959; Haramura and Katto, 1983). The model proposed by Haramura and Katto (1983) is known as microlayer model, focuses on the existence of a liquid microlayer of definite thickness beneath large vapor slugs or vapor mushroom on the heated surface. The liquid slugs are formed by coalescing bubbles from a number of adjacent nucleation sites (Figure 2.7a) and isolating thin liquid layer underneath the vapor mushroom known as vapor stem (Figure 2.7b). Vapor stem feed the large vapor bubble though the evaporation of the thin film of liquid separating the vapor mass from the heated surface. The large vapor bubble “hover” over the surface until accumulating sufficient vapor to detach. When the liquid microlayer evaporates during the “hovering” time, causes dryout before bubble detaches and CHF ensues (Figure 2.7c).

Kutateladze (1952) and Zuber (1959) independently arrived at a similar relationship to predict CHF for saturation pool boiling on upward facing orientation.

$$CHF_{sat} = C_{CHF,sat} h_{fg} \rho_v^{0.5} [\sigma g (\rho_l - \rho_v)]^{1/4} \quad (2.6)$$

Their correlation differed in the value of the constant,  $C_{CHF,sat}$ . Zuber (1959) fixed the constant at  $\pi/24$  (~0.131). Average values of  $C_{CHF,sat}$  given by Kutateladze (1952) for

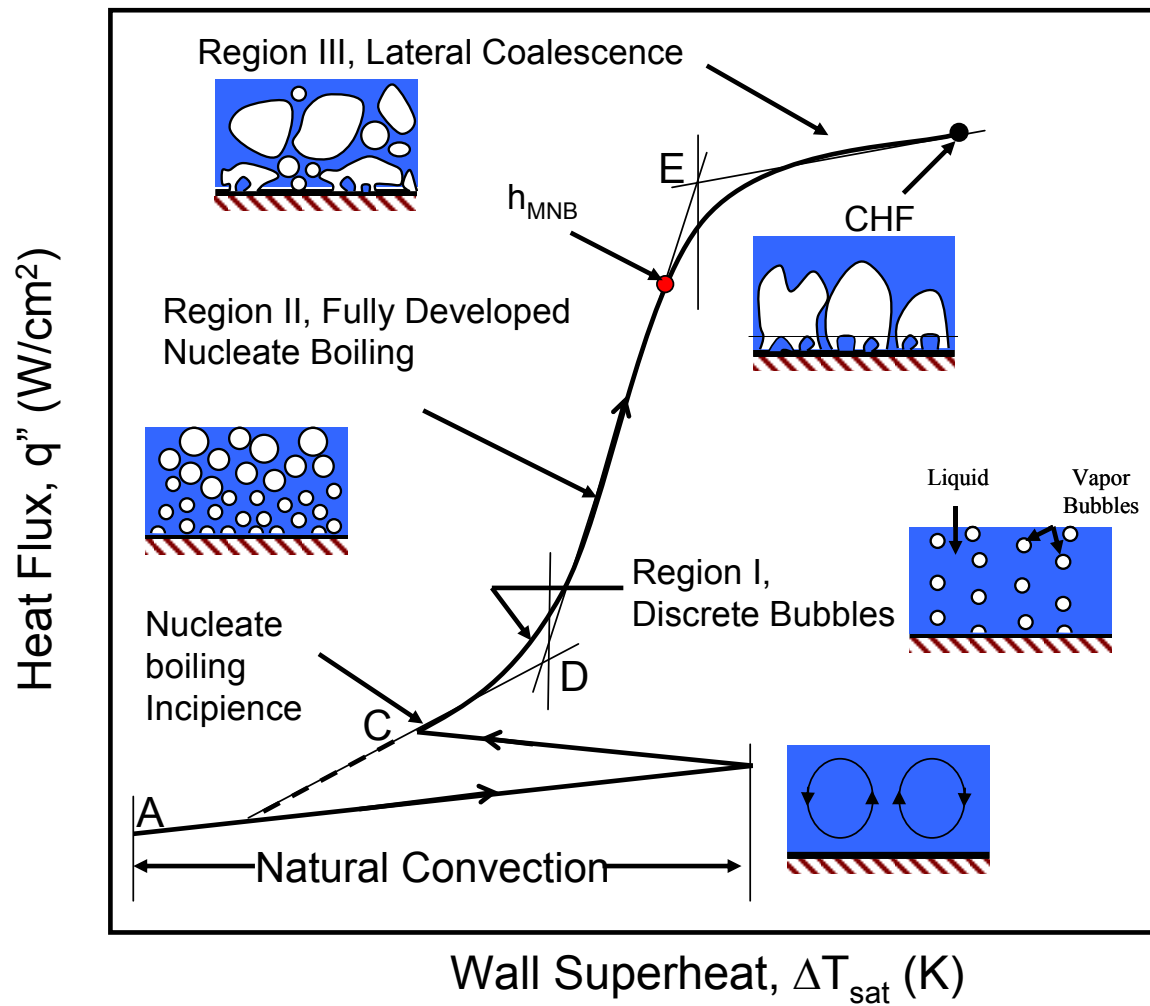


Figure 2.6 Typical nucleate boiling curves of dielectric liquids (El-Genk and Ali, 2010).

water, and organic liquids boiling on graphite disks, chrome plated disks, and wires of different composition range from 0.13 – 0.19. The value of the coefficient,  $C_{CHF,sat}$ , for electric and dielectric liquid have been shown to depend on the boiling surface characteristics (morphology, geometry, orientation, material properties (El-Genk and Parker, 2008, El-Genk and Bostanci, 2003; Priarone, 2005, Ali and El-Genk, 2012, 2013) as reported in the literature. The values of this coefficient for dielectric liquids such as FC-72, and HFE-7100 are higher than given by both Zuber and Kutateladze. The reported values for the critical heat flux coefficient,  $C_{CHF,sat}$  are 0.26 and 0.96 for FC-72 and HFE-7100 liquids on porous graphite, micro finned and microporous coated surface (e.g., Mudawar, Howard, and Gersey, 1997; Arik, Bar-Cohen, and You, 2007; Parker and El-Genk, 2006a,b; Parker and El-Genk, 2008; El-Genk and Parker, 2008)

To account for the effect of orientation on CHF, the coefficient,  $C_{CHF,sat}$  in equation 2.6 is multiplied by a function of the orientation angle,  $R(\theta)$ , obtained by normalizing the CHF at different inclination angle to that in the upward facing CHF. The modified correlation for CHF is given as:

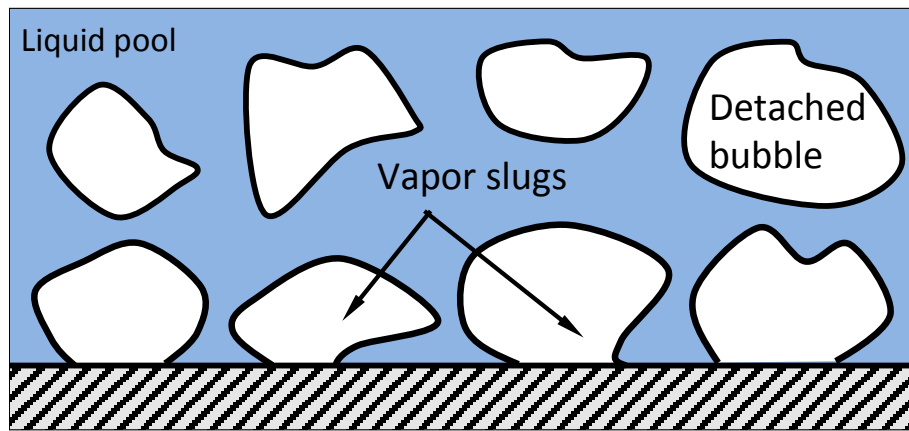
$$CHF_{sat} = C_{CHF,sat}(0^\circ)R(\theta)h_{fg}\rho_v^{0.5}[\sigma g(\rho_l - \rho_v)]^{1/4} \quad (2.7)$$

This correlation is in a good agreement between experimental CHF for dielectric liquids FC-72 and HFE-7100 on plane and porous graphite and other surfaces (Ali and El-Genk, 2013; Parker and El-Genk, 2006; Parker and El-Genk, 2008; El-Genk and Bostanci, 2003; Priarone, 2005, Ali and El-Genk, 2013; Rainey and You, 2001, Change and You, 1996; Reed and Mudawar, 1997).

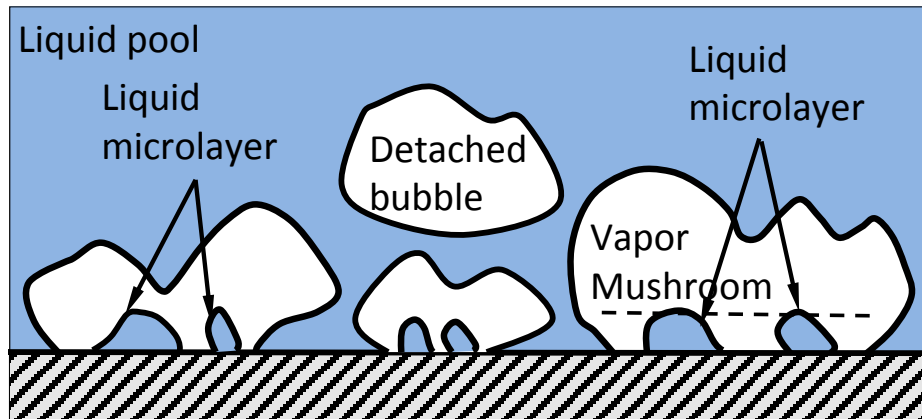
## **2.4 Nucleate Boiling Enhancements**

Thermal challenges associated with nucleate boiling using dielectric liquids have motivated recent studies (El-Genk and Ali, 2009, 2012; Kim, J. H., 2006; Furberg, 2006, 2011; El-Genk, suszko and Ali, 2013). These challenges include temperature excursion prior to boiling incipience and relatively lower nucleate boiling heat transfer rate. In attempt to enhance nucleate boiling and reduce or eliminate temperature excursion, many researchers have investigated experimentally nucleate boiling of dielectric liquids on different surfaces. These include micro-and macro-structured, porous surfaces, rough and

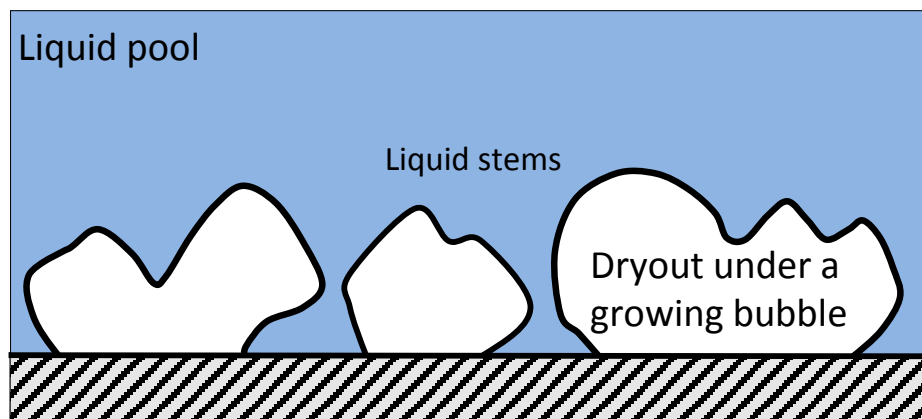




(a) Formation and detachment of vapor bubbles



(b) Vapor Mushroom and liquid micro layer



(c) CHF-dryout of liquid micro layer

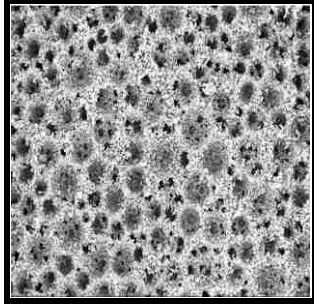
Figure 2.7 Vapor dynamic for triggering the critical heat flux (CHF).

micro-structured surfaces, and surfaces with applied micro-porous coatings. (e.g., Kim et al., 2008; El-Genk and Parker, 2008; Nimkar et al., 2006; Parker and El-Genk, 2006; El-Genk and Ali, 2009). The reported results showed a marked decrease or complete absence of temperature excursion and variable enhancements in heat transfer coefficient and CHF compared to plane surfaces. The degree of enhancement depends on the surface characteristics.

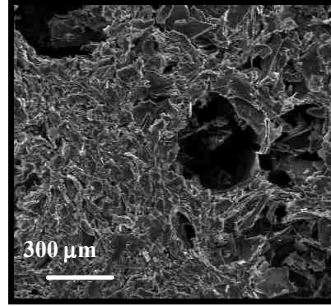
Figure 2.8 presents SEM images of surface morphology for selected surfaces investigated experimentally for enhancing nucleate boiling of dielectric liquids. The previous researchers contributed the enhancement in nucleate boiling to the increase of the active nucleation site density and/or wetted area of these surfaces. In addition to surface effect, other parameters affecting nucleate boiling of dielectric liquids are liquid thermophysical properties, subcooling, and the orientation of the boiling surface with respect to gravity (El-Genk and Parker, 2008; El-Genk and Bostanci, 2003b; Priarone, 2005; Howard and Mudawar, 1999; Howard, A. H., 1999; Ali and El-Genk 2012, El-Genk, Suszko, and Ali 2013). The next sections reviewed some of the reported studies on nucleate boiling enhancement of dielectric liquids with focuses on PF-5060, and FC-72 liquids.

#### **2.4.1 Effect of liquid thermophysical properties**

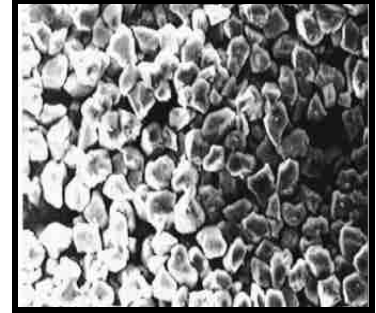
Arik and Bar-Cohen (2001) performed experiments that explored the effect of using HFE-7100 and HFE-7200 on CHF compared to FC-72. Reported CHF values for HFE-7100 and HFE-7200 were found to be 50-90 % higher than reported for FC-72 on similar surfaces (Change and You, 1996; Rainey and You, 2000,2001; El-Genk and Bostanci (2003a, b), El-Genk and Parker (2004, 2005), Parker and El-Genk (2006), and Priarone (2005), have carried out separate investigations comparing HFE-7100 and FC-72 dielectric liquids for boiling on Copper and porous graphite. Consistent with the results of Arik and Bar-Cohen (2001), CHF for HFE-7100 was higher than measured and found in the literature for FC-72. El-Genk and Bostanci (2003a,b) reported saturation CHF of HFE-7100 on plane Copper of  $24.5 \text{ W/cm}^2$ ; Priarone (2005) reported  $25.2 \text{ W/cm}^2$ . The CHF value reported by El-Genk and Parker (2005) is  $22.7 \text{ W/cm}^2$ . The average saturation CHF of FC-72 on plane Copper and silicon reported in the literature is  $16.3 \text{ W/cm}^2$  (Rainey and You, 2000; Rainey, You, and Lee, 2003). On porous graphite,



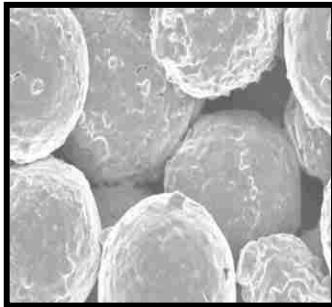
**MPC**  
Richard Furberg ( $3\text{A/m}^2$ )  
(2006,2008,2009)



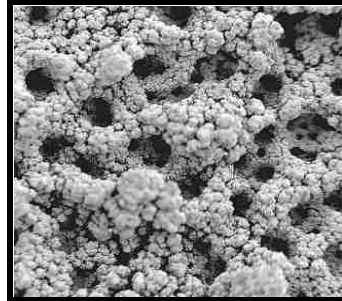
**Porous Graphite**  
El-Genk and Parker (2005)



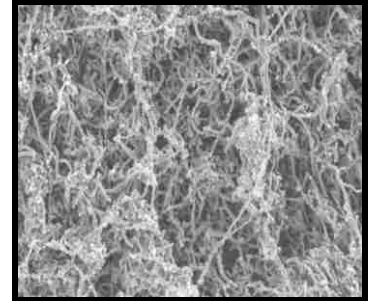
**Painting and brushing**  
You and colleagues (1995, 1996,  
1997, 2000, 2003)



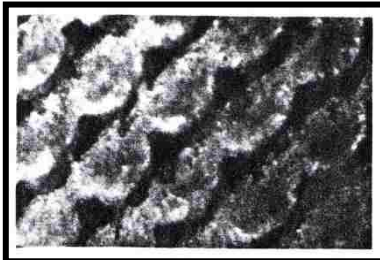
**Sintered Copper**  
McHale et al. (2011)



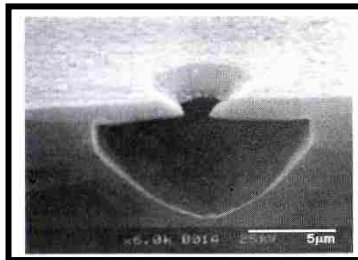
**MPC**  
( $<1.2\text{ A/cm}^2$ ) Kim, J. H.,(2006)



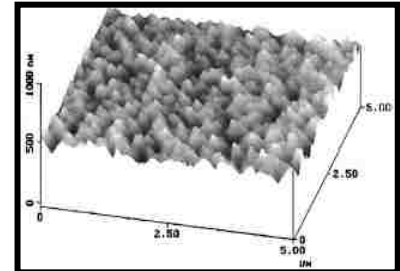
**Carbon Nano-Tubes**  
McHale and Garimella (2011)



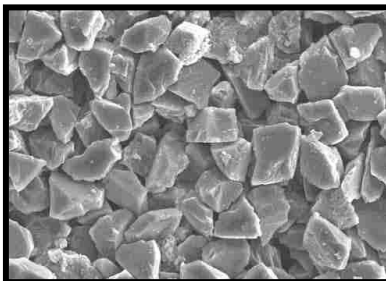
**Hitachi Thermoexel-E,**  
Marto and Lepere (1982)



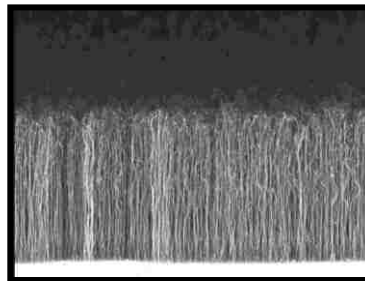
**Chemical etching**  
Kubo et al. (1999)



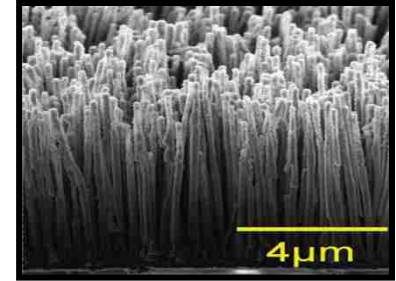
**Chemical etching**  
Honda, Takamatsu, Wei (2002)



**Microporous coating**  
Kim, Lee, and Han (2008)



**MWCNTs**  
Ahn, Sathyamurthi, and  
Banerjee (2009)



**Cu Nano-wires**  
Im, Joshi, Dietz, and Lee (2010)

**Figure 2.8 Selected surfaces for nucleate boiling enhancement of dielectric liquids.**

the reported saturation CHF of HFE-7100 is  $31.8 \text{ W/cm}^2$  and that of FC-72 on porous graphite is  $27.3 \text{ W/cm}^2$  (Parker and El-Genk, 2005). for FC-72 on similar surfaces (Change and You, 1996; Rainey and You, 2000,2001; El-Genk and Bostanci (2003a, b), El-Genk and Parker (2004, 2005), Parker and El-Genk (2006), and Priarone (2005), have carried out separate investigations comparing HFE-7100 and FC-72 dielectric liquids for boiling on Copper and porous graphite. Consistent with the results of Arik and Bar-Cohen (2001), CHF for HFE-7100 was higher than measured and found in the literature for FC-72. El-Genk and Bostanci (2003a,b) reported saturation CHF of HFE-7100 on plane Copper of  $24.5 \text{ W/cm}^2$ ; Priarone (2005) reported  $25.2 \text{ W/cm}^2$ . The CHF value reported by El-Genk and Parker (2005) is  $22.7 \text{ W/cm}^2$ . The average saturation CHF of FC-72 on plane Copper and silicon reported in the literature is  $16.3 \text{ W/cm}^2$  (Rainey and You, 2000; Rainey, You, and Lee, 2003). On porous graphite, reported saturation CHF of HFE-7100 is  $31.8 \text{ W/cm}^2$  and that of FC-72 on porous graphite is  $27.3 \text{ W/cm}^2$  (Parker and El-Genk, 2005).

In a recent study by Arik and Bar-Cohen (2010) investigating the effect on CHF enhancement on polished Silicon surface of using a mixture of FC-72/FC-40 10-20% mixing ratio by weight. Fluorinert Electronic liquid FC-40 has a higher saturation temperature ( $165^\circ\text{C}$  at atmospheric pressure) and 33% higher in surface tension than FC-72. Results showed an increase in CHF to  $56.8 \text{ W/cm}^2$  compared to  $25.2 \text{ W/cm}^2$  for pure FC-72 at the same experiment condition. These results were confirmed by Watwe and Bar-Cohen (1997) using the same liquid mixture. Similar work reported by other researchers confirmed different degrees of CHF enhancement on binary liquids mixtures compared to single liquids (Lee and Normington, 1993; Avedisian and Purdy, 1993). It is believed that the increase in the mixture latent heat of evaporation and surface tension, accompanying the depletion of the lower boiling point fluid in the wall region plays the major role in enhancing the critical heat flux for binary mixtures (Arik and Bar-Cohen, 2010).

#### **2.4.2 Effect of Surface Condition**

A simple method for changing surface condition is roughing it using sanding paper with different grit sizes. Ramilison, Sadasivan, and Lienhard (1992) used data obtained from the open literature for several boiling fluids on different rough surfaces to quantify

for the effect on CHF. They determined that CHF is influenced by the RMS roughness to the power 0.125. By taking into account the surface roughness, the scatter of the data was reduced from  $\pm 40\%$  to  $\pm 15\%$ . Ferjančič and Golobič (2006) confirmed that for FC-72 and water, increasing surface roughness increases CHF. Experiments with dielectric liquids confirm that the surface micro-features affect the boiling performance including CHF (e.g., Oktay, 1982; Change, J. Y., 1997; Chang and You, 1997b; Khann, Toh, and Pinjala, 2008; El-Genk et al., 2013).

Honda, Takamatsu, and Wei (2002) have investigated saturation and subcooled boiling ( $\Delta T_{\text{sub}} = 3, 25, \text{ and } 45 \text{ K}$ ) of both gas dissolved and degassed FC-72 on smooth silicon and  $\text{SiO}_2$  surfaces chemically etched to an RMS roughness of 25 – 32 nm. The nucleate boiling on the rough chip was significantly improved over that on the smooth chip. In saturated FC-72, the temperature excursions at boiling incipience were about 18 K on the smooth chip, but only about 12 K on the etched surface. The nucleate boiling heat transfer coefficient and CHF on rough chip also increased over that on the smooth chip at all levels of subcooling, and in gas dissolved and degassed liquid.

Rainey and You (2000) reported differences in saturation boiling of FC-72 on a machine roughened Copper and a polished Copper surface (Chang and You, 1996). The temperature excursion at incipient boiling on the polished Copper was 40 K and subsequent boiling ensued at 19 K. For the machine-roughened surface, these values were 27 K and 10 K, respectively. The heat transfer coefficient on the roughened surface was about 5 times higher, and the CHF increased by about 40%. These enhancements may be attributed to the trapped air in the small surface features.

Ferjančič and Golobič (2002) have studied experimentally nucleate boiling of FC-72 and water on horizontal and vertical ribbon heaters made of stainless steel on CHF. Surface treatment was performed with different sandpapers and etching in diluted acid. In the center, the average  $R_a$  ranged from 0.02 to 1.5  $\mu\text{m}$ . Results showed that, the pool boiling CHF of FC-72 on stainless increased from 87.6 to 115.4  $\text{kW/m}^2$  and the etched heater surface CHF on both stainless steel 302 and steel 1010 increased by 51%, compared to a sanded surface with the same  $R_a$ .

El-Genk, Souszko and Ali (2013) recently performed extensive study on the effect of surface roughness on nucleate boiling of dielectric liquid PF-5060. Eleven Copper

surfaces with an average roughness from 0.21 to 1.79  $\mu\text{m}$  were tested for saturation boiling in the upward facing orientation. Results showed a CHF increase from 19  $\text{W}/\text{cm}^2$  for Copper with an average roughness 0.21  $\mu\text{m}$  to 22  $\text{W}/\text{cm}^2$  for Copper with average roughness 1.79  $\mu\text{m}$  compared to about 15.7  $\text{W}/\text{cm}^2$  for smooth polished Copper (Average roughness  $\sim 0.039\mu\text{m}$ ). The reported maximum heat transfer coefficient for 1.79  $\mu\text{m}$  rough surface was  $\sim 2$  times higher than that for smooth Cu.

Surfaces partially or fully covered with carbon nano-tubes and Cu nano wires have been reported for nucleate boiling enhancement with promising results (Ujereh, Fisher, and Mudawar, 2007; Ahn et al.; 2009; McHale and Garimella, 2011, Ghiu and Joshi, 2005; Im, Lee, and Joshi, 2012; Im, Joshi, Dietz, and Lee, 2010). Carbon nano-tubes layer have been grown on both flat and structured silicon and Copper surfaces, , to study the effect on saturation boiling of FC-72 and PF-5060. The carbon nano-tubes generally increased nucleate boiling heat transfer and reduced or eliminated the temperature overshoot at boiling incipience (Ujereh, Fisher, and Mudawar, 2007). The CHF for FC-72 on a silicon surface fully coated with carbon nano-tubes increased by 6 - 44% over that of an uncoated silicon surface.

McHale et al. (2011) experimentally investigated pool boiling of HFE-7300 on smooth Copper, Copper-coated carbon nano-tubes (CNT), and surface with sintered copper particles coated with carbon nano-tubes. Results showed that, the hybrid (sintered with CNTs) surface achieved the lowest wall superheat at high heat flux with low temperature excursion prior to boiling incipience. For HFE-7300, the hybrid surface achieved more than 46% increase in CHF at a decreased wall superheat by 22.6% and the incipience temperature decreased by 29%, compared to plane Copper.

Hee Seok Ahn et al. (2009) investigated pool boiling of PF-5060 on silicon surface coated with multi-wall carbon nano-tubes (MWCNT) fabricated using chemical vapor deposition. Surfaces covered with 8-15 nm diameter CNT of different heights (9 and 25  $\mu\text{m}$ ) were tested for enhancing CHF compared to bare silicon surface under saturation and subcooled conditions. Results showed that increasing the height of CNT increased CHF, but also extended the wall superheat at CHF. On the 25  $\mu\text{m}$  high CNT this superheat was 40% higher and 25% higher for 9  $\mu\text{m}$  high CNT, compared to bare silicon.

Both types of CNT enhanced CHF of subcooled liquid over bare silicon. CHF on 25  $\mu\text{m}$  high CNT was 12% higher than on 9  $\mu\text{m}$  high CNT at 5 K subcooled condition.

Im et al. (2010) have examined the effectiveness of Copper nano-wires (NWs) attached to a silicon surface for enhancing nucleate boiling of degassed PF-5060 under saturation condition. Surfaces with 1-8  $\mu\text{m}$  high Copper nano wires were tested for nucleate boiling enhancement and results are compared to those on bare silicon surface. Results showed an increase in CHF on the surfaces with Copper nano wires compared to baseline silicon surfaces. CHF increased from 11.4  $\text{W}/\text{cm}^2$  on baseline surface to a maximum of 19.2  $\text{W}/\text{cm}^2$  on the surface with for sample of 2  $\mu\text{m}$  long nano wires. CHF then decreased to 12.4  $\text{W}/\text{cm}^2$  as Cu nano wires length increased to 8  $\mu\text{m}$ . The 2  $\mu\text{m}$  long Cu NWs showed reduced surface temperature prior to boiling incipience 23  $^{\circ}\text{C}$ , compared to 41  $^{\circ}\text{C}$  and 30  $^{\circ}\text{C}$  on plane surface and that with 8  $\mu\text{m}$  long Copper nano wires.

Enhancement in nucleate boiling of dielectric liquids on porous surfaces and surfaces with micro-porous coatings has been investigated widely. A micro-porous coating developed by O'Connor and You (1995), improved by Chang and You (1997a, b) and Kim et al. (2007), and used by others (Rainey and You, 2000, Kim, Rainey and You, 2002; Rainey, You, and Lee, 2003) have been shown to enhance boiling of dielectric liquids. These coatings, made of 1 – 20  $\mu\text{m}$  particles mixed with a volatile carrier and epoxy, are applied to the heated surface. The carrier evaporates and the particles remain behind, being bound together with the epoxy, leaving a microporous coating about 50  $\mu\text{m}$  thick. Chang and You (1997b) varied the coating composition and fabrication method and found that all the microporous coating performed similarly. They provide negligible increase to the surface area and the effective thermal conductivity is relatively low at about 0.95  $\text{W}/\text{m K}$  (O'Connor and You, 1995), due to the low thermal conductivity of epoxy binder. The pores of these coatings, believed to be on the order of 0.1 – 1.0  $\mu\text{m}$ , effectively trap air, increasing the total number of active nucleation sites. Using these coatings, the temperature excursion prior to boiling incipience was < 10 K and nucleate boiling ensued at a surface superheat of about 3 K. Boiling heat transfer rates were much higher than on smooth surfaces. In addition, CHF was greatly increased in both saturation and subcooled boiling of FC-72 (O'Connor J. P., 1994; O'Connor and You, 1995; Chang and You, 1997a, b; Kim et al., 2002; Rainey and You, 2002; Rainey, You, and Lee, 2003)

Ramaswamy et al. (2003) have investigated saturation boiling of FC-72 on single and multiple layers micro-fabricated copper and silicon surfaces. The surfaces were made of layers of copper plates bonded together with gold, or of silicon or copper in the case of a single layer. Rectangular channels first were cut into the top side of the plate, then in the bottom side perpendicular to those channels on top. The channels intersected, creating pores in the structure. The effect of the pores size, and the pitch and height of the structure were the experimental variables. The experiments were stopped when the temperature at the base of the structure reached 85 °C, or when the surface superheat was about 30 K, which was prior to reaching CHF. Comparisons were made to a solid copper block of the same dimensions. Results showed that increasing the pore size (90-230µm) and/or increasing the pores pitch (150-200 µm) increased the total thermal power removed at low surface superheat (4-12K), however, no significant enhancement was reported at high surface superheat (30K).

Ghiu and Joshi (2005) have used a single layer of copper microstructure, similar to that of Ramaswamy et al. (2003), to investigate the effect of varying the channel width and pitch in the microstructure on saturation boiling of PF-5060. Results showed measurable enhancement in the total power removed as the width of the micro-channels increased (65 – 105 µm) and the pitch decreased (0.2 – 0.7 mm). They reported no CHF data, as they terminated the experiments when the base temperature of the copper microstructures reached or exceeded 85 °C ( $\Delta T_{\text{sat}} = 29$  °C), which occurred prior to CHF.

Yoo-Han Kim et al (2008) have investigated the effect of surface treatment on enhancing nucleate boiling of PF-5060 in saturation and liquid subcooled (0, 5, and 10 K) boiling at different inclination (0°, 45°, and 90°). Plane, sanded (1.55 µm average roughness), and microporous coated Copper surfaces were tested. The microporous coating that is 45 µm thick produced by DOM technique similar to that of Rainey and You, 2001, was investigated. The sanded and the microporous coated surfaces showed similar increase in CHF by 70% compared to plane Copper surface.

Sriraman and Banerjee (2007) reported saturation and subcooled boiling of dielectric liquid PF-5060 on nano structured silicon. The structured surface consisted of array of 200 nm diameter fins of 100 nm height, and 1 µm pitch and fabricated using lithography process. Results showed an increase in the CHF for saturation boiling on the nano finned



surface. CHF continued to increase with increasing liquid subcooling up to 20 K. The reported increase in CHF was 41%, 19% and 27% for saturation, 10 K and 20 K subcooled boiling, compared to bare silicon surface.

Kim (2006) improved boiling heat transfer on microporous coatings with high thermal conductivity. By immersing a Copper substrate in a solution of sulfuric acid and cupric sulfate, a microporous Copper coating was deposited when subject to a potential difference between the anode and the cathode (heated surface). Different porous structures were grown using different current densities. Compared to the plane Copper; the  $h_{MNB}$  increased by ~50 – 600% and CHF increased by 20 – 50%. Another surface tested by Kim (2006) was made of nickel spheres soldered onto the surface using a procedure that resulted in a porous coating. He reported an increase in the  $h_{MNB}$  of up to 600%, compared to that on plane and 30 – 80% increase in the CHF.

Saturation boiling experiments with PF-5060 on smooth and micro-grooved Copper surface covered with microporous coating with Flower-Like CuO have been reported by Im et al. (2012). Alkali-assisted surface oxidation technique was used to fabricate the 4  $\mu\text{m}$  thickness CuO surface nanostructures. The nanostructure was believed to provide higher surface area-to-volume ratio to increase the CHF. Reported results showed that despite only having a thickness of 4  $\mu\text{m}$ , the CuO nanostructure increased CHF of PF-5060 by 58 % for the plane surface and 30 % for the micro-grooved one.

### **2.4.3 Effect of Surface Orientation**

Packaging of computer components may require different orientations with respect to gravity. Several studies investigating the effect of surface inclination on pool boiling of dielectric liquids have been performed (Mudawar, Howard, and Gersey, 1997; Chang and You, 1996; Howard and Mudawar, 1999; Rainey and You, 2001; El-Genk and Bostanci, 2003a,b; Priarone, 2005; Parker and El-Genk, 2006a,b; Parker and El-Genk, 2008). In general, the results are consistence to those obtained from non-dielectric liquids (Beduz, Scurlock, and Sousa, 1998; El-Genk and Guo, 1993; Nishikawa et al. 1984; Vishnev et al., 1976).

Chang and You (1996) have used smooth Copper surface measuring 10 x 10 mm for investigating the effect of surface orientation on saturation nucleate boiling of FC-72. At low surface superheats, the boiling heat transfer coefficient increased as the surface

inclination increased from  $0^\circ$  (upward facing) to  $90^\circ$  (vertical). Rainey and You (2001) reported similar results for smooth Copper measuring  $20 \times 20$  mm and  $50 \times 50$  mm for saturation boiling of FC-72. The nucleate boiling heat transfer rate increased for  $0^\circ < \theta < 45^\circ$ , then decreased as the inclination angle exceeded  $90^\circ$  (vertical). The difference in the boiling heat transfer rate diminished as the size of the boiling surface increased from  $10 \times 10$  mm to  $50 \times 50$  mm.

Wei and Honda (2003) reported that the nucleate boiling heat transfer rate in 25 K subcooled FC-72 was higher on a vertical smooth silicon surface ( $10 \times 10$  mm) than on the same surface in the horizontal upward orientation. On  $12.7 \times 12.7$  mm Copper surface for “near saturated” FC-72, the data of Reed and Mudawar (1997) indicated that at low surface superheats, nucleate boiling heat transfer improves as the surface inclination increases. At high surface superheats, the nucleate boiling heat transfer decreases as the inclination increases.

El-Genk and Bostanci (2003a, b) have performed experiments of saturated and subcooled boiling of HFE-7100 on a  $10 \times 10$  mm Copper surfaces. In saturation boiling at low surface superheat, the nucleate boiling heat transfer coefficient increased as the surface inclination,  $\theta$ , increased from upward facing ( $0^\circ$ ) to downward facing ( $180^\circ$ ). The trend is reversed at high surface superheats. For subcooled liquid, they reported that for  $0^\circ < \theta < 90^\circ$ , the heat transfer coefficient decreased slightly with increased inclination angle, but increased with increased subcooling. At low surface superheats, the nucleate boiling heat transfer rate was almost the same or increased slightly as the inclination angle increased.

Parker and El-Genk 2005 have investigated the effect of surface orientation on nucleate boiling and Critical Heat Flux (CHF) on porous graphite and smooth Copper surfaces measuring  $10 \times 10$  mm. The inclination angle of the surfaces increased from  $0^\circ$  (upward-facing) to  $60^\circ$ ,  $90^\circ$ ,  $120^\circ$ ,  $150^\circ$ , and  $180^\circ$  (downward facing). Results demonstrated significant increases in the nucleate boiling heat transfer coefficient and CHF on porous graphite, compared to those on smooth Copper. At low surface superheats, increasing the inclination angle increased the nucleate boiling heat transfer coefficient, which decreases with increased inclination angle at high surface superheats. These results, and the measured decrease in CHF with increased inclination angle, are

consistent with those reported earlier by other investigators for dielectric and non-dielectric liquids (Mudawar, Howard, and Gersey, 1997; Chang and You, 1996; Howard and Mudawar, 1999; Rainey and You, 2001; Priarone, 2005; Beduz, Scurlock, and Sousa, 1998; El-Genk and Guo, 1993; Nishikawa et al. 1984; Vishnev et al., 1976). On smooth surfaces and micro-porous coatings, the reported fractional decreases in CHF with increased inclination angle are almost identical, but markedly larger than those measured by (Chang and You, 1996; Howard and Mudawar, 1999; Rainey and You, 2001; El-Genk and Bostanci, 2003a,b; Priarone, 2005) on porous graphite. On these surfaces the reported CHF in the downward-facing position ( $180^\circ$  inclination) is  $\sim 10\text{-}20\%$  of that in the upward-facing position ( $0^\circ$  inclination), compared to  $\sim 53.3\%$  on porous graphite. CHF of FC-72 on porous graphite, which also decreased with increased inclination angle, are correlated using the general form suggested by Kutateladze (1961) to within  $\pm 5\%$  of the experimental data (Parker and El-Genk, 2006a,b; El-Genk and Parker 2008).

El-Genk et al. (2013) have recently performed experiments to investigate saturation nucleate boiling of PF-5060 dielectric liquid on eleven Cu surfaces measuring  $10 \times 10$  mm and with average roughness,  $R_a = 0.21\text{-}1.79 \mu\text{m}$  at 6 inclination angles of  $0^\circ$  (upward facing),  $60^\circ$ ,  $90^\circ$  (vertical),  $120^\circ$ ,  $150^\circ$ , and  $180^\circ$  (downward facing). Results showed that nucleate boiling heat transfer coefficient,  $h_{NB}$ , increases with increasing surface roughness and decreasing inclination angle. The highest values were in the upward facing orientation, while the lowest values were in the downward facing inclination. In the fully developed nucleate boiling region in the upward facing orientation,  $\theta = 0^\circ$ , the values of  $h_{NB}$  were correlated in terms of the applied heat flux as:  $h_{NB} = Aq^B$ . The coefficient “A” and exponent “B”, which are functions of surface roughness; “A”, increases from 0.15 to 0.25 and “B”, decreases from 0.76 to 0.67 as  $R_a$  increases from 0.21 to  $1.79 \mu\text{m}$ , respectively.

Ali and El-Genk (2013) have performed pool boiling experiments investigating the effect of inclination angle on saturation CHF of PF-5060 dielectric liquid on seven Microporous Copper (MPC) surfaces of different thickness from 80 to  $230 \mu\text{m}$ . The morphology of these surfaces, deposited using electrochemical processes, varied with the thickness. The inclination angles investigated are  $0^\circ$  (upward facing),  $60^\circ$ ,  $90^\circ$  (vertical),

120°, 150°, 160°, 170° and 180° (downward facing). CHF decreases with decreasing MPC surface thickness and increasing inclination angle. Saturation boiling CHF on the MPC surfaces in the upward facing orientation are 43-66 % higher than on smooth, polished Cu. For all MPC surfaces, CHF values in the downward facing orientation were ~28% of those in the upward facing orientation,  $\theta = 0^\circ$ . The developed CHF correlation accounts for the effects of MPC thickness and inclination angle and is in good agreement with the present experimental data, to within  $\pm 8\%$ .

Despite the minor discrepancies in the angular dependence of nucleate boiling heat transfer, there is a general agreement on the effect of inclination angle on CHF. Reported results showed CHF decreases slowly as the surface inclination increases up to 90° degrees (vertical), then rapidly decreases to its minimum value as the inclination approaches 180° (horizontal-downward facing) (Chang and You, 1996; Reed, 1996; Howard and Mudawar, 1999; Rainey and You, 2001; El-Genk and Bostanci, 2003a; Priarone, 2005; Parker and El-Genk 2006). CHF correlations and analytical models have been developed (El-Genk and Guo, 1993; Vishnev, 1976; Brusstar et al. 1997; Chang and You, 1996; El-Genk and Bostanci, 2003a; Howard and Mudawar, 1999), for dielectric and non-dielectric liquids.

## ***2.5 Bubble departure diameter and frequency***

Fritz (1935) had introduced the earliest correlation of bubble departure diameter as a function of the contact angle. The expression was derived by balancing the buoyant and surface tension forces for steam and Hydrogen bubbles at low heat flux and atmospheric pressure. An expression for bubble departure diameter is obtained by equating buoyant and surface tension forces acting on the bubble was introduced by Zuber (1959). Cole (1967) had shown that the force balance on the bubble at departure represents a condition of static equilibrium. The results for bubble departure diameter showed a deviation between experimental and the theoretical results obtained by Fritz (1935) and Zuber (1963). Such difference was attributed to the partial satisfaction of the static equilibrium, due to vigorous ebullition. In a similar analysis of balancing the forces on the bubble at the moment of departure, Ruckenstein (1961) obtained an expression for the departure diameter considering the buoyant and drag forces only. In addition, the drag and acceleration forces were included in a correlation introduced by Roll and Myers (1964).

High speed visualization have been performed by many researcher to study the effect of surface heat flux and surface characteristics on bubble departure diameter in saturation boiling of FC-72 (Rini et al. ,2001; Nimkar et al.,2006; Ramswamy et al., 2002, Hutter et al., 2010). On synthetic diamond transparent plate, the bubble size was measured directly from the video images at surface heat flux of 4-10 W/cm<sup>2</sup> by Rini (2001). Results showed that the mean departure diameter ranged 400-500 and was not a function of the heat flux and  $\mu\text{m}$ . A slight increase in the bubble departure diameter with increased surface heat flux was reported by Nimkar (2006). They measured the bubble departure diameter and detachment frequency in saturation boiling of FC-72 on Si surface with reentrant cavities of a surface heat flux 1-9 W/cm<sup>2</sup>. The bubble departure diameter increased from 260-450  $\mu\text{m}$  with increased surface heat flux. For the same range of heat fluxes the investigated detachment frequency increased from 55 to 68 Hz.

Ramswamy et al. (2002) have reported values of the bubble departure diameter in saturation boiling of FC-72 on Si surface with interconnected micro channels of different geometries and at different surface superheat,. The pore diameter was found to be the most influential on the bubble departure diameter. The bubble departure diameter increased with increasing both pore size and surface superheat. For all geometries investigated, the reported bubble departure diameter varied between 500-700  $\mu\text{m}$  at surface superheats up to 11 K. At low surface superheats (4-6) K, the bubble departure frequency was independent of the structure geometry and surface temperature, ranged from 170 to 220 Hz.

Hutter et al (2010) have measured the bubble detachment frequency, and departure diameter in saturation boiling of FC-72 bubbles on silicon surface with artificial cavities. The cavities had cylindrical shape with a mouth diameter of 10 mm and depth of 40, 80, and 100 mm. The measured bubble departure diameter at low range of surface superheats (1-5 K) increased linearly from 200-500  $\mu\text{m}$  depending on the wall superheat for all cavities under atmospheric pressure. For the same range of surface superheats, the reported bubble detachment frequency was 10 to 40 Hz for cavities with 80 and 100  $\mu\text{m}$  depths.

McHale and Garimella (2008, 2010) have performed high speed visualization study at 8000 frames/sec of saturation boiling of FC-77 dielectric liquid on smooth and rough

aluminum surfaces with average roughness of 0.03 and 5.89 mm. The bubble departure diameter increased with decreased surface roughness and surface heat flux. The measured bubble departure diameter on smooth surface varied from 600  $\mu\text{m}$  to 2 mm as the heat flux increased from 2-11  $\text{W}/\text{cm}^2$ . There was less significant increase in the measured departure diameter on the rough surface with increased heat flux. The measured diameter on the rough surface was 400-500  $\mu\text{m}$  for the same range of surface heat fluxes. The bubble departure frequency was 40-150 and 80-200 Hz on smooth and rough surfaces, respectively.

El-Genk et al. (2013) have investigated the effect of surface roughness on the bubble departure diameter and bubble release frequency. The Copper surfaces had average roughness of 0.21 to 1.79  $\mu\text{m}$ . At least 5 ebullition cycles was recorded of isolated bubble at many active sites of the same surface using a CD camera at 210 frames/seconds. Results showed that the bubbles are independent of surface roughness, averaging 427  $\mu\text{m}$  and 39 Hz, respectively.

## **2.6 Active nucleation site density**

Active sites densities for bubble nucleation of dielectric liquids of FC-72 and FC-77 on smooth and roughened surfaces, and micro structured surfaces have been reported (Ramswamy et al., 2002; McHale and Garimella, 2008, 2010). The active nucleation site density could be estimated using proposed mathematical models or, through visualizing using high speed images and analyzing the nucleate boiling results. Ramswamy et al. (2002) observed a number of FC-72 bubble active sites on their interconnected micro-channels structured surface and calculated the active site density.

Mathematical models for determining the active nucleation site density are generally driven based on the thermophysical properties of the liquid and surface characteristics (Lorenz, 1971; Yang and Kim, 1988; Benjamin and Balakrishnan, 1997; Kocamustafaogullari and Ishii, 1983; Hibiki and Ishii, 2003). Surfaces characteristics include the cavity mouth size and the angle assuming conical shape (Lorenz, 1971; Yang and Kim, 1988) and surface roughness (Benjamin and Balakrishnan, 1997). Kocamustafaogullari and Ishii (1983) assumed that the active nucleation site density in pool boiling is influenced by fluid properties. A correlation was introduced as a function of liquid and vapor properties, and departure bubble diameter. They compared their

correlation with various existing experimental data and concluded that the correlation gave fairly good predictions. Benjamin and Balakrishnan (1997) have introduced a correlation for the active nucleation site density in pool boiling of different pure liquids at low and moderate heat fluxes. Stainless steel and aluminum surfaces with different surface finish, obtained by polishing with different emery paper, were used. The average surface roughness,  $R_a$  was  $0.2 - 1.2 \mu\text{m}$ . They derived their correlation as a function of the average surface roughness,  $R_a$  and new coefficient similar to that proposed by Rohsenow (1952) to account for the surface liquid interaction. Similar study has been carried out by Benjamin and Balakrishnan (1997) using binary mixture of acetone and carbon tetrachloride. A new parameter that counts for the surface physical properties and variation of the physical properties of the binary mixture was introduced to the primary equation.

Hibiki and Ishii (2003) have introduced a mathematical model for predicting the active nucleation site density in pool and flow boiling. The model accounts for the effect of contact angle, critical cavity radius, and surface superheat on the active site density. It covered a wide range of static contact angle,  $\theta$ , from as low as  $5^\circ$  up to  $90^\circ$ . and was validated using by predicts of other models and experimental data for different liquids, with deviation of  $\pm 50\%$ . In that work, the active nucleation sites density is predicted based on the fully developed nucleate boiling portion of the boiling curve. This approach equates the total rate of the thermal heat removed from the surface and the volume of the generated bubbles on the surface. The total rate of the heat removed is simply a function of the bubble departure diameter, detachment frequency and the surface density of active nucleation sites.

MPC surfaces have been investigated experimentally to enhance nucleate boiling of dielectric liquids and the reported results are very promising. For these surfaces the increased wetted surfaces and/or the active site density would affect the potential for enhancing nucleate boiling and increase CHF. The morphology and microstructure of MPC surfaces varied with thickness and so the degree of enhancement that need to be investigated. In addition, nucleate boiling of dielectric liquids such as PF-5060 on MPC surfaces for immersion cooling of high power chips is not reported in the literature. The effects of inclination angle on nucleate boiling of dielectric liquids on MPC surfaces need

to be explored. The next section describes the experimental setup used in the present work. The specific objectives of this research are listed in the Introduction section.



### 3. Deposition of MicroPorous Copper Surfaces

Electrodeposition of a thin layer, usually metallic on a metal surface, is made by the action of electric current passing through an electrochemical cell. The cell consists of two electrodes (Cathode, and anode) submerged in electrolyte that carries the ions of the deposited metal layer. When electric current is passing through the electrolyte, the surface to be plated (Cathode) is negatively charged. The potential difference between the two electrodes forces the positive ions in the electrolyte to migrate towards the negative electrode surface, chemically reduced and form a thin metal layer. This process has been widely and commercially used in electroplating industry.

The MicroPorous Copper (MPC) surfaces for enhancing nucleate boiling of dielectric liquids are fabricated using electrochemical deposition process with high current density ( $>1 \text{ A/cm}^2$ ) for a short period of time. The surfaces initially deposited are delicate, easily to crack and peel easily off the substrate. A second stage of electrodeposition at low current density for a long period of time or annealing strengthen the MPC surfaces enough to be handled and assembled in a test section to perform pool boiling experiments. SEM images of the deposited MPC surfaces after each stage of deposition are presented to demonstrate the changes in surface morphology with thickness. The next subsection reviews the reported work on MicroPorous surfaces for enhancing nucleate boiling of dielectric liquids ( Bliss et al, 1969; Albertson, 1977; Kim, 2006; Furberg R., 2006; Kim et al., 2007; Li et al., 2008; Furberg et al., 2006, 2008, 2009; Furberg and Palm, 2011, Shin, et al, 2003). The effects of the deposition parameters on surface morphology and nucleate boiling results are summarized

#### **3.1 Review of prior work**

Bliss et al. (1969) have performed electrochemical deposition of thin layers of different metals. A 127  $\mu\text{m}$  thick layers of Copper, Nickel, Tin, Cadmium, and Chromium have been deposited using high current density on a 1-inch diameter tube to enhance nucleate boiling of water. The Microporous Copper, Chrome, and Cadmium enhanced nucleate boiling by as much as of 300%. Enhancement of nucleate boiling of R-12 on a deposited Copper layer has been reported by Albertson (1977). Results showed that, electroplating at very high current density for a short time builds a structure with

dendrites and nodules. A current density of  $100 \text{ mA/cm}^2$  for only 20 seconds of deposition was used to electroplate a 3/4 inch diameter pipe with Copper dendrites structure. Similar deposition of Copper nano-dendrites structure was done using high current density of  $3 \text{ A/cm}^2$  for different periods of time (Shin et al. 2003). The high electrode potential and highly hydrogen concentration in the electrolyte, forms hydrogen bubbles on the cathode surface during deposition. These bubbles mask the cathode surface locally from the formation of the basic dendrite (Shin et al., 2003). Experiments have been performed to investigate the effects of deposition time, electrolyte concentration, and electrolyte additives on the morphology of the deposited structure (Shin and Lui, 2004). Results showed that the deposition time and current density had the greatest effects on the density and size of the pores in the deposited microstructure (Figure 3.1). Similar results were reported by other researchers (Furberg R., 2006; Li et al., 2008; Furberg et al., 2006)

Kim (2006) has performed electrochemical deposition of Copper using current density of ( $0.33$  to  $1.2 \text{ A/cm}^2$ ) for enhancing nucleate boiling of FC-72. Figure 3.2 a-f presents SEM images of the MicroPorous Copper structure deposited by Kim at different current density. At low current density ( $<1 \text{ A/cm}^2$ ) no hydrogen gas bubbles were formed during deposition of the MPC surfaces. The deposited Copper formed hills and valleys without surface pores (Figures 3.3 a-d). At high current density ( $>1 \text{ A/cm}^2$ ) the formation of pores and dendrites, attributed to the release of the hydrogen gas bubbles at the cathode surface during deposition was apparent (Figures 3.3 e-f). The deposited MPC surfaces using low or high current density were delicate and mechanically fragile (Kim, 2006; Furberg, 2006; Li et al., 2008, El-Genk and Ali, 2009, 2010).

To demonstrate the weakness of the deposited microstructure, air was blown over deposited MPC surface at short distances (5-60 mm) at pressure of 7 bar for 180 seconds. (Furberg, 2006,2011). The microporous structure almost completely eroded when exposed to pressurized air flow at 60 mm distance. Additional processes have been reported in the literature to enhance the mechanical strength of the deposited microporous Copper structure, (Furberg R., 2006; Li et al., 2008; Furberg and Palm, 2011). Annealing at or above  $600^\circ\text{C}$  for more than 5 hours was examined to increase the adhesion of the deposited Copper layers to the Cu substrate. After annealing, the morphology of

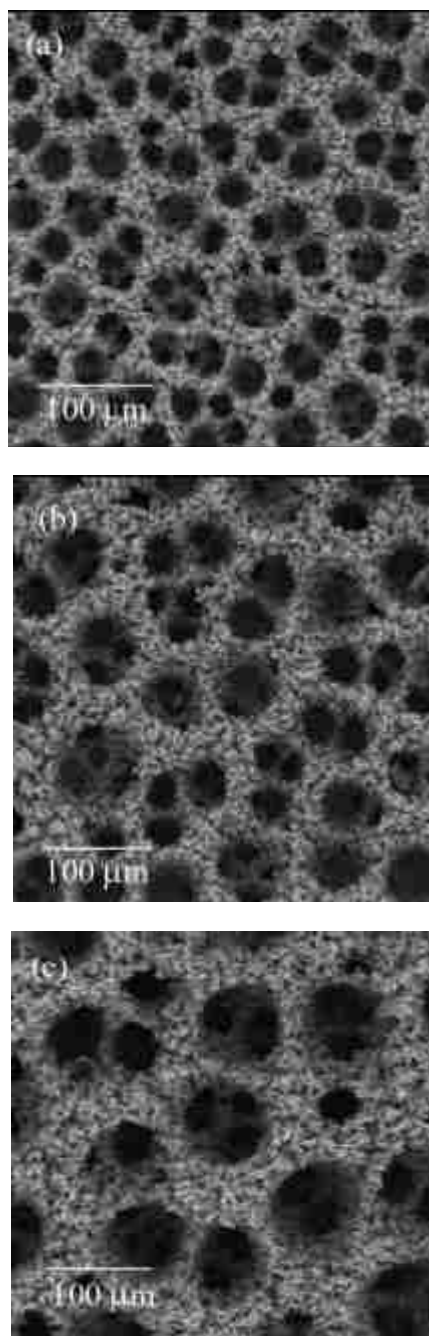
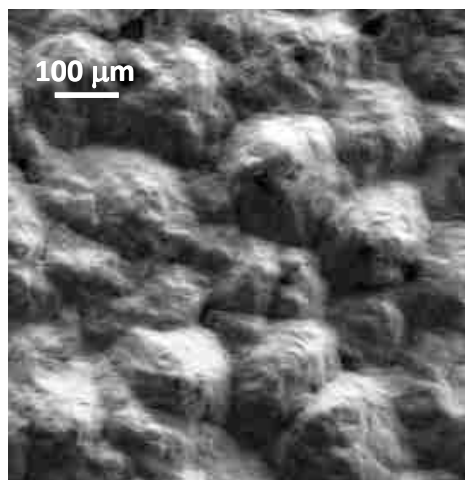
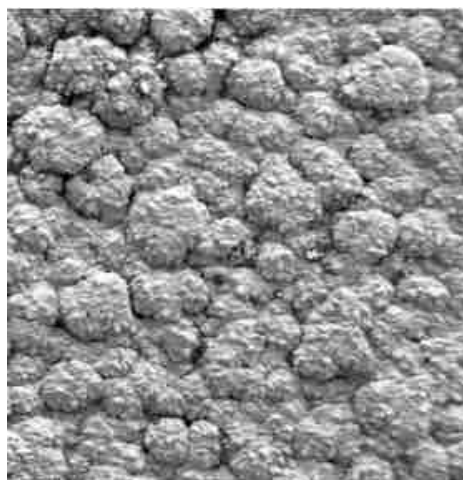


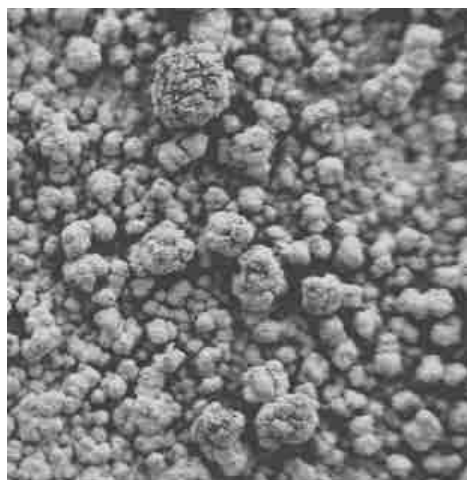
**Figure 3.1 SEM images on the effect of deposition time on structure pore size for the same concentration and current density of  $3 \text{ A/cm}^2$  for (a) 5 Seconds (b) 10 Seconds (c) 15 Seconds (Shin et al 2003, 2004).**



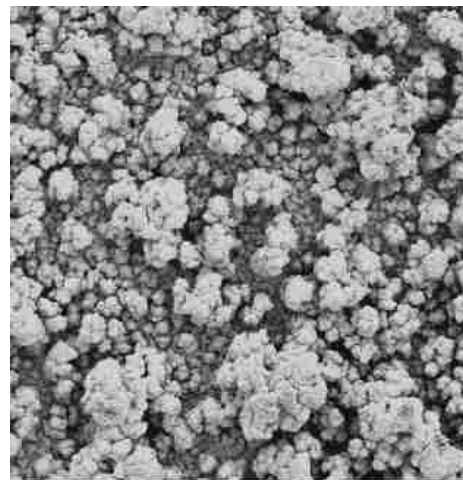
**(a) 0.166 A/cm<sup>2</sup>**



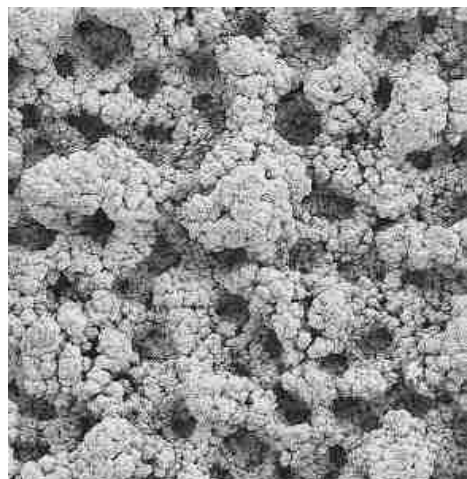
**(b) 0.25 A/cm<sup>2</sup>**



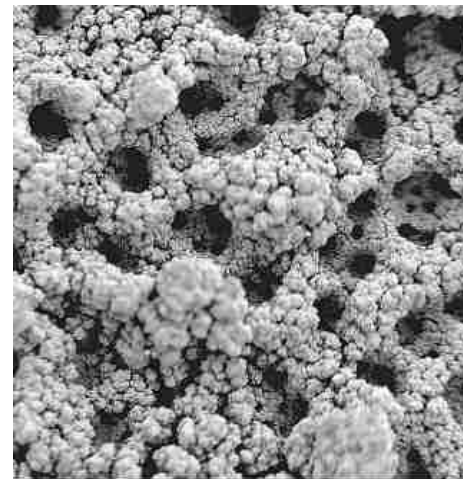
**(c) 0.33 A/cm<sup>2</sup>**



**(d) 0.5 A/cm<sup>2</sup>**



**(e) 1.0 A/cm<sup>2</sup>**



**(f) 1.2 A/cm<sup>2</sup>**

**Figure 3.2 SEM images of the deposited MPC structure at different current densities (Kim, 2006).**

the microporous structure did not change (pore size, thickness of the structure, pore density), but the submicron features of the structure changed (Figure 3.3). The grain size of the nano-dendrites branches grew during annealing, increasing the interconnectivity and enhancing the adhesion and mechanical strength of the structure (Furberg, R., 2011). Another method for increasing the mechanical strength of the deposited MPC thin film is to continue the deposition at very low current density for a long period of time. In this stage using current density of  $\sim 55 \text{ mA/cm}^2$  for a 1.5-2 hrs has been reported by Albertson (1977). A second stage of deposition at very low current density for more than one hour was used by Kim (2006) to strengthen the micro structure fabricated.

In summary, the reported work in the literature showed two distinguished stages of fabricating MPC surfaces using conventional electrochemical deposition process. The first stage is to apply electrochemical deposition using intermediate or high current density ranging from  $0.33$  to  $3 \text{ A/cm}^2$  to create the basic features of the MPC surfaces. The surface morphology of the deposited structure strongly depends on the current density and the deposition time. In this stage, the deposited surface is delicate and weak to be handled or tested in pool boiling experiments, unless it is strengthened. To increase the mechanical stability and adhesion of the deposited structure to the substrate, two approaches have been reported. The first is annealing at relatively high temperature for few hours, while the second is to continue the electrochemical deposition at very low current density for a long period of time. The next section describes the fabrication process of MPC surfaces in this research.

MicroPorous Copper surfaces are fabricated using two successive stages of electrochemical deposition. The first stage used high electric current density ( $3 \text{ A/cm}^2$ ) for a short period of time, depending on the thickness. The main features of the deposited MPC surfaces such as surface pores, volume porosity, and thickness are created in the first stage. To increase the mechanical strength of the structure, electrochemical deposition continued (second stage) at low current density for longer period of time. SEM images are taken after each stage of deposition to assess the effect of deposition time and the thickness of MPC on the surface morphology.

### **3.1.1 Surface preparation**

Prior to conducting the electrochemical deposition, the Copper surface is prepared

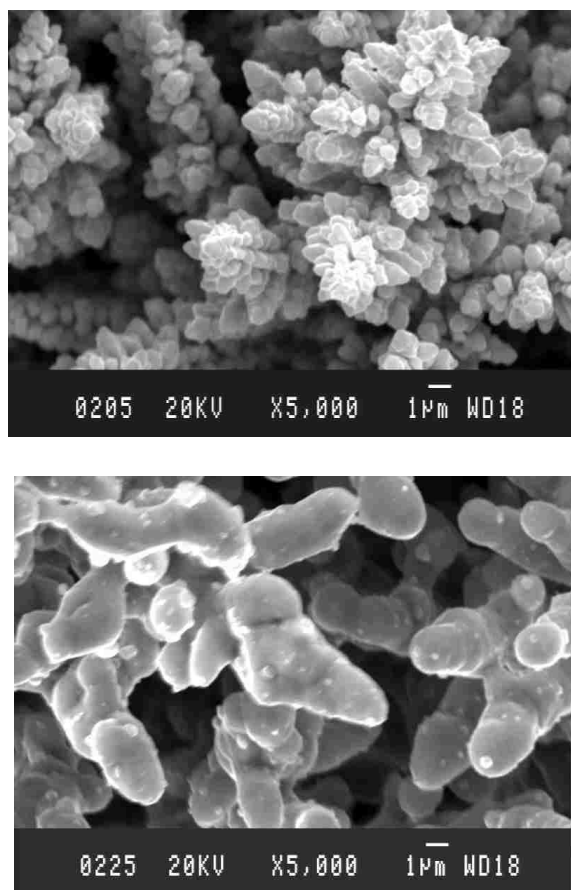
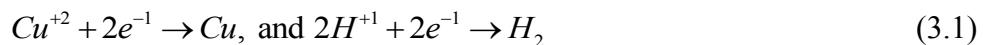


**Figure 3.3 SEM images of deposited MPC structure before (top) and after (Lower) annealing at 600 °C for 5 hours (Furberg, 2006).**

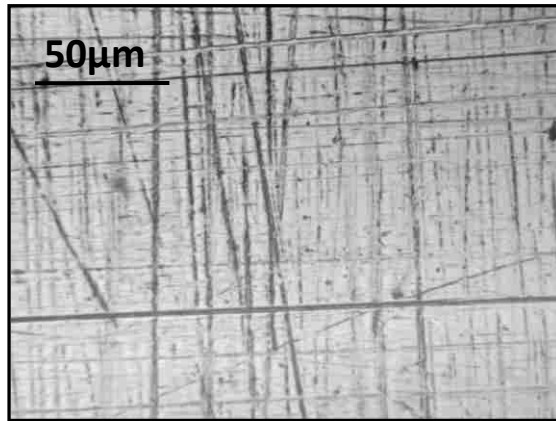
using consistent procedures. In addition, this procedure is required to insure the uniformity and strong adhesion of the deposited layer to the Cu substrate. First, a machined rough Copper surface is prepared using 400-grit emery paper to remove the large scratches then sanded using 1500-grit emery paper to remove the small dents. The Copper surface is brushed and polished, using polishing liquid (Brasso), cotton swabs and brushing tool, and rinsed with water and alcohol. Figure 3.4 shows microscopic images of the plane Copper substrate after it is prepared with the 400-grit, 1500-grit, emery paper and smoothed polished. The measured average surface roughness of the Cu surfaces following these stages are 0.58, 0.21, and 0.04  $\mu\text{m}$ , respectively. Finally, the prepared Cu surface is immersed in diluted hydrochloric acid to remove organic and nonmetallic film before the electrochemical deposition of MPC.

### 3.1.2 Setup and procedures

The electrochemical deposition of MicroPorous layers of different thickness is accompanied with the formation of  $\text{H}_2$  gas bubbles at the cathode surface. Figure 3.5 shows a schematic of the setup of the electrochemical deposition process. The 10 mm x 10 mm x 1.6 mm thick smoothed Copper substrates are laid out horizontally in the electrochemical cell parallel to a Copper anode. The anode has a larger surface area than the cathode (4.5-5  $\text{cm}^2$ ) to ensure uniform deposition onto the small area cathode. The chemical composition of the electrolyte ensures that the rate of electrochemical deposition is not limited by the supply of the Copper ions from the electrolyte. Both the cathode and the anode are fully immersed in electrolyte solution of sulfuric acid and Copper sulfate separated by 2 cm, and connected to an external power supply source controlled by PC computer (Figure 3.5). The electrolyte solution contains both  $\text{Cu}^{+2}$  and  $\text{H}^+$ , and when the electric current is supplied to the electrochemical deposition cell, the  $\text{Cu}^{+2}$  and  $\text{H}^+$  ions in the electrolyte solution undergo two simultaneous reduction reactions at the cathode:



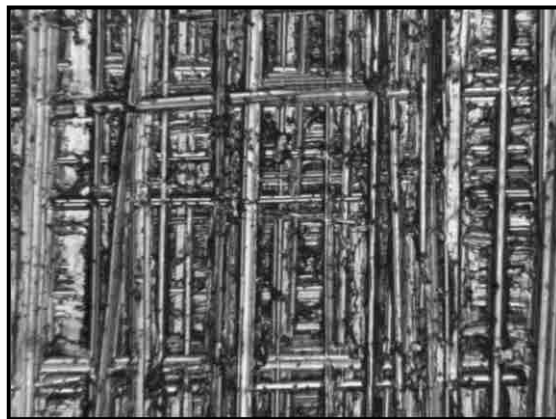
The thickness and the basic microstructure of the deposited MPC layers are established in the first stage using current density of 3  $\text{A}/\text{cm}^2$  for tens of seconds depending on the thickness. The micro-structure produced in the first stage is similar to



**(a) Smooth polished finish**



**(b) 1500 Grit finish**



**(c) 400 Grit s finish**

**Figure 3.4 Microscopic images of plane Copper substrate after treatment using emery of 400 and 1500-grit emery paper.**



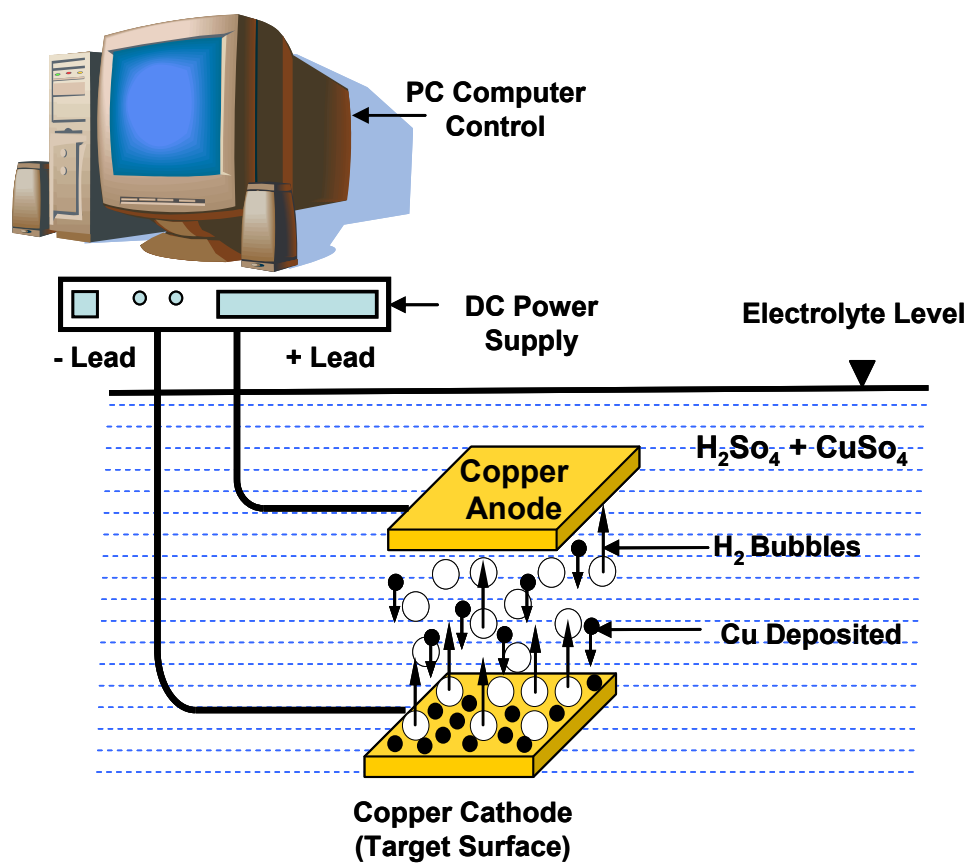


Figure 3.5 A Schematic of the electrochemical deposition setup at high current density.

the nano-dendrites structure reported in the literature (Shin, et al 2003, Shin and Liu 2005, Furberg 2006, Furberg et al 2008, Li et al 2008). This micro structure, which is very delicate to handle, is strengthened by continuing the electrochemical deposition at very low current density for additional 10's of minutes. During this stage, the rate of disposition of the Cu atoms into the cathode is very low, negligibly changing the thickness of the nano-dendrites surface layers. The deposition Cu atoms partially fill out the nano-dendrites and some of the macro-pores changing the surface morphology. A detailed description of the morphology of the deposited MicroPorous structure, supported with Scanning Electronic Microscope images (SEM) after each stage of the electrochemical deposition process, is given next.

### **3.1.3 Surface morphology and SEM**

During the stage of high current density ( $3 \text{ A/cm}^2$ ) electrochemical deposition, the columns of rising hydrogen bubbles at the cathode surface form the circular macro-pores. These macro-pores are surrounded by a complex microstructure of branching Cu nano-dendrites. The continuous migration of  $\text{Cu}^{+2}$  and  $\text{H}^+$  from the electrolyte solution to the cathode surface sustains the growth of the nano-dendrites, increasing the thickness of the deposited layer. The rising columns of hydrogen bubbles increase the average opening of the macro-pores as the thickness of the deposited layer increases. Because of the ionic mobility of  $\text{H}^+$  ions is higher than that of  $\text{Cu}^{+2}$  ions, the former migrate to the cathode faster, increasing the number and generation rate of the hydrogen bubbles. The initially deposited Cu nano-dendrites provide additional active reduction sites for incoming  $\text{H}^+$  and  $\text{Cu}^{++}$  ions, sustaining the generation of the hydrogen bubbles and the growth of the Cu nano-dendrites.

The generation and rising of the hydrogen bubbles locally produce orderly patterned macro-pores, a few to 10's of micron in diameter. On the other hand, the pores within the Cu nano-dendrites structure are very small, ranging in size from a fraction of micron to a few microns. SEM images at different magnifications of the deposited MicroPorous Copper surfaces after the first stage are presented in Figures 3.6 -3.11 (left columns). They clearly show the formation of macro-pores, as a result of the generation of the hydrogen gas bubbles at the cathode surface, surrounded by the Cu nano-dendrites. In addition to increasing the opening of the macro-pores, increasing the thickness of the

nano-dendrites layer slightly increases the volume porosity, which at the end of the first stage ranges 93.1% to 94.9%, and almost independent of the thickness. Table 3.1 summarizes the electrochemical deposition conditions and the estimated thickness and volume porosity of different MPC layers deposited.

**Table 3.1 Deposition conditions and characteristics of deposited MPC surfaces.**

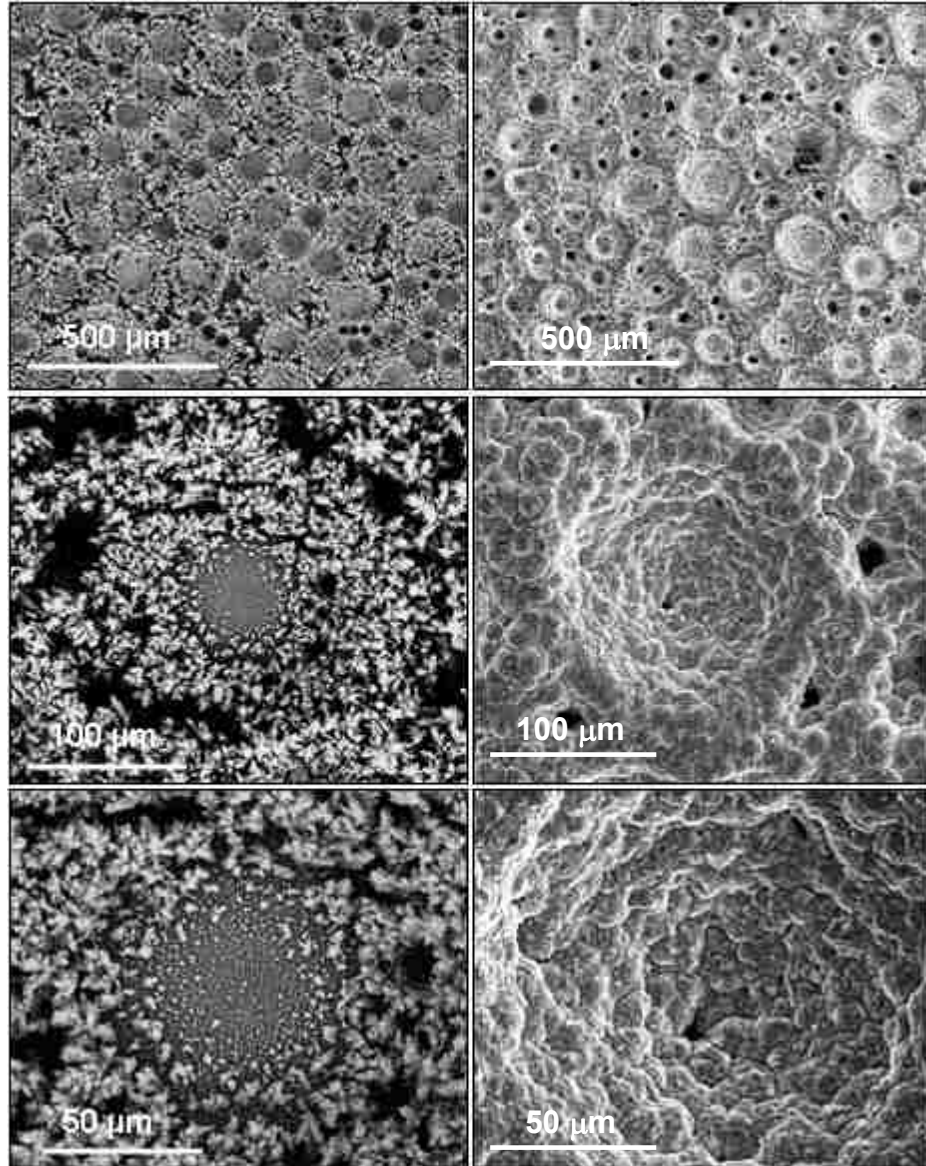
Deposited MPC layer	Electrolyte strength (mol/lit)	Current density (A/cm <sup>2</sup> )		Est. Thickness, $\delta_{MPC}$ ( $\mu$ m)	Est. Porosity, (%)	
		1st	2nd		1st	2nd
1	0.8 CuSO <sub>4</sub> + 1.5 H <sub>2</sub> SO <sub>4</sub>	3	V. low	80.0 $\pm$ 1.31	94.9	52.1
2		3	V. low	95.1 $\pm$ 1.81	94.5	65.3
3		3	V. low	115.1 $\pm$ 1.63	94.4	70.6
4		3	V. low	139.4 $\pm$ 2.64	93.8	73.9
5		3	V. low	171.1 $\pm$ 3.13	93.7	76.8
6		3	V. low	197.4 $\pm$ 3.61	93.6	79.0
7		3	V. low	230.3 $\pm$ 4.2	93.1	80.6

As indicated earlier, the deposited MPC microstructures in the first stage is very delicate, easily chipped and cracked. The mechanical strength of the deposited MPC surfaces is enhanced by continuing deposition, but at a very low current density for 10's of minutes. During this phase of deposition, the production of hydrogen ceases because of the low electrode potential. Also, the deposition rate of Cu atoms onto the cathode is very low to change the thickness, but it changes the surface morphology and reduces the volume porosity (Table 3.1). The resulting microstructure is rugged and excellent for handling in the boiling experiments, and has lower volume porosity, but larger wetted surface area. However, the average volume porosity of the deposited MPC decreases, but its value increases with increased thickness (Table 3.1). Figures 3.6-3.11 (right columns) show SEM images at different magnifications of the MPC surfaces at the end of the second stage. These are used in the present pool boiling experiments. These images indicate that the second stage of electrochemical disposition strengthens the microstructure, by filling out the branches and some of the originally open macro-pores with Cu nano-and micro-particles. These open pores range from 30-60  $\mu$ m in diameter, depending on the thickness of the deposited layer. The filled out macro-pores effectively

increase the wetted surface area for nucleate boiling, as indicated by the large and deep hemi-spherical depressions in the SEM images.

In summary, mechanically stable MicroPorous Copper surfaces of different thicknesses are deposited on Cu substrate using two successive stages of electrochemical deposition. The basic micro-structure with patterned open macro-pores surrounded by fine and dense Cu dendrites, forms during the first stage using high current density ( $3 \text{ A/cm}^2$ ) for short period of time. The thicker the deposited layer, the larger are the macro-pores and the denser is the surrounding Cu dendrites at the end of the first stage. The deposited microstructure at the end of the first stage is highly porous ( $\varepsilon > 90\%$ ), but fragile and delicate to handle. Strengthening this microstructure is accomplished by continuing the electrochemical disposition process at a much lower current density for 10's of minutes with the same electrolyte. In this stage, the very low rate of disposition of the Cu atoms strengthens the microstructure by filling up the Cu dendrites and some of the open macro-pores, insignificantly changing the thickness but changing the surface morphology. The micro-porous structure at the end of the second has lower volume porosity and larger wetted surface area.

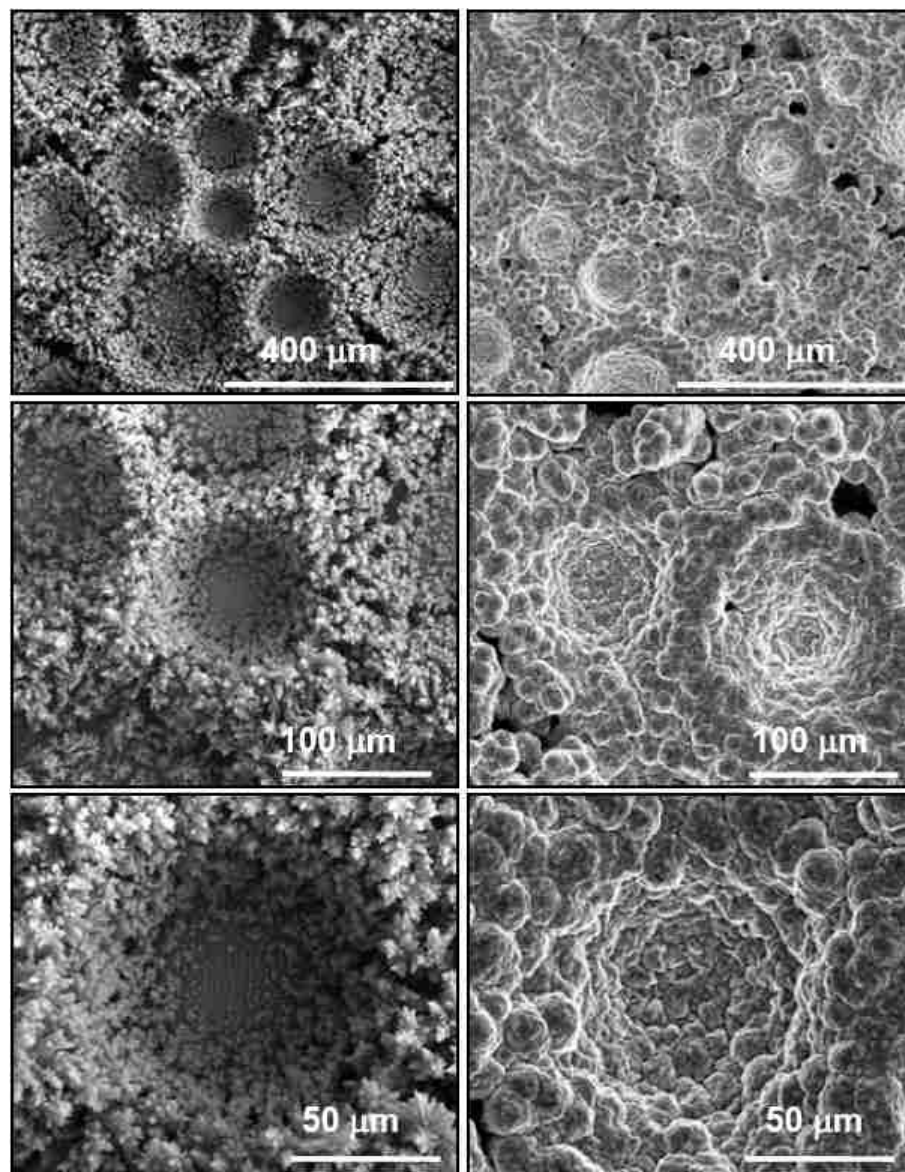
The increased wetted surface area due to the formation of semi-spherical depressions and the formation of micro-sized Cu particles on the surface during the second stage of deposition could enhance nucleate boiling, investigated for saturation boiling of the PF-5060 dielectric liquid. MicroPorous surface of different thicknesses (Table 3.1, Figures 3.6b–3.11b) are assembled into separate test sections for performing the pool boiling experiments which are discussed in the next chapter.



(a) After 1<sup>st</sup> stage

(b) After 2<sup>nd</sup> stage

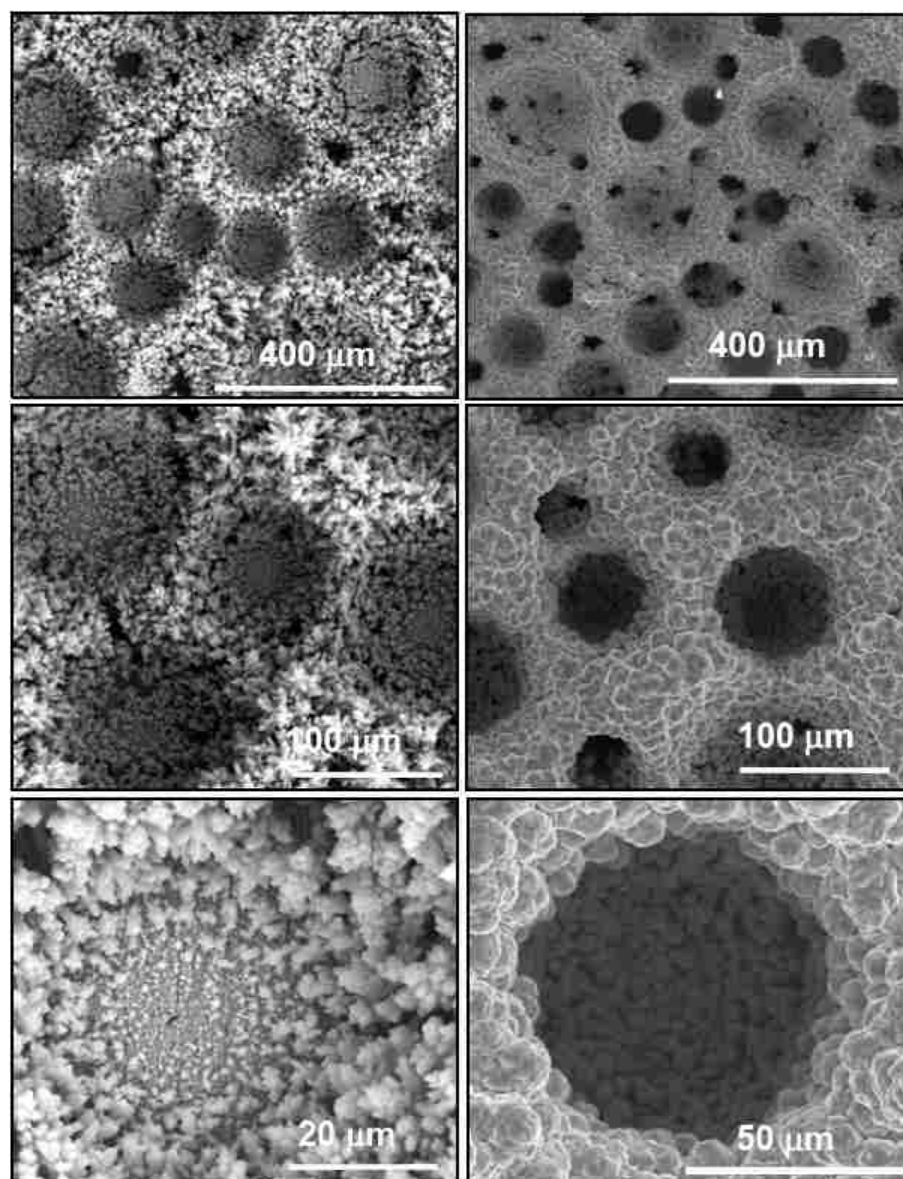
Figure 3.6 SEM images of layer # 1 after 1<sup>st</sup> and 2<sup>nd</sup> stage of deposition (Thickness  $80 \pm 1.81 \mu\text{m}$ ).



(a) After 1<sup>st</sup> stage

(b) After 2<sup>nd</sup> stage

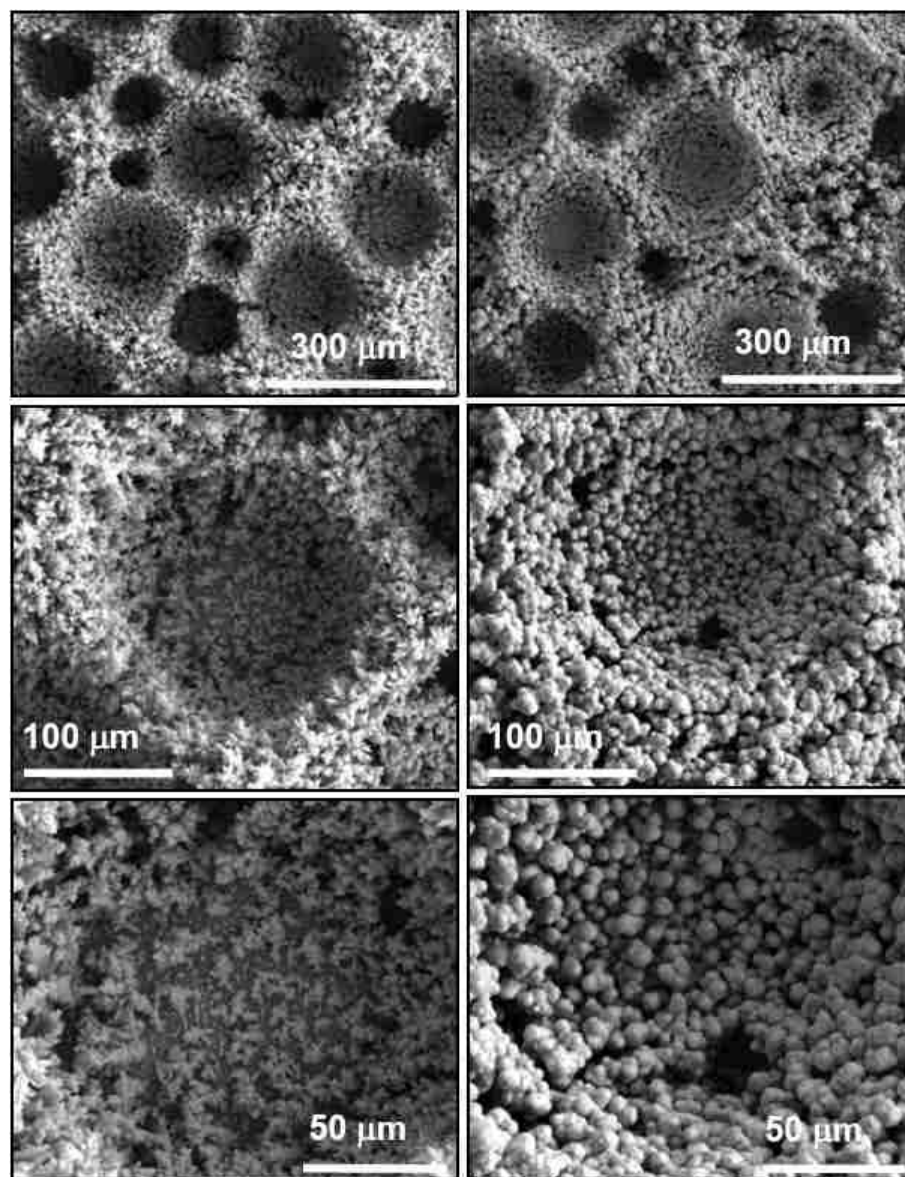
Figure 3.7 SEM images of layer # 2 after 1<sup>st</sup> and 2<sup>nd</sup> stage of deposition (Thickness  $95.1 \pm 1.81 \mu\text{m}$ ).



(a) After 1<sup>st</sup> stage

(b) After 2<sup>nd</sup> stage

Figure 3.8 SEM images of layer # 4 after 1<sup>st</sup> and 2<sup>nd</sup> stage of deposition (Thickness  $139.4 \pm 2.64 \mu\text{m}$ ).

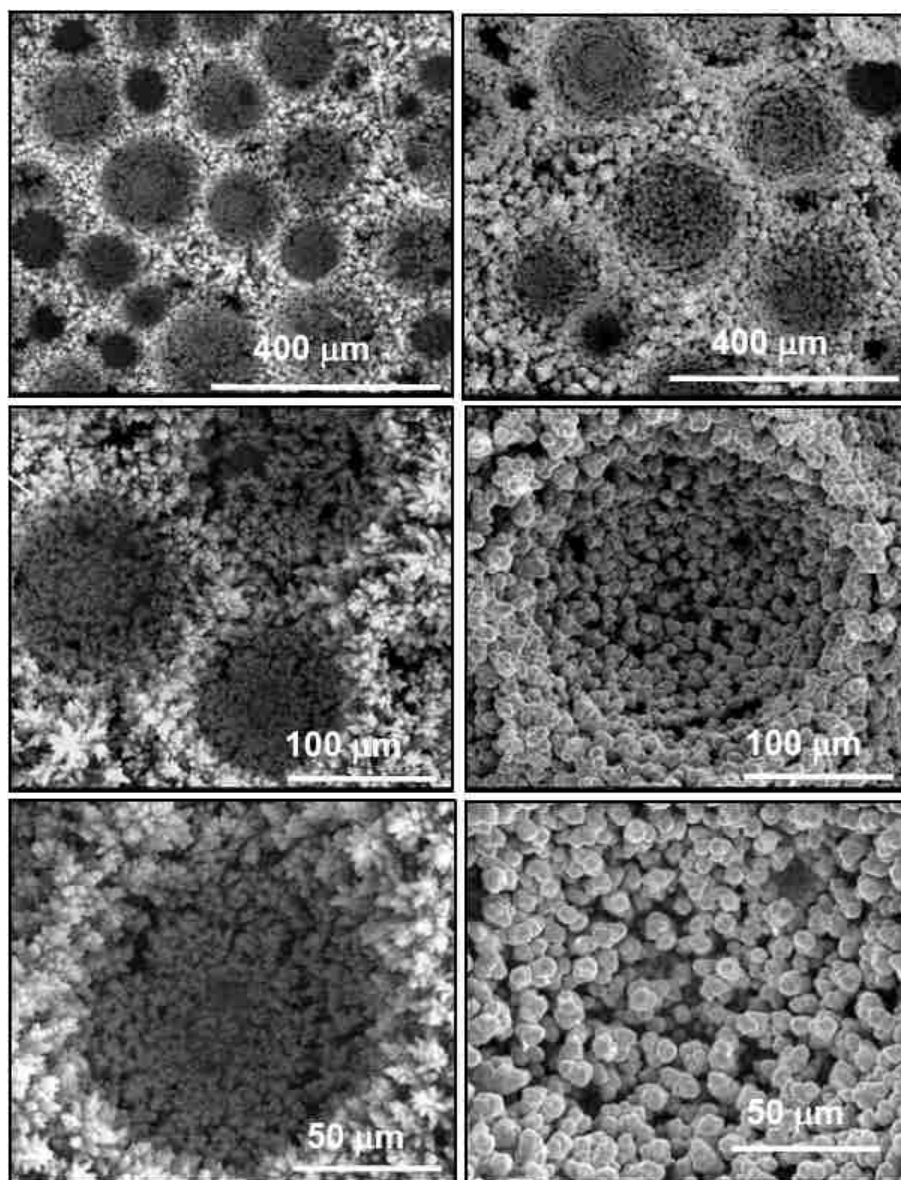


(a) After 1<sup>st</sup> stage

(b) After 2<sup>nd</sup> stage

Figure 3.9 SEM images of layer # 5 after 1<sup>st</sup> and 2<sup>nd</sup> stage of deposition (Thickness  $171.1 \pm 3.13 \mu\text{m}$ ).

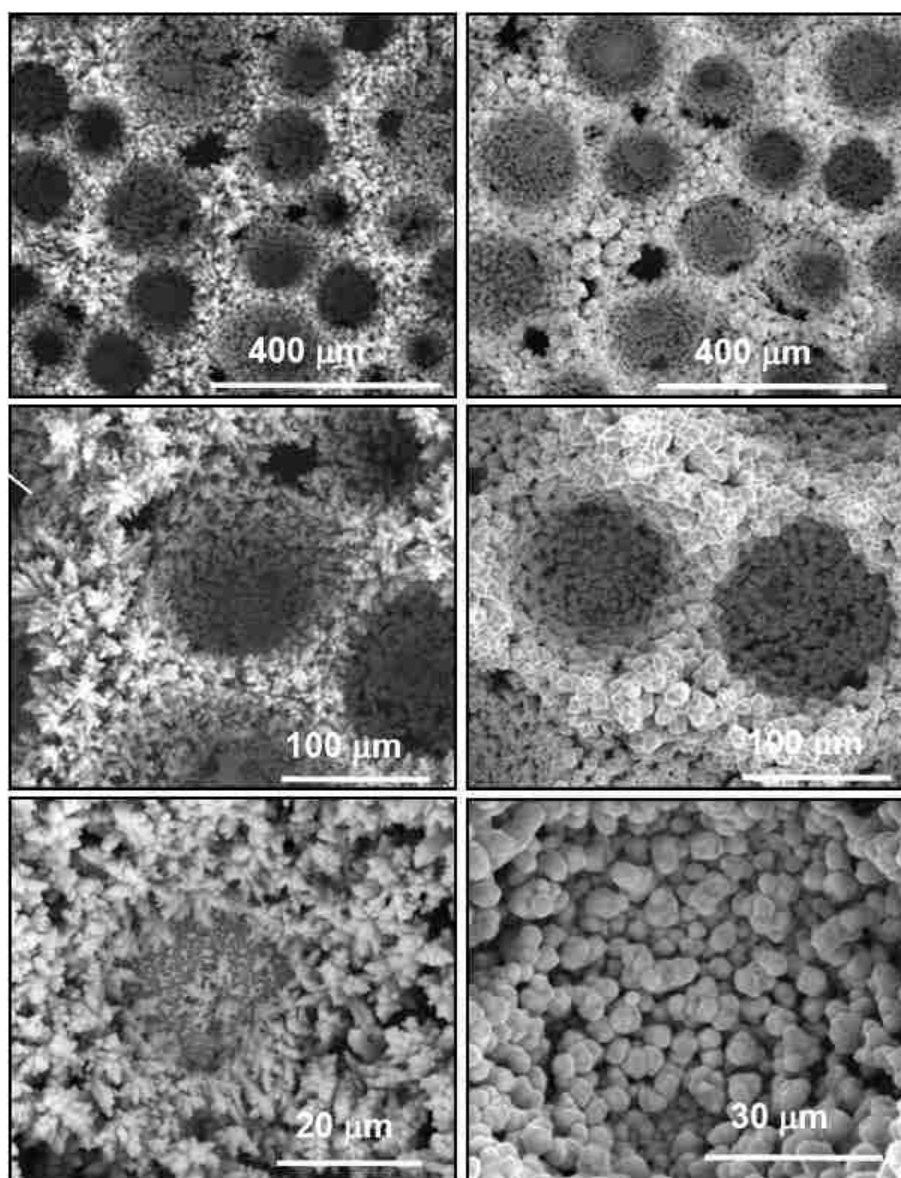




(a) After 1<sup>st</sup> stage

(b) After 2<sup>nd</sup> stage

Figure 3.10 SEM images of layer # 6 after 1<sup>st</sup> and 2<sup>nd</sup> stage of deposition (Thickness  $197.4 \pm 3.61 \mu\text{m}$ ).



(a) After 1<sup>st</sup> stage

(b) After 2<sup>nd</sup> stage

Figure 3.11 SEM images of layer # 7 after 1<sup>st</sup> and 2<sup>nd</sup> stage of deposition (Thickness  $230.3 \pm 4.2 \mu\text{m}$ ).

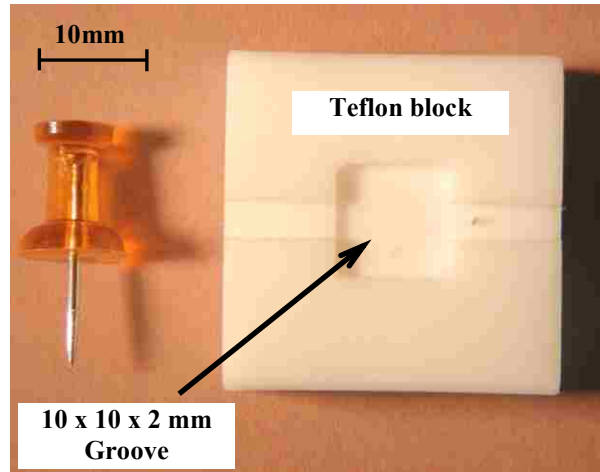
## 4. Pool Boiling Experiments

This chapter describes the saturation pool boiling experiments carried out in this research using PF-5060 dielectric liquid at 0.085 MPa (local pressure in Albuquerque, NM). The test section, pool boiling facility, and experimental procedures are discussed. The facility used and the experimental setup and the procedures are similar to those used earlier by El-Genk and Bostanci (2003a, b), El-Genk and Parker (2005, 2006) and Parker (2008).

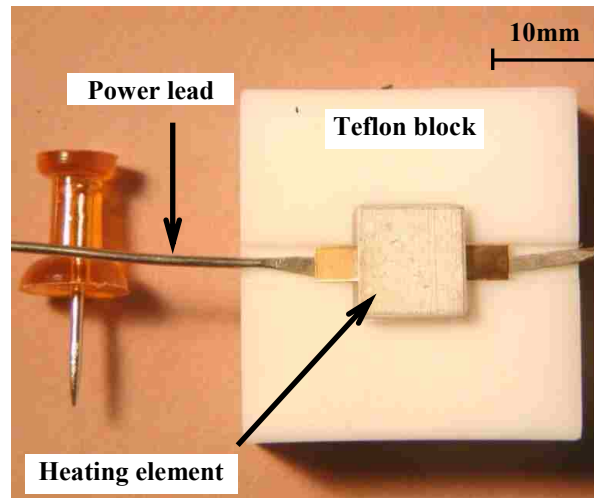
### 4.1 Test Section

The assembled test section for conducting pool boiling experiments consists of a Teflon block (30 x 30 x 12.7 mm) with a 2 mm deep square cavity (10 x 10 mm) at the center of its top surface (Figure 4.1a). The MPC surface with Copper substrate is attached to an underlying heating element. The heating element of a total resistance 16  $\Omega$  can provides up to 250 W dissipated power (Figure 4.1b). A high thermal conductivity epoxy is used to reduce the interfacial resistance between the heating element and the Copper substrate. The MPC surface and the underlying heating element are placed inside the central cavity at the surface of the Teflon block. This block provides good thermal insulation; reduce side heat losses from the heating element, and ensuring that the generated heat by the heating element is transferred to the boiling surface.

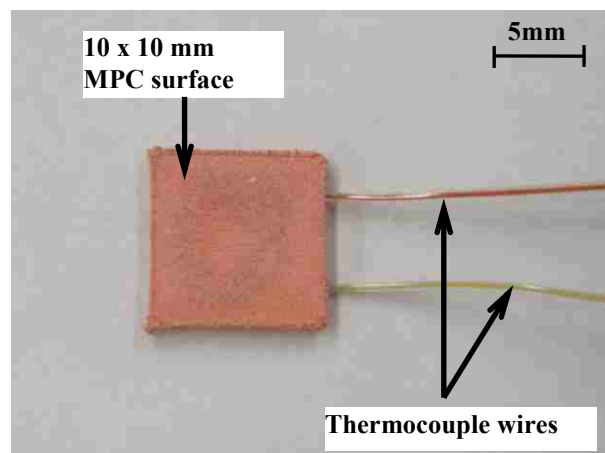
A Thermal analysis has been performed using ANSYS, a commercial finite element numerical analysis package, to estimate the heat losses from the test sections (El-Genk and Parker, 2006, 2008; Parker, 2008). The analysis compares the heat generation rate by the heating element to that removed by nucleate boiling and natural convection from the exposed heated surface and through the sides of the test section in the liquid. The results showed that about 0.5% of the total thermal power generated in the heater has lost through the top of the epoxy filler, and slightly more than 1% of the total power was lost through the four vertical sides of the Lexan frame, and slightly more than 1% from the bottom of the Lexan frame. The total heat losses were estimated to be less than 3%. The thermal analysis results were validated by performing experiments using the assembled test section with thermocouples embedded in the thermal insulation, between the Teflon block and Lexan frame. The measured temperatures closely matched those calculated by



(a) Teflon block with a central square cavity



(b) Heating element with power leads.



(c) MPC surface with thermocouples inserted in the Cu substrate

Figure 4.1 Test section assembly.

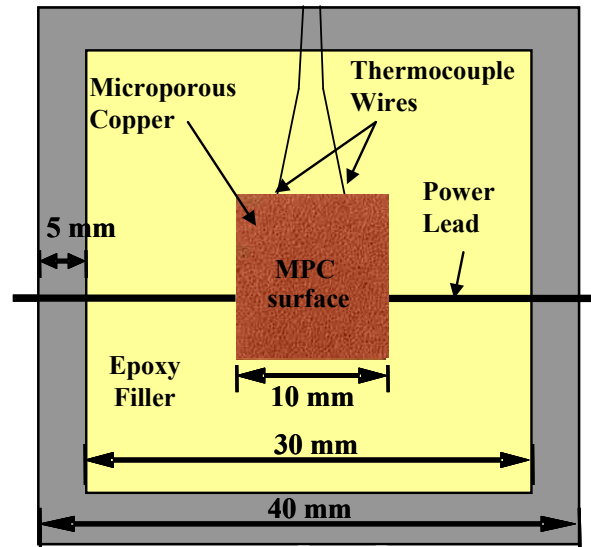
ANSYS (ANSYS Inc., [www.ANSYS.com](http://www.ANSYS.com)), validating the thermal analysis and the estimates of the side heat losses.

The MPC and the Teflon block is encased in a Lexan frame with closed bottoms and the top shallow cavity is filled with special epoxy that is chemically compatible with dielectric liquids. This epoxy ensures that, only the top faces of MPC is exposed for boiling. Figure 4.2 shows a schematic and still photograph of the assembled MicroPorous Copper test section for the experiments. Two K-type thermocouples are installed into 0.6 mm diameter horizontal holes drilled on one side, 0.8 mm from the bottom surface and 5 mm deep into the Cu substrate. The measuring tips of these thermocouples are securely attached to the Cu substrate inside the holes using thermally conducting epoxy (Figure 4.1c). The average readings of these thermocouples after correction for conduction to the surface are taken as an average surface temperature for constructing the pool boiling curves.

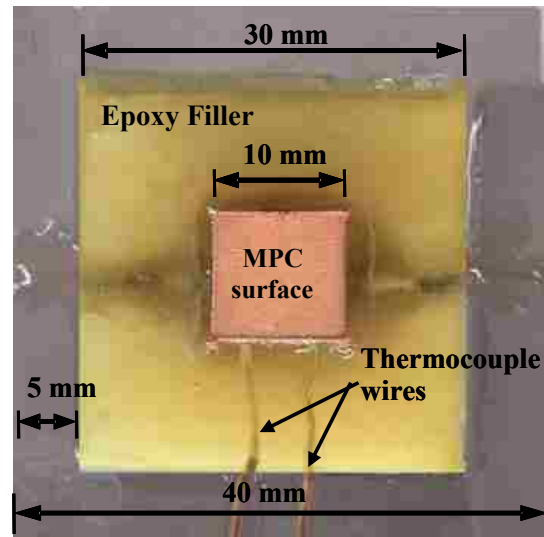
## **4.2 Experimental setup**

A schematic diagram of the experimental setup is shown in Figure 4.3. The pool boiling facility used for the present experiments (El-Genk and Bostanci, 2003; El-Genk and Parker, 2008; Ali and El-Genk, 2013) comprises the following components: (a) A heated water bath in an acrylic tank, (b) A polycarbonate test vessel filled with the dielectric liquid, (c) The assembled test section mounted onto a rotation assembly, (d) Equipment for controlling and monitoring the water bath temperature, the dielectric liquid pool temperature, and the boiling surface, (e) A computer controlled DC power supply to adjust the input power to the heating element, and to monitor and record the voltage drop across and the current through the element, (f) A computer controlled data acquisition unit, and (g) A cooling water loop with a reflux condenser and two submerged coils in the test vessel with a water supply chiller with temperature control. The undercover cooling coil condenses the vapor generated in the experiment. The submerged cooling coils maintain the liquid pool temperature constant at the desired values in saturation and subcooled boiling experiments. Figures 4.4 show a still photograph of the experimental setup for performing the pool boiling experiments.

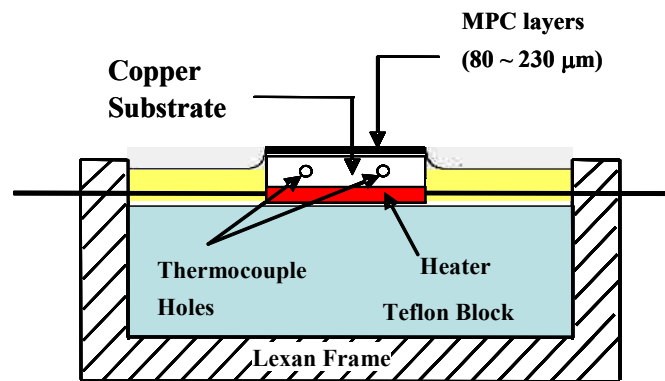
An acrylic block measuring 40 x 40 x 20 mm was used to attach the test section to a rotational assembly in the test vessel (Figure 4.5). A square of Superlock fastener on the



(a) Plane view (Schematic)



(b) Plane view (photograph)



(c) Sectional view

Figure 4.2. Cross sectional views of the fully assembled test section with MicroPorous Copper.

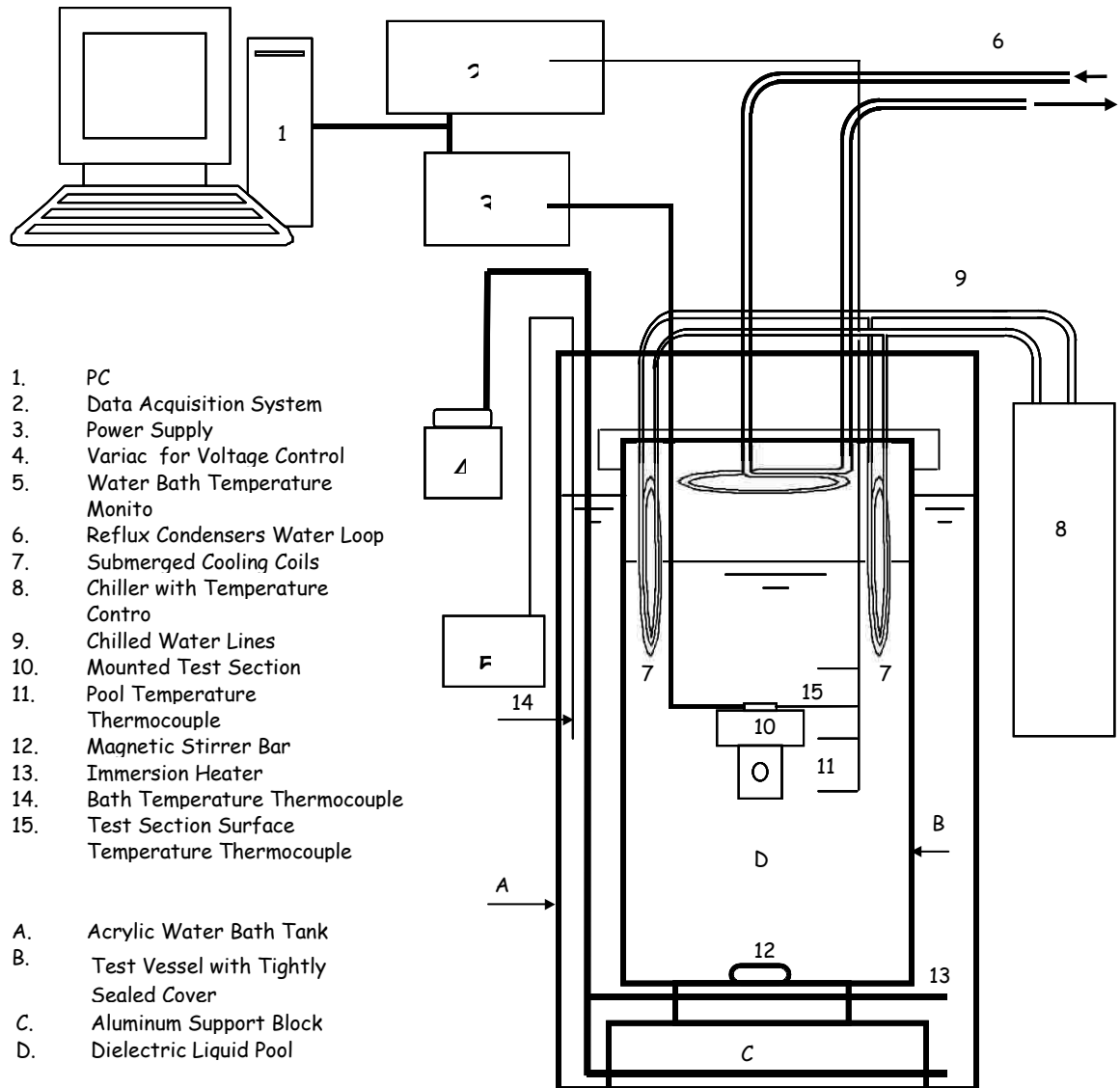


Figure 4.3 Line diagram of the pool boiling test facility (El-Genk and Parker, 2005).

top of the acrylic block and the bottom of the test section, holds the assembled test section firmly in place during the experiments at a various inclination angles. An acrylic rod is inserted through the center of and welded to the acrylic block. Two wheel bearings are placed on each end of the rod. A square piece of blue acrylic is attached to the back half of the rod provided a contrasting background for the photographs and video (Figure 4.5). The rotation assembly consists of two arms and the angle indicator (Figure 4.6 a, b) of the inclination angle of the test section as read from a protractor glued to the outside of the test vessel. These arms extend through the cover of the test vessel with 1/8 inch diameter brass rods. Thus, the inclination angle of the test section to the desired value is adjusted using the extended arms without a need to open the test vessel.

The test vessel is made of 1/2 inch thick Lexan is 290 mm high, 120 mm deep, and 140 mm wide (Figure 4.7c). The entire vessel is assembled using fast curing solvent cement and all inside edges are perfectly sealed with epoxy. An O-ring that fits into a groove in the top cover ensures a tight seal of the test vessel in the experiment. Within the test vessel, there are two wheel wells in which the rotational bearings sit (Figure 4.7c). The cover of the test vessel provides access to the heating element leads, temperature measurements in the pool and assembled test section, the cooling coils, and the rotation mechanism (Figure 4.7b). The cover extends to the edges of the lip of the test vessel. The pool temperature, monitored using submerged thermocouples suspended in the pool, is taken as the average of the readings by the two thermocouples placed 5-10 millimeters from the surface (Figure 4.7a).

The reflux condenser is mounted on the inside of the vessel cover and the cooling coils (Figure 4.7 b) are submerged in the liquid pool. The coil on the inside of the vessel cover plate condenses the vapor produced in the experiments, thus maintaining a constant liquid pool height and vapor pressure in the test vessel. The submerged coils, cooled with water from a chiller, help to control the liquid pool temperature, remove the heat dissipated during the boiling experiments, and maintain the dielectric liquid at the saturation temperature. All throughputs are properly sealed both on the inside and outside. Because dielectric liquids have very low surface tension and are highly wetting, the test vessel is tightly sealed to prevent leakage. The test vessel sits inside a heated water bath to help maintain the temperature of the dielectric liquid in the test vessel near



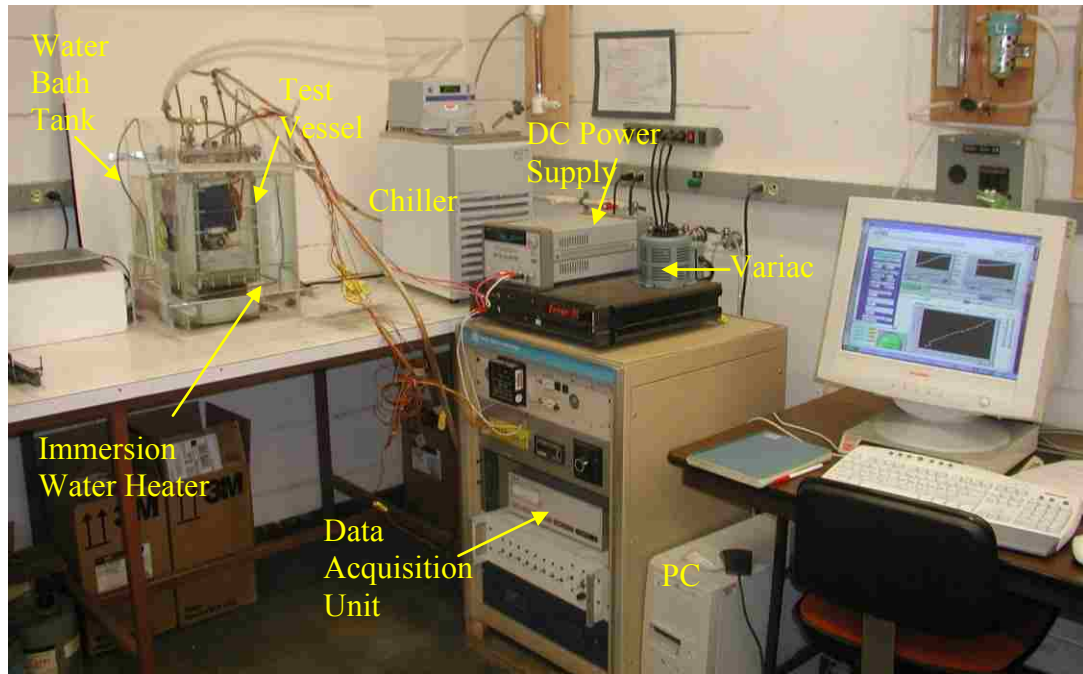


Figure 4.4 Photograph of the pool boiling facility (Parker, 2008).

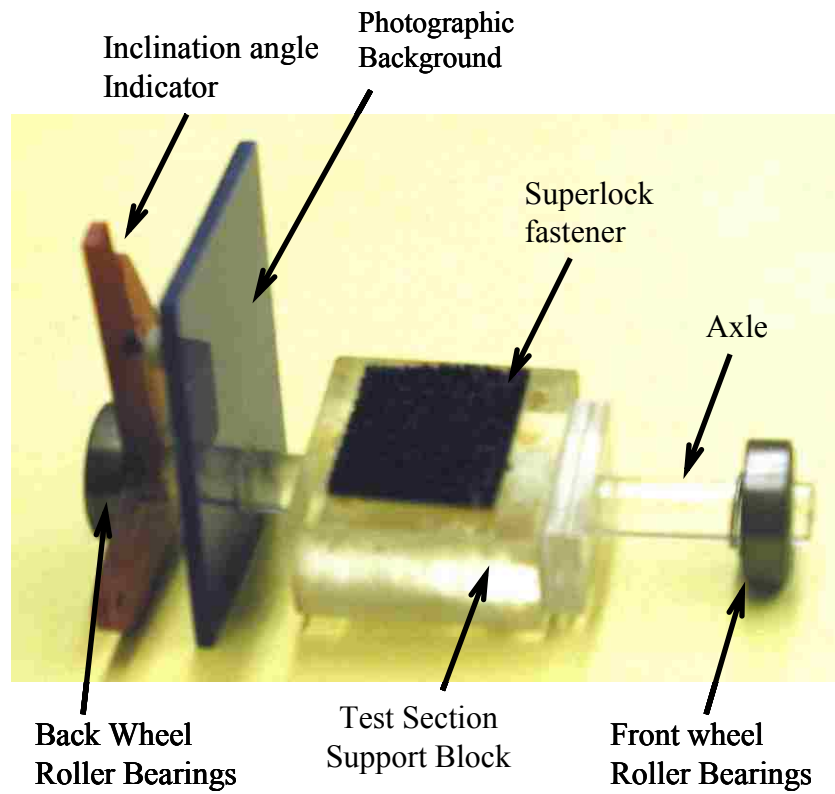
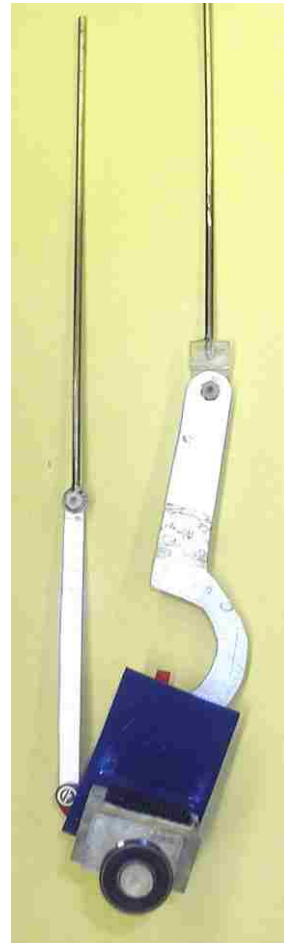


Figure 4.5 Fully assembled test section support (Parker, 2008).



(a) Rotation control mechanism



(b) Assembled rotation assembly and  
control mechanism

**Figure 4.6 Photographs of rotation assembly and fully assembled rotation mechanism (Parker, 2008).**

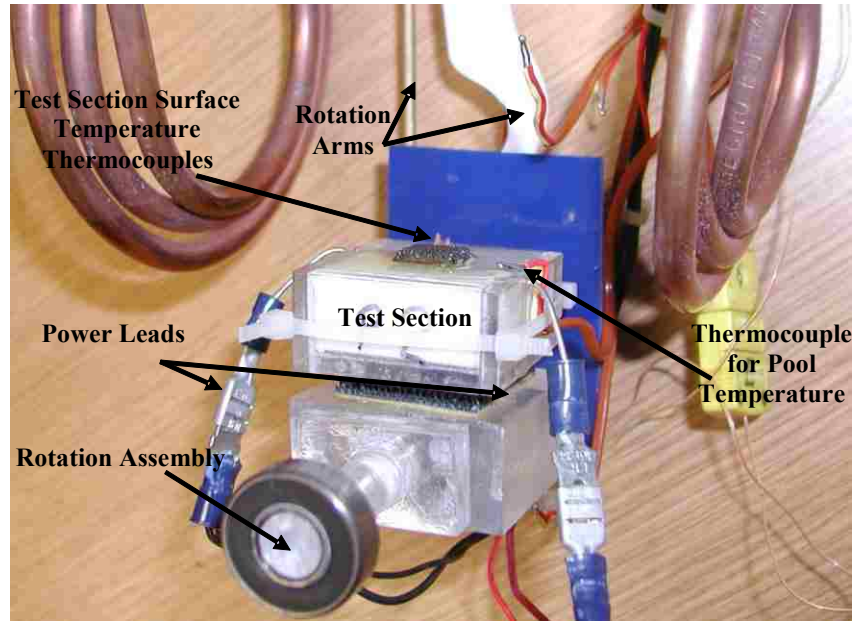
the target value and minimize side heat losses from the vessel wall. An immersion heater sitting at the bottom of the tank of the heated water bath (Figures 4.3 and 4.4). The test vessel sits inside the tank of the water bath on a submersible magnetic stirrer to accelerate degassing of the dielectric liquid in the test vessel before performing the pool boiling experiments.

### **4.3 Experimental Procedures**

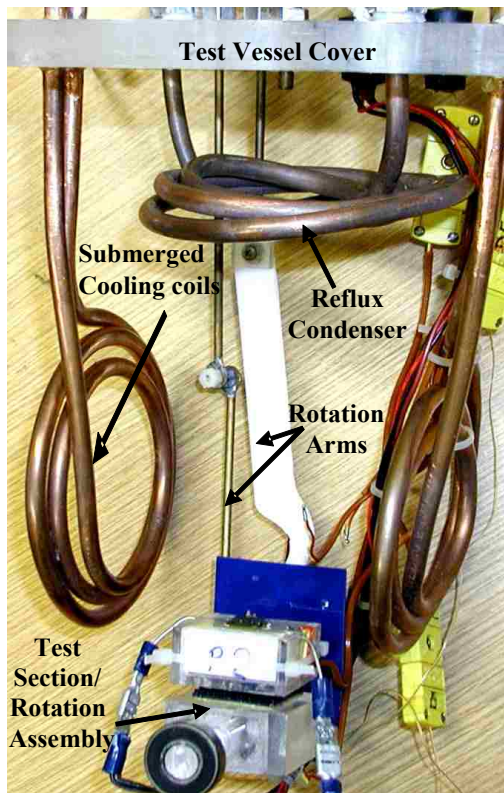
The test vessel is partially filled with the dielectric liquid and the assembled test section is immersed in the liquid pool such that the surface in the upward-facing position ( $0^\circ$ ) is at least 8 cm below the free liquid pool surface. The assembled test vessel is then placed inside the hot water bath tank. Due to the high air solubility in dielectric liquids 48% by volume for PF-5060 (You et al., 1995) out-gassing the liquid pool in the sealed test vessel is accomplished by allowing it to boil for several hours, while maintaining the temperature of the water bath 5-10 K above the saturation temperature of dielectric liquid (Table 1.1) and turning on the magnetic stirrer at the bottom of the pool in the test vessel on (Figures 4.3 and 4.4). The released gas is intermittently vented out by opening a release valve in the cover plate of the test vessel (Figure 4.7c).

The pool boiling experiments begin by turning off the magnetic stirrer, venting any residual gas or vapor in the vessel to ensure the liquid is under atmospheric pressure (0.085 MPa). The electric power to the heating element in the test section is incrementally increased via increasing the applied voltage in increments of  $< 0.2$  V. As the nucleate boiling heat flux increases, the incremental increase in the applied voltage to the heating element is adjusted down to ensure that the maximum increase in the input power to the heater is no more than 0.1 W at a time (or the increase in the surface heat flux is  $< 0.2$  W/cm<sup>2</sup>). When approaching CHF, the incremental increase in the heater's power is gradually reduced further to less than 0.05 W, to accurately determine the CHF values and avoid the temperature surge, which may burn the heating element. The applied voltage and the current through the heating element are measured simultaneously to determine the dissipation heat flux.

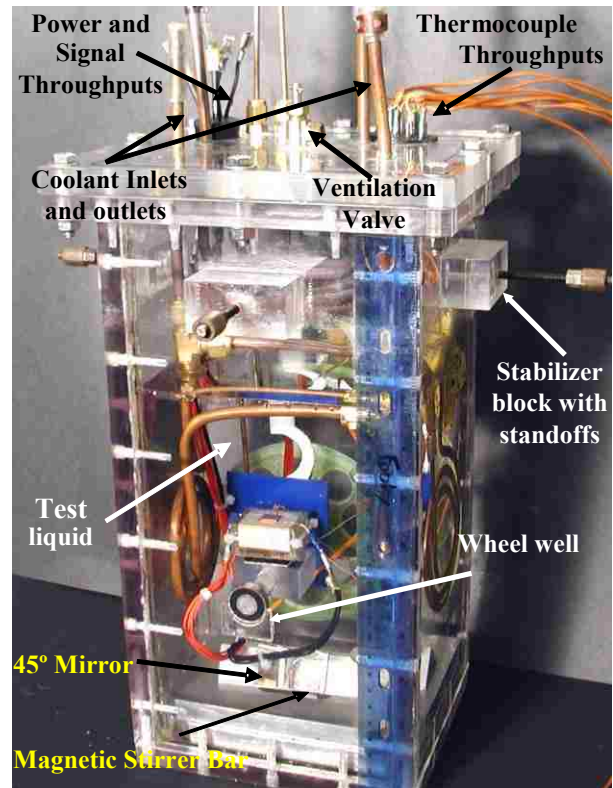
Following each incremental increase in the heater's power, the dissipated heat flux and average surface temperature are recorded at steady state. This is when the changes in two successive average temperature measurements are within  $\pm 0.2$  K which is of the



(a) Test section on rotational mechanism



(b) Reflux condenser and submerged cooling coils



(c) Assembled test vessel

Figure 4.7 Photographs of pool boiling test vessel and assembly (Parker, 2008).

order of the precision of the thermocouple readings. Each of these measurements is the average of 30 subsequent readings by the two thermocouples embedded in the Copper substrate of the MPC surface. It usually takes 20-30 seconds after incrementally increasing the electrical power to the heating element to reach steady state.

Figure 4.8 shows the boiling curves based on individual temperature measurements by the two thermocouples embedded in the Cu substrate. The measured temperatures by the two different thermocouples are consistent ensuring the accuracy of the conducted boiling curve constructed based on the average temperature of the two thermocouples readings. At CHF, the temperature difference between the measurements of the two thermocouples could be as much as 1-3 K, which matches well the results of the thermal analysis discussed earlier. To avoid burning the heating element at CHF, when any of the two surface thermocouples detect an increase of 30 K in two consecutive steady state average surface temperature readings, it is considered an indication of reaching CHF, and the experiments are terminated.

The experimental uncertainties are determined from the manufacturers' stated uncertainties associated with measuring instruments including . These uncertainty are combined to estimate the uncertainty for each individual measurements in the experiments (See appendix A). The estimated experimental uncertainties are  $\pm 0.2$  K in temperature measurements and  $< \pm 1\%$  in the applied voltage and current measurements. The estimated uncertainty in nucleate boiling heat flux is  $\pm 1.3\%$ ,  $\pm 1\%$  in the measured surface area,  $\pm 3\%$  in the surface heat flux and  $\pm 2.3\%$  in the heat transfer coefficient. The variation in the surface superheat at CHF can be as much as 1-3 K due to the hydrodynamic instability of the liquid-vapor interface on the surface.

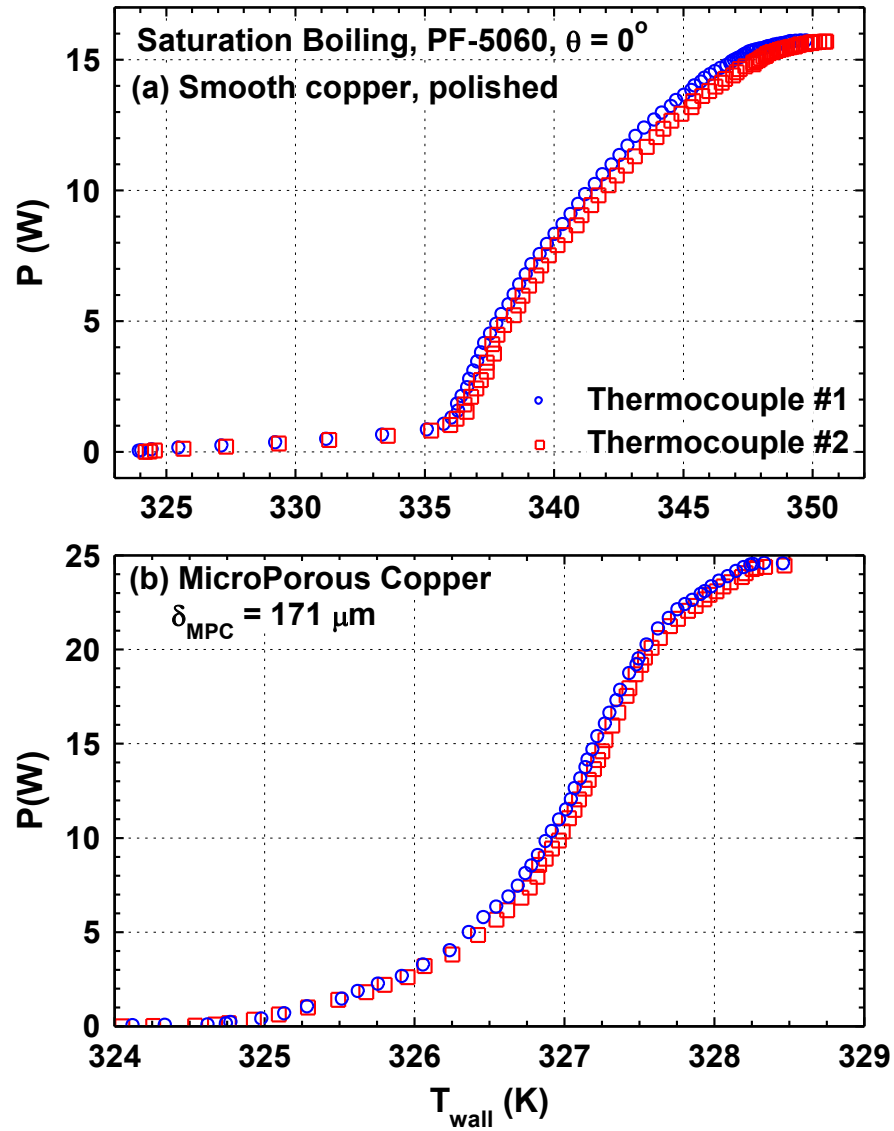


Figure 4.8 Saturation boiling curves on smooth Copper and MPC surfaces based on the readings of two thermocouples (Fig. 4.2c).

## 5. Saturation Nucleate Boiling

Experiments investigated the effect of inclination angle,  $\theta$ , and thickness of MPC Copper surfaces ( $\delta_{MPC}$ ) on saturation nucleate boiling of degassed PF-5060 dielectric liquid as well as the bubble departure diameter and detachment frequency during saturation boiling of PF-5060 in upward facing orientation. The MPC surfaces investigated that are 80, 95, 140, 171, 197, 230  $\mu\text{m}$ -thick at nine inclination angles of  $0^\circ$  (upward facing),  $30^\circ$ ,  $60^\circ$ ,  $90^\circ$  (vertical),  $120^\circ$ ,  $150^\circ$ , and  $180^\circ$  (downward facing). Results of nucleate boiling of PF-5060 are compared to those measured on plane Copper with an average roughness,  $R_a$ , of 0.039  $\mu\text{m}$ .

In the upward facing orientation, a correlation is developed for the obtained values of the fully developed nucleate boiling heat transfer coefficient,  $h_{NB}$ , in terms of the applied heat flux and thickness of MPC,  $\delta_{MPC}$ . In addition, the transient growth of vapor bubbles at discrete sites on various MPC surfaces is recorded using CD Camera at 210 frames/seconds. The results of the bubble departure diameter and detachment frequency are used to estimate the surface average density of active sites for bubble nucleation on different MPC surfaces. For consistency, the present experiments are carried out using degassed PF-5060 and conditioned MPC surfaces.

### 5.1 Conditioning of MPC Surfaces

Conditioning of MPC surfaces is achieved after conducting several pool boiling experiments, each lasting typically 4-5 h, separated by cool down intervals of 2-14 h. When they used for the first time, MPC surfaces experience conditioning, results in a gradual increase in the surface superheat and decrease in nucleate boiling heat transfer coefficient with little effect on CHF. On these surfaces the excursion in surface temperature is much smaller than those reported in the literature on plane Cu and silicon surfaces (Rainey and You, 2000; Parker and El-Genk, 2005; El-Genk and Bostanci, 2003; Chang et al., 1998; O'Connor, You, and Chang, 1996; Kim et al, 2007). The obtained nucleate boiling and heat transfer coefficient curves for two different MPC surfaces during conditioning ( $\delta_{MPC} = 85$  and  $230 \mu\text{m}$ ) are shown in Figures 5.1a and 5.1b. The results show that the saturation boiling curves on the conditioned MPC surfaces in the last two tests are almost identical, and so are the heat transfer coefficient curves in

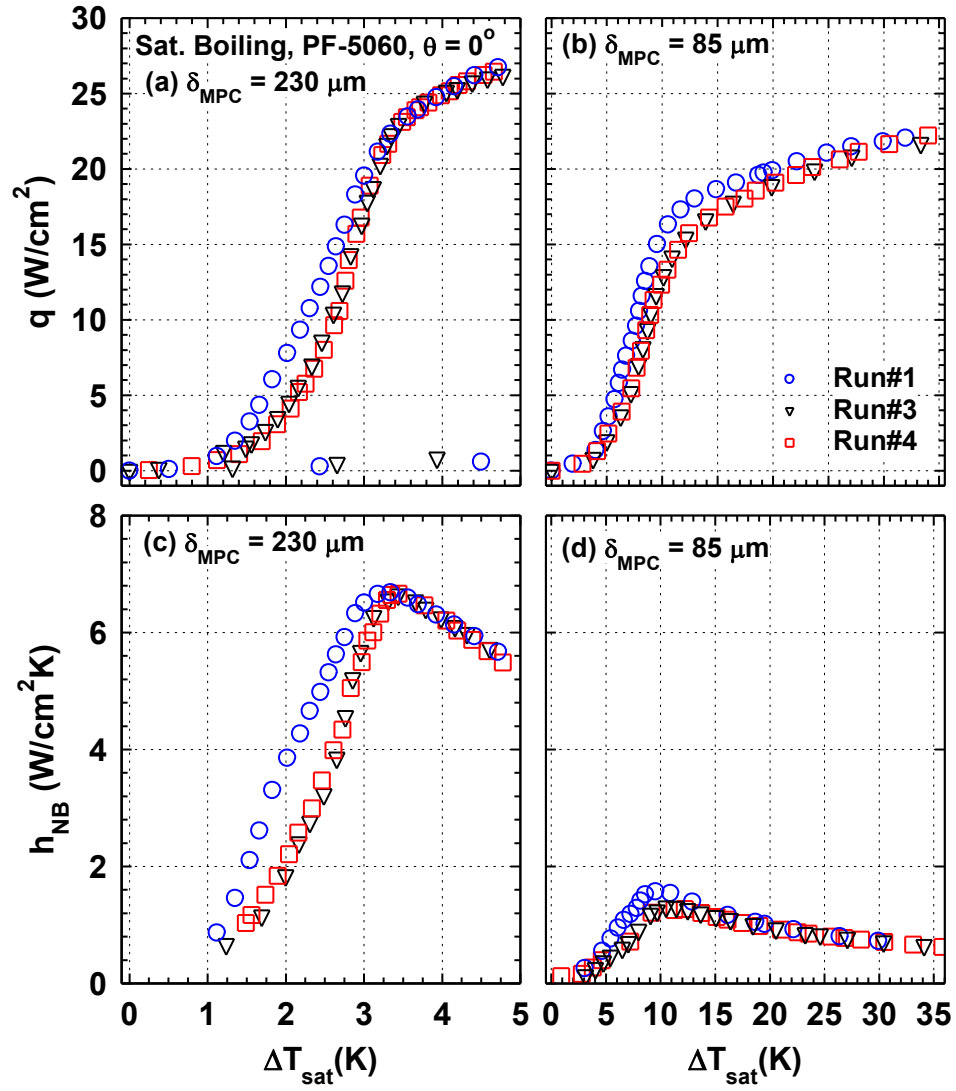


Figure 5.1 Conditioning of saturation boiling curves of PF-5060 on MPC surfaces.



Figures 5.1c and 5.1d. For consistency, all nucleate boiling curves presented and discussed next in the chapter are for degassed PF-5060 liquid on conditioned MPC surfaces.

Figure 5.2a-5.2d shows the saturation pool boiling and heat transfer coefficient curves of PF-5060 liquid in upward facing on two conditioned MPC surfaces having thicknesses of 95  $\mu\text{m}$  and 197  $\mu\text{m}$ . For each MPC thickness, two different test sections are tested in separate experiments to confirm the reproducibility of the fabrication process. The results in these figures confirm the reproducibility of the boiling curves and the fidelity of the procedure used for fabricating MPC surfaces and running the experiments.

## **5.2 Boiling Hysteresis**

In order to ensure that not the thermal inertia of the boiling surface and the assembled test section, but rather the surface characteristics and liquid properties affect the nucleate boiling results. Separate experiments are performed to quantify the boiling hysteresis. Identical experiments are conducted with the same MPC surface, the pool boiling curves are recorded with ascending (or increasing heat flux) and descending (or decreasing heat flux) input power to the heating element of the test section and compared in Figures 5.3a and 5.3b. These figures clearly show that the nucleate boiling curve obtained by incrementally increasing and decreasing input power is almost identical. The absence of boiling hysteresis confirms that the nucleate boiling results in the present experiments are solely depends on the morphology of MPC surfaces and the thermophysical properties of the PF-5060.

## **5.3 Nucleate Boiling Results**

The obtained saturation pool boiling curve of PF-5060 on 230  $\mu\text{m}$ -thick MPC surface with embedded photographs is shown in Figure 5.4. It consists of three distinct boiling regions in addition to natural convection. In region I of discrete bubbles, at low-superheat and low heat flux, not all potential nucleation sites are active, but their number increase with increased heat flux. In region II of fully developed nucleate boiling, at higher heat flux than in the discrete bubble region, is characterized by a steep slope of the boiling curve indicative of the increased density of the active bubble nucleation sites.

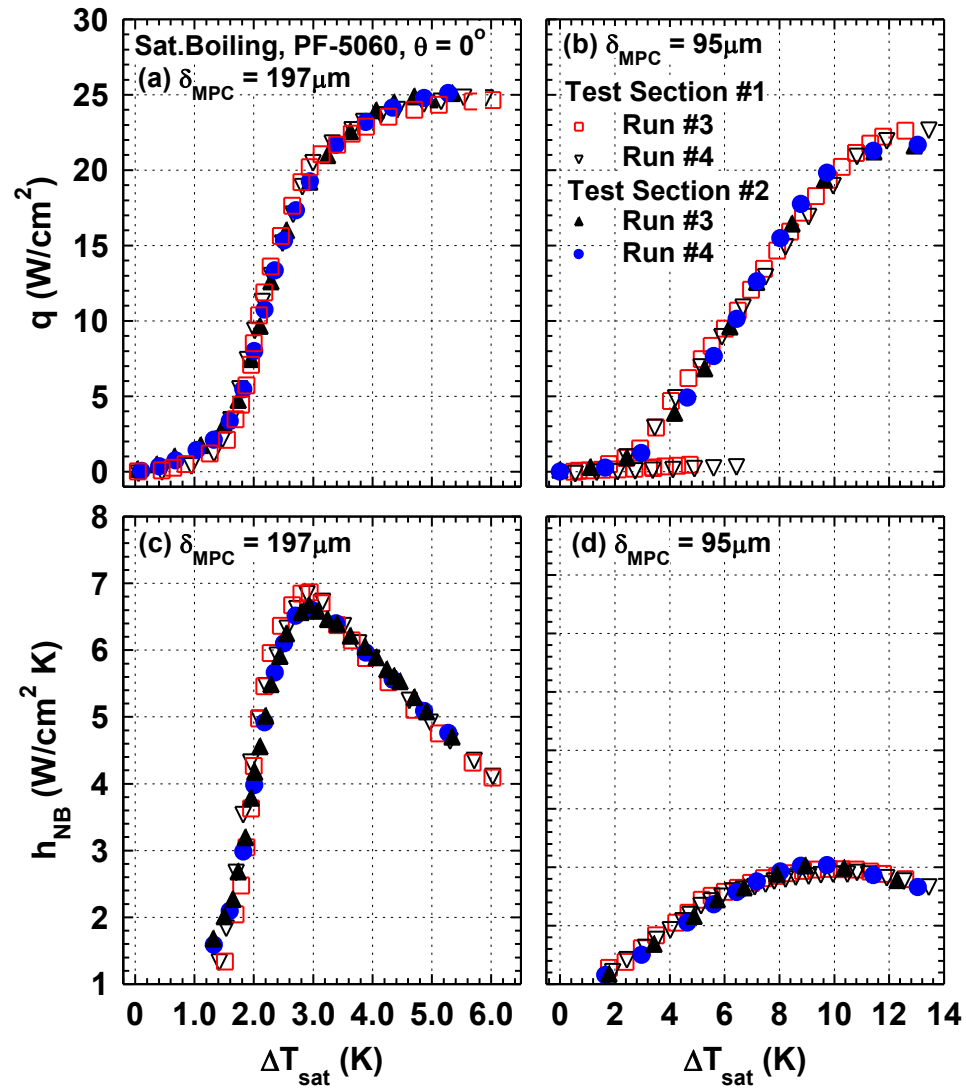


Figure 5.2 Reproducibility of saturation pool boiling curves.

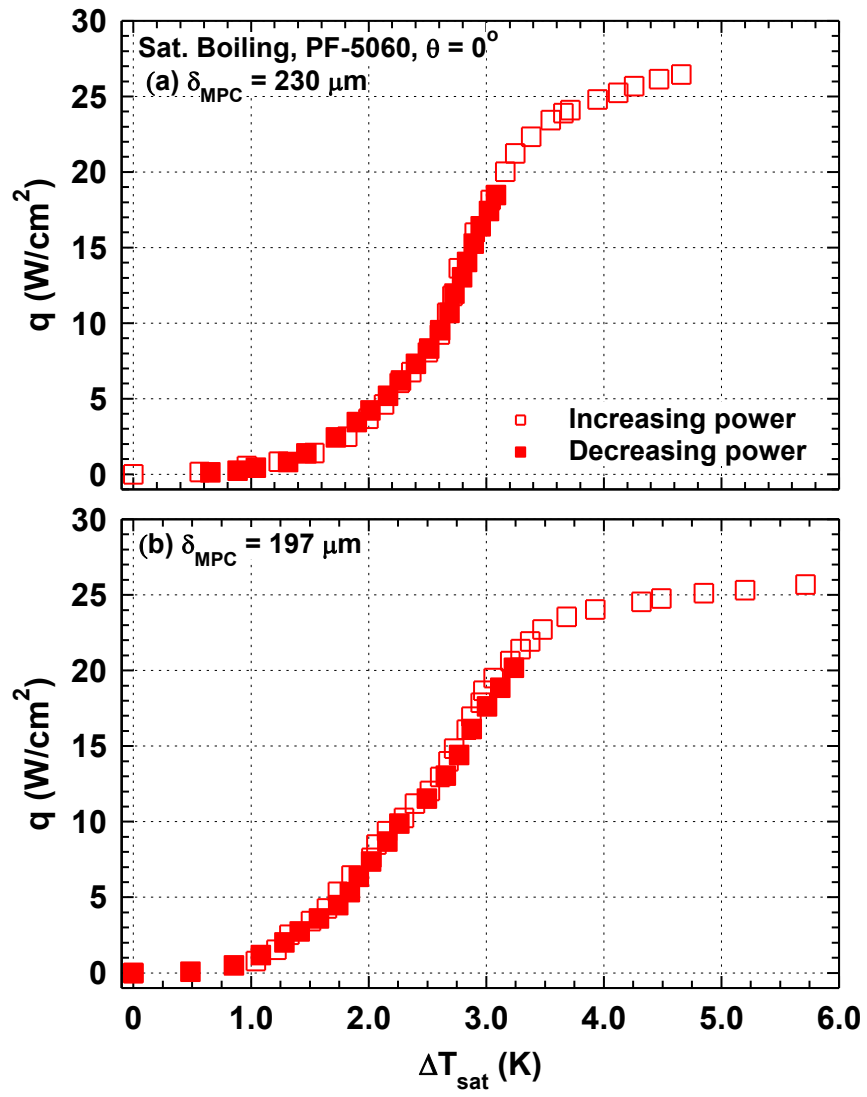


Figure 5.3 Hysteresis of saturation boiling curves of PF-5060 on MPC surfaces.

The maximum nucleate boiling heat transfer coefficient,  $h_{MNB}$ , occurs near the end of this region (Solid square symbol, Figure 5.4). In addition to the high density of the active nucleation sites on the surface, lateral coalescence among growing and departing vapor bubbles is negligible, but increases with increasing heat flux. With further increase in the heat flux, lateral bubble coalesce hinders the heat removal from the surface, decreasing the slope of the boiling curve as it transitions into Region III (Figure 5.4). In this region, the gradually decreasing slope of the boiling curves is caused by the increased lateral coalescence of the growing and departing bubbles, forming large vapor masses near the boiling surface. Consequently, the increase in the nucleate boiling heat transfer coefficient with increasing surface superheat is significantly lower than in regions I and II. Region III extends to CHF marked with the solid circle symbols in Figure 5.4. The nucleate boiling heat transfer coefficient at CHF is lower than  $h_{MNB}$  and the corresponding surface superheat is higher. Thus, operating in the fully developed nucleate boiling region is preferable in industrial application. Since most of electronic components operate in the standby mode for typically long time, the heat dissipation is low and cooling of the chip could be by natural convection, investigated next.

## 5.4 Natural Convection

Natural convection ensues when the wall temperature is higher than the bulk temperature within the liquid layer adjacent to the wall. The buoyant force circulates the cold liquid from the bulk to replace the hot liquid rising at the heated wall. In the present experiments, the MPC surfaces are uniformly heated, the dissipated heat removal rate in the natural convection is proportional to  $(T_w - T_b)^{1.2}$ . The present natural convection data for PF-5060 on MPC surfaces are compared to those reported earlier by other investigators for PF-5060 and FC-72 on micro-porous coatings, micro-fined surfaces and surfaces with micro-reentrant cavities (e.g. Parker and El-Genk 2005; El-Genk, 2012) are shown in Figures 5.5. The present natural convection data for PF-5060 on MPC in Figure 5.5a are correlated as:

$$q_{_{NC}} = 0.0444 (T_w - T_b)^{1.2} \quad (5.1)$$

Equation 5.1 fit the data to within  $\pm 10\%$ . Figure 5.5b shows the heat removal rate by natural convection of PF-5060 dielectric liquid from the MPC surfaces is  $\sim 26\%$  higher

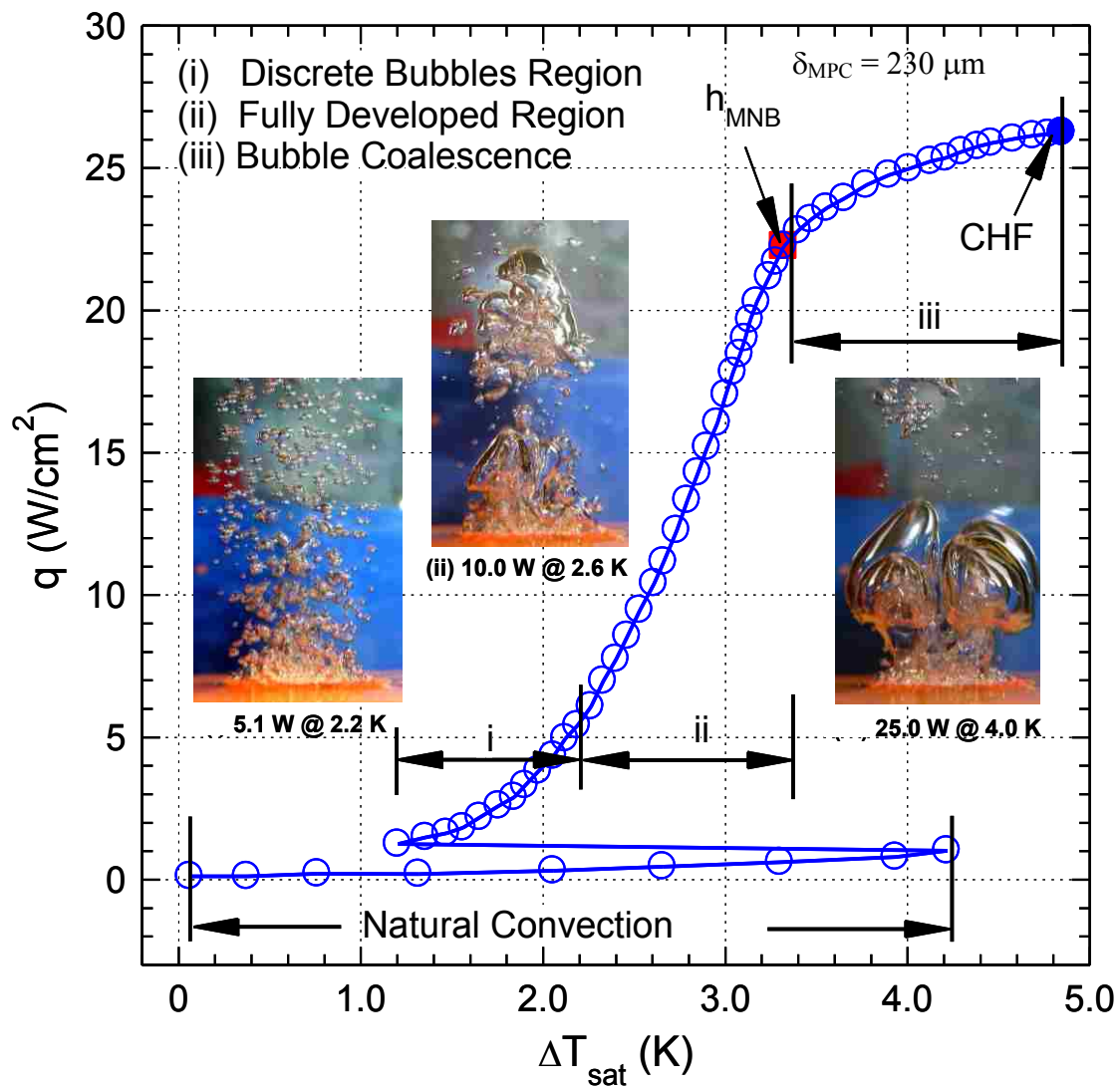


Figure 5.4 Saturation boiling curve of PF-5060 on 230  $\mu m$ -thick MPC surfaces in the upward facing orientation.

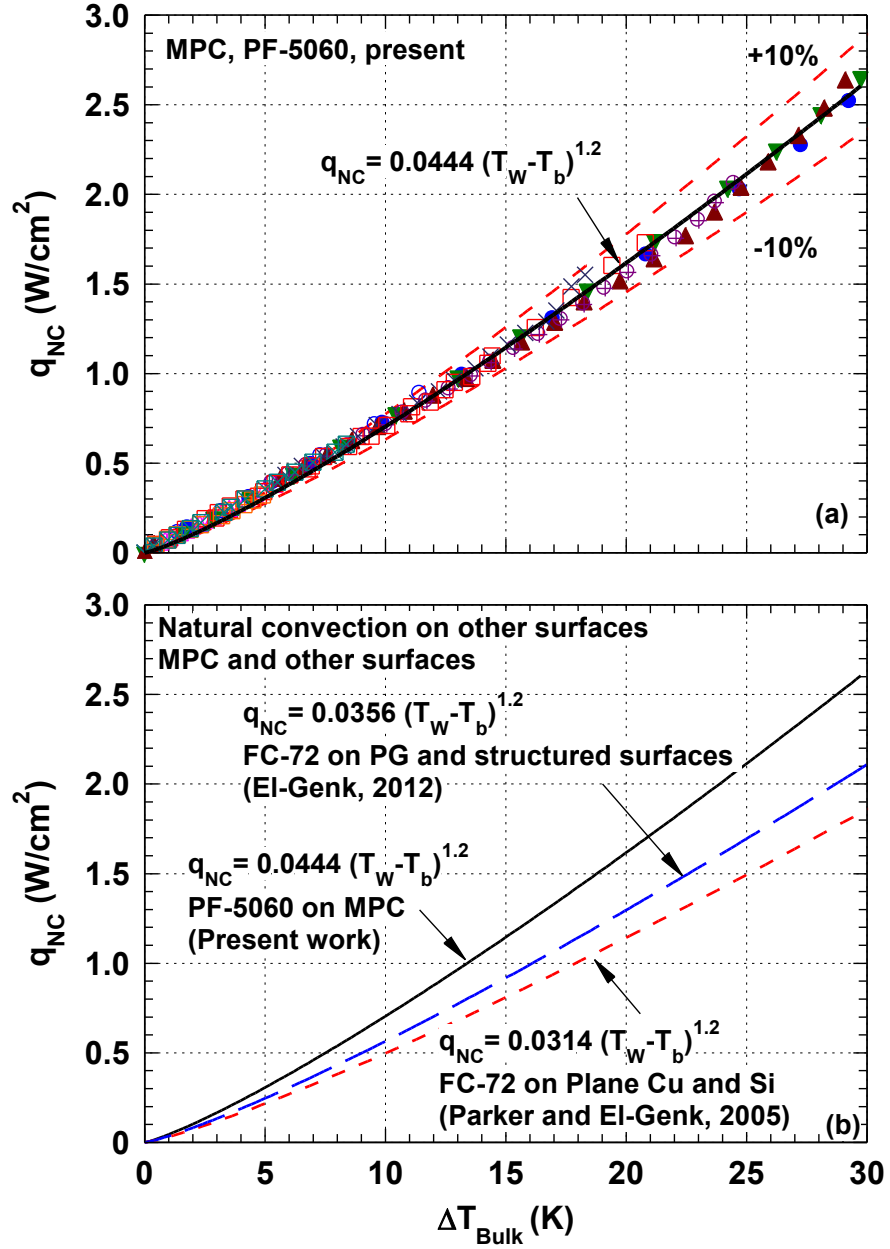


Figure 5.5 Natural convection data of dielectric liquids on smooth, porous, micro-structured, and MPC surfaces.

than of FC-72 on porous graphite, structured surfaces, and surfaces with micro particles coating and 41% higher than on plane Copper and silicon surfaces. Natural convection in the present experiments dominates until nucleate boiling incipience (Figure 5.4). The next section presents the present nucleate boiling results.

## 5.5 Nucleate Boiling and Heat Transfer Coefficient

Reported results in the literature on nucleate boiling of dielectric liquids on plane Copper and silicon surfaces showed a large extension of surface temperature prior to boiling incipience. On MPC surfaces there no or little temperature excursion prior to boiling incipience. The next subsections present and discuss the effects of MPC surface thickness,  $\delta_{MPC}$ , and surface orientation on saturation nucleate boiling of PF-5060.

### 5.5.1 Effect of MPC surface thickness

The saturation nucleate boiling and heat transfer coefficient curves of PF-5060 on conditioned MPC surfaces of different thickness (95-230  $\mu\text{m}$ ) in the upward facing orientation ( $\theta = 0^\circ$ ) are shown in Figure 5.6a and 5.6b. These Figures show a little temperature excursion prior to boiling incipience on MPC surfaces with nucleate boiling starting at surface temperature  $< 5$  K, compared to high surface superheat at boiling incipience that on smooth Copper surface ( $\sim 12$  K).

The saturation pool boiling curves for PF-5060 show that increasing the applied heat flux progressively increases the surface superheat until reaching CHF (Solid square symbols, Figure 5.6). The nucleate boiling heat transfer coefficient,  $h_{NB}$ , initially increases with increased surface superheat to a maximum,  $h_{MNB}$  (Solid circle symbols, Figure 5.6c and d), and then decreases with further increase in the surface superheat until reaching CHF. The  $h_{MNB}$ , near the end of the fully developed nucleate boiling region, and is much higher than that at CHF and occurs at much lower surface superheat. The results in Figures 5.6 confirm that the MPC surface of different thickness,  $\delta_{MPC}$ , significantly enhance saturation boiling of PF-5060 dielectric liquid and increase CHF compared to smooth Copper. Increasing the thickness of MPC surfaces from 95 to 230  $\mu\text{m}$  increases CHF from  $\sim 22\text{-}26$   $\text{W}/\text{cm}^2$ , compared to  $\sim 16$   $\text{W}/\text{cm}^2$  CHF on smooth Copper. CHF values on MPC surfaces occur at much lower superheats than on smooth Cu. The surface superheats,  $\Delta T_{\text{sat}}$  at CHF on MPC surfaces range from 5-14 K, depending on the

thickness compared to  $\Delta T_{\text{sat}} = 25 \text{ K}$  on smooth Copper. While CHF increase with increased MPC thickness, the  $h_{\text{NB}}$  increases up to  $\delta_{\text{MPC}}$  of  $171 \mu\text{m}$  and then decreases with further increase in MPC thickness. Depending on  $\delta_{\text{MPC}}$ , the  $h_{\text{MNB}}$ , ranges from of  $2 - 7.8 \text{ W/cm}^2 \text{ K}$  and occurs at surface superheats of  $2.8\text{-}9.2 \text{ K}$ . The highest  $h_{\text{MNB}}$  on the MPC surface that is  $171 \mu\text{m}$  thick ( $7.8 \text{ W/cm}^2 \text{ K}$ ) occurs at  $\Delta T_{\text{sat}}$  of only  $2.7 \text{ K}$ , compared to  $2.0, 4.8$  and  $6.7 \text{ W/cm}^2 \text{ K}$  and  $\Delta T_{\text{sat}}$  of  $9.2, 4.3 \text{ K}, 2.93 \text{ K}$ , and  $2.88 \text{ K}$ , on  $\delta_{\text{MPC}}$  of  $95, 140$  and  $230 \mu\text{m}$  thick, respectively (Figure 6b). The  $h_{\text{MNB}}$  for  $\delta_{\text{MPC}} = 171 \mu\text{m}$  is about 10 folds that on smooth Copper ( $< 0.7 \text{ W/cm}^2 \text{ K}$ ) and the surface superheat ( $2.8 \text{ K}$ ) is much lower than that on smooth Copper ( $21.5 \text{ K}$ ) (Figure 5.6a-5.6b).

The results presented in Figure 5.6 are for the upward facing orientation. The results on the effect of MPC surface inclination, from upward facing ( $\theta = 0^\circ$ ) to downward facing ( $\theta = 180^\circ$ ) on nucleate boiling of PF-5060 dielectric liquid on MPC surface of different thicknesses are presented and discussed next.

### 5.5.2 Effect of surface orientation

Figures 5.7a-d compare the obtained nucleate boiling and heat transfer coefficient curves in for the  $85, \text{ and } 115 \mu\text{m}$ -thick MPC surfaces at inclinations angle of  $0^\circ, 60^\circ, 90^\circ, 120^\circ, 150^\circ$ , and  $180^\circ$ . For the same heat flux, increasing the thickness of MPC and/or decreasing the inclination angle, decreases the surface superheat, thus enhancing the nucleate boiling heat transfer coefficient,  $h_{\text{NB}}$ . The maximum heat transfer coefficient,  $h_{\text{MNB}}$ , which occurs near the end of the fully developed nucleate boiling region of the pool boiling curve, indicated by the solid circle symbols in Figures 5.7c and 5.7d. are the highest in the upward facing orientation ( $\theta = 0^\circ$ ) and decreases with increased inclination angle to the lowest value in the downward facing ( $\theta = 180^\circ$ ). The corresponding surface superheat decreases with increasing surface inclination. CHF is indicated by solid square symbol in Figures 5.7a-d. The CHF and  $h_{\text{NB}}$  decrease with increasing surface inclination and occur at slightly lower surface superheats. These results are applicable for all MPC surfaces investigated in this research. For all inclination angles,  $h_{\text{NB}}$  increases with increasing the MPC thickness up to  $171 \mu\text{m}$  and then decreases with further increase in the thickness.



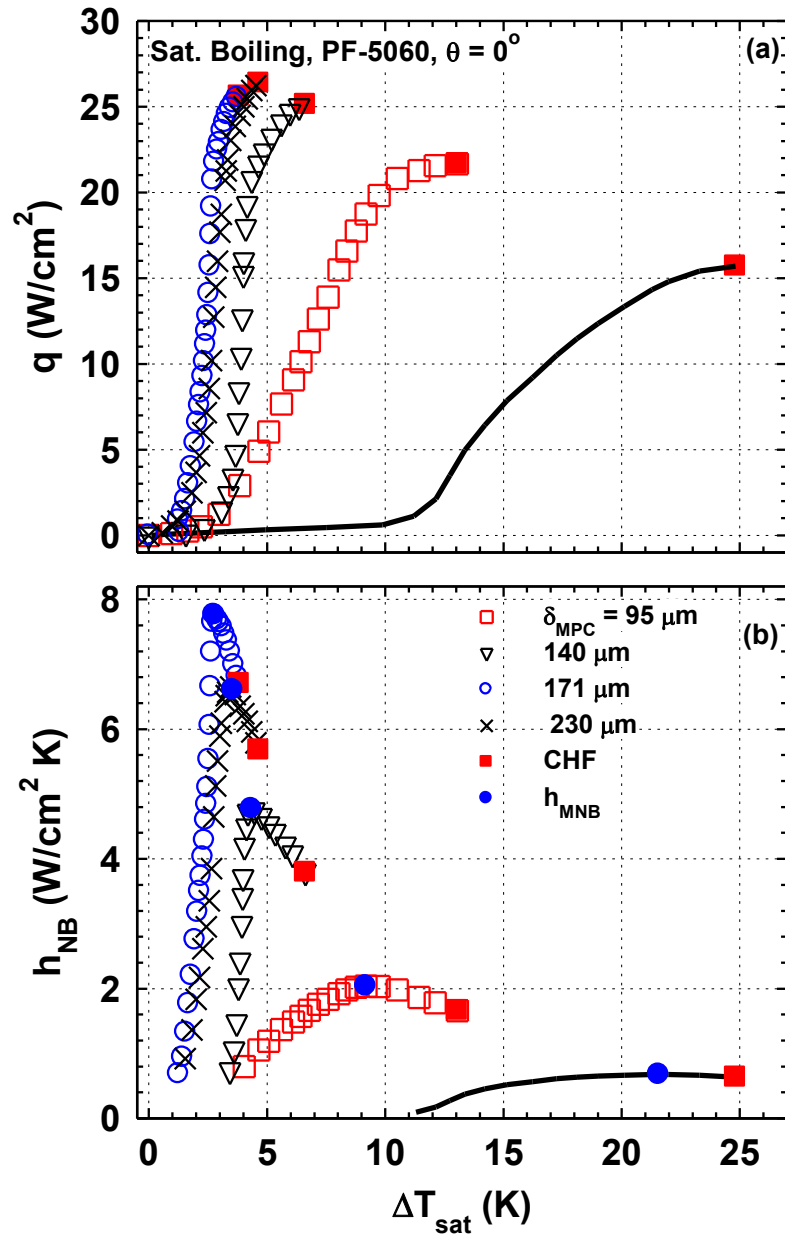


Figure 5.6 Effect of  $\delta_{MPC}$  on saturation boiling of PF-5060 in the upward facing orientation.

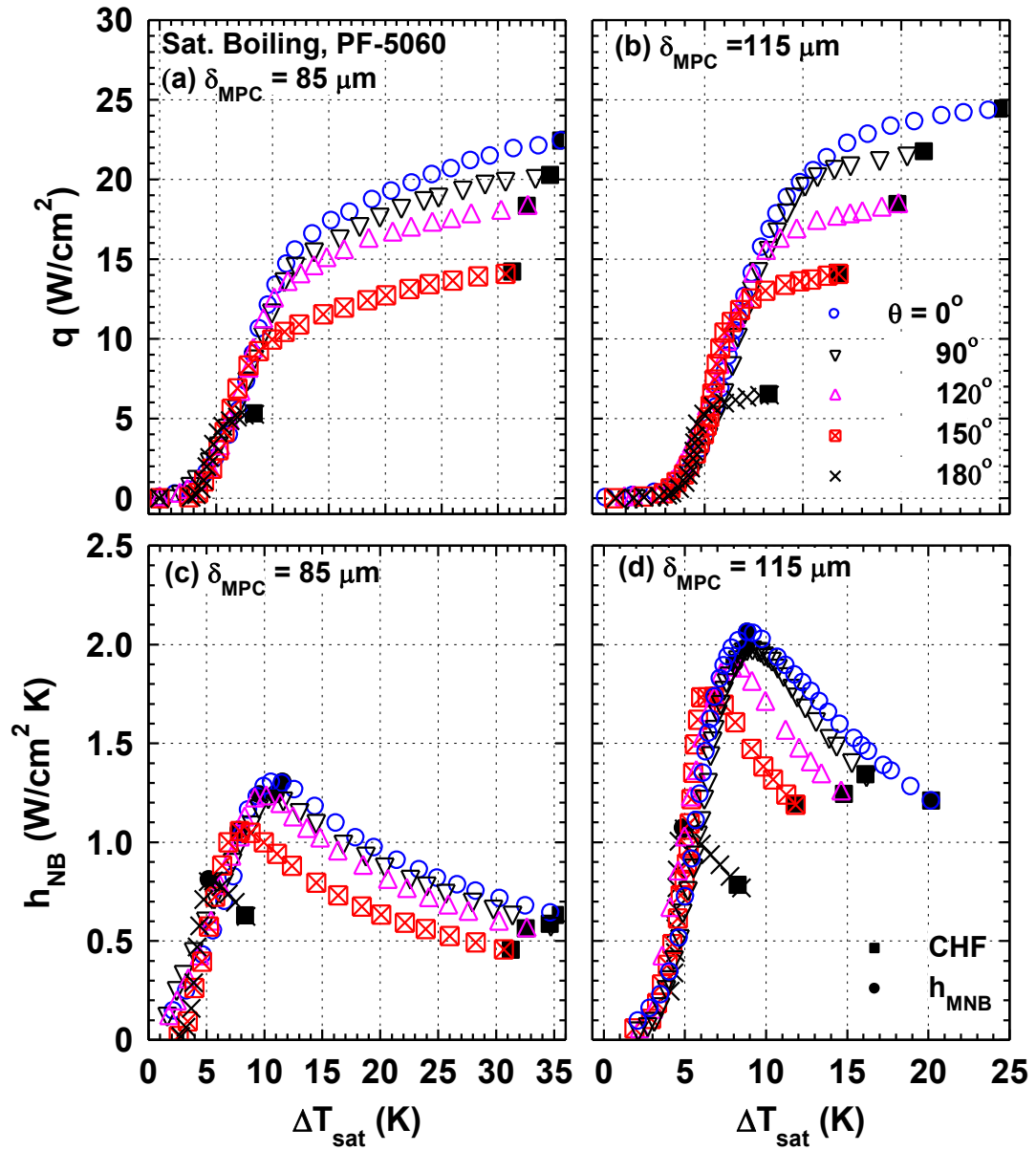


Figure 5.7 Effect of inclination angle on saturation boiling of PF-5060 on MPC surfaces.

In industrial applications of nucleate boiling, it is preferable to operate at or  $h_{MNB}$ , on the left side of the boiling curve (fully developed region, Region II) to have sufficient safety margin from CHF. Thus, a correlation for the fully developed nucleate boiling heat transfer coefficient,  $h_{NB}$ , is a useful tool for such application. The next section correlate the present values of  $h_{NB}$  for saturation boiling of PF-5060 on MPC surfaces in the upward facing orientation ( $\theta = 0^\circ$ ).

### 5.5.3 Nucleate boiling heat transfer correlation

Figures 5.8a-5.8c each present the results of experiments performed at the same condition with 80, 115, and 171  $\mu\text{m}$ -thick MPC surfaces. These Figures that plots the  $h_{NB}$  values versus the surface superheats, confirm the reproducibility of the results. The values of  $h_{NB}$  for saturation boiling of PF-5060 liquid on MPC surfaces in the upward orientation,  $\theta = 0^\circ$  are correlated as:

$$h_{NB}(\delta_{MPC}, 0^\circ) = A q^B \quad (5.2)$$

Figure 5.8d, which compares the correlations for MPC surface of different thicknesses. shows that  $h_{NB}$  increases with increasing,  $q$ , ending with the  $h_{MNB}$  (closed circle symbol), and with increasing  $\delta_{MPC}$  up to 171  $\mu\text{m}$ , and decreases with further increase in  $\delta_{MPC}$ . In equation 5.2, the coefficients A and B functions of  $\delta_{MPC}$  are correlated as:

$$A(\delta_{MPC}, 0^\circ) = 7.7 \times 10^{-3} \delta_{MPC}^{0.92} \quad (5.3a)$$

$$B(\delta_{MPC}, 0^\circ) = 0.05 + 7.93 \times 10^{-3} \delta_{MPC} - 2.45 \times 10^{-5} \delta_{MPC}^2 \quad (5.3b)$$

These correlation for “A” and “B” are within  $\pm 11\%$  and  $\pm 5\%$  of the present experimental data for all values of  $\delta_{MPC}$  from 80  $\mu\text{m}$  to 230  $\mu\text{m}$ , respectively. The coefficient “A” increases from 0.4 to 0.91 as the  $\delta_{MPC}$  increases from 80-230  $\mu\text{m}$  (Figure 5.10a). The exponent “B”, which presents the slope of the fully developed nucleate boiling curve, increases from 0.5 to 0.7 with increasing  $\delta_{MPC}$  from 80  $\mu\text{m}$  to close to 162  $\mu\text{m}$  and then to 0.57 for 230  $\mu\text{m}$ -thick MPC (Figure 5.9b). Figure 5.10 compares the experimental values for  $h_{NB}$  in the upward facing orientation to the predicted values using Equations 5.2 and 5.3 for MPC surfaces of different thicknesses (80-230 $\mu\text{m}$ ). The correlation for  $h_{NB}$  agrees to within  $\pm 11\%$  with the experimental data for all MPC surface investigated in this work.

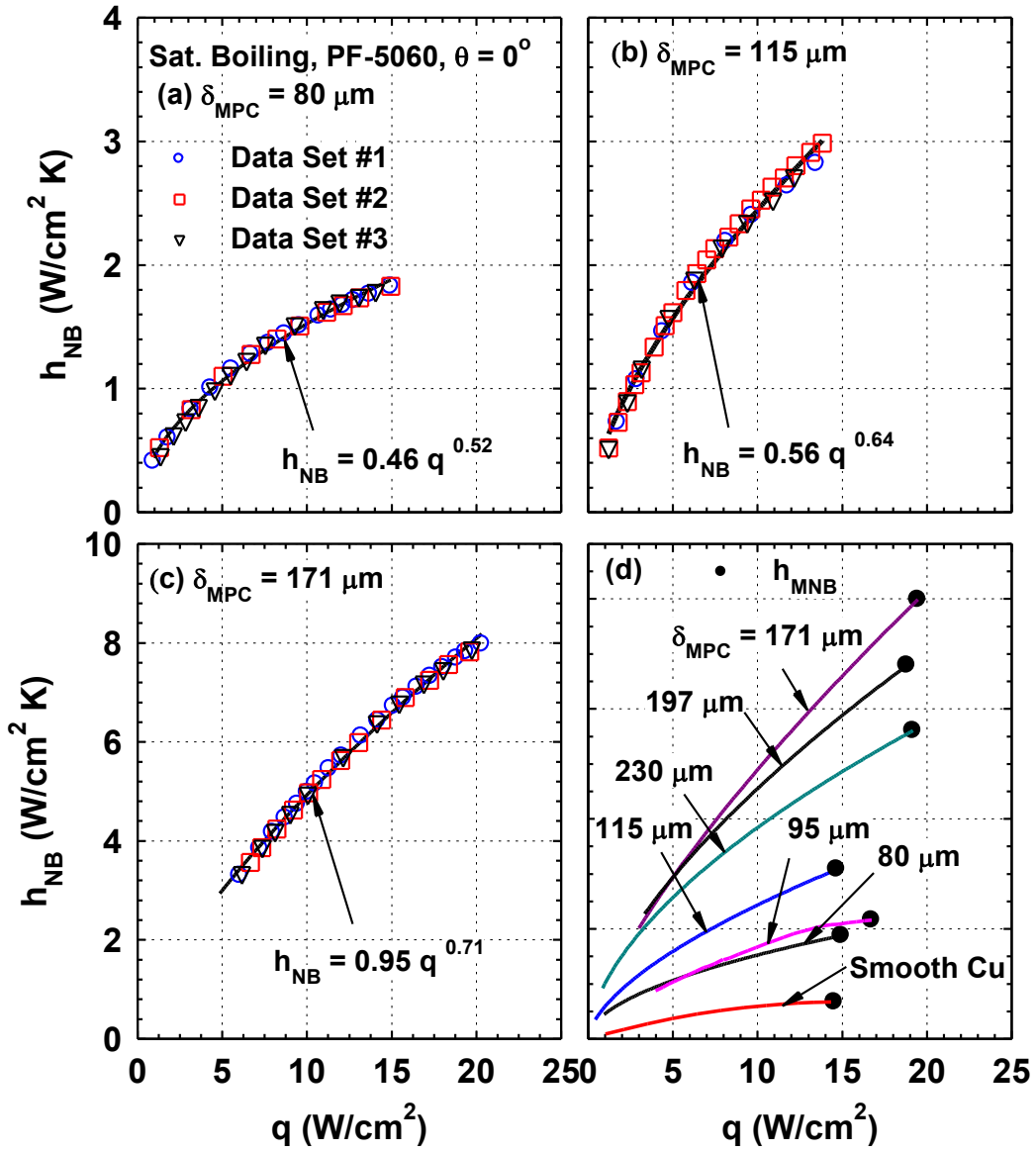


Figure 5.8 Developed correlation of saturation boiling  $h_{NB}$  on of PF-5060 on MPC of different thicknesses.

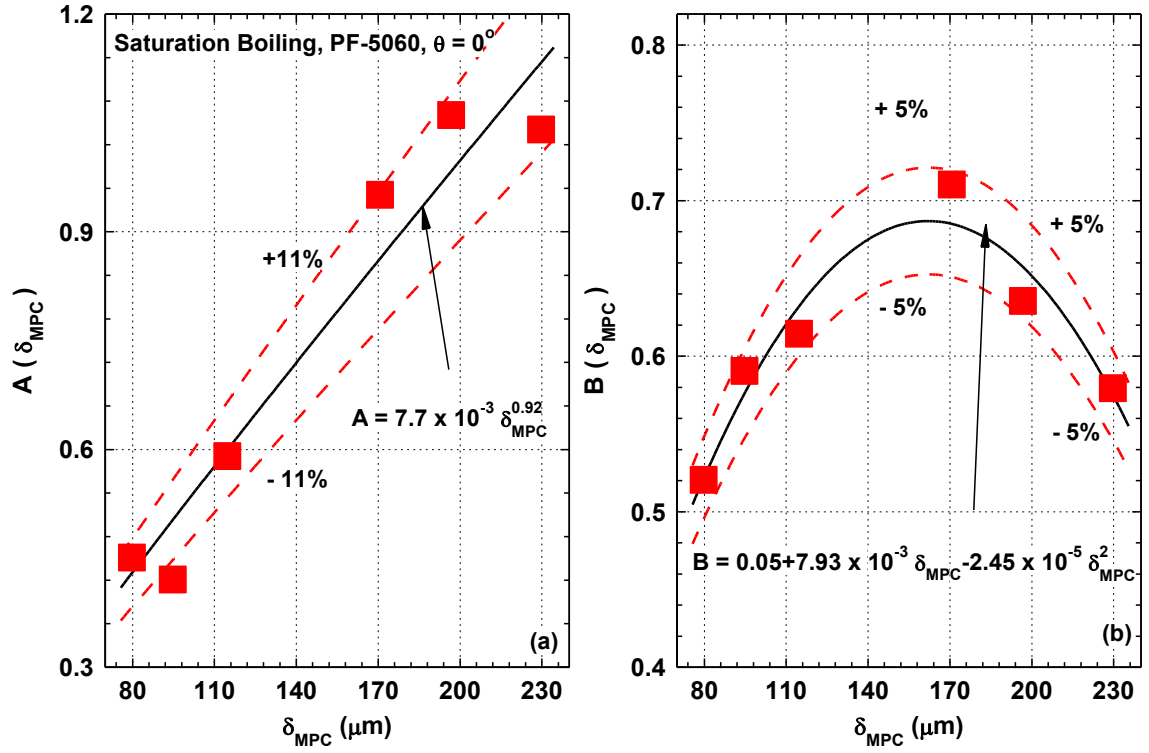


Figure 5.9 Coefficients for fully developed nucleate boiling heat transfer correlation on MPC surfaces.

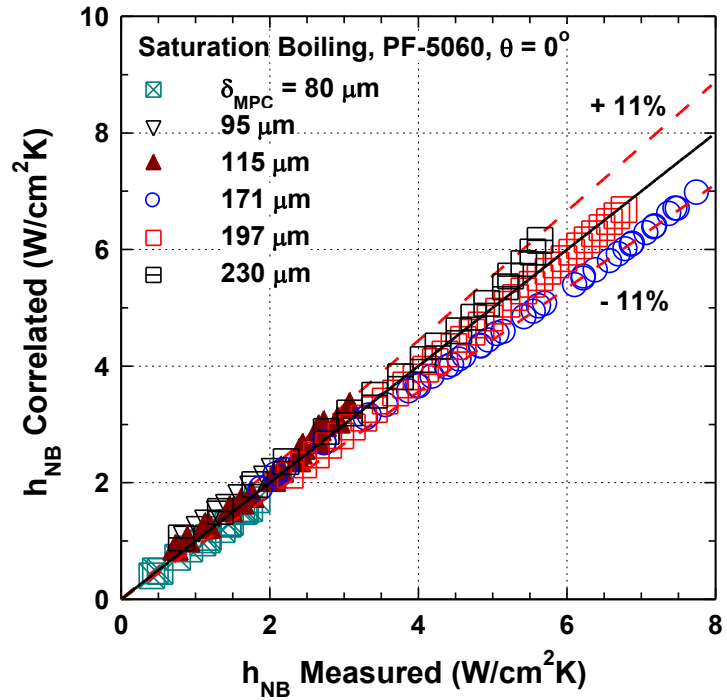


Figure 5.10 Comparison of predicted and measured  $h_{NB}$  values for saturation boiling of PF-5060 on MPC surfaces.

The values of fully developed nucleate boiling heat transfer,  $h_{NB}$ , on the present MPC surfaces are compared in Figure 5.11 to those reported in the literature for PF-5060 and other dielectric liquids on different surfaces. These include, microporous coating (MPCo), porous Graphite (PG), microporous Copper (MPC) Copper with nano wired (CNWs), Copper Oxides nano structure (Cuo NS) and Copper with sintered Copper particles (e.g., McHale and Garimella, 2011; Im, Lee, and Joshi, 2012; Im et al., 2010; El-Genk and Parker, 2005; kim and Han, 2008). For the same range of applied heat flux,  $q$ , the  $h_{NB}$  values on the present MPC surfaces with thickness  $\delta_{MPC} < 115 \mu m$ , are comparable to those reported for other dielectric liquid on other surfaces. For thicker MPC surfaces,  $\delta_{MPC} > 115 \mu m$ , the present values of  $h_{NB}$  are significantly higher than other surfaces at low and high surface heat flux. For example, at heat flux of  $15 W/cm^2$ , the  $h_{NB}$  of PF-5060 on  $230 \mu m$  thick MPC is 30 % and 83 % higher than the  $h_{NB}$  of FC-72 liquid on microporous Copper (MPC) (Kim, J.H., 2006) and porous Graphite (PG) (El-Genk and Parker, 2008) surfaces. These values increased to 77% and 144% when  $171 \mu m$ -thick MPC is compared to microporous Cu and PG surfaces at the same heat flux.(Figure 5.12).

Figure 5.12a and 5.12b show the effect of  $\delta_{MPC}$ , and inclination angle on the  $h_{MNB}$  (Figure 5.12a) and the corresponding surface superheats at which  $h_{MNB}$  occurs (Figure 5.12b). For all inclination angles, the  $h_{MNB}$  increases with increasing  $\delta_{MPC}$  up to  $171 \mu m$  and then decreases for thicker surfaces. The value of  $h_{MNB}$  is the highest in the upward facing orientation and decreases with increasing inclination angle. It decreases slowly from upward facing ( $\theta = 0^\circ$ ) up to vertical orientation ( $\theta = 90^\circ$ ), and then decreases at a higher rate with further increase in the inclination angle to the lowest value in the downward facing orientation ( $\theta = 180^\circ$ ) (Figure 5.12). The surface superheats at  $h_{MNB}$  occurs, decreases slowly from upward facing to the vertical orientation and faster as the inclination angle increases to that for the downward facing orientation ( $\theta = 180^\circ$ ).

The presented results show that MPC surface significantly enhance nucleate boiling heat transfer compared to plane Copper surfaces mostly by increasing the active site for bubble nucleation. This depends on surface morphology of the MPC surfaces, which varies with thickness and so is the degree of enhancement. To examine the effect of surface morphology on enhancing nucleate boiling, in the next section the transient

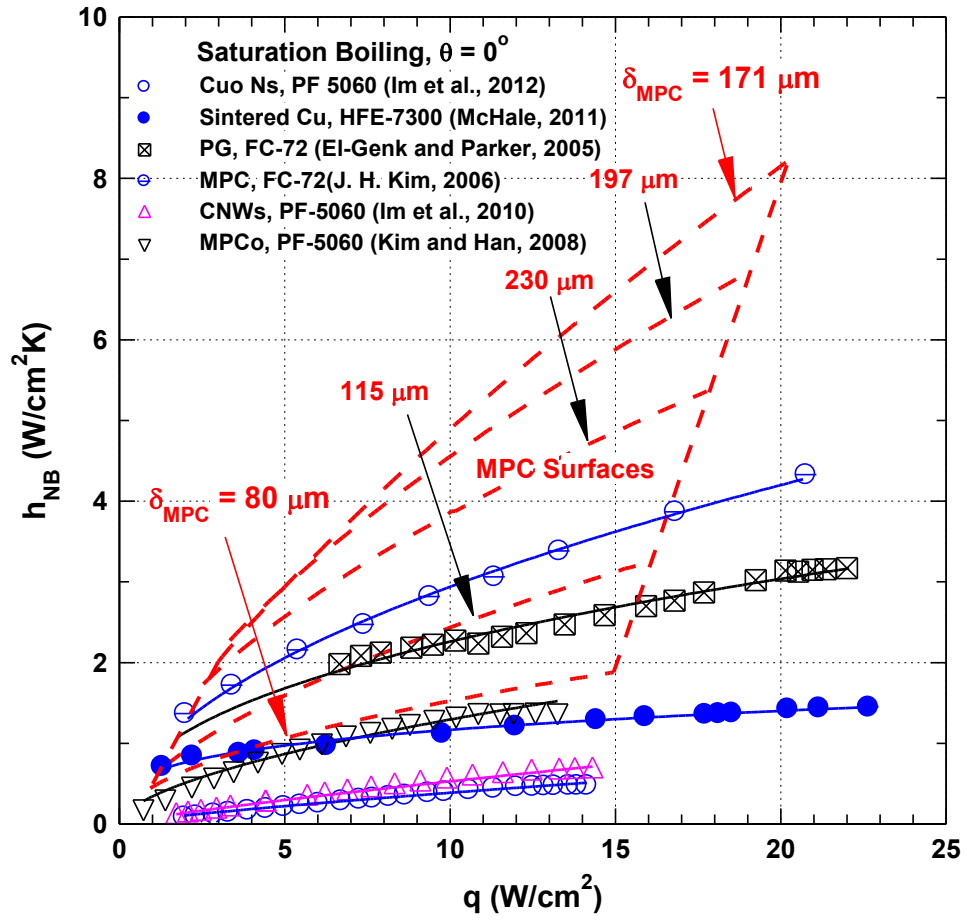


Figure 5.11 Comparison of present values for  $h_{NB}$  of PF-5060 on MPC with those reported for PF-5060 and other dielectric liquids on micro-structured, microporous coating, and other MPC surfaces.

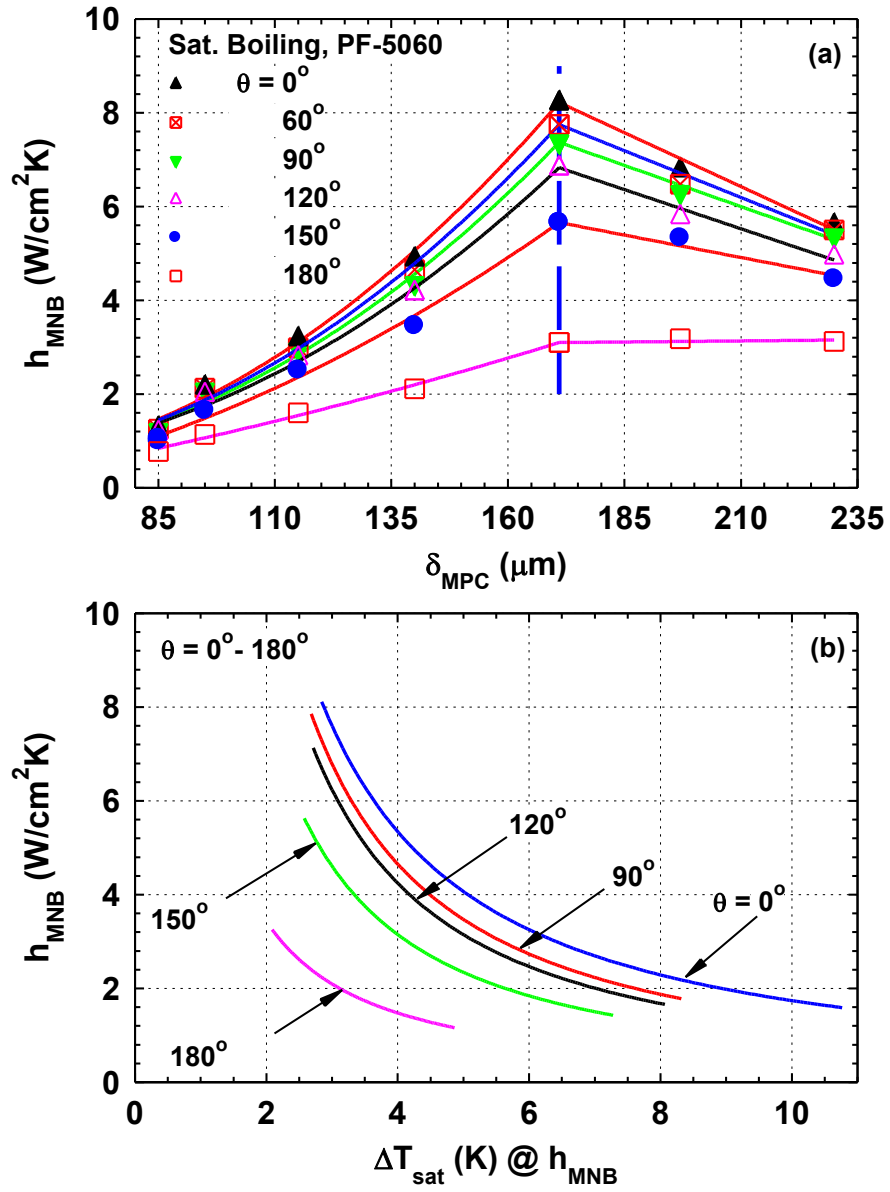


Figure 5.12 Present values of  $h_{MNB}$  for saturation boiling of PF-5060 on MPC surfaces at different inclinations.



growth of discrete bubbles on various MPC surfaces is recorded using high speed CD camera at 210 frames/seconds. The results are used to determine the values of bubble departure diameter and detachment frequency of discrete bubbles as well as estimate the surface average density of active nucleation sites, as a function of surface superheats.

## 5.6 Transient Bubble Growth

Figure 5.13 shows pictures of discrete bubbles on the 80  $\mu\text{m}$ -thick MPC surface at different stage of growth. These photographs are taken with a speed of 210 frame/s camera at an applied heat flux of 0.45-0.5  $\text{W}/\text{cm}^2$ . Because of the modest recording speed, it was not possible to capture images of the growing bubbles earlier than 4.717 ms.

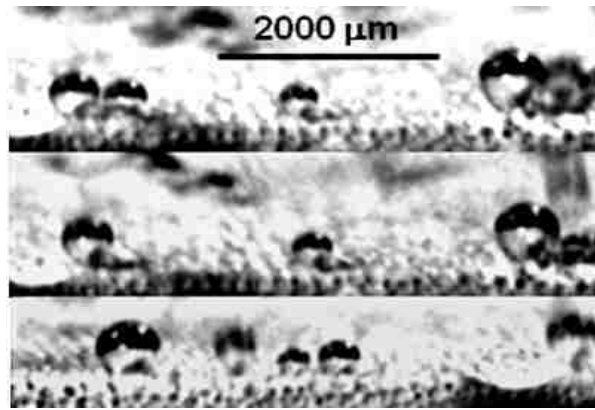


**Figure 5.13 Photographs growing bubbles at discrete sites on 80  $\mu\text{m}$ -thick MPC during saturation boiling of PF-5060.**

Figure 5.14a and 5.14b show a sequence of photographs of the transient growth of a discrete bubble on MPC surfaces with  $\delta_{\text{MPC}} = 115 \mu\text{m}$  and  $140 \mu\text{m}$ . The time  $t_b = t_o$ , is when recording of the bubble growth transient begins and the last frames of the bubble in Figure 5.14 are just prior to departure. The bubble departure actually occurs later within less than a frame, or 4.761 ms. The transient growth of the bubble and the determination of its departure diameter and detachment frequency are based on the recordings of 3-5 ebullition cycles, at some sites on the surface.

Figure 5.15a-5.15d compares the diameters of the growing discrete bubbles on four different MPC surfaces in upward facing orientation ( $\theta = 0^\circ$ ). On each MPC surface, the bubble diameter increases proportional to the square root of the time growth,  $\sqrt{t_b}$ . These results are consistent with the data reported in the literature for thermally driven bubble

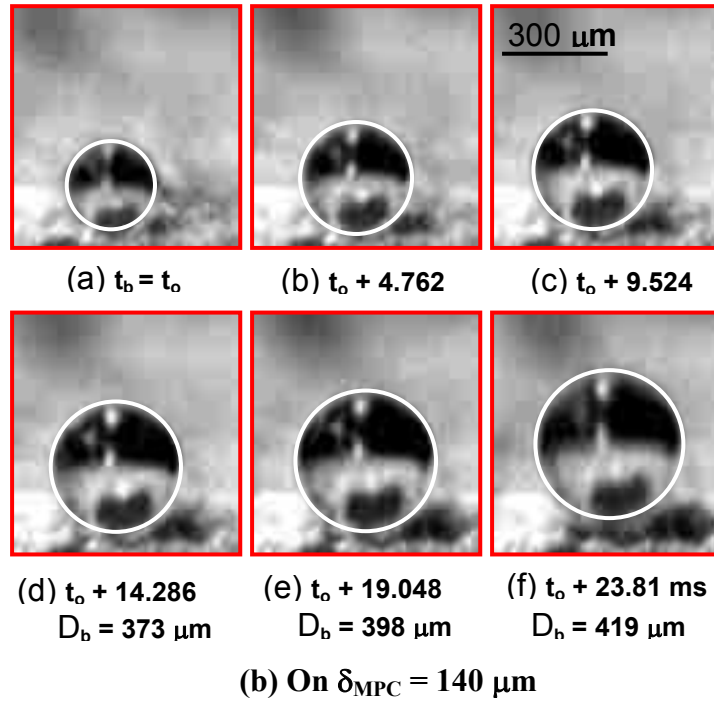
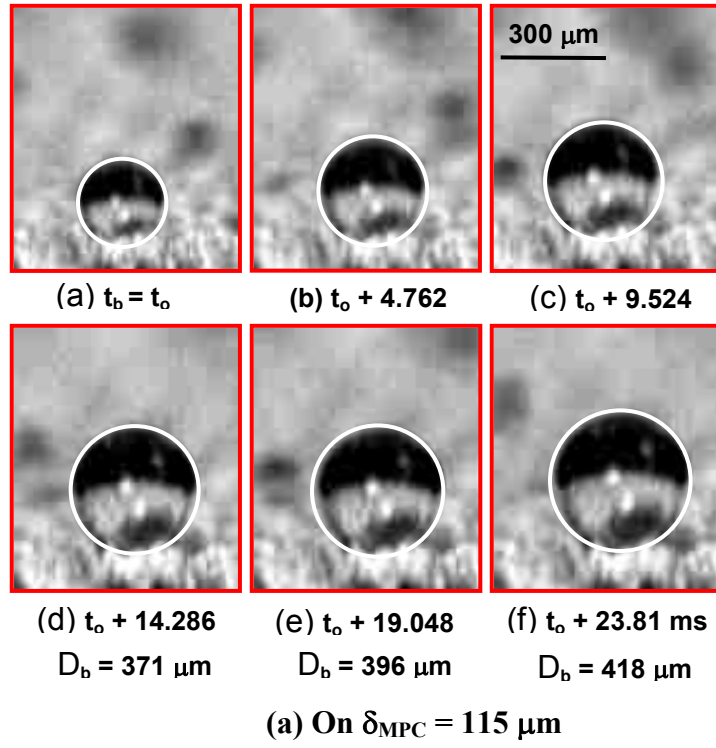


**Figure 5.14 Transient Growth Images of discrete bubble in saturation boiling of PF-5060 on MPC surfaces in the upward facing orientation.**

growth (Rini, Chen and Chow, 2001; Zuber, N., 1963, 1959). In Figure 5.15a-d, for the departure diameter, the growth time,  $t_b$ , is increased a half of frame or 2.381 ms. The calculated departure diameter,  $D_d$ , and the corresponding bubble growth time,  $t_d$ , for each MPC surfaces are indicated by the dash lines in Figures 5.15a-5.15d.

Figure 5.16 presents the obtained data for transient bubble growth on the present MPC surfaces. The bubble growth is independent of the thickness of the MPC surface but increases with time,  $t_b$ , as.

$$D_b = 0.21 + 0.043 t_b^{0.5} \quad (5.4)$$

This correlation fits the data in Figure 5.16 to within  $\pm 5\%$ . The calculated determined bubble departure diameter and detachment frequency on five MPC surfaces are presented in Figures 5.17a and b. For each MPC surface, the bubble departure diameter and bubble departure frequency is presented for not less than 5 discrete bubbles. The values of the bubble departure diameter and detachment frequency in Figure 5.17a and b independent of the thickness of the MPC surfaces and consistent to within  $\pm 8\mu\text{m}$  and  $\pm 2\text{ Hz}$ , respectively.

El-Genk and Bostanci (2003) have measured the average bubble departure diameter in saturation HFE-7100 on plane Cu at 0.085 MPa to be 550  $\mu\text{m}$ . In saturation boiling of FC-72 dielectric liquid at 0.1 MPa, Rini et al. (2001) reported a departure bubble diameter of 400-500  $\mu\text{m}$ . Hutter et al. (2010) reported an average detachment diameter of the same liquid on a silicon chip of 200-1000  $\mu\text{m}$ , depending on the wall superheat. The thermophysical properties of FC-72 and PF-5060 are the same, except the surface tension of PF-5060 is 20% higher than for FC-72 (10 N/m for FC-7s, 12 N/m for PF-5060). It would be expected that at the same system pressure and surface superheat, the bubble detachment diameter increase as the liquid surface tension increased.

The measured bubble departure diameter and release frequency, for saturation boiling of PF-5060 at 0.085 MPa, are used to estimate the active nucleation site density on the present MPC surfaces. Figure 5.18 plots the estimate of surface average density of active nucleation sites in saturation boiling of PF-5060 dielectric liquid on the present MPC surfaces versus Jacob number ( $Ja$ ). These results are for the fully developed nucleate boiling region. The surface average density of active nucleation sites on MPC surfaces of different thickness ranges from 1000-10000 sites/ $\text{cm}^2$  compared to 300-1000 sites/ $\text{cm}^2$  for

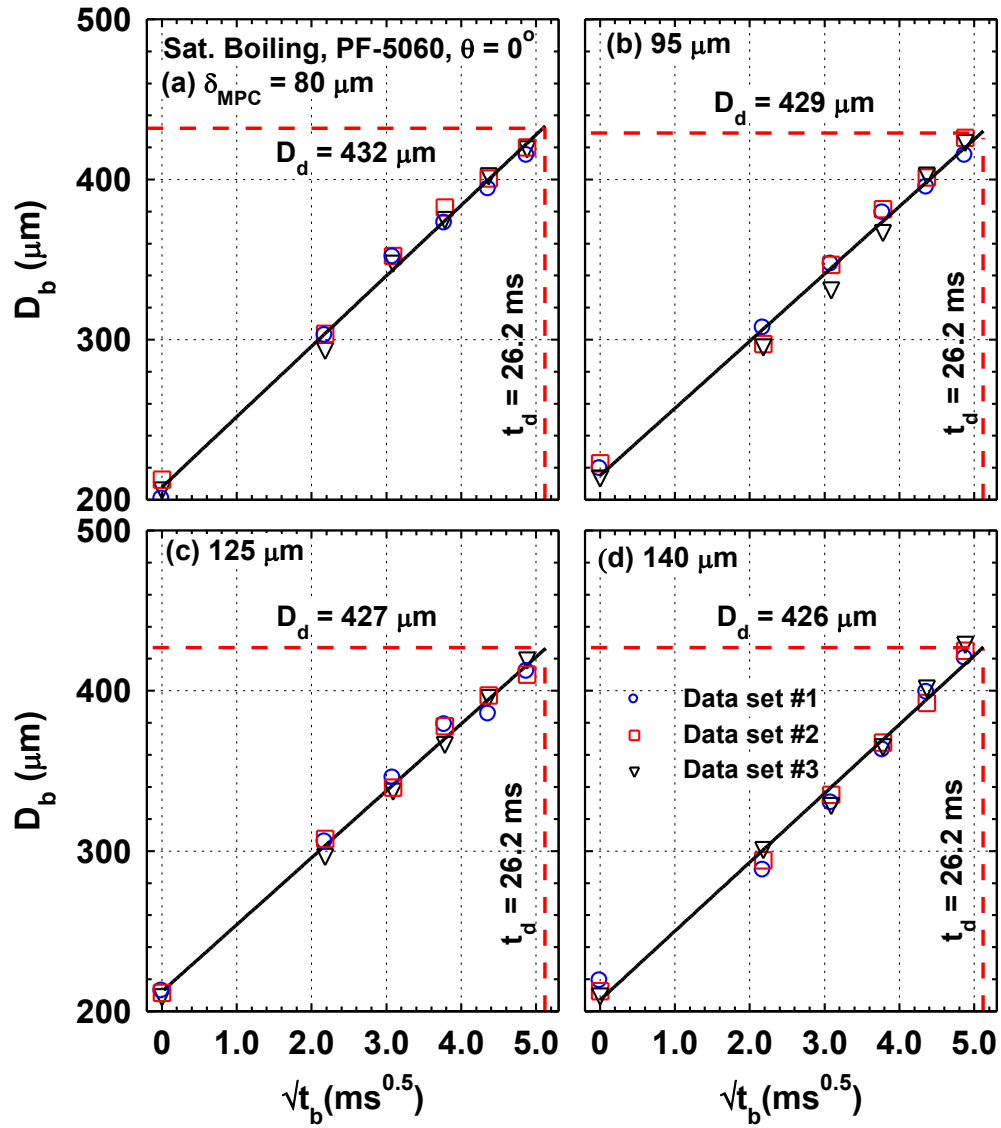


Figure 5.15 Bubbles diameter during transient growth in saturation boiling of PF-5060 on Upward Facing on MPC surfaces in the upward facing orientation.

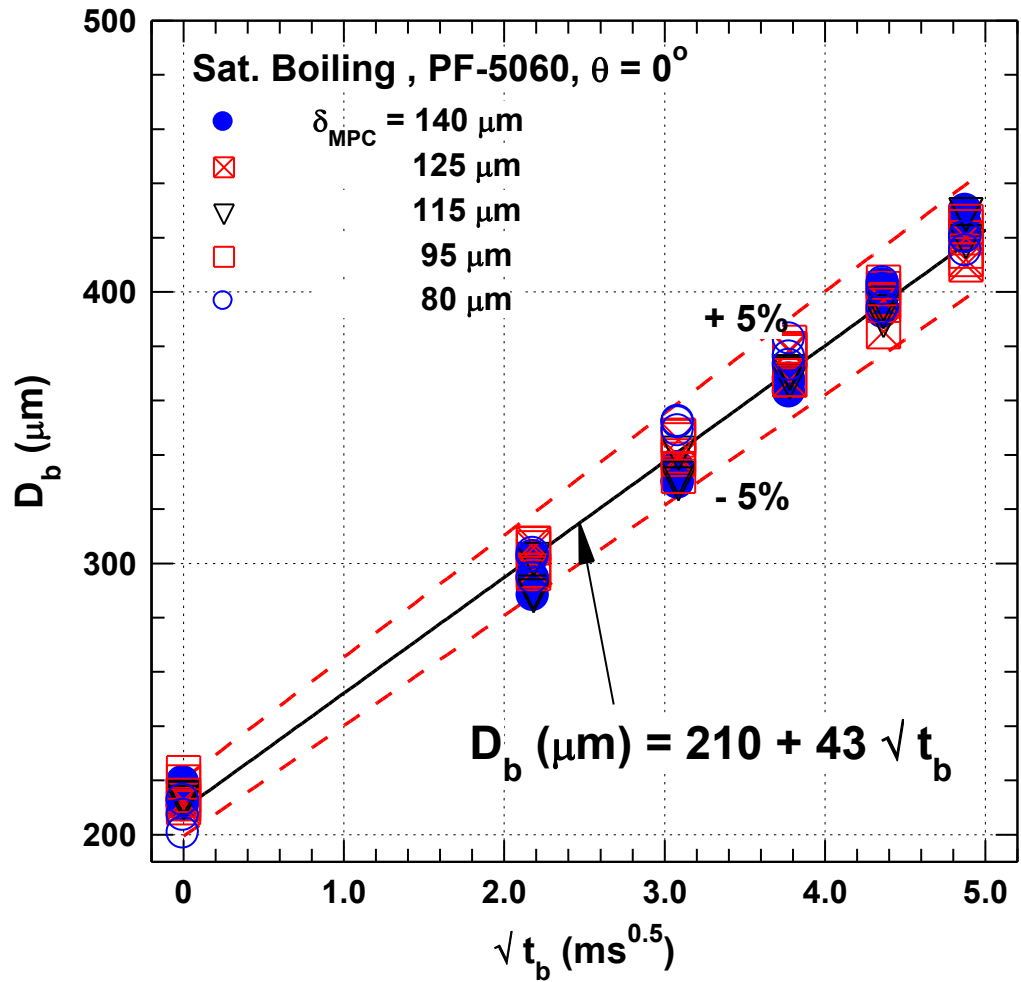


Figure 5.16 Bubbles transient growth diameter in saturation boiling of PF-5060 on MPC surfaces in the upward facing orientation.

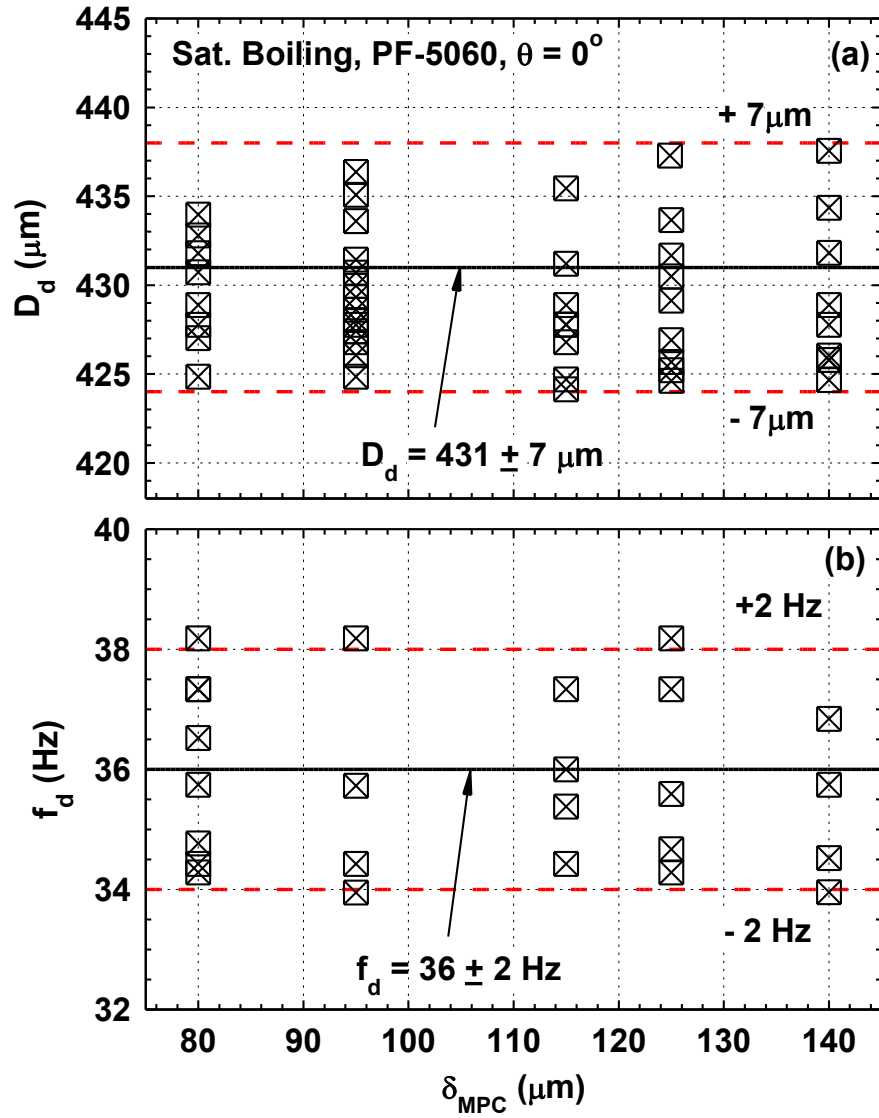


Figure 5.17 Bubble departure diameter and detachment frequency in saturation boiling of PF-5060 on MPC surfaces in the upward facing orientation.

FC-77 dielectric liquid on surfaces covered with sintered copper particles (McHale and Garimella, 2010). Nimkar et al. (2006) have also measured the bubble departure diameter and detachment frequency in saturation boiling of FC-72 at 0.1 MPa on surface with micro-cavities. They estimated the density of active site of  $\sim 2000$  sites/cm<sup>2</sup> and independent on the surface superheat (Figure 5.18).

## 5.7 Summary and Conclusion

This chapter presented and discussed the results of saturation boiling of PF-5060 dielectric liquid experiments on MPC surfaces at different inclination angle. The MPC surfaces that are 80, 95, 140, 171, 197, 230  $\mu\text{m}$ -thick are investigated in saturation boiling at nine inclination angles of 0° (upward facing), 30°, 60°, 90° (vertical), 120°, 150°, and 180° (downward facing). The experimental results presented and discussed in this chapter are for degassed PF-5060 liquid and conditioned MPC surfaces. Conditioning the MPC surfaces is accomplished by conducting 4-6 pool-boiling experiments, separated by duration of 2 or more hours, at the same conditions. The pool boiling curves for the conditioned MPC surfaces are almost identical with no boiling hysteresis. The temperature excursion prior to boiling incipience on the MPC surfaces is either absent or  $< 5$  K.

In upward facing orientation increasing MPC surface thickness from 80 $\mu\text{m}$  to 230  $\mu\text{m}$  showed to increase CHF, while the fully developed nucleate boiling heat transfer coefficient,  $h_{\text{NB}}$ , showed to increase up to 171 $\mu\text{m}$  and decreases with further increase in the thickness. The highest values of the nucleate boiling heat transfer coefficient,  $h_{\text{MNB}}$ , from the slope of the pool boiling curves, occurs at the end of the fully developed nucleate boiling region. This is when all potential sites for bubble nucleation on the surface are active. In upward facing orientation, the present values of  $h_{\text{MNB}}$  (7.8 W/cm<sup>2</sup> K) is the highest representing a 10 folds increase compared to those on smooth polished Copper ( $\sim 0.78$  W/cm<sup>2</sup> K). The present values of  $h_{\text{NB}}$  are correlated in terms of the surface heat flux as:  $h_{\text{NB}} = A q^{\text{B}}$ . The coefficient “A” and exponent “B” are functions of the thickness of MPC surfaces. The developed correlation for  $h_{\text{NB}}$  in the upward facing orientation as function of the MPC surface thickness is within  $\pm 10\%$  of the present experimental measurements.

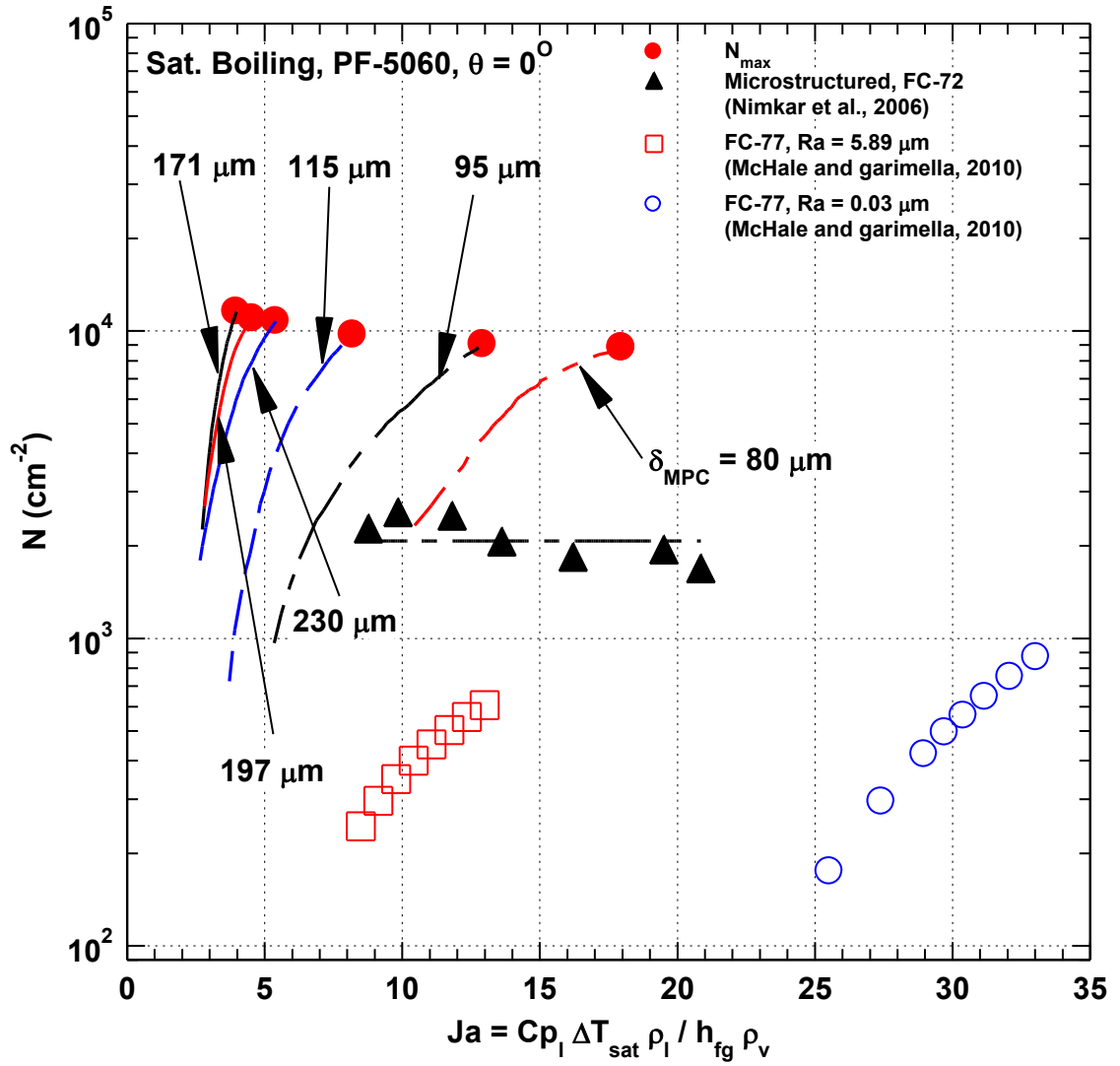


Figure 5.18 Comparison of the surface average density of active nucleation sites in saturation boiling of PF-5060 on MPC, FC-77 on Aluminum, and FC-72 on Silicon surfaces.



Transient growth of vapor bubbles on MPC surfaces (80, 95, 115, 125, and 140  $\mu\text{m}$  thick) are recorded for a several ebullition cycles. The growth is proportional to the square root of time, confirming that the bubbles are in the thermal growth stage. The developed correlation for the transient growth of the bubbles is in a good agreement with the measurements to within  $\pm 5\%$ . Determined bubble departure diameter,  $D_d$ , and detachment frequency,  $f_d$ , for saturation boiling of PF-5060 dielectric liquid in the upward facing orientation are independent of surface morphology. The determined values of  $D_d = 431 \pm 7 \mu\text{m}$  and  $f_d = 36 \pm 2 \text{ Hz}$  are used to calculate the surface average density of active nucleation site. It ranges from 1000-10000 sites/ $\text{cm}^2$  compared to 300-1000 sites/ $\text{cm}^2$  for FC-77 on rough Aluminum surfaces.

Results on the effect of MPC surface thickness,  $\delta_{\text{MPC}}$ , and surface orientation angle,  $\theta$ , on CHF in saturation boiling of PF-5060 liquid are presented and discussed in the next chapter.

## 6. Saturation Boiling Critical Heat Flux

This chapter presents and discusses the effect of inclination angle,  $\theta$ , and the MPC surface thickness,  $\delta_{MPC}$ , on saturation CHF of degassed PF-5060 dielectric liquid on conditioned MPC surfaces, 80, 95, 140, 171, 197, 230  $\mu\text{m}$ -thick at nine inclination angles of  $0^\circ$  (upward facing),  $30^\circ$ ,  $60^\circ$ ,  $90^\circ$  (vertical),  $120^\circ$ ,  $150^\circ$ , and  $180^\circ$  (downward facing). The measured CHF values are correlated in terms of the inclination angle and thickness of MPC surfaces.

### 6.1 Effect of MPC thickness

Figures 6.1a and b compare the obtained saturation pool boiling curves for PF-5060 liquid on the 85 and 230  $\mu\text{m}$ -thick MPC surfaces at inclination angles of  $0^\circ$ ,  $60^\circ$ ,  $90^\circ$ ,  $120^\circ$ ,  $150^\circ$ , and  $180^\circ$ . The last data point in the nucleate boiling curve indicates CHF, condition determined as described previously in the experimental procedure. Increasing the thickness, increases CHF values and decreases the corresponding surface superheat decrease. This trend is detected by comparing the pool boiling curves in Figures 6.1a and b, for two different MPC surface thicknesses at different inclination angles.

The magnitudes of CHF on the MPC surfaces are much higher and occur at much lower surface superheats than on plane Cu (Figure 5.6a). In the upward facing orientation, the CHF values range from 22.4 to 26.2  $\text{W}/\text{cm}^2$  for MPC thickness ranges from 80  $\mu\text{m}$  to 230  $\mu\text{m}$  (Figure 6.2a) compared to  $\sim 16 \text{ W}/\text{cm}^2$  CHF on plane Copper surface (Figure 5.1). For the same range of  $\delta_{MPC}$ , the surface superheat,  $\Delta T_{\text{sat}}$ , at CHF ranges from 4.6 to 15 K (Figure 6.2b) compared to 25 K on plane Cu (Figure 5.6a). The present experimental CHF values in the upward facing orientation are correlated as a function of  $\delta_{MPC}$  with within  $\pm 4\%$  (Figure 6.2a). The surface superheats at CHF are also correlated in term of MPC thickness within  $\pm 12\%$  (Figure 6.2b). For all MPC surfaces investigated in this work, increasing the inclination angle decreases CHF and the corresponding surface superheat. The effect of inclination angle on CHF is presented and discussed next.

### 6.2 Effect of inclination angle

Previously reported work on the effect of inclination angle on CHF of dielectric

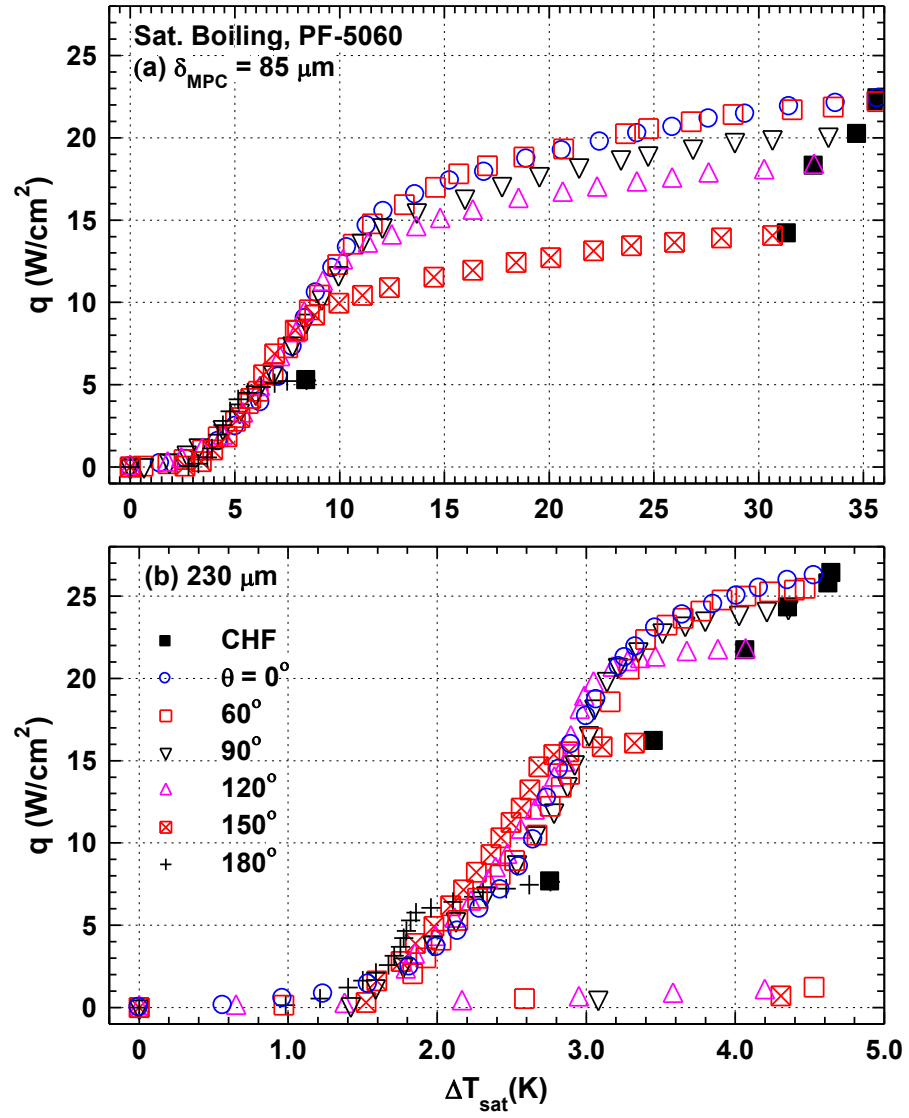


Figure 6.1 Effect of inclination on saturation boiling CHF on MPC surfaces of different thickness at different inclination angles.

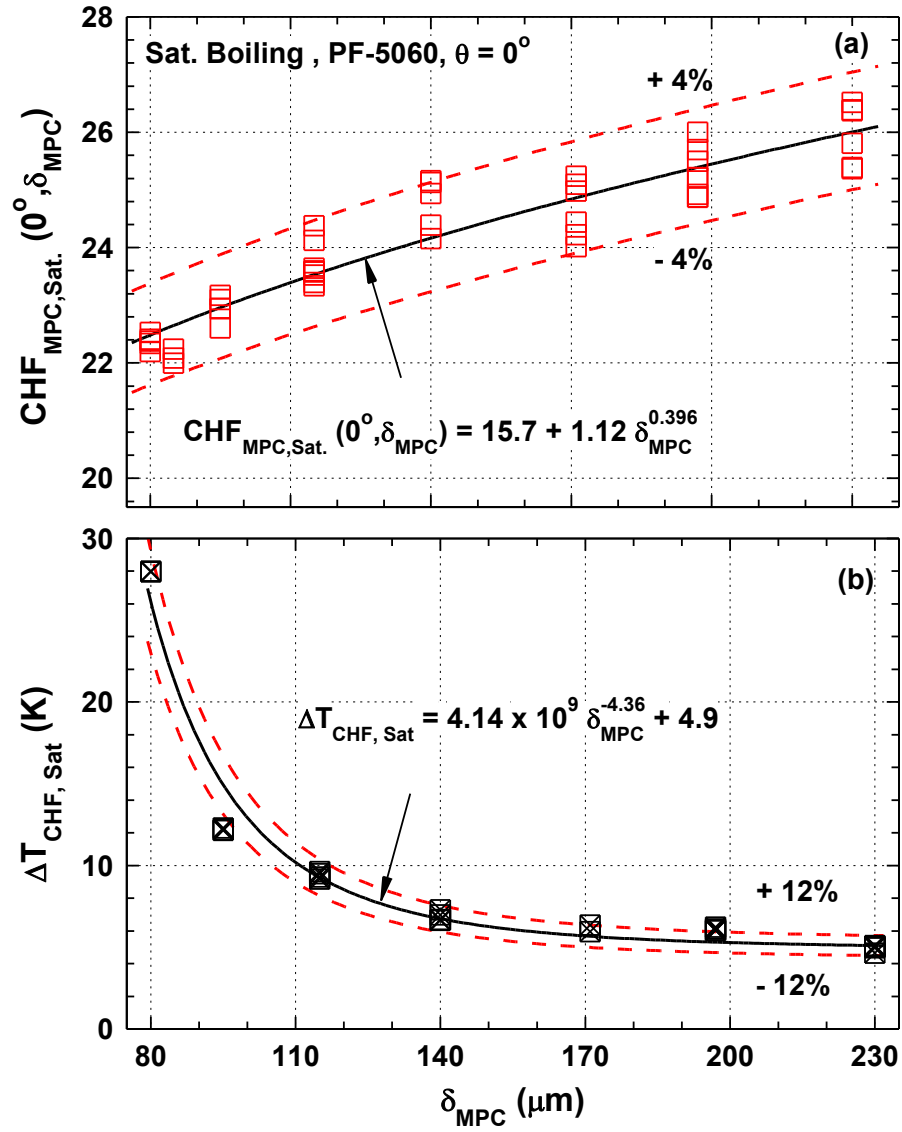


Figure 6.2 Dependence of saturation boiling CHF, and  $\Delta T_{\text{sat@CHF}}$  on the thickness of MPC surfaces in the upward facing orientation.

liquids showed the highest values occur at upward facing ( $\theta = 0^\circ$ ). The CHF decreases with increased inclination slowly up to  $90^\circ$  and then much faster beyond  $90^\circ$  to the lowest value in downward facing orientation ( $\theta = 180^\circ$ ) (El-Genk and Parker; 2004a; Parker and El-Genk 2005; Chang and You1996; Reed and Mudawar 1997; Howard and Mudawar 1999; Priarone, 2005; Ali and El-Genk 2011). Despite the induced mixing by rising bubbles on inclined surfaces, the increased accumulation of the vapor in the boundary layer increases the resistance to the heat transfer and triggers CHF earlier than in the upward facing orientation. In the downward facing orientation, the growing bubbles coalesce into large globules that extend sideways along the surface. Vapor released at the edges of test section stimulates liquid upward flow from the pool toward the heated surface, flattening the vapor globules and limiting their growth downward. The vapor release, followed by accumulation, then the release occurs cyclically until CHF (El-Genk and Parker, 2008; El-Genk and Ali, 2012; Ali and El-Genk, 2013).

The results in Figure 6.3 show the effects of inclination angle and MPC thickness on saturation boiling CHF of PF-5060 liquid. For reference this figure also presents the measured CHF values versus the inclination angle for smooth Cu surface with an average roughness of  $0.039 \mu\text{m}$ . The CHF values on these surfaces are different, but decrease slowly with increasing inclination angle up to  $90^\circ$  (vertical), and then decrease faster with further increase in inclination angle. CHF values are lowest in the downward facing orientation ( $\theta = 180^\circ$ ). CHF increases with increasing the thickness of the MPC surface, but the magnitude of the increase decreases with increasing inclination angle (Figure 6.3). The values for saturation boiling of PF-5060 liquid on MPC are consistently higher than on smooth plane Copper surface. The CHF on the  $230 \mu\text{m}$ -thick MPC surface in the upward facing orientation is  $\sim 20\%$  higher than on the  $85 \mu\text{m}$ -thick surface and  $\sim 67\%$  higher than on smooth Cu (Figure 6.3).

The present results show that the CHF values for saturation boiling of PF-5060 on MPC surfaces are high and the corresponding surface superheats are significantly lower than plane Cu. To further quantify the enhancement in CHF for saturation boiling of PF-5060 on MPC surfaces, the measured values in upward facing orientation are compared in Figure 6.4 to those reported in the literature on other surfaces. These include microporous coated (MPCo), micro wired (MWs), nano finned (NF) silicon,

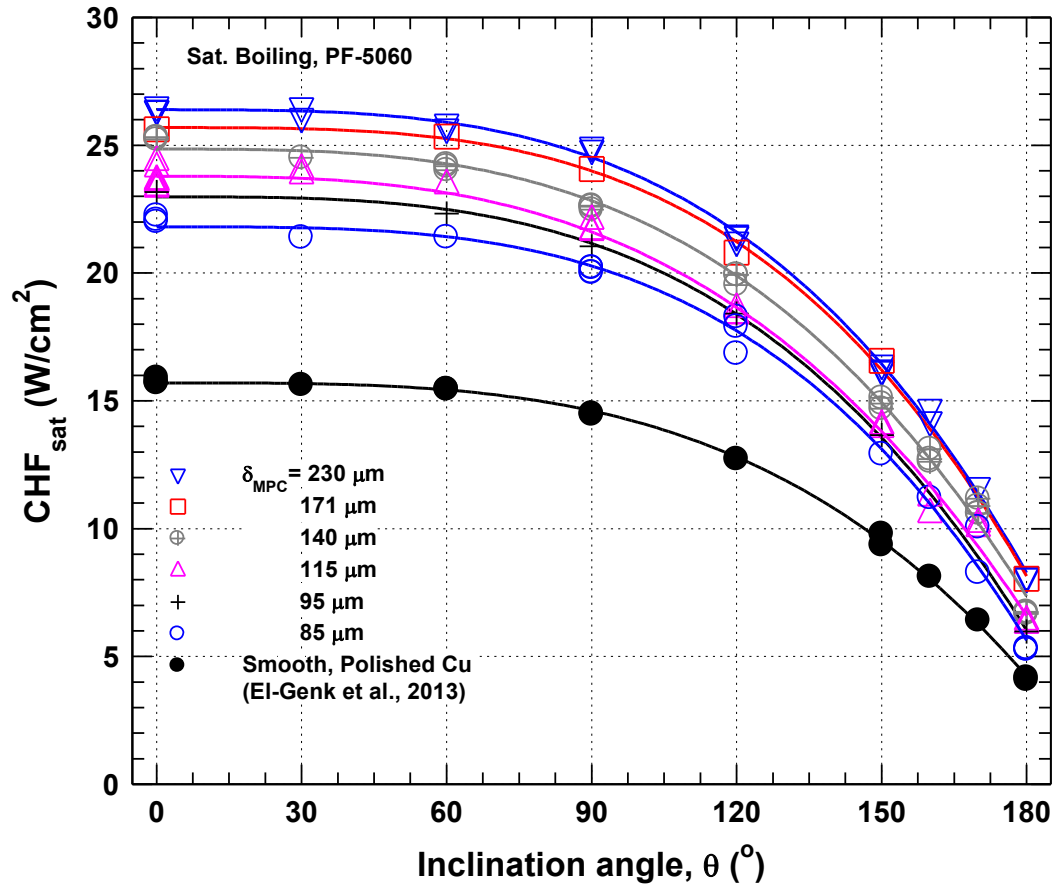


Figure 6.3 Effect of inclination angle on saturation boiling CHF of PF-5060 on different thickness MPC surfaces.

nano-structured (NS) Cu, and plane Copper and silicon surfaces (e.g., Ghiu and Joshi, 2005; Im, Lee, and Joshi, 2012; Im, Joshi, Dietz, and Lee, 2010; Gerlash, and Joshi, 2005; Sriraman and Banerjee, 2007; Kim and Han, 2008; El-Genk, Suszkoo and Ali, 2013 ). The reported values of CHF on these surfaces are 38% - 91% of the present values on MPC, and the corresponding surface superheats, which vary from 17 K to 42 K, are also higher than on the present MPC surface ( $< 15$  K). The present values of  $\Delta T_{sat}$  at CHF correspond to a surface temperature  $< 66.5$  K, which are significantly lower than recommended for the chip junctions' temperature recommended by the industry ( $< 85$  °C). Compared to plane Copper, the value of  $\Delta T_{sat}$  at CHF on MPC surface are 36%-67% higher (depending on MPC thickness) (Figure 6.4).

Still photographs of saturation nucleate boiling near CHF are recorded on different MPC surfaces and on plane Copper (Figure 6.5). Near CHF the boiling images on smooth Copper and MPC surfaces of different thickness ( $\delta_{MPC} = 95\text{-}230$   $\mu\text{m}$ ) are quite similar. However, CHF is lowest on smooth Copper and increases with increasing the MPC thickness surface. Conversely, the surfaces superheats at CHF on smooth copper are the highest and decrease with increasing the thickness of MPC surface. The present CHF values on MPC surfaces at different inclinations are presented and correlated next.

### 6.3 Critical heat flux correlation

The values of CHF on MPC surfaces (80-230  $\mu\text{m}$ -thick) at inclination angles from  $0^\circ$  (Upward facing) to  $180^\circ$  (Downward facing) are correlated using an expression similar to the developed independently by Kutateladze (1952) and Zuber (1959), recently confirmed for dielectric and dielectric liquids (El-Genk and Bostanci, 2003; El-Genk and Parker, 200x; El-Genk and Ali, 2012; Ali and El-Genk, 2013) as:

$$CHF_{MPC,sat}(\theta, \delta_{MPC}) = C_{MPC,sat}(\theta, \delta_{MPC}) (\rho_v^{0.5} h_{fg} [\sigma g(\rho_l - \rho_v)]^{0.25}) \quad (6.1)$$

The liquid and vapor properties, ( $h_{fg}$ ,  $\sigma$ ,  $\rho_l$ ,  $\rho_v$ ) in this correlation are evaluated at the saturation temperature. The coefficient  $C_{MPC,sat}(\theta, \delta_{MPC})$  on the right hand side of this correlation depends on the thickness and inclination angle of the MPC surface. For other surfaces, this coefficient had been shown to depend on the surface characteristics (morphology, porosity, microstructure and material properties) and the dielectric liquid

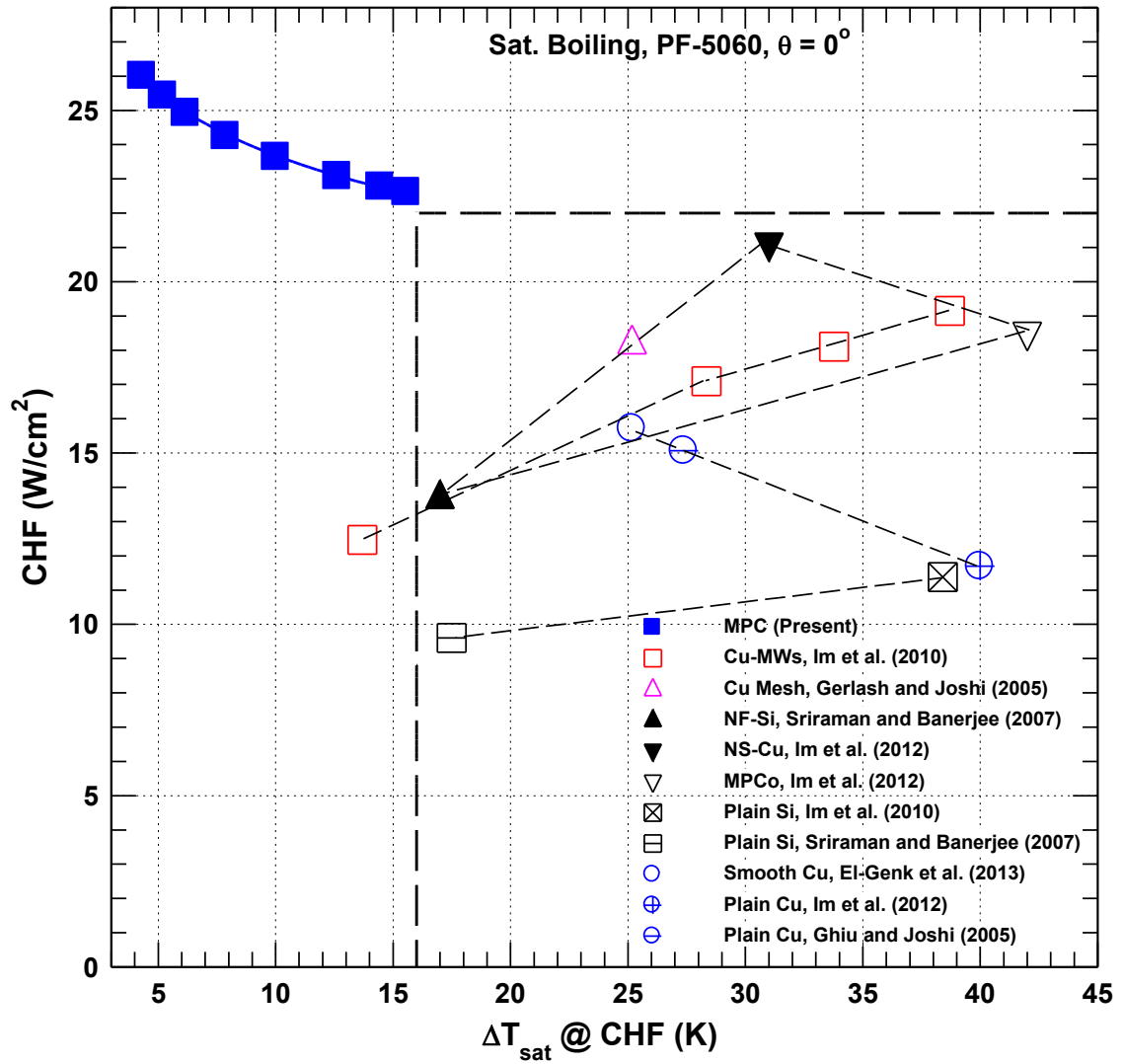


**Figure 6.4 Comparison of saturation boiling CHF of PF-5060 dielectric liquid and the  $\Delta T_{\text{sat}}$  on MPC surfaces with reported values on other surfaces.**



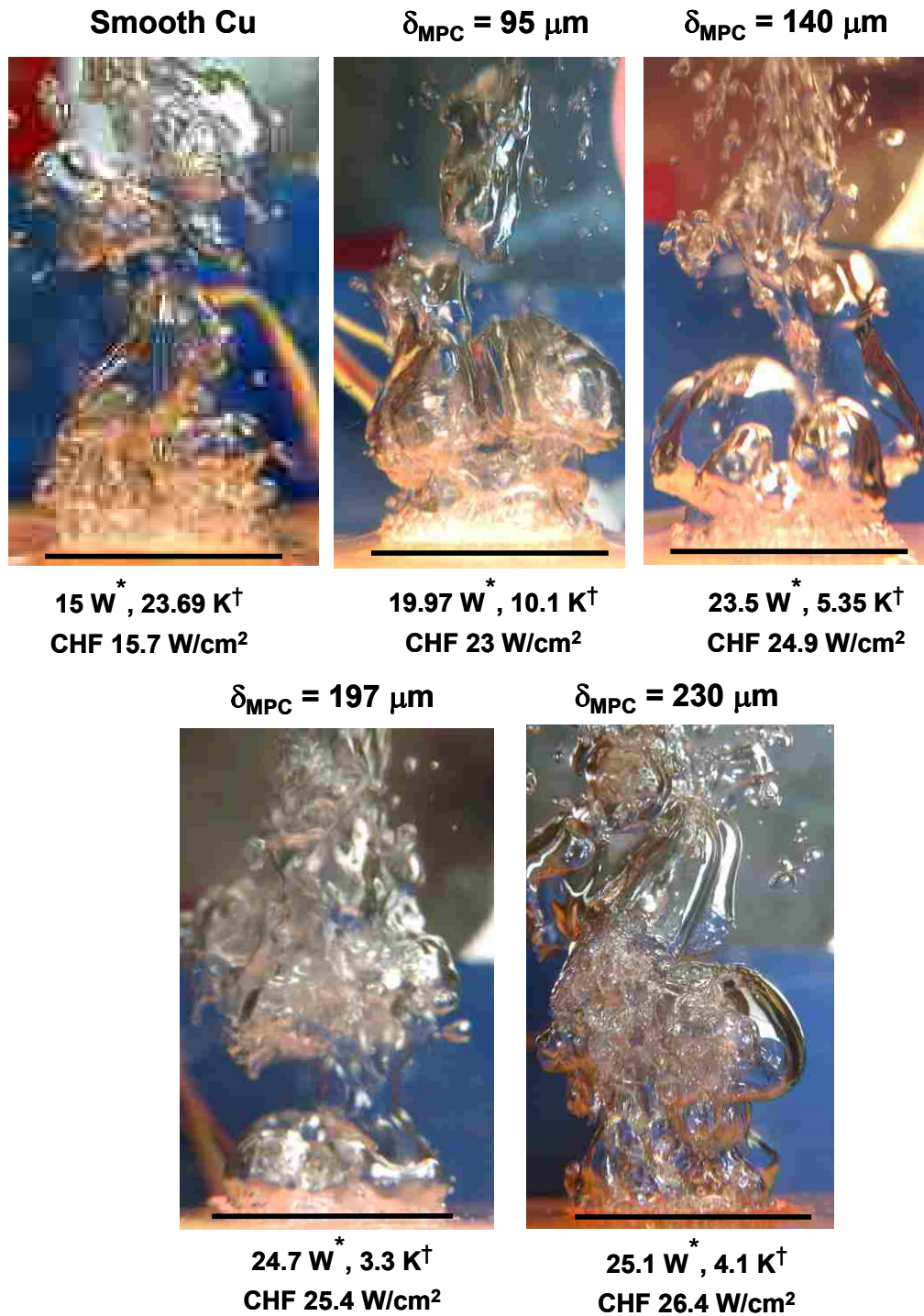


Figure 6.5 Still photographs of saturation boiling of PF-5060 near CHF on smooth and MPC surfaces in the upward facing orientation (\* applied heat flux, † corresponding  $\Delta T_{\text{sat}}$ ).

and none dielectric liquids properties (Chang and You, 1996,1997 El-Genk and Bostanci, 2003a; Priarone, 2005, El-Genk and Parker 2005; Ali and El-Genk 2012).

For the present MPC surfaces, the coefficient on the right hand side of Equation 6.1 can be expressed as:

$$C_{MPC,sat}(\theta, \delta_{MPC}) = C_{MPC,sat}(0^\circ, \delta_{MPC}) R_{MPC}(\theta) \quad (6.2)$$

The first term on the right hand side of Equation 6.2,  $C_{MPC,sat}(0^\circ, \delta_{MPC})$ , is the CHF coefficient for saturation boiling in the upward facing orientation ( $\theta=0^\circ$ ) which represents the effect of surface characteristics. It is correlated in terms of the thickness of MPC surface (Figure 6.6) as:

$$C_{MPC,sat}(0^\circ, \delta_{MPC}) = 0.1486 + 0.0083 \delta_{MPC}^{0.431} \quad (6.3)$$

This expression is within  $\pm 4\%$  of the current experimental values on MPC surfaces (figure 6.6). Multiple experiments conducted with conditioned MPC surfaces improved the statistics of the CHF and CHF coefficient values in the upward facing (Figures 6.2 and 6.6). The values on MPC surfaces are much higher than those recommended by Kutateladze (1952) and Zuber (1959) for water and other organic liquids on metal surfaces of different geometries and surface finish. They are also different, but consistent with those reported for saturation pool boiling of FC-72 and HFE-7100 on porous graphite and surface with microporous coatings (Raieny and You, 2001; El-Genk and Bostanci, 2003a; Priarone, 2005; El-Genk and Parker, 2008).

The second term on the right hand side of Equation 6.2,  $R_{MPC}(\theta)$ , represents the effect of surface inclination angle,  $\theta$ , on saturation boiling CHF of PF-5060 on MPC surfaces. This terms correlated based on the present CHF values, is similar to those reported for dielectric liquids, such as FC-72 and HFE-7100 on various surfaces (Chang and You, 1996; El-Genk and Bostanci, 2003a; Priarone, 2005; El-Genk and Ali, 2012; Ali and El-Genk, 2013). These include CHF for saturation boiling of FC-72 on plane copper (Priarone, 2005) and micro-porous coatings (Chang and You, 1996), saturation boiling of HFE-7100 liquid on plane Copper (El-Genk and Bostacni, 2003, Priarone, 2005), porous graphite (El-Genk and Parker 2004), and PF-5060 on MPC surfaces (El-Genk and Ali, 2012; Ali and El-Genk, 2013).

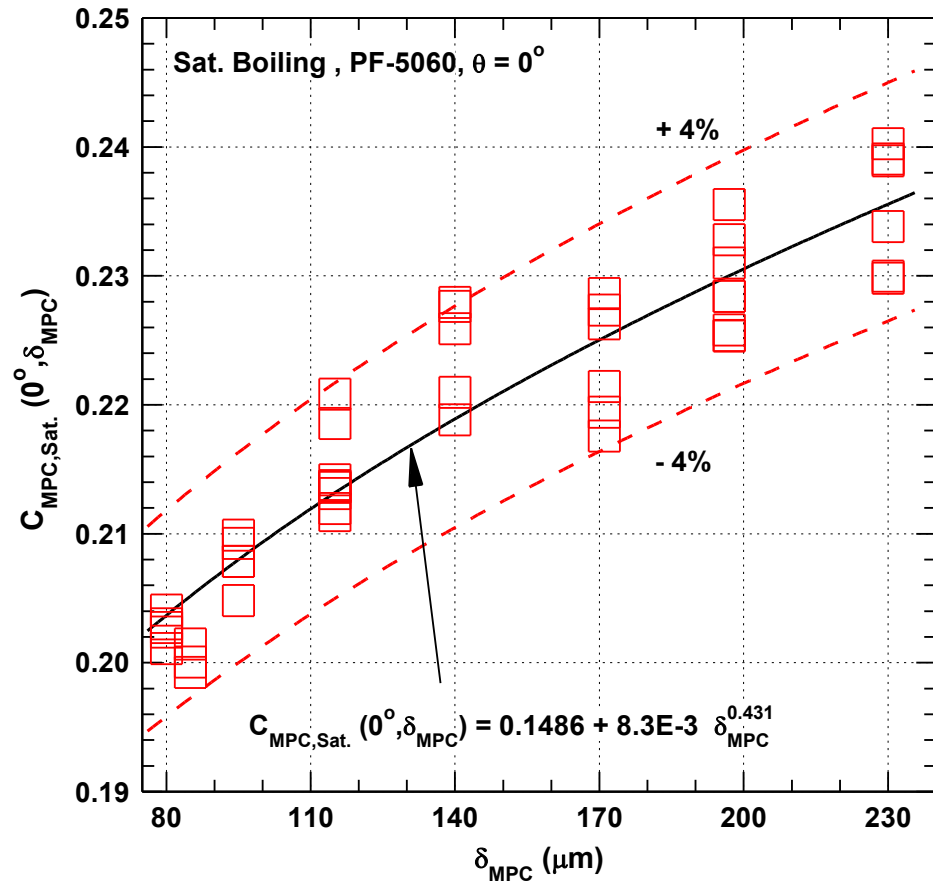


Figure 6.6 CHF coefficient for Saturation boiling of PF-5060 dielectric liquid on MPC surfaces in the upward facing orientation.

The normalized CHF values at different inclination angle to that in the upward facing orientation ( $\theta = 0^\circ$ ) were correlated as follows:

Chang and You (1996):

$$R(\theta) = [1 - 0.0012 \theta \tan(0.414 \theta) - 0.122 \sin(0.318 \theta)] \quad (6.4a)$$

El-Genk and Bostanci (2003):

$$R(\theta) = \left[ (1 - 0.00127 \theta)^{-4} + (3.03 - 0.016 \theta)^{-4} \right]^{-0.25} \quad (6.4b)$$

Priarone (2005) ( $0^\circ \leq \theta \leq 175^\circ$ )

$$R(\theta) = 1 - 0.001117\theta + 7.79401 \times 10^{-6} \theta^2 - 1.37678 \times 10^{-7} \theta^3 \quad (6.4c)$$

El-Genk and Parker (2005):

$$R(\theta) = \left[ (1 - 0.000796 \theta)^{-4} + (1.8 - 0.00703 \theta)^{-4} \right]^{-0.25} \quad (6.4d)$$

Similarly, to quantify the effect of surface inclination on CHF, Figure 6.7 plots the normalized CHF values to those in the upward facing orientation ( $\theta^\circ$ ),  $R_{MPC}(\theta)$ , versus the inclination angle as:

$$R_{MPC}(\theta) = 1 - 5.0 \times 10^{-8} \theta^{3.17} \quad (6.5)$$

The dependence of  $R_{MPC}(\theta)$  on the inclination angle is almost identical for all surfaces, including plane Copper. The normalized CHF values are within  $\pm 6\%$  from the mean, except for  $\theta > 150^\circ$ ,  $R_{MPC}(\theta)$  values are within  $\pm 15\%$  from the mean (Figure 6.7). For all surfaces, CHF values in the downward facing orientation are  $\sim 28\%$  of the values in the upward facing orientation.

Figure 6.8 compares the present experimental values of CHF for saturation boiling of PF-5060 dielectric liquid on MPC surfaces of different thicknesses at inclination angles from  $0^\circ$  to  $180^\circ$ , versus the calculated by the present correlation (Equations 6.1). The results in Figure 6.8 show that the developed CHF correlation is in a good agreement with the experimental data to within  $\pm 8\%$ . The proposed CHF correlations accounts for the effect of the morphology thickness and inclination angle of MPC surfaces, this is useful tool for industrial applications. In these applications the thermal or heat transfer equipment operate normally at surface heat flux  $\leq 70\%$  of CHF and the heated surface at different orientation angle.

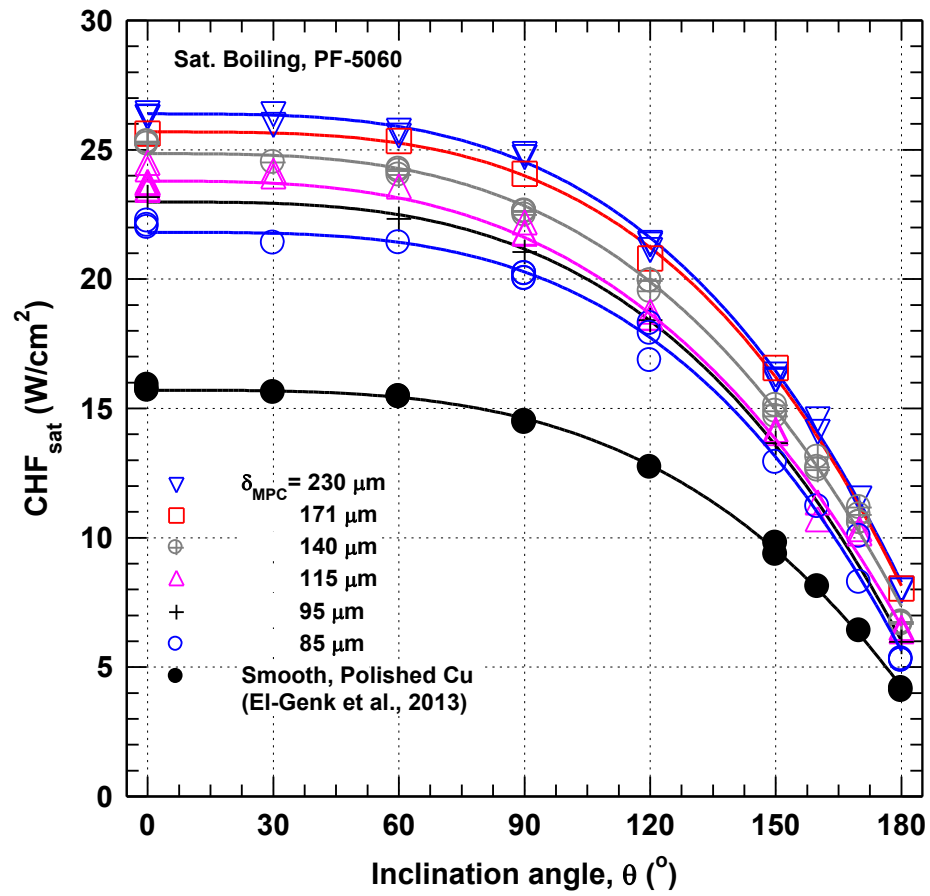


Figure 6.7 Normalized saturation boiling CHF of PF-5060 on smooth Copper and MPC surfaces.

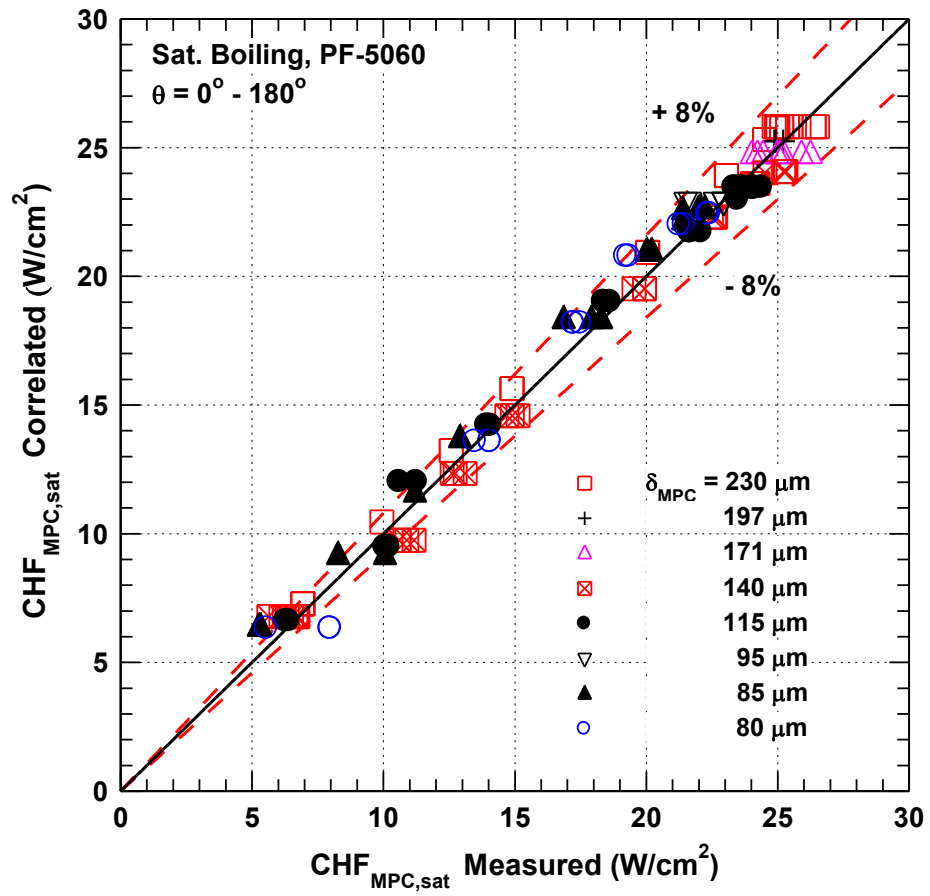


Figure 6.8 Comparison of experimental versus correlated values of saturation boiling CHF of PF-5060 on MPC surfaces at different inclination angle.

In the next chapter, the results on nucleate boiling heat transfer (Chapter 5) and CHF (Chapter 6) are incorporated into a numerical analysis that investigate the potential of using Cu spreaders with MPC surfaces for increasing the total thermal power removed from underlying chip and mitigate the effect of hot spots. The results of the effects of hot spot area and heat flux ratio, and thermal interface material between the underlying chip and the spreader on the total thermal power removed, spreaders foot print area, and the chip maximum temperature are presented and discussed in the next chapter (Chapter 7).

## 7. Composite Spreaders for Immersion Cooling of Computer Chips with Central Hot Spots

This chapter investigates the performance of heat spreaders comprised of Cu substrate and MPC surface of different thicknesses for cooling underlying chip with a central hot spot (Figure 7.1). The analysis quantifies the effect of changing the thickness of the Cu substrate (1.6 to 3.2 mm) and of MPC surface (80-197  $\mu\text{m}$ ) with a given thermal interface material (TIM) ( $0.19\text{ }^{\circ}\text{C}\cdot\text{cm}^2/\text{W}$ ) between the chip and the composite spreaders. The investigated spreaders are for cooling 10 x 10 mm underlying chip with a single CHS has an area of 1 and 4  $\text{mm}^2$  with HFR varies from 1 (uniform) to 6 (non-uniform). The total thermal resistances and the contribution of each individual resistance on the chip maximum temperature are presented. The results are also compared to those calculated for plane Cu spreaders of the same thicknesses as the Cu substrates of the composite spreaders. The calculated quantities are (a) the footprint area of the spreader; (b) the total thermal power removed; and (c) the chip maximum surface temperature at the hot spot.

Further analysis is performed to quantify the effect of the TIM impedance on the calculated results. A polymer foil TIM sheet between the Cu substrate and the underlying chip is applied to the numerical analysis for a number of spreaders. The results of the numerical analysis using TIM impedance of 0.02 and  $0.19\text{ }^{\circ}\text{C}\cdot\text{cm}^2/\text{W}$  are presented and compared.

### 7.1 *Prior work*

The performance of composite spreader comprised of a Copper substrate ( $\text{Cu} \leq 1.6\text{ mm}$  thick) and thin layer of porous graphite, ( $\text{PG} \geq 0.4\text{ mm}$  thick) for cooling 10 x 10 and 15 x 15 mm underlying chip with uniform dissipated heat flux has been investigated numerically by El-Genk et al (2005) and El-Genk and Saber (2006). The spreaders surfaces were cooled by saturation or subcooled boiling of FC-72 dielectric liquid. Results showed that the composite spreaders increased the total thermal power removed at relatively low chip temperature, compared to plane Copper spreaders of the same total thickness of 2 mm. With saturation boiling of FC-72 liquid, the total thermal power removed by composite spreaders for 10 x 10 and 15 x 15 mm chips were 53 and 85 W, compared to 54 W and 78 W for Copper spreaders. The footprint area of the Cu-PG



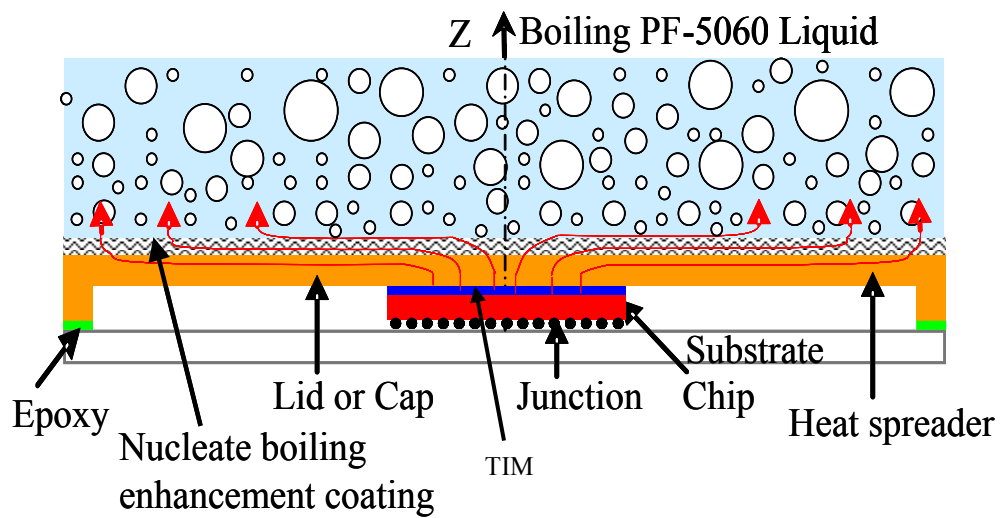


**Figure 7.1 A schematic of a composite spreader for immersion cooling nucleate boiling of PF-5060 dielectric liquid of high power computer chips.**

composite spreader was larger than plane Cu spreader, but the maximum chip surface temperature was lower. Results also showed that while subcooled nucleate boiling increases the total thermal power removed from the spreader surface, compared to saturation boiling, it increases the maximum surface temperature of the chip and the footprint area of the spreader. The chip maximum temperature for composite spreaders cooled by saturation and 30 K subcooled boiling of FC-72 were 61 K and 69 K, compared to 71 K and 74 K with plane Copper spreaders of the same thickness.

El-Genk and Saber (2008) extended the thermal numerical analysis of the Cu-PG composite spreaders for a non-uniform heat flux at the surface of 10 x 10 mm underlying chip. The dissipated thermal power by the chip had a cosine shape with a variable peak to average heat flux ratio  $\sim 2.5$ . The surface areas of the composite spreader were smaller, the total thermal resistances were lower, and the removed thermal powers were higher than those for Cu spreaders. When the peak to average heat flux ratio was 2.467, the composite spreader cooled with saturation and 30 K subcooled nucleate boiling of FC-72 removed 39.48 and 72.0 W, compared to 43.0 and 65.3 W with a Cu spreader. The total thermal resistance of the composite spreaders (0.284 and 0.68 °C/W) was much smaller than with the Cu spreaders (0.51 and 0.83 °C/W). The chip maximum temperature of 62.37 and 72.2 K was much lower than Cu spreader (72.67 and 76.30 K), when the composite spreader was cooled by saturation and 30 K subcooled boiling of FC-72..

XU (2006) performed a numerical thermal analysis investigating cooling of a single and multi-core processor with multiple hot spots. The effects of varying hot spot power density, size, and total CPU power level have been evaluated. The performed analysis was for a die, 20 x 20 mm in footprint area and power dissipation of 200 watts was assumed in the model. The two square heat spreaders were 25 x 25 x 2 mm and 100 x 100 x 5 mm. Results for the single core processor, showed a linear increase in the thermal resistance with the local hot spot power density at given CPU power level and hot spot size, while the junction temperature increases linearly with total CPU power level at given hot spot density and size. Results showed that the hot spot size significantly impacts on the thermal resistance. For the multi-core processor package, the thermal resistance was about 0.1 °C/W for a chip with 2 x 2 mm hot spot and power density of 200 W/cm<sup>2</sup>.

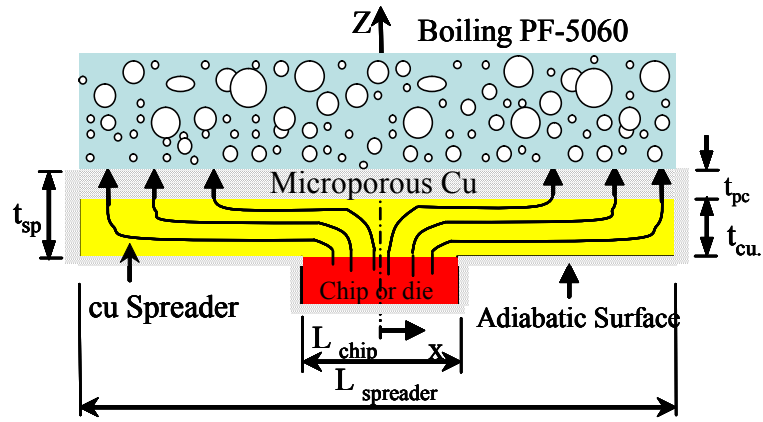
Hashimoto et al (2010) developed a vapor chamber heat spreader for cooling high heat flux chips. The prototype had an evaporator, condenser and an adiabatic section. Several evaporator plates with different microstructures for enhancing nucleate boiling under different thermal loads were investigated. Evaporator surface was enhanced by soldering different mesh size of Cu screens and with a thin layer of sintered Copper particles. Results showed that with a screen mesh evaporator, the removed heat load was  $2 \text{ W/mm}^2$ , but at unaccepted high evaporator temperature ( $200^\circ\text{C}$ ). For sintered Copper powder evaporator with  $50 \text{ }\mu\text{m}$  diameter particles, a heat load of  $8.5 \text{ W/mm}^2$  was supported at an evaporator temperature  $< 80^\circ\text{C}$ .

The above review of the literature on spreaders with surfaces for enhancing nucleate boiling has been limited, particularly for high power computer chips with hot spots. The following sections in this chapter address this issue for Cu spreaders with MPC surfaces.

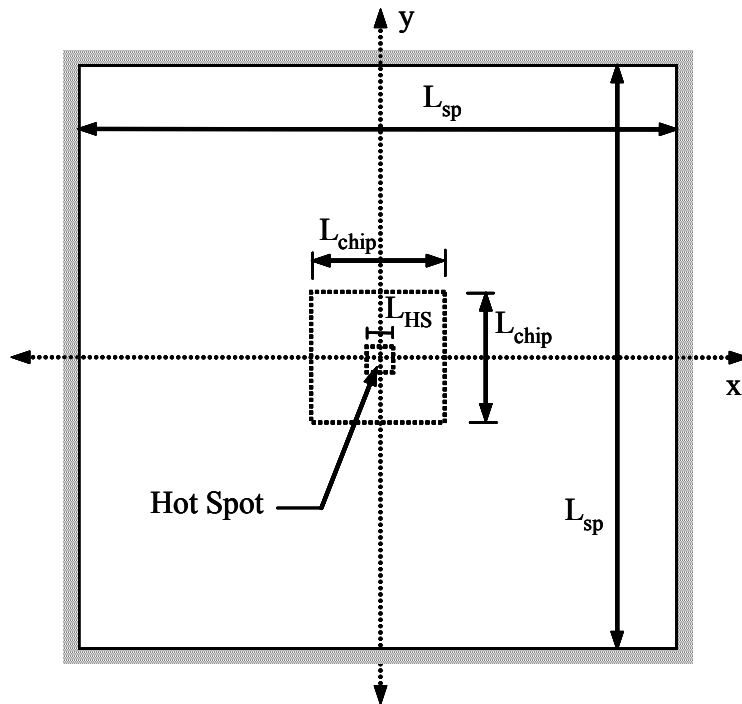
## **7.2 Problem Statement**

The analyzed composite spreaders have a total thickness  $t_{sp}$ , and consist of a Cu substrate that is  $t_{cu}$  thick and a MPC surface that is  $t_{MPC}$  thick (Figure 7.2). In Figures 7.2a, b and c, a computer chip measuring ( $10 \times 10 \text{ mm}$ ) is centered below the spreader. The spreader has a square surface area measuring  $L_{sp} \times L_{sp}$ . These dimensions are determined in the numerical simulation analysis, subject to the specified values of the saturation nucleate boiling heat transfer coefficient of the PF-5060 dielectric liquid obtained experimentally on the MPC surfaces. Figure 7.3 compares the experimental curves of saturation pool boiling and nucleate boiling heat transfer coefficient for PF-5060 on plane Copper and different MPC surfaces. The curves of the nucleate boiling heat transfer coefficient are used in the present numerical thermal analysis of the spreaders. In Figure 7.3, the last data points in the curves, indicated by the closed circle symbols, mark CHF. This figure also shows that nucleate boiling heat transfer coefficients,  $h_{NB}$ , for PF-5060 initially increases with increased surface temperature to a maximum,  $h_{MNB}$ , and then decreases with further increase in surface temperature. The values of  $h_{MNB}$ , indicated by the solid square (Figure 7.3) are much higher than that at CHF and occur at much lower surface temperature. The values of both CHF and  $h_{MNB}$  increase as the thickness of the MPC surface increases, and are much higher than those reported for PF-5060 on plane Cu.

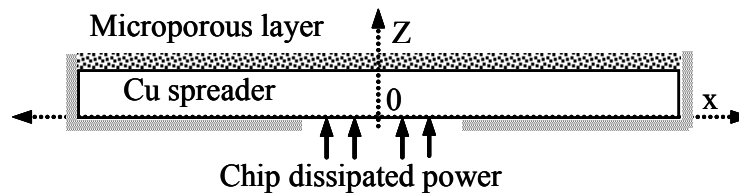
The present numerical analysis assumes a single underlying chip with a square central



(a) A schematic



(b) Plan view



(c) Elevation plan

Figure 7.2 A schematic and cross sectional views of a spreader comprised of a Cu substrate and a MPC surface.

hot spot measuring 1x1 or 2 x 2 mm. The hot spot's heat flux is up to 6 times that of the chip's surface average outside the hot spot. The analysis also assumes that the sides and bottom of the composite spreader are perfectly insulated (or adiabatic), while the top MPC surface of the spreader is cooled by saturation nucleate boiling of PF-5060 dielectric liquid. The thermal analysis initially assumes perfect contact between the underlying chip and the spreaders then quantify the effects of applying TIM between the chip and the lower face of the composite spreader.

The thermal conductivities of the Cu substrate and of the MPC surfaces saturated with PF-5060 liquid, the experimental curves of  $h_{NB}$ , and the dimensions of the chip are specified in the input to the numerical thermal analysis. The footprint area of the spreader and the spatial temperature distributions at the surfaces of the spreader and the underlying chip are calculated, as detailed later. In addition, the total thermal power dissipated by the chip and removed from the spreader surface by nucleate boiling is calculated subject to the following conditions specified at the spreader surface:

- (a)  $h_{NB}$  of saturation boiling of the PF-5060 liquid at the center of the spreader surface is that corresponding to 90% of CHF in the boiling experiments. This condition is indicated by solid upside triangle symbols in Figure 7.3;
- (b)  $h_{NB}$  at the corners of the spreader surface is that measured in the experiments at 1.0 °C higher surface temperature than at incipient boiling. This condition is indicated by the upside down solid triangle symbols in Figure 7.3.

The performed steady state thermal analysis of the present spreader (Figure 7.2) involves 3-D conduction (x, y, z) in the Copper substrate and in the MPC surface saturated with the PF-5060 dielectric liquid. Owing to the high effective thermal conductance ( $k_{eff} / t_{MPC} = 4.3- 23.9 \times 10^5 \text{ W/m}^2 \text{ K}$ ) of the MPC surfaces, compared to those of the Copper substrate ( $k_{Cu}/t_{Cu} = 1.25-2.5 \times 10^5 \text{ W/m}^2 \text{ K}$ ), the heat conduction through these surfaces is effectively one dimensional. The effective thermal conductivities of MPC,  $k_{eff}$ , are calculated in terms of these of Cu and PF-5060 liquid and the estimated volume porosity (Table 3.1), as follows:

$$K_{eff} = \varepsilon K_b + (1 - \varepsilon) K_{Cu} \quad (7.1)$$

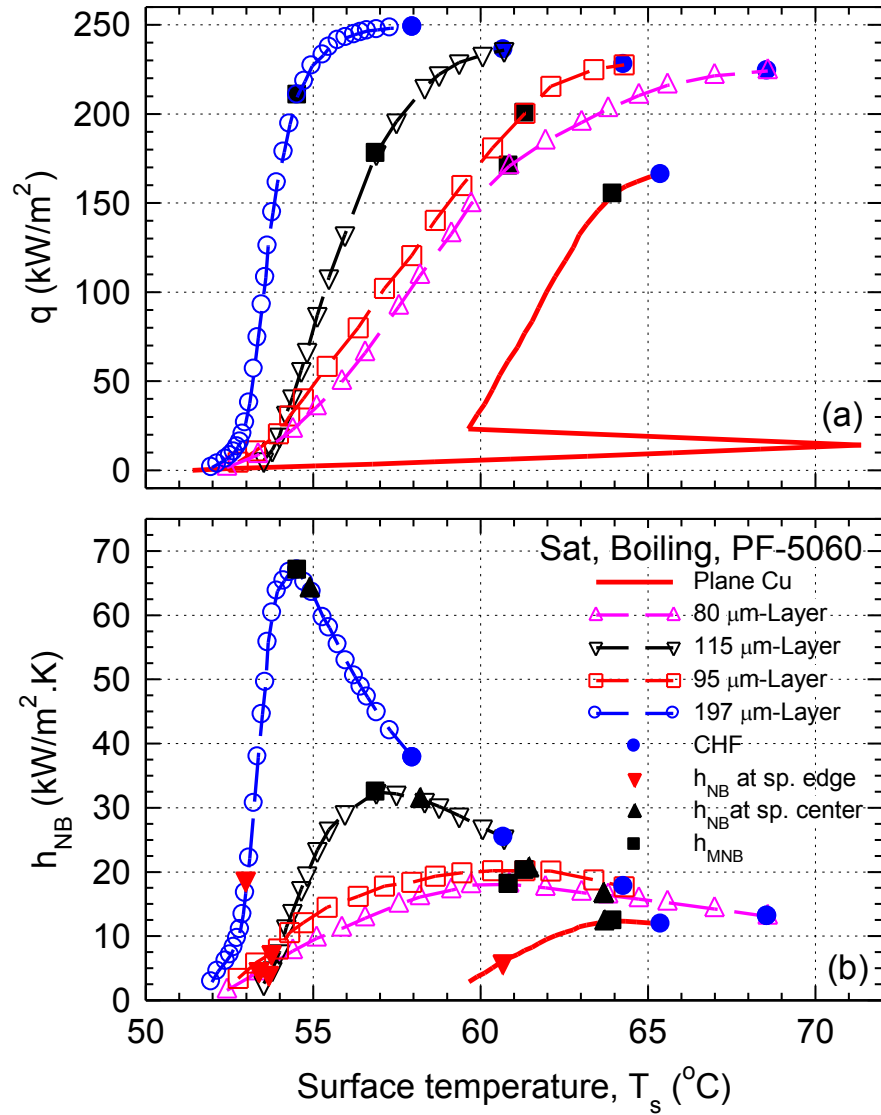


Figure 7.3 Experimental saturation pool boiling and nucleate boiling heat transfer coefficient curves of PF-5060 dielectric liquid on plane Cu and MPC surfaces.

The calculated  $k_{\text{eff}}$  for MPC decreases with increased thickness, ranging from 84.1 W/m K. for the 197  $\mu\text{m}$ -thick MPC surface to 191.6 W/m K for the 80  $\mu\text{m}$ -thick MPC surface..Table 7.1 lists the estimated values for the different MPC layers.

**Table 7.1 Properties of electrochemical deposited MPC surfaces.**

Thickness ( $\mu\text{m}$ )	80.0 $\pm$ 1.31	95.1 $\pm$ .81	115.1 $\pm$ 1.63	197.4 $\pm$ 3.6
Estimated volume Porosity, $\varepsilon$ (%)	52.1	65.3	70.3	80.6
Estimated thermal conductivity, $K_{\text{eff}}$ (W/m.K)	191.63	138.83	118.84	84.1
Estimated thermal conductance (W/m <sup>2</sup> .K)	2.39x10 <sup>6</sup>	1.46x10 <sup>6</sup>	1.03x10 <sup>6</sup>	0.43x10 <sup>6</sup>

The 2-D temperature distributions at the chip surface and at the top surface of the Cu substrate are calculated from the energy balance at the interfaces between the underlying chip and the Cu substrate and between the Cu substrate and the Cu-micro-porous surface. The 2-D temperature distribution at the MPC surface of the spreader is determined from equating the heat flow to and removed from the surface by saturation nucleate boiling of the PF-5060 dielectric liquid. The side temperatures of the spreader and those at the bottom of the Cu substrate are calculated subject to the specified adiabatic condition at these surfaces.

### **7.3 Approach and methodology**

The numerical calculations are carried out using an iterative approach in which initial value of the spreader footprint and dissipated thermal power by the chip are assumed. They are changed incrementally in subsequent iteration until the condition (a) above for the  $h_{\text{NB}}$  at the center of the spreader surface is satisfied. Then, the chip dissipated power and the footprint area of the spreader, are incrementally increased until both (a) and (b) conditions above are simultaneously satisfied. The accuracy of the numerical calculations is verified by examining the error in the overall energy balance. With a solver tolerance of  $1.0 \times 10^{-4}$ , the estimated error in the overall energy balance is 0.1%. In addition to the calculated temperature distributions at the chip and the spreader surfaces, the output includes the spreader's footprint dimensions, the total thermal power dissipated by the underlying chip, and the chip maximum surface temperature.

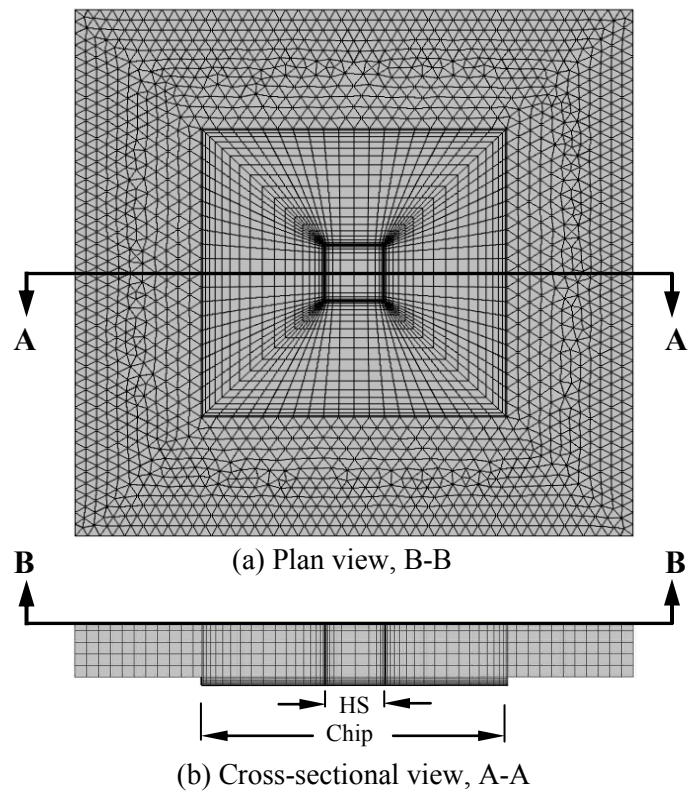


**Figure 7.4 Numerical mesh grid used in the present numerical thermal Analysis of composite spreaders.**



## **7.4 Numerical analysis and meshing grid**

The numerical thermal analysis of the spreaders is carried out using COMSOL multi-physics, finite element commercial software version 4.0a, subject to the boundary conditions stated earlier. The software implements the solution of the 3-D, steady state, coupled heat conduction equations in the Copper substrate and the MPC surface of the spreader using a stationary iterative solver with a generalized minimum residual algorithm (GMRES). To ensure calculations accuracy, a solver tolerance of  $1.0 \times 10^{-4}$  and a fine mesh grid are used. The used numerical mesh grid consists of quadrilateral elements in the central  $10 \times 10$  mm region of the spreader above the underlying chip with a CHS and hexahedral elements in the rest of the spreader.

Figure 7.4a shows the numerical mesh grid and elements at the surface of the spreader and Figure 7.4b shows the grid in a cross-sectional view of the Cu substrate and the MPC surface. The total number of the mesh elements used, increase as the thickness of the Cu substrate increases. The number of the mesh elements used in the present analysis increases from  $4.5 \times 10^4$  for the spreader comprised of a 1.6 mm thick Cu substrate and 197  $\mu\text{m}$  thick MPC surface to  $35 \times 10^4$  for the spreader with 3.2 mm thick Cu substrate and 80  $\mu\text{m}$ -thick MPC surfaces. The sensitivity of the numerical solution to change the number of mesh elements is tested. Selected calculations are repeated using finer numerical grid of  $6.0 \times 10^5$  mesh elements. The results showed no significant effect on the solution convergence or the calculated values of temperature, thermal power removed, and thermal resistance.

## **7.5 Results and Discussion**

This section presents and discusses the results of the numerical thermal analysis investigating the performance of the composite spreaders with MPC surfaces. The analysis quantifies the effect of changing the Cu substrate, and the thickness of MPC surface for cooling  $10 \times 10$  mm underlying chip with fixed  $1 \text{ mm}^2$  or  $4 \text{ mm}^2$  CHS area and HFR up to 6 and of changing the TIM between the underlying chip and the Cu Substrate. The results presented next for  $4 \text{ mm}^2$  CHS area and no thermal TIM include, the total thermal power dissipated by the underlying chip and removed by saturation boiling of PF-5060 dielectric liquid from the spreader surface, and the 2-D spatial

temperature distribution at the Chip surface and the footprint area of the spreader as functions of the thicknesses of the Cu substrate and MPC surfaces.

### 7.5.1 Total thermal power removed and footprint area without TIM

The thermal power dissipated by the 10 x 10 mm underlying chip with a single CHS and removed from the spreader's surface, without a TIM, are plotted in Figures 7.5a-c versus distance along the spreader surface, measured from its center. ( $x = y = 0$ ), for the 80 and 115  $\mu\text{m}$ -thick MPC and plane Copper. This analysis assumes perfect contact between the Cu substrate and underlying chip. The symbols in these figures indicate the spreaders with Cu substrate thicknesses,  $t_{\text{Cu}}$  from 1.6 to 3.2 mm, for the chip with a 2 x 2 mm CHS and  $\text{HFR} = 3$ . The dashed curves in these figures are for the same spreaders, but with uniform heat dissipation by the underlying chip (i.e., No CHS,  $\text{HFR} = 1$ ). The last data points in the curves in these figures mark half-widths of the spreaders ( $0.5 L_{\text{sp}}$ ), which are directly proportional to their footprint areas.

The results in Figures 7.5a and b clearly show that, the total thermal power removed from the surface of the composite spreaders are much higher than that removed by a plane Copper spreader (Figure 7.5c). Despite the lower values of  $h_{\text{NB}}$  on the 80  $\mu\text{m}$ -thick MPC surface, the total thermal powers removed from the surfaces of the spreaders are higher than those removed using the same spreaders, but with a 115  $\mu\text{m}$ -thick MPC surface. The higher nucleate boiling heat transfer coefficient on the 115  $\mu\text{m}$ , compared to that on the 80  $\mu\text{m}$ -thick surface of the spreaders favors axial versus lateral heat flow in the Cu substrate. This reduces the spreader's surface area and in turn, the total thermal power removed, which depends on the surface average nucleate boiling heat transfer coefficient and more strongly on the footprint area of the spreader. Increasing the thickness of the Cu substrate decreases the spreading thermal resistance, effectively increasing the total thermal power removed, but also the corresponding footprint areas of the spreader (Figures 7.5a and b).

For example, the total thermal powers removed by saturation nucleate boiling of PF-5060 dielectric liquid from the spreaders with a 115  $\mu\text{m}$ -thick MPC surface and 1.6 mm thick Cu substrate are 40.3 W and 43.9 W, when the underlying chip has a 4 mm<sup>2</sup> CHS and uniform heat dissipation, respectively. These spreaders have footprint areas of 28.95

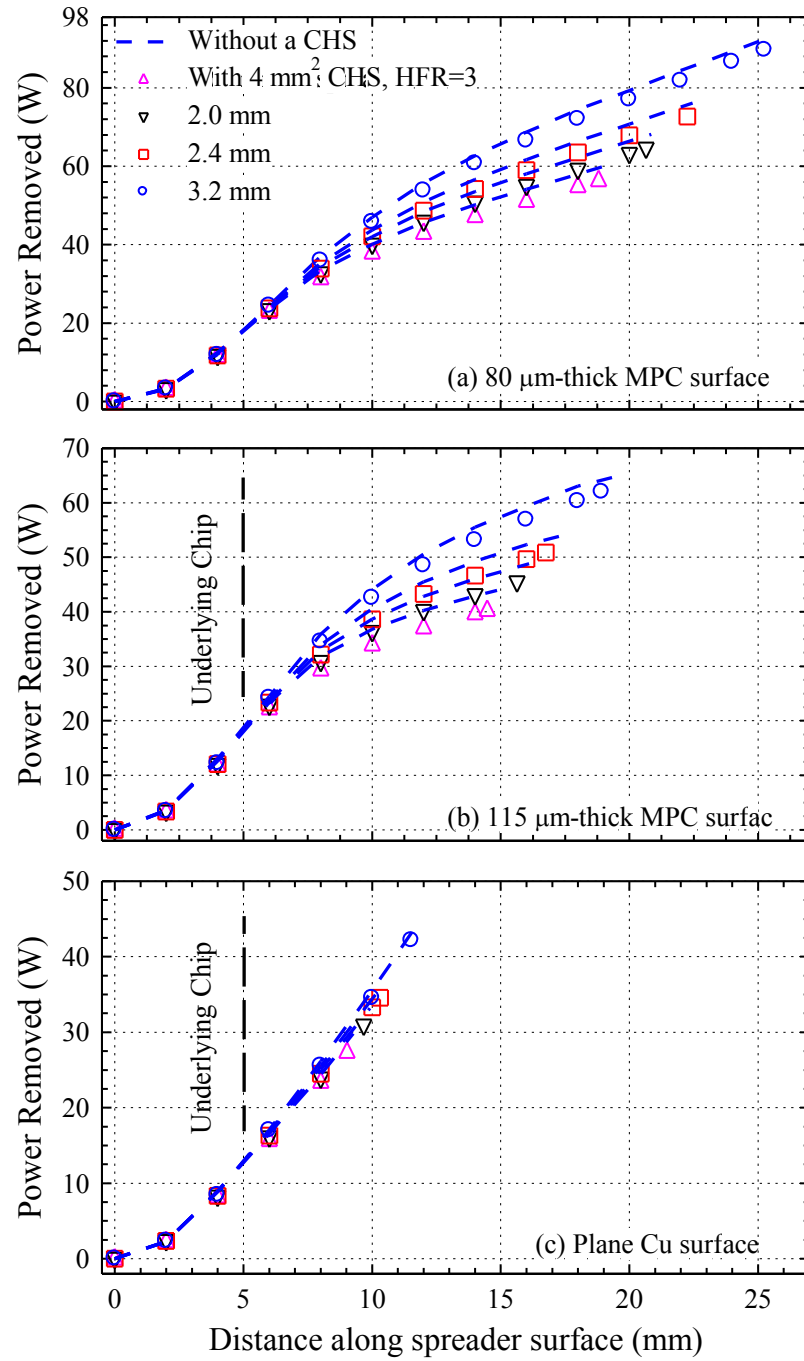


**Figure 7.5 Thermal power dissipation by underlying chip and removed from spreader surface assuming no thermal interface material.**

x 28.95 mm and 29.55 x 29.55 mm, compared to 37.6 x 37.6 mm and 38.2 x 38.2 mm and 55.4W and 60.15W of removed thermal power for the same underlying chips using the same spreaders, but with 80  $\mu\text{m}$ -thick MPC surfaces. Doubling the thickness of the Cu substrate to 3.2 mm increases the footprint areas as well as the total thermal power removed using the spreaders with plane 115  $\mu\text{m}$  and 80  $\mu\text{m}$  thick MPC surfaces by 70.9-80.4% and 53.8-58.9%, respectively. These values of total thermal power removed and footprint areas are much less when plane Copper spreader is utilized for cooling the underlying chip (Figure 7.5c). For 1.6 mm thick Cu spreader, the total thermal powers removed are 27.39 and 29.79, and footprint areas of 9 x 9 mm and 9.27 x 9.27 mm, when the underlying chip has a 4 mm<sup>2</sup> CHS and uniform heat dissipation, respectively. For 3.2 mm plane Copper spreader, the footprint area and total thermal power remove increase by 64.1% and 53.9% respectively.

The results delineated in Figure 7.5 also shows that for the 10 x 10 mm underlying chip with a 2 x 2 mm CHS and HFR of 3, the total thermal powers removed are slightly lower than with a uniform heat dissipation by the chip. The footprint areas of the spreaders are also larger. For the underlying chip with a single CHS, the spreaders with 3.2 mm-thick Cu substrates and 115  $\mu\text{m}$  and 80  $\mu\text{m}$  thick MPC surfaces could remove a total of 62.0 W and as much as 89.65 W of thermal power. These spreaders have footprint areas of 37.85 x 37.85 mm and 50.5 x 50.5 mm, respectively (Figures 7.5a, b). When the heat dissipated by the 10 x 10 mm underlying chips is uniform, the removed thermal powers increase slightly to 64.8 and 92.75 W and the footprint areas of these spreaders increase to 37.95 x 37.95 mm and 50.8 x 50.8 mm, respectively. With plane Copper spreaders, the total thermal power removed and footprint area decrease to 42.15 W and 11.52 x 11.52 mm and as much as 44 W and 11.69 x 11.69 mm for the underlying chip with 2 x 2 mm CHS and uniform heat dissipation, respectively (Figure 7.5c).

### **7.5.2 Chip Maximum temperature at hot spot**

One of the objectives of the performed numerical analysis is to investigate the potentials of using composite spreaders cooled by saturation nucleate boiling of PF-5060 for mitigating the effect of CHS in the underlying chip. The analysis is performed with heat flux at the 2 x 2 mm CHS that is three times the surface average heat flux outside the CHS (or HFR = 3). The obtained results are presented in Figures 7.6 a, and b, for the

spreaders with 80 and 197  $\mu\text{m}$ -thick MPC surfaces on different Cu substrate thicknesses,  $t_{\text{Cu}} = 1.6\text{-}3.2$  mm. Also the results for Cu spreaders of the same thickness and same condition are calculated and presented (Figure 7.6 c). The calculated spatial temperature distributions at the underlying chip surface are compared to those for the chip with a 4  $\text{mm}^2$ CHS (solid curves) with uniform power dissipation (dashed curves).

Increasing the thickness of the MPC surface, which increases the  $h_{\text{NB}}$ , decreases the footprint areas of the spreaders, and the total thermal power removed by saturation nucleate boiling of PF-5060 liquid from the surface of the spreaders (Figure 7.5), and hence decreases the chip's surface temperature (Figure 7.6). For example, on the spreaders with 197  $\mu\text{m}$ -thick MPC surface, the values of  $h_{\text{NB}}$  are much higher than on the 80  $\mu\text{m}$ -thick MPC surface (Figure 7.3), resulting in a much lower chip surface temperatures (Figure 7.6). With the plane Cu spreaders, the chip temperature at the CHS are lower than with the composite spreaders having 80  $\mu\text{m}$ -thick surface but at much lower values of the total thermal power removed (Figure 7.5c). These results indicate the potential of using MPC surface with Cu spreaders to increase the total thermal power removed at much lower or comparable maximum chip temperatures to those with plane Cu spreaders (Figure 7.6).

In general, immersion nucleate boiling cooling with the composite spreaders investigated in this work effectively reduces the chip surface temperature at the CHS (Figure 7.6). Using spreaders with 197 and 80  $\mu\text{m}$ -thick MPC surfaces, the difference between the surface temperature at the center and the edge of the chip with a hot spot,  $\Delta T_{\text{chip}}$ , is  $< 3.1$  K and  $< 5.3$  K respectively (Figure 7.7). For the same spreaders, this temperature difference is slightly higher than those for the underlying chip with uniform heat dissipation,  $\Delta T_{\text{chip}} < 1.8$  and  $3.8$   $^{\circ}\text{C}$ , respectively. Such low temperature differences across the chip would reduce thermal stresses and hence, the degradation in the chip performance and service life; an advantage of immersion cooling nucleate boiling.

The results in Figure 7.7 show that the maximum surface temperature of the chip with a CHS ranges from  $65.3$   $^{\circ}\text{C}$  to  $70$   $^{\circ}\text{C}$  and from  $57.1$   $^{\circ}\text{C}$  to  $59.3$   $^{\circ}\text{C}$ , when using spreaders with 80 and 197  $\mu\text{m}$ -thick Cu MPC surfaces, respectively. These temperatures are  $15$   $^{\circ}\text{C}$  -  $7.9$   $^{\circ}\text{C}$  lower than the lowest recommended by the chip manufacturer ( $85$   $^{\circ}\text{C}$ ). Thus, the proper choice of Cu spreader with a MPC surface depends on weighting the increase

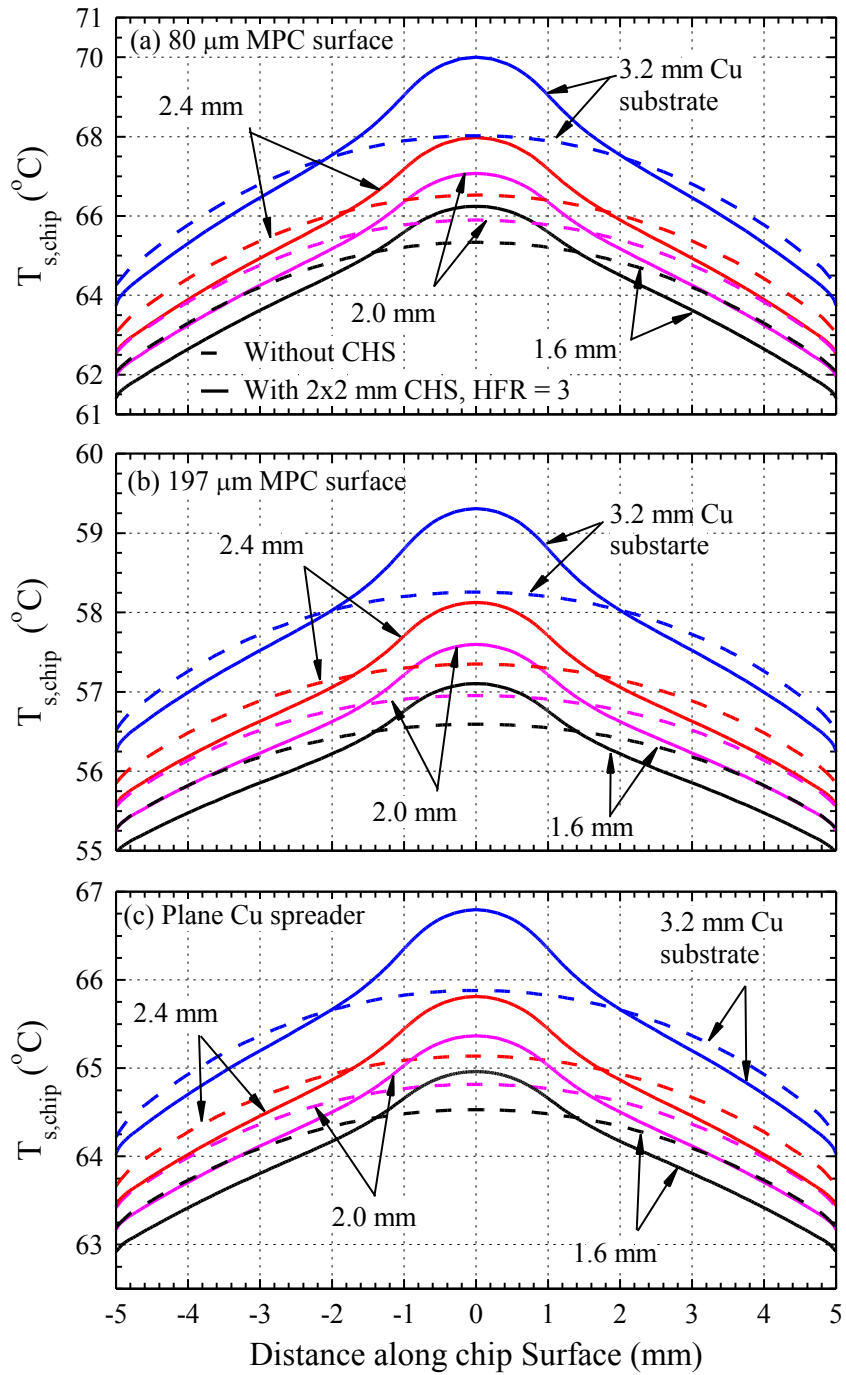


**Figure 7.6** Temperature distributions at the surface of the chips with and without a central hot spot.

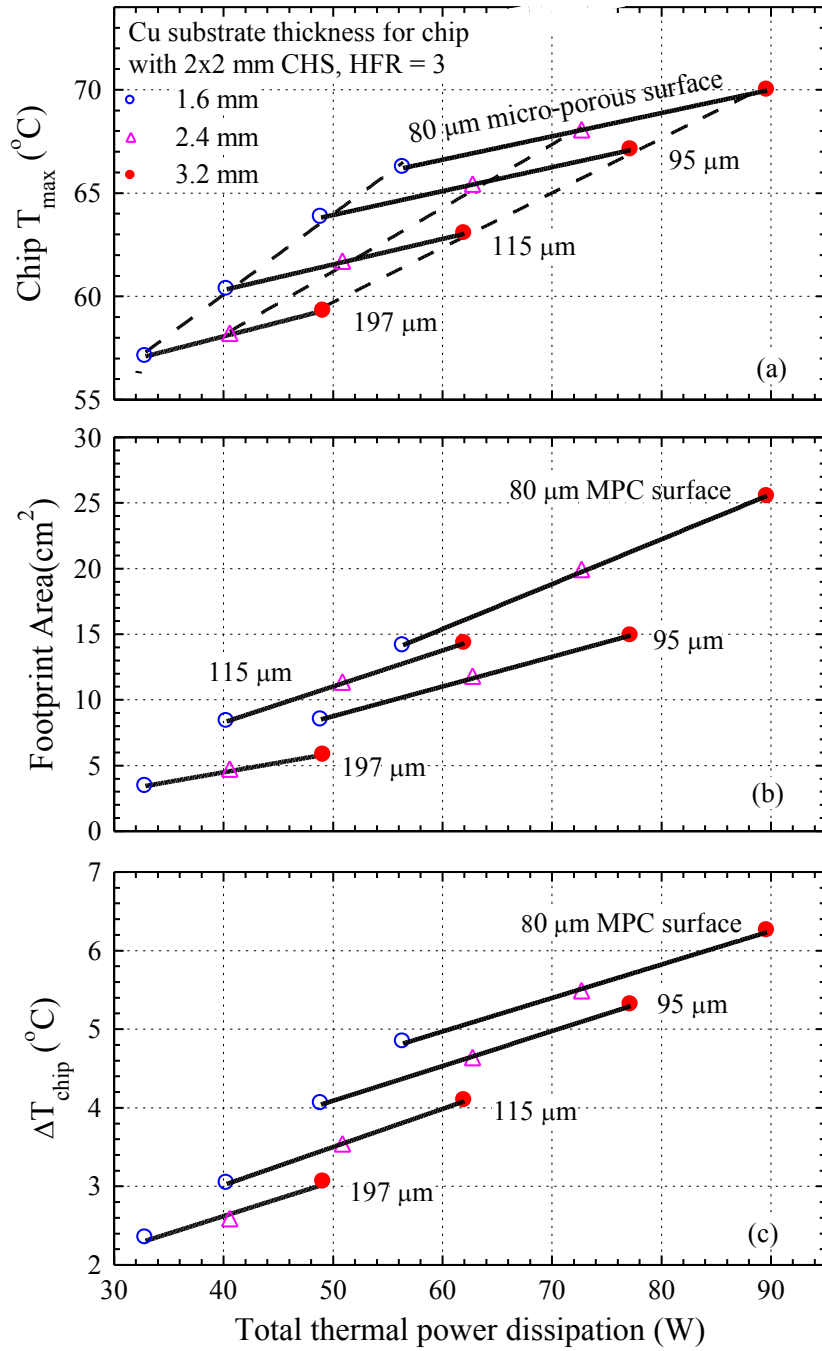


**Figure 7.7 Comparison of composite spreaders performance for immersion cooling of 10 x 10 mm underlying chip with 2 x 2 mm CHS having HFR=3.**

in the total thermal power removed from the spreader surface by immersion cooling nucleate boiling versus the maximum chip surface temperature.

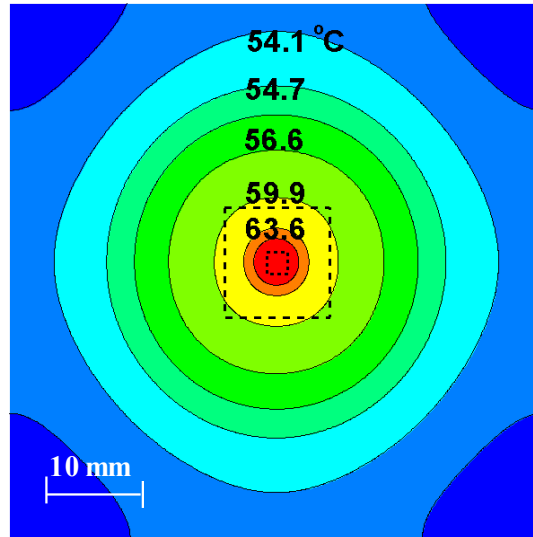
### 7.5.3 Effect of MPC surface thickness

The performance results of the investigated spreaders with MPC surfaces and Cu substrates of different thicknesses for immersion nucleate boiling cooling of an underlying chip of 10 x 10 mm with a 4 mm<sup>2</sup> CHS and HFR =3 are compared in Figure 7.7a-c. They plot the calculated maximum chip maximum temperature, footprint areas of the spreaders and the rise in the chip maximum surface temperature due to presence of CHS,  $\Delta T_{\text{chip}}$ , versus the total thermal power removed from the spreader surface. The highest total thermal powers removed and chip maximum surface temperatures, and the largest footprint areas and rises in the chip surface temperature are associated with using the composite spreaders with 80  $\mu\text{m}$ -thick MPC surfaces. Conversely, the lowest total thermal powers removed and chip maximum surface temperatures and the smallest footprint areas and rises in the chip surface temperature are associated with using the spreaders with 197- $\mu\text{m}$  thick MPC surfaces.

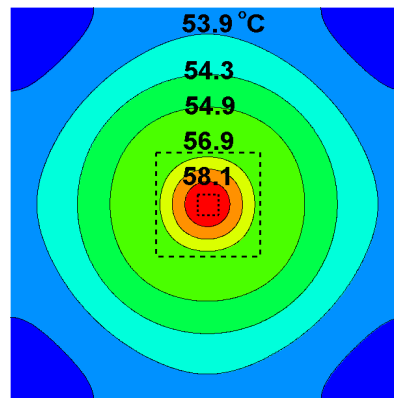
These results are caused by the nucleate boiling heat transfer coefficient being the highest on the 197  $\mu\text{m}$ -thick and the lowest on the 80- $\mu\text{m}$  thick MPC. For the same thickness of MPC surface, increasing the thickness of the Cu substrate of the spreader increases not only the chip's maximum surface temperature and the rise in the chip surface temperature (Figure 7.7a and c), but also the total thermal power removed from the surface of the spreader. The highest thermal power removed of 89.65 W for the chip with a 4 mm<sup>2</sup> CHS and HFR=3, is with the spreader having a 3.2 mm-thick Cu substrate and 80  $\mu\text{m}$ -thick MPC surface. For that spreader, the chip has a maximum temperature of about 70 °C and 25 cm<sup>2</sup> footprint areas.

Figure 7.8 presents contours of the calculated surface temperatures of the spreaders with 80, 115, and 197  $\mu\text{m}$ -thick MPC surfaces, for cooling the 10 x 10 mm underlying chip with a 2 x 2 mm CHS and HFR = 3. The underlying chip is indicated by the outer dashed square and the 2 x 2 mm CHS is indicated by the inner smaller square in the images in Figure 7.8. The images in these figures reflect the relative sizes of the footprint areas of the spreaders with a 3.2 mm-thick Cu substrate and different MPC surfaces. The

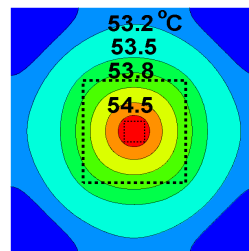




(a) 80  $\mu\text{m}$  MPC, 89.65 W



(b) 115  $\mu\text{m}$  MPC, 62 W



(c) 197  $\mu\text{m}$  MPC, 49.1 W

Figure 7.8 Surface temperature contours and footprints of composite spreaders with 3.2 mm-thick Cu substrate and MPC surfaces of different thicknesses.

spreader with the 197- $\mu\text{m}$  thick MPC surface (Figure 7.8c) runs the coolest, has the smallest footprint area, but removes the smallest amount of dissipated thermal power by the underlying chip (49.1 W). Conversely, the composite spreader with the thinnest MPC surface (80  $\mu\text{m}$ -thick) has the largest footprint area (Figure 7.8a), runs the hottest, but removes the largest amount of dissipated thermal power by underlying chip (89.65 W).

#### **7.5.4 Effects of TIM and HFR at CHS**

The numerical analysis results presented and discussed previously didn't count for the effect of the thermal resistance of the TIM material and of varying the area and local heat flux at the chip's CHS. To quantify the effect of TIM impedance on the performance of the spreaders, a polymer foil THERMFLOW<sup>TM</sup> T558 TIM sheet between the Cu substrate and the underlying chip is applied in the numerical thermal analysis. This TIM is a phase-change, electrically nonconductive, and thermally enhanced polymer for high power chips and electronic packaging applications. At room temperature, this material is solid but becomes soft at high temperatures ( $> 45\text{ }^{\circ}\text{C}$ ), conforming to the matting surfaces of the interface with a light clamping pressure. The TIM impedance is  $0.19\text{ }^{\circ}\text{C}\cdot\text{cm}^2/\text{W}$  at a clamping pressure of 69 kPa and  $70\text{ }^{\circ}\text{C}$  (Thermflow, 2012). In addition to the TIM, the analyses also varied the values of: (a) the CHS area (1 and  $4\text{ mm}^2$ ) (b) local heat flux ratio at CHS, HFR, from 1-6, and (c) the thickness of the Cu substrate (1.6-3.2 mm) for the composite spreader with 80  $\mu\text{m}$ -thick MPC surface.

The performance surfaces of the composite and plane Cu spreaders are compared in Figures 7.9a and b. These surfaces are grids compromised of equal-thickness lines of the Cu spreaders or the Cu substrate of the MPC spreaders, and intersecting lines of the values of HFR at the CHS (1-6). The performance surfaces in Figure 7.9a are for a chip with a  $1\text{ mm}^2$  CHS and those in Figure 7.9b are for a chip with a  $4\text{ mm}^2$  CHS. The performance surface for the MPC spreaders is much wider than for the plane Cu spreaders of the same thicknesses. Increasing the CHS area expands the performance surface of the MPC spreaders, but only slightly that of the plane Cu spreaders. The thermal powers removed by the MPC spreaders are  $\sim 2$  times those removed by the plane Cu spreaders of almost the same thicknesses, when the CHS area is  $1\text{ mm}^2$  (Figure 7.9a). However, the corresponding chip maximum surface temperatures are  $5.79\text{-}13.36\text{ }^{\circ}\text{C}$  higher than with the plane Cu spreaders (Figures 7.9a, b). This is because the thermal

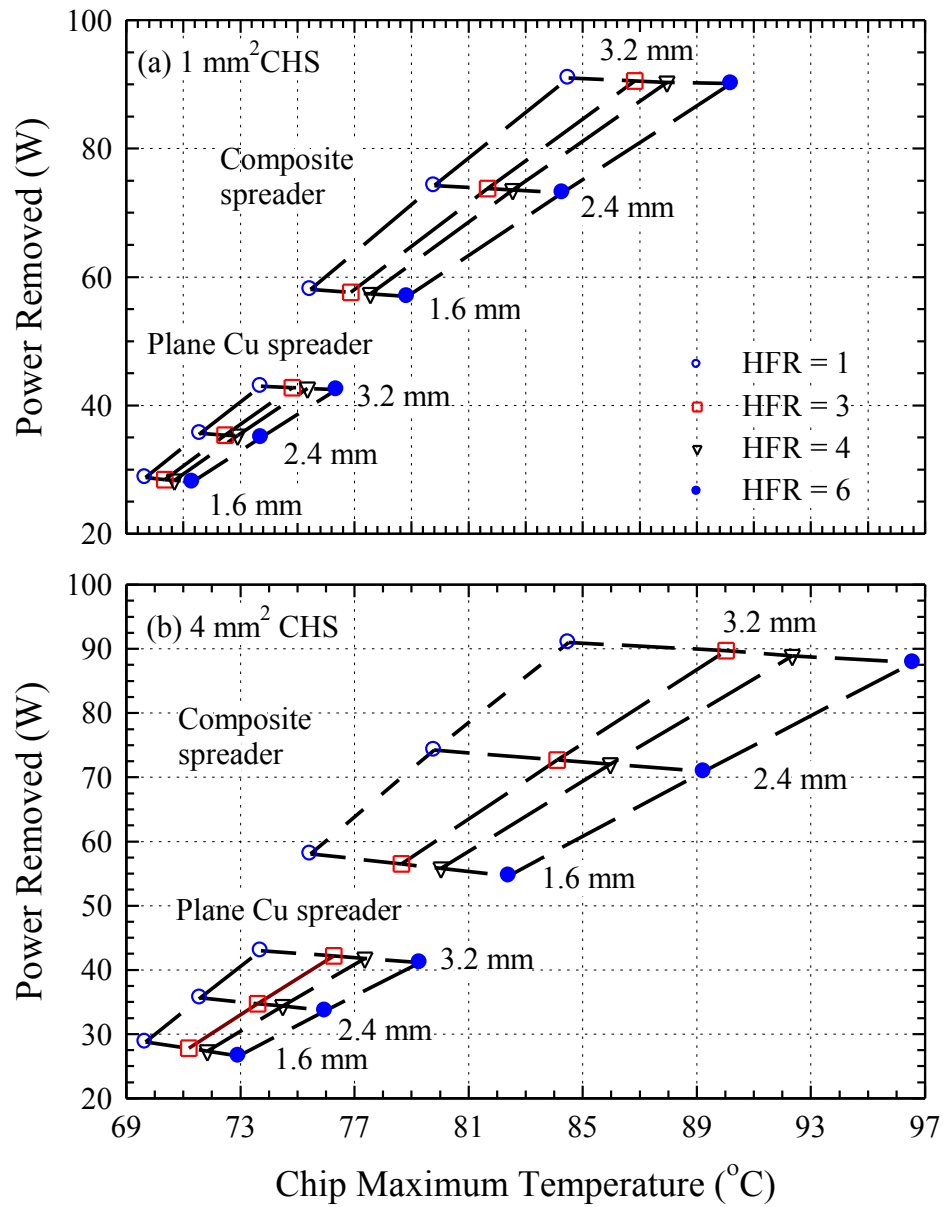


Figure 7.9 Effect of CHS area and HFR on the performance of the composite and plane Cu spreaders.

powers removed by MPC spreaders are higher and the footprint areas are larger than those of the plane Cu spreaders.

With a MPC spreader with a 1.6 mm thick Cu substrate, when HFR = 6 the local heat flux at the 1 mm<sup>2</sup> and 4 mm<sup>2</sup> CHS of the underlying chip is 325.43 and 273.3 W/cm<sup>2</sup>, respectively. For the same HFR, increasing the thickness of the Cu substrate of the composite spreader to 3.2 mm increases the local heat flux at the 1 and 4 mm<sup>2</sup> CHS to 514.85 and 439.25 W/cm<sup>2</sup>, respectively. With plane Cu spreaders, the removed thermal powers and the local heat fluxes at the Chip's CHSs are much lower than with the MPC spreaders. For a 1.6 mm thick plane Cu spreader, when HFR = 6 the local heat flux at the chip's 1 and 4 mm<sup>2</sup> CHSs is 160.6 and 133 W/cm<sup>2</sup>, respectively. For the same HFR, increasing the thickness of the plane Cu spreader to 3.2 mm increases to 242.7 W/cm<sup>2</sup> and 205.8 W/cm<sup>2</sup>, respectively, the local heat flux at the 1 and 4 mm<sup>2</sup> CHS of the underlying chip. The distinct differences in the performance of the composite and plane Cu spreaders affect their total thermal resistances and the maximum surface temperatures of the underlying chip. These effects and the values of the individual thermal resistances as well as the total thermal resistances of the plane Cu and composite spreaders are discussed next.

### 7.5.5 Spreader's thermal resistance

The total thermal resistance,  $R_{TOT}$ , of the composite spreaders is the sum of those for: (a) saturation boiling at the MPC spreader surface,  $R_{boil}$ , (b) heat conduction in the 80- $\mu$ m thick MPC saturated with PF-5060 dielectric liquid,  $R_{MPC}$ , (c) heat conduction in the TIM between the Cu substrate and the underling chip,  $R_{TIM}$ , and (d) heat spreading in the Cu substrate,  $R_{sp}$ , as:

$$R_{TOT} = (T_{chip,max} - T_{sat}) / Q = R_{TIM} + R_{sp} + R_{MPC} + R_{boil} \quad (7.2)$$

The individual thermal resistances in this equation are defined as:

$$R_{TIM} = \frac{TI_{TIM}}{A_{chip}}, \quad (7.3a)$$

$$R_{sp} = \frac{T_{chip,max} - \bar{T}_{Cu}}{Q} - R_{TIM}, \quad (7.3b)$$

$$R_{MPC} = \frac{\bar{T}_{cu} - \bar{T}_{s,MPC}}{Q}, \quad (7.3c)$$

$$R_{boil} = \frac{\bar{T}_{s,MPC} - T_{sat}}{Q}, \quad (7.3d)$$

The average surface temperatures of the Cu substrate,  $\bar{T}_{cu}$ , and the MPC surface layer,  $\bar{T}_{s,MPC}$ , are expressed, respectively, as:

$$\bar{T}_{cu} = \left( \int_{-0.5L_{sp}}^{+0.5L_{sp}} \int_{-0.5L_{sp}}^{+0.5L_{sp}} T_{cu}(x, y) dx dy \right) / L_{sp}^2, \quad (7.4a)$$

$$\bar{T}_{s,MPC} = \left( \int_{-0.5L_{sp}}^{+0.5L_{sp}} \int_{-0.5L_{sp}}^{+0.5L_{sp}} T_{s,MPC}(x, y) dx dy \right) / L_{sp}^2, \quad (7.4b)$$

For the plane Cu spreader, the total resistance is given as:

$$R_{TOT} = (T_{chip,max} - T_{sat}) / Q = R_{TIM} + R_{sp} + R_{boil} \quad (7.5)$$

While the  $R_{TIM}$  (Equation 7.3a) is independent of the total thermal power removed by the spreaders,  $Q$ ,  $R_{boil}$ ,  $R_{MPC}$ , and  $R_{sp}$ , and hence the spreader's total resistance,  $R_{TOT}$ , depend on  $Q$ , the chip maximum surface temperature at CHS, and the average top surface temperatures of the Cu substrate or the MPC surface. Note that for the same  $TI_{TIM}$ , as the chip's footprint area increases, the TIM's thermal conduction resistance,  $R_{TIM}$ , decreases. The individual and total thermal resistances for the plane Cu and composite with 80  $\mu m$  MPC spreaders of the same Cu substrate thickness are plotted in Figures 7.10a and b versus the HFR, at the 4 mm<sup>2</sup> CHS of the underlying chip. The results in these figures are for different thicknesses of the Cu substrate in the composite and plane Cu spreaders (1.6-3.2 mm).

The heat spreading resistance,  $R_{sp}$ , is practically independent of the thickness of the plane Cu spreaders (Figure 7.10a). For the composite spreaders, however, the heat spreading resistance,  $R_{sp}$ , increases slightly as the thickness of the Cu substrate increases (Figure 7.10b). For both the MPC and plane Cu spreaders,  $R_{sp}$  increases linearly with the HFR (Figure 7.10), but is higher for the composite spreaders. The larger footprint areas of the composite spreaders increase their heat spreading resistances. However, these resistances are much lower than for the plane Cu spreaders of almost the same thickness. The plane Cu spreaders remove much less thermal powers and have smaller footprint areas than for the plane Cu spreaders of almost the same thickness. The plane Cu spreaders remove much less thermal powers and have smaller areas (Figure 7.10).

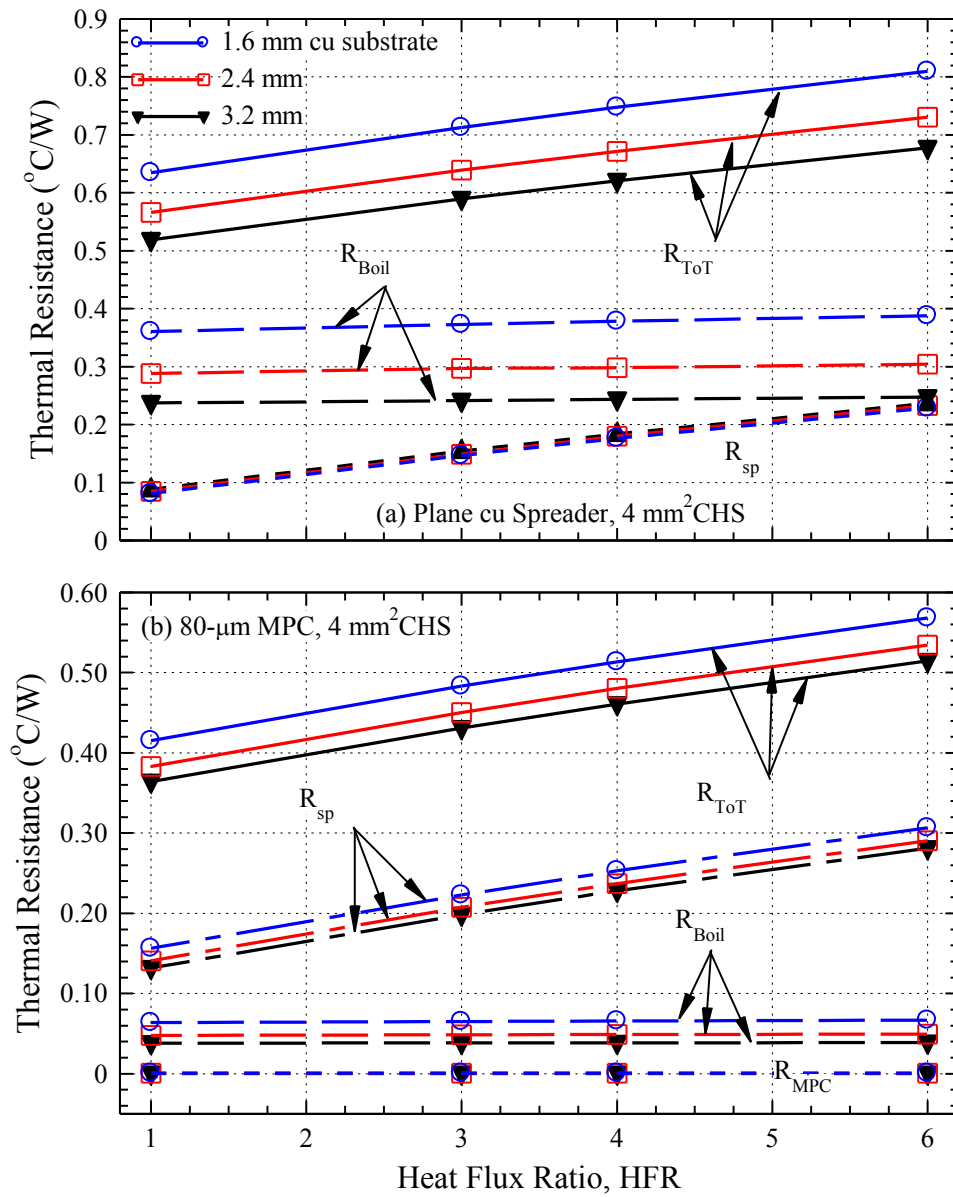


Figure 7.10 Comparison of the thermal resistances for composite and plane Cu spreaders.

The resistance for saturation boiling of,  $R_{\text{Boil}}$ , is almost independent of the value of HFR at the CHS of the underlying chip, but that for composite spreaders is much lower than on plane Cu (Figures 7.10a and b). This is because the values of nucleate boiling heat transfer coefficients on MPC are much higher than on plane Cu and the corresponding surface temperatures are lower (Figure 7.3). The thermal interface material resistance,  $R_{\text{TIM}}$ , is constant ( $0.19 \text{ }^{\circ}\text{C/W}$ ) and independent of the value of HFR at the CHS of the underlying chip as well as the total thermal power removed from the spreader surface. It depends on the surface area of the underlying chip, which in the present analysis is constant  $1 \text{ cm}^2$ .

The total thermal resistances,  $R_{\text{TOT}}$ , of the Cu and composite spreaders increase as either the HFR at the Chip's CHS increases or the thickness of the Cu substrate decreases (Figure 7.10). The highest total resistance is that of the 1.6 mm thick plane Cu spreader when  $\text{HFR} = 6$  ( $0.81 \text{ }^{\circ}\text{C/W}$ ). This resistance is 42.6% higher than that of the composite spreader ( $0.568 \text{ }^{\circ}\text{C/W}$ ) with the same Cu substrate thickness of 1.6 mm (Figure 7.10). When  $\text{HFR} = 6$ , increasing the thickness of the plane Cu spreader to 3.2 mm decreases its total thermal resistance to  $0.677 \text{ }^{\circ}\text{C/W}$ . This resistance is 31.6% higher than that of the composite spreader ( $0.515 \text{ }^{\circ}\text{C/W}$ ) with the same Cu substrate thickness. For both the plane Cu and composite spreaders, the increases in the total thermal resistance are associated with decreases in the total thermal power removed and the spreaders' footprint areas

### 7.5.6 Chip Surface Temperature

This section compares the various contributions to the total thermal resistances of the plane Cu and composite spreaders and the maximum surface temperatures of the underlying chip at the CHSs. For the results in Figure 7.11, the thickness of the Cu spreaders and that of the Cu substrate of the composite spreaders is the same; 2.4 mm. The analysis is for a  $10 \times 10 \text{ mm}$  chip with 1 and  $4 \text{ mm}^2$  CHSs, TIM impedance of  $0.19 \text{ }^{\circ}\text{C-cm}^2/\text{W}$ , and  $\text{HFR} = 6$ . Results show that the primary contributor to the total thermal resistances of the composite spreaders is that of heat spreading in the Cu substrate,  $R_{\text{sp}}$ , followed by  $R_{\text{TIM}}$ ,  $R_{\text{boil}}$ , and then  $R_{\text{MPC}}$  (Figure 7.11a). By contrast, the primary contributor to the total thermal resistances of the plane Cu spreaders is  $R_{\text{boil}}$ , followed a distance second by  $R_{\text{TIM}}$  and then  $R_{\text{sp}}$  (Figure 7.11b). This is because of the low nucleate

boiling heat transfer coefficient of PF-5060 dielectric liquid on plane Cu and the small footprint areas of the plane Cu spreaders.

For the underlying chip with  $1 \text{ mm}^2$  CHS, the total thermal power removed from the MPC surface of the composite spreader by saturation nucleate boiling of PF-5060 dielectric liquid is 73.13 W and the maximum surface temperature at the CHS of the underlying chip is  $84.27^\circ\text{C}$ . This temperature reflects a total rise above the saturation temperature of PF-5060 dielectric liquid ( $51.4^\circ\text{C}$  in Albuquerque, NM),  $\Theta_{\text{TOT}} = 32.87^\circ\text{C}$  ( $R_{\text{TOT}} = 0.45^\circ\text{C/W}$ ). The largest contribution to the maximum temperature at the chip's CHS is that of heat spreading,  $\Theta_{\text{sp}} = 15.39^\circ\text{C}$  ( $0.208^\circ\text{C/W}$ ), followed close second by that of heat conduction in TIM,  $\Theta_{\text{TIM}} = 13.9^\circ\text{C}$  ( $0.19^\circ\text{C/W}$ ), then saturation boiling at the spreader's top surface,  $\Theta_{\text{Boil}} = 3.54^\circ\text{C}$  ( $0.048^\circ\text{C/W}$ ) (Figure 7.11a). The heat conduction through the MPC surface layers contributes only  $0.04^\circ\text{C}$  ( $0.00055^\circ\text{C/W}$ ) to the total increase in the chip maximum surface temperature.

Figure 7.11a also shows the results for the same composite spreader, but for chip's CHS area of  $4 \text{ mm}^2$ . With this CHS area, the removed total thermal power decreases to 70.9 W, but the chip's maximum surface temperature at the CHS increases to  $89.24^\circ\text{C}$ . The contributions to this temperature due heat spreading and saturation boiling are  $\Theta_{\text{sp}} = 20.76^\circ\text{C}$  and  $\Theta_{\text{Boil}} = 3.58^\circ\text{C}$ , while those due to heat conduction in TIM and the MPC t surface layer are  $\Theta_{\text{TIM}} = 13.47^\circ\text{C}$  and  $\Theta_{\text{MPC}} = 0.035^\circ\text{C}$ . With the  $4 \text{ mm}^2$  CHS area, the total thermal resistance of the MPC spreader is  $0.5337^\circ\text{C/W}$  and the underling chip experiences a total temperature rise of  $\Theta_{\text{TOT}} = 37.84^\circ\text{C}$  above the saturation temperature of the PF-5060 liquid ( $51.4^\circ\text{C}$  in Albuquerque, NM) .

For the plane Cu spreader of the same thickness as the Cu substrate of the composite spreader (2.4 mm), the total thermal powers removed for the underlying chip with 1 and  $4 \text{ mm}^2$  CHSs and  $\text{HFR} = 6$  are only 35.05 and 33.64 W (Figure 7.11b). The corresponding chip maximum surface temperatures are  $73.7^\circ\text{C}$  and  $76.0^\circ\text{C}$ , respectively. For the chip with a  $1 \text{ mm}^2$  CHS, the total thermal resistance of the 2.4 mm thick plane Cu spreader is  $0.636^\circ\text{C/W}$  and  $0.731^\circ\text{C/W}$  when the chip has a larger CHS of  $4 \text{ mm}^2$ . These resistances are much higher than those of the composite spreader of almost the same thicknesses, which remove more than twice the thermal power of the plane Cu spreaders. The total contribution to the chip maximum surface temperature ( $73.7^\circ\text{C}$ ) is the sum of those due



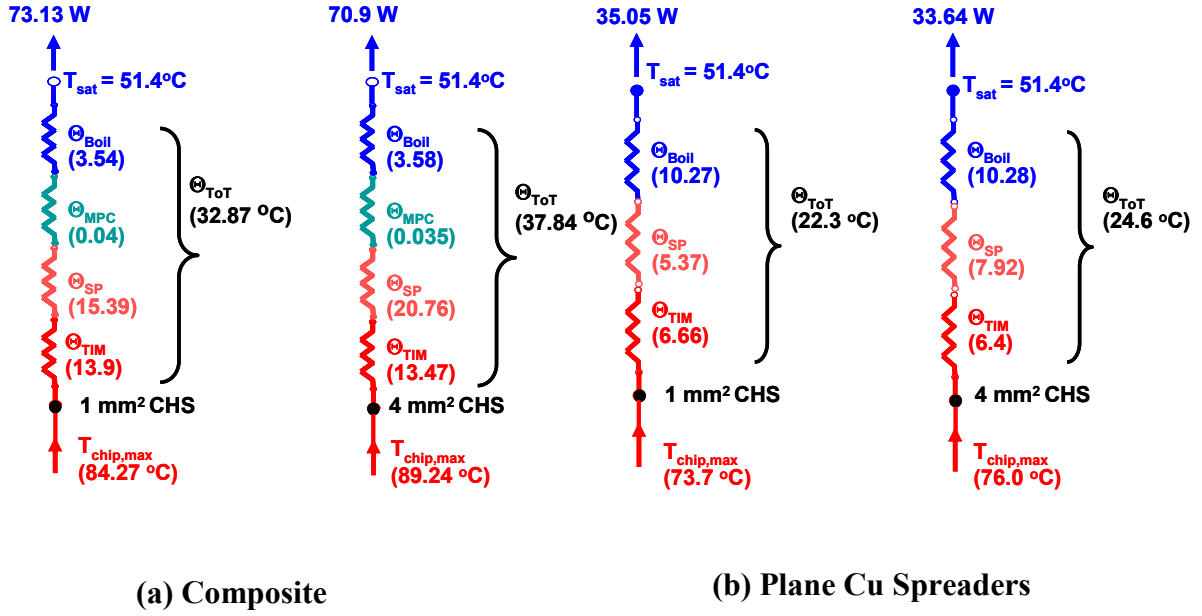


Figure 7.11 Comparison of the calculated chip maximum surface temperatures and the removed total thermal power: (a) plane Cu (b) MPC spreaders [HFR=6,  $t_{Cu}$ =2.4mm,  $TI_{TIM}$ =0.19 °C-cm<sup>2</sup>/W and CHS= 1 and 4 mm<sup>2</sup>].

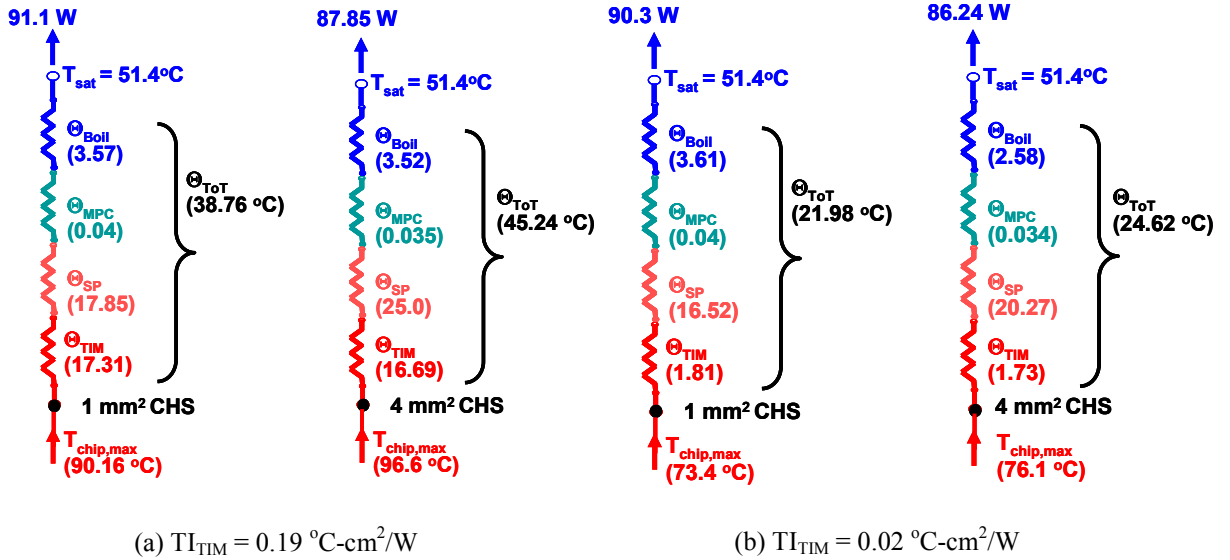


Figure 7.12 Comparison of the calculated chip maximum surface temperatures and the removed total thermal power: (a)  $TI_{TIM} = 0.19$  °C-cm<sup>2</sup>/W (b)  $TI_{TIM} = 0.02$  °C-cm<sup>2</sup>/W [HFR=6,  $t_{Cu}$ =3.2mm, and CHS= 1 and 4 mm<sup>2</sup>].

saturation boiling,  $\Theta_{\text{Boil}} = 10.27$  °C, heat conduction in TIM,  $\Theta_{\text{TIM}} = 6.66$  °C and heat spreading,  $\Theta_{\text{sp}} = 5.37$  °C (Figure 7.11b). Increasing the Chip's CHS area to 4 mm<sup>2</sup> increases the chip maximum surface temperature at CHS to 76 °C, reflecting the increase in total the thermal resistance. The contributions of the individual resistances to the total temperature rise for the underlying chip are shown in Figure 7.11b.

In actual applications, the chip maximum surface temperatures could be lower and the removed thermal powers could be higher than those calculated in the present analysis. This is because the analysis did not account for the heat removed from the sides and bottom surface of the spreaders (Figure 7.1). In addition the TIM resistance is responsible for the highest contribution to the temperature rise across the composite spreaders. Thus lowering the TIM resistance could lower the total resistance of the composite spreaders, increase the total thermal removed, and reduce the maximum chip surface temperature at the CHS areas.

The numerical analysis is extended to investigate the effect of reducing the thermal impedance of TIM on the calculated total thermal power removed, chip maximum surface temperature, and footprint area for both Copper and composite MPC spreaders. The analysis varied the thickness of the Cu or Cu substrate thickness of the composite spreader with 80 µm-thick MPC surface from 1.6-3.2 mm. In this analysis, the underlying chip has 1 and 4 mm<sup>2</sup> CHSs and HFR of 1-6 and the TIM impedance is 0.02 °C-cm<sup>2</sup>/W. The obtained results are compared to those discussed earlier in this chapter for the same composed spreaders but with TIM impedance of 0.19 °C-cm<sup>2</sup>/W.

The results show that decreasing the resistance of  $TI_{\text{TIM}}$  between the Cu substrate and the underlying chip markedly decreases the chip's maximum temperatures at CHSs, but only slightly the total thermal powers removed by the composite spreaders with the same Cu substrate thickness (Figure 7.12). This Figure compares the effect of changing TIM resistance on chip maximum temperature and the total thermal power removed by the composite spreader with 3.2 mm cu substrate and 80-µm thick MPC surface but for different area of the CHS when HFR of 6. Results in Figure 7.12a are for  $TI_{\text{TIM}} = 0.19$  °C-cm<sup>2</sup>/W and that in Figure 7.12b are for  $TI_{\text{TIM}} = 0.02$  °C-cm<sup>2</sup>/W. Figure 7.11a shows that for underlying chip with 1 and 4 mm<sup>2</sup> CHSs, the total thermal powers removed by the composite spreaders are 90.3 W and 86.24 W, compared to 91.1 W and 87.85 W in

Figure 12a. The corresponding chip's maximum surface temperatures at CHSs of 73.4 °C and 76.1 °C are significantly lower than those of 90.16 °C and 96.6 °C. The chip's maximum surface temperatures at CHSs in Figures 7.12a and b are much lower than those recommended by the chip manufactures (< 85 - 125 °C, depending on application).

## **7.6 Summary and closing marks**

A 3-D steady state numerical thermal analysis is performed to investigate the potential of Cu spreader with thin layer of MPC surface for immersion cooling of 10 x 10 mm underlying computer chip with 1 x 1 mm or 2 x 2 mm CHS. The composite spreaders are comprised of 1.6-3.2 mm-thick Cu substrates, for efficient heat spreading, and MPC surfaces (80-197 µm-thick) for enhancing nucleate boiling. The spreaders are cooled by saturation boiling of PF-5060 dielectric liquid, for which the experimentally obtained nucleate boiling heat transfer coefficient curves on MPC surfaces of different thicknesses are used in the present numerical thermal analysis. The analysis investigates the effects of changing the thicknesses of the Cu substrates and the MPC surfaces on the performance of the spreaders and their potential for mitigating the effect of the hot spot

For the thermal analysis using perfect contact between the underlying chip and the lower face of the composite spreaders, results show that the highest removed thermal power dissipated (89.65 W) by the underlying chip with a CHS is with the thickest Cu substrate (3.2 mm), but the thinnest MPC surface (80 µm). This composite spreader, however, has the largest footprint area (25.5 cm<sup>2</sup>), and results in the highest CHS temperature (70 °C). This temperature is only 2.0 °C higher than that for the same chip, but with uniform heat dissipation. Composite spreaders with higher  $h_{NB}$  (197 µm-thick MPC) have smaller footprint areas and hence remove lower thermal powers at lower chip maximum temperature at the CHS.

Second numerical analyses is also performed to investigate the effects of the local heat flux at the chip's 1 and 4 mm<sup>2</sup> CHS, and the thermal impedance of TIM ( $TI_{TIM}$ ), between the Cu substrate and the underlying chip, on the spreaders' total thermal resistance and thermal power removed as well as the Chip's maximum temperature. The analyses varied the heat flux ratio at the CHSs (HFR) from 1 to 6 times that of the chip's surface average outside the hot spot. Lowering the  $TI_{TIM}$  from 0.19 to 0.02 °C-cm<sup>2</sup>/W

markedly decreases the chip's maximum temperatures at CHSs and only slightly the thermal powers removed by the MPC spreaders with the same Cu substrate thickness

The composite spreaders mitigate the effect of the CHSs by limiting the increase in the chip's maximum surface temperature to only a few degrees, even when the HFR is 6. It is worth noting that in immersion nucleate boiling cooling application, the chip's maximum surface temperature could be somewhat lower than those calculated in the present analysis, which did not take credit for the heat removal, likely by forced convection, from the sides and bottom surfaces of the spreaders and the die. In addition, lowering the TIM impedance would lower chip's maximum surface temperature which is a primary concern to electronic cooling.

## 8. Summary and Conclusions

This research investigated experimentally the potential of microporous copper (MPC) surfaces of different thicknesses to enhance nucleate boiling and increase Critical Heat Flux (CHF) of dielectric liquid PF-5060 for immersion cooling applications. MPC surfaces of different thicknesses (80–230  $\mu\text{m}$ ), fabricated using conventional electrochemical deposition at high current density, have different morphology and microstructure. The PF-5060 liquid is chemically inert, environmentally friendly, and has low enough saturation temperature ( $\sim 54^\circ\text{C}$  at 0.10 MPa) to help maintain the chip junctions temperature below that recommended by the chip manufacturer (85–120  $^\circ\text{C}$ , depending on the application).

The MPC surfaces are fabricated using two successive stages of electrochemical deposition. The first stage of is carried out under high current density for a short period of time, followed by a second stage at low current density for longer time to increase the mechanical stability of the deposited MPC surfaces. The SEM images after each stage of deposition showed that the basic micro-structure of the deposited MPC surface is established in the first stage using a current density of 3  $\text{A}/\text{cm}^2$  for a few seconds, depending on the thickness. During the first stage, the deposited Copper atoms on the cathode surface nucleate and grow rapidly in the form of fine and dense dendrites that surround open, circular macro-pores. The hydrogen bubbles evolving at the cathode are responsible for the formation of the patterned arrangement and the size of the openings of the macro-pores.

The initially deposited micro-structures with volume porosities ( $>90\%$ ) and orderly arranged macro-pores are very delicate for handling, easily chipped and cracked. To strengthen these micro-structures, electrochemical deposition continued at much lower current density for additional 10's of minutes. During this stage, the rate of deposition of the Cu atoms into the cathode is very low, negligibly changing the thickness of the Cu dendrite surface layer. The Cu atoms partially fill out the dendrites structure and some of the macro-pores change the surface morphology and the volume porosity but increase the interconnection between the branches, hence strengthen the structure.. The strengthened Cu surface layers become less porous (65–80 %), but the wetted area of the surface

increases due to the resulting micro-porous morphology and the formation of rounded depressions in the surface layers. The adhesion of the Cu micro-porous surface layers to the Cu substrates is very good for handling during the fabrication of the test section

To ensure consistency of the results, all saturation pool boiling experiments reported in this Dissertations are for degassed PF-5060 dielectric liquid and uniformly heated and conditioned 10 x 10 mm MPC surfaces (80, 95, 115, 140, 171, 197, 230  $\mu\text{m}$  thick) at different inclination angles. These are  $0^\circ$  (upward facing),  $30^\circ$ ,  $60^\circ$ ,  $90^\circ$  (vertical),  $120^\circ$ ,  $150^\circ$ , and  $180^\circ$  (downward facing). The MPC surfaces are conditioned, by performing several experiments at same conditions, separated by at least 2 hours and someone a couple of days. The experiments demonstrated the reproducibility of the measurements and the absence of boiling hystercics. Thus, confirming that nucleate boiling in the present experiments was not influenced by the thermal inertia of the heated surface but solely depends on the thermophysical properties of the PF-5060 and morphology and microstructure of the MPC surfaces.

In order quantify the effects of MPC thickness and orientation on nucleate boiling heat and CHF, the present results are compared to those for smooth polished Cu of the same dimensions at the same experimental conditions. In addition, results are compared to those reported in the literature for other micro-structured surfaces and microporous coatings. In additions, high-speed videos are recorded of the transient growth of nucleating vapor bubbles on MPC surfaces in the upward facing orientation. The captured images are used to determine the detachment diameter and the frequency of the ebullition cycle of the bubbles, as well as estimate the surface density of active sites for bubble nucleation.

The values of the saturation nucleate boiling heat transfer coefficient,  $h_{\text{NB}}$ , in the upward facing orientation are correlated as a function of the applied heat flux. The values of the maximum heat transfer coefficients, at the end of the fully developed nucleate boiling,  $h_{\text{MNB}}$ , are in terms of the thickness and inclination angle of MPC surfaces for saturation boiling of PF-5060 dielectric liquid.

The MPC surfaces enhance nucleate boiling with no or little temperature excursion prior to boiling incipience ( $< 5\text{K}$ ) of PF-5060. The experimental measurements demonstrated large enhancements in both  $h_{\text{NB}}$  and CHF. In the upward facing orientation,

the values of  $h_{\text{MNB}}$  ( $7.8 \text{ W/cm}^2\text{K}$  occurs at  $\Delta T_{\text{sat}} = 2.7 \text{ K}$ ) is the highest,  $\sim 10$  times that on smooth polished Copper ( $0.78 \text{ W/cm}^2\text{K}$  occurs at  $\Delta T_{\text{sat}} = 22 \text{ K}$ ). The developed correlation for  $h_{\text{NB}}$  in the upward facing orientation as function of the MPC surface thickness is within  $\pm 10\%$  of the present experimental measurements. CHF on MPC surfaces not only increases with increased thickness, but also the corresponding surface superheat decreases.. CHF increases from 22 to 26  $\text{W/cm}^2$  as the MPC surface thickness increases from 80  $\mu\text{m}$  to 230  $\mu\text{m}$  while the corresponding surface superheat decreases from 15 to 5 K. The CHF values on MPC surfaces in the upward facing orientation are 39% to 59% higher than on a smooth Cu surface. The corresponding surface superheats at CHF on MPC are much lower than those on smooth Copper surface.

Surface inclination also affects nucleate boiling and CHF. At low surface superheats, increasing inclination angle increases the nucleate boiling heat transfer coefficient. At high surface superheats, the trend is reversed and the nucleate boiling heat transfer coefficients decrease as inclination angle increases. The surface inclination angle decreases CHF and the corresponding surface superheat. CHF decreases slowly as surface inclination increases from upward facing ( $0^\circ$ ) to vertical ( $90^\circ$ ), then decreases more rapidly with further increase in inclination angle, to that in the downward facing orientation ( $180^\circ$ ). On MPC surfaces, saturation boiling CHF for PF-5060 dielectric liquid decreases with increasing inclination angle, but increases with increased thickness of MPC surfaces. Regardless of the thickness, CHF values in the downward facing orientation are  $\sim 28\%$  of their values in the upward facing orientation. The values of CHF are correlated in terms of the MPC thickness and the surface inclination angle. The developed correlation is in good agreement with experimental data to within  $\pm 8\%$ .

The recorded enhancements in both saturation CHF and nucleate boiling heat transfer coefficient in the present research are partially be attributed to the combined effects of surface morphology, the relatively high volume porosity of MPC surfaces, and increased wetted surface area caused by hemi-spherical depression in the MPC surfaces. The micro-sized Cu particles on the MPC surfaces increase the numbers the active sites for bubbles nucleation, enhancing nucleate boiling.

The transient growth of vapor bubbles on MPC surfaces (80, 95, 115, 125, and 140  $\mu\text{m}$  thick) are recorded for a number of ebullitions cycles and selected discere sites. The

bubbles diameter increases proportional to the square root of time, confirming that the growth is thermally controlled. The developed correlation for the transient growth diameter of the bubbles is in good agreement with the measurements to within  $\pm 5\%$ . The bubble departure diameter,  $D_d$ , and frequency,  $f_d$ , for saturation boiling of PF-5060 dielectric liquid in the upward facing orientation are independent of surface morphology. The determined values of  $D_d = 431 \pm 7 \mu\text{m}$  and  $f_d = 39 \pm 2 \text{ Hz}$ , are used to calculate the average surface density of active nucleation sites. The determined values range from 1000-10000 sites/ $\text{cm}^2$  compared to 300 -1000 sites/ $\text{cm}^2$  for FC-77 on rough ( $R_a = 5.89 \mu\text{m}$ ) Aluminum surfaces (McHale and Garimella, 2010).

The present results of  $h_{NB}$  are incorporated in a numerical thermal analysis investigating performance of Cu spreaders with MPC surfaces for cooling a 10 x 10 mm underlying high power chip with a central hot-spot (CHS). In the analysis the dimensions of the CHS are 1 x 1 mm to 2 x 2 mm and the heat flux at the CHS is up to 6 times that of the chip surface average outside the hot spot. The analysis also varied the thermal conductance of the thermal interface materials (TIM) between Cu substrate of the spreader and the underling chip from 0.19 to 0.02  $^\circ\text{C}\cdot\text{cm}^2/\text{W}$ . The spreader MPC surface is cooled by saturation boiling of PF-5060 dielectric liquid.

The numerical results confirmed the effectiveness of the Cu spreaders with MPC surface for immersion cooling nucleate boiling of high power chips. They could remove  $> 85 \text{ W}$  of dissipated thermal power by underlying chip at junctions' temperature  $< 100^\circ\text{C}$ . With a TIM impedance of 0.19  $^\circ\text{C}\cdot\text{cm}^2/\text{W}$ , a spreader with a 3.2 mm-thick Cu substrate and 80  $\mu\text{m}$ -thick MPC surface removes 90.1 W and 87.85 W for the chip with a 1 and 4  $\text{mm}^2$  CHS and heat flux ratio (HFR) at CHSs = 6. The corresponding chip maximum surface temperatures at the CHSs are 90.16  $^\circ\text{C}$  and 96.6  $^\circ\text{C}$ , respectively. Decreasing the TIM impedance to 0.02  $^\circ\text{C}\cdot\text{cm}^2/\text{W}$  decreases the chip's maximum surface temperatures to 73.4 and 76.1 $^\circ\text{C}$ , but slightly changes the removed thermal power to 90.3 W and 86.24 W, respectively.



## 9. Recommendations for Future Work

This chapter suggests future research to expand on the results presented in this Dissertation. Suggestions for future research to investigate MPC surfaces for enhancing nucleate boiling and expand the limits of the developed correlations are summarized below:

*(1) Investigate the effect of liquid subcooling on nucleate boiling and CHF for PF-5060 on MPC surfaces of different thickness.*

The proposed correlations for  $h_{NB}$  and CHF are useful tools to design and operate thermal devices associated with nucleate boiling in industrial application. These correlations account for the thickness of MPC and inclination angles. Perform experiments to investigate the effect of liquid subcooling on nucleate boiling of PF-5060 on MPC surfaces at different inclination and incorporate the obtained results into these correlations. This would extend their applicability to wide ranges of parameters for industrial applications.

*(2) Perform experiments to validate the numerical analysis results of investigating the potential of using MPC in heat spreaders for cooling high power chips.*

Numerical analysis is carried out to investigate the potential of using MPC in heat spreaders cooled by saturation boiling of PF-5060 to increase the total thermal power remove from underlying chip with a CHS. Results showed, spreaders with MPC effectively increased the total thermal power removed while keep the maximum temperature at the CHS low enough and mitigate the hot spot effect by lowering the temperature gradient across the chip surface. Performing experiments using composite spreaders with footprint areas calculated as by the numerical analysis to validate the numerical analysis results.

## 10. References

- 3M, Tables of Saturation Properties of HFE-7100, FC-72 and PF-5060, 2010, [www.3M.com](http://www.3M.com).
- 3M, Technical Data Sheets, 2010, [www.3M.com](http://www.3M.com).
- Ahn, S. A., Sathyamurthi, V., and Banerjee, D., 2009, "Pool Boiling Experiments on a Nano-Structured Surface," *IEEE Transactions on Component and Packaging Technology*, 32(1), 156-165.
- Albertson, C.E., 1977, "Boiling heat transfer surface and method," US Patent # 4018,264.
- Ali, A. F., and El-Genk, M. S., 2012a, "Effect of inclination on saturation boiling of PF-5060 dielectric liquid on 80 and 137  $\mu\text{m}$  thick copper micro-porous surfaces," *International Journal of Thermal Sciences*, 53, 42-48.
- Ali, A. F., and El-Genk, M. S., 2012b, "Spreaders for immersion nucleate boiling of a computer chip with a central hot spot," *Journal of Energy Conversion and Management*, 53(1), 259- 267.
- Ali, A. F., and El-Genk, M. S., 2013, "An Investigation of the Effect of Inclination on Critical Heat Flux of PF-5060 Dielectric Liquid on Microporous Copper Surfaces" ASME IMECE2013, San Diego, California, paper#IMECE2013-65503
- ANANDAN, S. S., and RAMALINGAM, V., 2008, "Thermal Management of Electronics: A review of Literature," *Thermal Science*, 12(2), 5-26.
- Anderson, T. M., and Mudawar, I., 1989, "Microelectronic Cooling by Enhanced Pool Boiling of a Dielectric Fluorocarbon Liquid," *ASME J. Heat Transfer*, 111, 752-759.
- Arik, M., and Bar-Cohen, A., 2001, "Ebullient Cooling of Integrated Circuits by Novec Fluids," *Proc. Pacific Rim Intersociety, Electronics Packaging Conference*, Kauai, Hawaii, USA.
- Arik, M., and Bar-Cohen, A., 2010, "Pool Boiling of Perfluorocarbon Mixtures on Silicon Surfaces," *International Journal of Heat and Mass Transfer*, 53, 5596-5604.
- Arik, M., Bar-Cohen, A., and You, S. M., 2007, "Enhancement of Pool Boiling Critical Heat Flux in Dielectric Liquids by Microporous Coatings," *Inter. J. Heat & Mass Transfer*, 50(5-6), 997-1009.
- Avedisian, C.T. and Purdy, D.J., 1993, "Experimental study of pool boiling critical heat flux of binary fluid mixtures on an infinitive horizontal surface," *Advances in Electronic Packaging*, EEP, 4(2), 909-915

- Baldwin, C. S., and Bhavnani, R. Jaeger, 1998, "Towards Optimizing Enhanced Surfaces for Passive Immersion Cooled Heat Sinks," Proceedings Intersociety Conf. on Thermal and Thermotechnical Phenomena in Electronic Systems, 399-407.
- Bar-Cohen, A., and Wang, P., 2009, "On-chip Hot Spot Remediation with Miniaturized Thermoelectric Coolers," Microgravity Sci. Technol, 21(Suppl 1), S351-S359
- Bar-Cohen, A., Tong, W., and Simon, T. W., 1992, "Theoretical aspects of nucleate pool boiling with dielectric liquids," Journal of Thermal Science, 1(1), 46-57.
- Beduz, C., Scurlock, R. G., and Sousa, A. J., 1988, "Angular Dependence on Boiling Heat Transfer Mechanisms in Liquid Nitrogen," Advances in Cryogenic Engineering, (R. Fast, Ed.) Plenum Press, NY, 33, 363-370.
- Benjamin, R., and Balakrishnan, A., 1996, "Nucleate pool boiling heat transfer of pure liquids at low to moderate heat fluxes," International Journal of Heat and Mass Transfer, 39, 2495-2504.
- Bliss, F. E., Hsu, S. T., and Crawford, M., 1969, "An Investigation into the Effects of Various Plating on the Film Coefficient During Nucleate Boiling from Horizontal Tubes," International Journal of Heat and Mass Transfer, 1, 1061-1072.
- Brusstar M. J., Merte H., Keller R. B., and Kirby B. J., 1997, "Effects of heater surface orientation on the critical heat flux: I. An experimental evaluation of models for subcooled pool boiling," Int. J. Heat Mass Transfer, 40, 4007-4019.
- Carey, V. P., 1992, Liquid-Vapor Phase Change Phenomena: An Introduction to the Thermophysics of Vaporization and Condensation Processes in Heat Transfer Equipment, Hemisphere Publishing Corporation, New York, USA
- Cengel, A. Y., 2002, Heat Transfer: A Practical Approach, McGraw-Hill, 2nd edition., New York, USA.
- Chang J. Y., and You, S. M., 1997b, "Enhanced Boiling Heat Transfer from Microporous Surfaces: Effects of a Coating Composition and Method," Inter. J. Heat & Mass Transfer, 40, 4449-4460.
- Chang, J. Y., 1997 "Enhanced Boiling Heat Transfer from Micro-Porous Surfaces," Ph.D. Dissertation, Mechanical Engineering Dept., University of Texas at Arlington, Arlington, TX.
- Chang, J. Y., and You, S. M., 1996, "Heater Orientation Effects on Pool Boiling of Microporous Enhanced Surfaces in Saturated FC-72," ASME J. Heat Transfer, 118, 937-943.
- Chang, J. Y., and You, S. M., 1997a, "Boiling Heat Transfer Phenomena from Microporous and Porous Surfaces in Saturated FC-72," Inter. J. Heat & Mass Transfer, 40, 4437-4447.

- Chang, J., You, S., and Haji-Sheikh, A., 1998, "Film Boiling Incipience at the Departure From Natural Convection on Flat, Smooth Surfaces," *J. Heat Transfer*, 120, 402-409.
- Cole, R., 1967, "Frequency and departure diameter at sub-atmospheric pressures," *American Institute of Chemical Engineers Journal*, 13, 779-783.
- El-Genk M. S., and Ali A. F., 2010, "Saturation and subcooled boiling on copper nanodendrites surfaces," *Proceedings 14th international heat transfer conference*, Paper # IHTC14-22108.
- El-Genk, M. S., 2012, "Nucleate Boiling Enhancements on Porous Graphite and Microporous and Macro-Finned Copper," *Heat Transfer Engineering*, 33(3), 175-204, 2012
- El-Genk, M. S., 2012, "Nucleate Boiling Enhancements on Porous Graphite and Microporous and Macro-Finned Copper Surfaces," *AICHE 2009 D. Q. Kern Award Paper*, *J. Heat Transfer Engineering*, 33(3), 175-204.
- El-Genk, M. S., and Ali, A. F., 2009, "Saturation Boiling of PF-5060 Dielectric Liquid On Micro-Porous Copper Dendrites Surfaces," *Proceedings of the ASME Heat Transfer Summer Conference HT2009*, July 19-23, San Francisco, California USA.
- El-Genk, M. S., and Ali, A. F., 2010a, "Enhancement of saturation boiling of PF-5060 on microporous copper dendrite surfaces," *Journal of heat transfer*, 132(7), 071501-1-9.
- El-Genk, M. S., and Ali, A. F., 2010b, "Enhanced Nucleate Boiling on Copper Microporous Surfaces," *Int. J. Multiphase Flow*, 36, 780-792.
- El-Genk, M. S., and Bostanci, H., 2003a, "Saturation Boiling of HFE-7100 from a Copper Surface, Simulating a Microelectronic Chip," *Inter. J. Heat & Mass Transfer*, 46, 1841-1854.
- El-Genk, M. S., and Bostanci, H., 2003b, "Combined Effects of Subcooling and Surface Orientation on Pool Boiling of HFE-7100 from a Simulated Electronic Chip," *Experimental Heat Transfer*, 16, 281-301.
- El-Genk, M. S., and Guo, Z., 1993, "Transient Boiling From Inclined and Downward-facing Surfaces in a Saturated Pool," *Inter. J. Refrigeration*, 16, 414-422.
- El-Genk, M. S., and Parker, J. L., 2004a, "Pool Boiling in Saturated and Subcooled HFE-7100 Dielectric Fluid From a Porous Graphite Surface," *Proc. 9th Intersociety Conference on Thermal Phenomena*, 1, 655-662.
- El-Genk, M. S., and Parker, J. L., 2004b, "Pool Boiling in Saturated and Subcooled FC-72 Dielectric Fluid From a Porous Graphite Surface," *Proc. ASME International Mechanical Engineering Congress (IMECE-2004)*, Paper IMECE2004-59905.

- El-Genk, M. S., and Parker, J. L., 2005, "Enhanced Boiling of HFE-7100 Dielectric Liquid on a Porous Graphite Surface," *Energy Conversion and Management*, 46, 2455-2481.
- El-Genk, M. S., and Parker, J. L., 2008, "Nucleate boiling of FC-72 and HFE-7100 on Porous Graphite at Different Orientations and Liquid Subcooling," *Energy Conversion and Management*, 49, 733-750.
- El-Genk, M. S., and Saber, H. H., 2006, "Composite Spreader for Submersion Cooling of a Computer Chip with Non-Uniform Heat Dissipation," *Proceeding Thermal and Thermomechanical Phenomena in Electronic Systems, and 10<sup>th</sup> intersociety conference (ITHERM 2006)*, 591-598.
- El-Genk, M. S., and Saber, H. H., 2008, "Composite Spreader for Cooling Computer Chip With Non-Uniform Heat Dissipation," *IEEE Transactions on Components and Packaging Technology*, 31(1), 165-172.
- El-Genk, M. S., and Saber, H. H., Parker, J. L., 2005, "Efficient Spreaders for Cooling High-Power Computer Chips," *Applied Thermal Engineering*, 27, 1072-1088.
- El-Genk, M. S., Saber, H. H., and Parker, J. L., 2005, "Thermal Analysis of Composite Copper/Porous Graphite Spreaders for Immersion Cooling Applications," *Proc. Conference on Integration and Packaging of MEMS, NEMS, and Electronics (InterPack'05)*, San Francisco, CA, IPACK2005-73226, 305-314.
- El-Genk, M. S., Suszko, A., and Ali, A. F., 2013, "Effects of Surface Roughness and Inclination angle on Nucleate Boiling of PF-5060 Dielectric Liquid on Copper," *ASME IMECE2013*, San Diego, California, IMECE2013-65512.
- Estes, K. A., and Mudawar, I., 1995, "Comparison of Two-Phase Electronic Cooling using Free Jets and Sprays," *ASME J. Electronic Packaging*, 117, 323-332.
- Ferjančič K., and Golobič, I., 2002, "Surface Effects on Pool Boiling CHF," *Experimental and Thermal Fluid Science*, 25, 565-571.
- Ferjančič, K., Rajšelj, D., and Golobič, I., 2006, "Enhanced Pool Boiling CHF in FC-72 from a Modulated Porous Layer Coating", *J. Enhanced Heat Transfer*, 13(2), 175-184.
- Fritz, W., 1935, Berechnung des maximalvolumen von dampfblasen. *Physikalische Zeitschrift* 36, 379–388.
- Furberg, R., 2006, "Enhanced Boiling Heat Transfer from a Novel Nanodendritic Microporous Copper Structure," Ph.D. Dissertation. KTH School of Industrial Engineering and Management, Stockholm, Sweden.
- Furberg, R., and Palm, B., 2011, "Boiling heat transfer on a dendritic and micro-porous surface in R134a and FC-72," *Applied Thermal Engineering*, 31(16), November 2011, 3595-3603.

Furberg, R., Khodabandeh, R., Palm, B., Li, S., Toprak, M., and Muhammed, M., 2008, "Experimental Investigation of an Evaporator Enhanced With a Micro-Porous Structure in a Two-Phase Thermosyphon Loop," Proceedings of 2008 ASME Summer Heat Transfer Conference, HT2008, August 10-14, Jacksonville, Florida USA.

Furberg, R., Palm, B., Li, S., Toprak, M., and Muhammed, M., 2009, "The Use of a Novel Nano-And Micro-Porous Structure For Enhanced Boiling In a Plate Heat Exchanger," Journal of Heat Transfer (special edition on porous media heat transfer), 131(10), Paper # 101010, 1-8.

Geisler, K. J. L., and Bar-Cohen, A., 2005, "Surface Effects on Confinement-Driven Pool Boiling Enhancement in Vertical Parallel-Plate Channels," Proc. ASME Summer Heat Transfer Conference, HT2005, 2, 195-205.

Ghiu, C.-D., and Joshi, Y. K., 2005, "Boiling Performance on Single-Layered Enhanced Structures," ASME J. Heat Transfer, 127(7), 675-683.

Griffith, P., 1957, "The Correlation of Nucleate Boiling Burnout Data," ASME Paper No. 57-HT-21.

Hall, D. D., and Mudawar, I., 1999, "Ultra-high critical heat flux (CHF) for subcooled water flow boiling-II. High-CHF database and design parameters," Int. J. Heat Mass Transfer, 42, 1429-145.

Han, C. L., Jeongbae, K., Byung, D.-Oh, and Moo, H. K., 2004, "Single bubble growth in saturated pool boiling of binary mixtures," International Journal of Multiphase Flow, 30(6), 697-710.

Haramura, Y., and Katto, Y., 1983. "A New Hydrodynamic Model of Critical Heat Flux, Applicable Widely to both Pool and Forced Convection Boiling on Submerged Bodies in Saturated Liquids," Inter. J. Heat & Mass Transfer, 26(3), 389-399.

Hashimoto, M., Kasai, H., Usami, K., Ryoson, H., Yazawa, K., Weibel, J. A., and Garimella, S. V., 2010, "Nano Structured Two-Phase Heat Spreader For Cooling Ultra-High Heat Flux Sources," Proceedings of the 14th International Heat Transfer Conference IHTC14, Washington, DC, USA, IHTC1422765

Hibiki, T., and Ishii, M., 2003, "Active nucleation site density in boiling systems. International Journal of Heat and Mass Transfer, 46, 2587-2601.

Honda, H., and Wei, J. J., 2003 "Advances in Enhanced Boiling Heat Transfer From Electronic Components," JSME International Journal, Series B: Fluids and Thermal Engineering, 46, 479-490.

Honda, H., Takamastu, H., and Wei, J. J., 2002, "Enhanced Boiling of FC-72 on Silicon Chips With Micro-Pin-Fins and Submicron Scale Roughness," ASME J. Heat Transfer, 124, 383-390.

Howard, A. H., 1999, "Effects of Orientation and Downward-Facing Convex Curvature on Pool Boiling Critical Heat Flux," Ph.D. Dissertation, Purdue University, West Lafayette, IN.

Howard, A. H., and Mudawar, I., 1999, "Orientation Effects on Pool Boiling Critical Heat Flux (CHF) and Modeling of CHF for Near-Vertical Surfaces," *Inter. J. Heat & Mass Transfer*, 42, 1665-1688.

Hsu, Y. Y., 1962, "On the Size Range of Active Nucleation Cavities on a Heating Surface," *ASME J. of Heat Transfer*, 84, 207-216.

Hutter, C., Kenning, D.B.R., Sefianea, K., Karayiannis, T.G., Linb, H., Cummins, G., and Walton, A.J., 2010, "Experimental pool boiling investigation of FC-72 on silicon with artificial cavities and integrated temperature micro-sensors," *Experimental Thermal and Fluid Science*, 34 (4), 422-433.

Im, Y., Dietz, C., Lee, S. S., and Joshi, Y., 2012, "Flower-Like CuO Nanostructures for Enhanced Boiling," *Nanoscale and Microscale Thermophysical Engineering*, 16, 145-153

Im, Y., Joshi, Y., Dietz, C., and Lee, S. S., 2010, "Enhanced Boiling of a Dielectric liquid on copper nanowire surfaces," *Int. Journal of Micro-Nano Scale Transport*, 1(1), 79-96.

ITRS, International Technology Roadmap for Semiconductors, 2007.

Jeon, S., Jo, B., and Banerjee, D., 2011, "Enhancement of Saturation Boiling of PF-5060 on Microporous Surface," *Proceedings of the ASME/JSME 2011 8th Thermal engineering joint conference*, March 14-17, Honolulu, Hawaii, USA, Paper # AJTEC2011-44408

Katsuta, M., 1977, "Boiling heat transfer of thin liquid with an impinging jet," in *Proc. 14<sup>th</sup> Nat. Heat Transf. Symp. Jpn.*, 154-156.

Khan, N., Toh, K. C., and Pinjala D., 2008, "Boiling Heat Transfer Enhancement Using Micro-Machined Porous Channels for Electronics Cooling," *Heat Transfer Engineering*, 29(4), 366-374.

Khan, N., Toh, Pinjala K.C., Kripesh, V., and Seung Wook Yoon, 2008, "Two phase cooling with heat transfer enhancement for BGA package," *Thermal and Thermomechanical Phenomena in Electronic Systems (ITHERM 2008)*, *Proceeding on. 11<sup>th</sup> Intersociety Conference on*, 79- 85.

Kim, J. H., 2006, "Enhancement of Pool Boiling Heat Transfer using Thermally-Conductive Microporous Coating Techniques," Ph.D. Dissertation, University of Texas at Arlington, Arlington, TX.

Kim, J. H., Kashinath, M. R., Kwark, S. M., and You, S. M., 2007, "Optimization of Microporous Structures in Enhanced Pool Boiling Heat Transfer of Saturated R-123, FC-

72, and Water,” Proc. ASME-JSME Thermal Engineering Summer Heat Transfer Conference, July-2007, Vancouver, BC, Canada, HT2007-32339.

Kim, S.J., Bang, I. C., Baongiorno, J., and Hu, L. W., 2006, “Effects of Nanoparticle Deposition on Surface Wettability Influencing Boiling Heat Transfer in Nanofluids,” *Applied Physics Letters*, 89(15), 153107-1-3

Kim, Y.-H, Lee, K.-J., and Han, D., 2008, “Pool boiling enhancement with surface treatments,” *Heat mass transfer*, 45,55-60.

Kline, S. J., and McClintock, F. A., 1952, “Describing Uncertainties in Single-Sample Experiments,” *ASME Mechanical Engineering*, 75, 3-8.

Kocamustafaogullari, G., and Ishii, M., 1983, “Interfacial area and nucleation site density in boiling systems,” *Int. J. Heat Mass Transfer*, 26, 1377-1387.

Kubo, H., Takamatsu, H., and Honda, H., 1999, “Effects of Size and Number Density of Micro-Reentrant Cavities on Boiling Heat Transfer from a Silicon Chip Immersed in Degassed and Gas Dissolved FC-72,” *J. Enhanced Heat Transfer*, 6(2-4), 151-160.

Kutateladze, S. S., 1952, “Heat Transfer in Condensation and Boiling,” Technical report AEC-tr-3770.

Launay, S., Fedorov, A. G., Joshi, Y., Cao, A., and Ajayan, P. M., 2006, “Hybrid Micro-Nano Structured Thermal Interfaces for Pool Boiling Heat Transfer Enhancement,” *Microelectronics Journal*, 37(11), 11581164.

Lee, T. Y. T., and Normington, P. J. C., 1993, “Application of dielectric binary mixtures in electronic cooling-nucleate pool boiling regime,” *Advances in Electronic Packaging*, ASME, 4(2), 927–935.

Li, S., Furberg, R., Toprak, M., Palm, B., and Muhammed, M., 2008, “Nature-Inspired Boiling Enhancement by Novel Nanostructured Macroporous Surfaces,” *Advanced Functional Materials*, 18(15), 2215–2220.

Lin, S.-C., and Banerjee, K., 2008, “Cool Chips: Opportunities and Implications for Power and Thermal Management,” *IEEE Transactions on Electron Devices*, 55(1), 245-255.

Lorenz, J.J., 1971, “The effects of surface conditions on boiling characteristics,” Ph.D. Thesis, Massachusetts Institute of Technology, Cambridge, MA, USA.

Marto P., and Lepere, V., 1982, “Pool Boiling Heat Transfer from Enhanced Surfaces to Dielectric Fluids,” *ASME J. of Heat Transfer*, 104, 292-303.

McFadden, P. W. and Grassman, P., 1963, “The relation Between Bubble Frequency and Diameter During Nucleate Pool Boiling,” *Int. J. Heat and Mass Transfer*, 5, 169-173.



McHale, J. P. , and Garimella, S. V., 2010, "Bubble nucleation characteristics in pool boiling of a wetting liquid on smooth and rough surfaces," *International Journal of Multiphase Flow*, 36(4), 249-260.

McHale, J.P. , and Garimella, S.V., 2008, "Measurements of bubble nucleation characteristics in pool boiling of a wetting liquid on smooth and roughened surfaces," *Proceedings ASME Summer Heat Transfer Conference HT2008-56179*, Florida, FL, 2008, 619-629.

McNiel, A., 1992, "Pool Boiling Critical Heat Flux in a Highly Wetting Liquid," Masters Thesis, Mechanical Engineering Dept., University of Minnesota, Minneapolis, MN.

Misale, M., Guglielmini, G., Frogheri, M., and Bergles, A. E., 1999, "FC-72 Pool Boiling from Finned Surfaces Placed in a Narrow Channel: Preliminary Results," *Heat and Mass Transfer*, 34(6), 449-452.

Monde, M., and Katto, Y., 1978, "Burnout in a high heat-flux boiling system with an impinging jet," *Int. J. Heat Mass Transfer*, 21, 295-305.

Mudawar, I., 1992, "Direct immersion cooling for high power electronic chips," in *Proc. I-Therm III: Intersoc. Conf. Thermal Phenom. Electron. Syst.*, Austin, TX, Feb. 3-5, 74-84.

Mudawar, I., 2001, "Assessment of High-Heat-Flux Thermal Management Schemes," *IEEE Transaction on Components and Packaging Technology*, 24(2), 122-141.

Mudawar, I., Howard, A. H., and Gersey, C. O., 1997, "An Analytical Model for Near Saturated Pool Boiling Critical Heat Flux on Vertical Surfaces," *Inter. J. Heat & Mass Transfer*, 40, 2327-2339.

Nakayama, W., Daikoku, T., Kuwahara, H., and Nakajima, T., 1980, "Dynamic Model of Enhanced Boiling Heat Transfer on Porous Surfaces Part I: Experimental Investigation," *ASME J. Heat Transfer*, 102(3), 445-450.

Nimkar, N. K., Bhavnani, S. H., and Jaeger, R. C., 2006, "Benchmark Heat Transfer Data for Microstructured Surfaces for Immersion-Cooled Microelectronics," *IEEE Trans. On Components and Packaging Tech.*, 29(1), 89-97.

Nishikawa, K., Fujita, Y., Uchida, S., and Ohta, H., 1984, "Effect of Surface Configuration on Nucleate Boiling Heat Transfer," *International. Journal of. Heat and Mass Transfer*, 27, 1559-1571.

O'Connor, J. P., 1994, "Enhancement of Pool Boiling Heat Transfer in Highly Wetting Dielectric Liquids," Ph.D. Dissertation, Mechanical Engineering Department, University of Texas at Arlington, TX.

O'Connor, J. P., and You, S. M., 1995, "A Painting Technique to Enhance Pool Boiling Heat Transfer in Saturated FC-72," *ASME J. Heat Transfer*, 117, 387-393.

O'Connor, J., You, S., and Chang, J., 1996, "Gas-Saturated Pool Boiling Heat Transfer From Smooth and Microporous Surfaces in FC-72," ASME J. Heat Transfer, 118, 662-667.

Oktay, S., 1982, "Departure from Natural Convection (DNC) in Low-Temperature Boiling Heat Transfer Encountered in Cooling Micro-Electronic LSI Devices," Proc. Seventh International Heat Transfer Conference, Munich, Fed. Rep. Germany, 113-118.

Parker, J. L. and El-Genk, M. S., 2008, "Subcooled Boiling of HFE-7100 Dielectric Liquid on Copper Surfaces with Corner Pins," Proc. 5th European Thermal-Sciences Conferences, May 18-22, Eindhoven, the Netherlands.

Parker, J. L., 2008, "Pool Boiling of Dielectric Liquids on Porous Graphite and Extended Copper Surfaces," Ph.D. Dissertation, Chemical and Nuclear Engineering Dept., University of New Mexico, Albuquerque, NM.

Parker, J. L., and El-Genk, M. S., 2005, "Enhanced Saturation and Subcooled Boiling of FC-72 Dielectric Liquid," Inter. J. Heat and Mass Transfer, 48, 3736-3752.

Parker, J. L., and El-Genk, M. S., 2006, "Effect of Surface Orientation on Nucleate Boiling of FC-72 on Porous Graphite," ASME Journal of Heat Transfer, 128, 1159-1175.

Parker, J. L., and El-Genk, M. S., 2006, "Subcooled Boiling of Dielectric Liquids on Porous Graphite at Different Orientations," Proceedings 13th International Heat Transfer Conference, Sydney, Australia, Paper # BOI-36.

Parker, J. L., and El-Genk, M. S., 2007, "Enhanced Saturation Boiling of HFE-7100 Dielectric Liquid on Extended Copper Surfaces," Proc, ASME, JSME Summer Heat Transfer conference, July 8-12, Vancouver, British Columbia, Canada, Paper # HT2007-32496.

Peterson, G. , 1994, An Introduction to Heat Pipes: Modeling, Testing, and Applications, New York, Wiley and Sons.

Priarone, A., 2005, "Effect of Surface Orientation on Nucleate Boiling and Critical Heat Flux of Dielectric Fluids," International Journal of Thermal Sciences, 44, 822-831.

Rainey, K. N., and You, S. M., 2000, "Pool Boiling Heat Transfer from Plain and Microporous, Square Pin-Finned Surfaces in Saturated FC-72," ASME J. Heat Transfer, 122, 509-516.

Rainey, K. N., and You, S. M., 2001, "Effects of Heater Size and Orientation on Pool Boiling Heat Transfer from Microporous Coated Surfaces," International Journal of Heat and Mass Transfer, 44, 2589-2599.

Rainey, K. N., You, S. M., and Lee, S., 2003, "Effect of Pressure, Subcooling, and Dissolved Gas on Pool Boiling from Microporous Surfaces in FC-72," ASME J. Heat Transfer, 125, 75-83.

- Ramaswamy, C., Joshi, Y., Nakayama, W., and Johnson, W., 2002, "High-speed Visualization of Boiling from an Enhanced Structure," *Int. J. Heat & Mass Transfer*, 45, 4761-4771.
- Ramaswamy, C., Joshi, Y., Nakayama, W., and Johnson, W., 2003, "Effects of Varying Geometrical Parameters on Boiling From Microfabricated Enhanced Structures," *ASME J. Heat Transfer*, 125, 103-109.
- Ramilison, J., Sadasivan, P., and Lienhard, J., 1992, "Surface Factors Influencing Burnout on Flat Heaters," *ASME J. Heat Transfer*, 114(1), 287-290.
- Reed, S. J., 1996, "Elimination of Boiling Incipience Temperature Drop and Enhancement of Boiling Heat Transfer in Highly Wetting Fluids Through Low Contact Force Attachments," M. S. Thesis, Mechanical Engineering, Purdue University, West Lafayette, IN.
- Reed, S. J., and Mudawar, I., 1997, "Elimination of Boiling Incipience Temperature Drop in Highly Wetting Fluids using Spherical Contact With a Flat Surface," *Inter. J. Heat & Mass Transfer*, 42, 2439-2454.
- Refai-Ahmed, G., 2007, "Thermal Challenges in the Present and Next Generation of PC Processors," Conference on Integration and Packaging of MEMS, NEMS, and Electronics (InterPack'07), Vancouver, BC, Canada, Paper # IPACK2007-3506, 1029-1032.
- Rini, D. P., Chen, R.-H., and Chow, L. C., 2001, "Bubble Behavior and Heat Transfer Mechanism in FC-72 Pool Boiling," *Experimental Heat Transfer: A Journal of Thermal Energy Generation, Transport, Storage, and Conversion*, 14, 27-44.
- Rohsenow, W.M., 1952, "A method of correlating heat transfer data for surface boiling of liquids," *Transactions of the ASME* 74, 969-976.
- Roll, J. B., and Myers, J. M., 1964, "The Effect of Surface Tension on Factors in Boiling Heat Transfer," *Journal of American Institute of Chemical Engineers*, 10(4), 530-534.
- Ruckenstein, E., 1961, "A physical model for nucleate boiling heat transfer from a horizontal surface," *Buletinul Institutului Politehnic Bucuresti (Romania)* 23, 79-88.
- Shin, H.C., and Liu, M., 2004, "Copper foam structures with highly porous nanostructured walls," *Chemistry of materials Journal*, 16, 5460-5464.
- Shin, H.C., Dong, J., and Liu, M., 2003, "Nanoporous structure prepared by an electrochemical deposition processes," *Journal of Advanced Materials*, 15, 1610-614.
- Sriraman, S. R., and Banerjee, D., 2007, "Pool boiling studies on nano-structured surfaces," In. *ASME Int. Mechanical Engineering Congress and Exposition*, Paper # IMECE2007-42581, Seattle, USA.

- Tilton, D. E., and Tilton, C. L., 1993, "High heat flux spray cooling," U.S. Patent 5220804.
- Ujereh, S., Fisher, T., and Mudawar, I., 2007, "Effects of Carbon Nanotube Arrays on Nucleate Pool Boiling," *International Journal of Heat and Mass Transfer*, 50(19-20), 4023-4038.
- Vemuri, S., and Kim, K. J., 2005, "Pool Boiling of Saturated FC-72 on Nano-Porous Surface," *International communication in Heat and Mass Transfer*, 32, 27-31.
- Vishnev, I. P., Filatov, I. A., Vinokur, Ya. G., Gorokhov, V. V., and Svalov, G. G., 1976, "Study of Heat Transfer in Boiling of Helium on Surfaces with Various Orientations," *Heat Transfer-Soviet Research*, 8, 104-108.
- Wang, C.H., and Dhir, V. K., 1993a, "Effect of surface wettability on active nucleation site density during pool boiling of saturated water," *ASME Journal of Heat Transfer*, 115, 659-669.
- Warrier, G. R., Basu, N., and Dhir, V. K., 2002, "Interfacial Heat Transfer of Subcooled Boiling at Low Pressures," *International Journal of Heat Mass Transfer*, 45(19), 3947-3959.
- Watwe, A., Bar-Cohen, A., and McNeil, A., 1997, "Combined Pressure and Subcooling Effects on Pool Boiling from a PPGA Chip Package," *Journal of Electronic Packaging*, 119, 95-105.
- Wei, J. J., and Honda, H., 2003, "Effects of Fin Geometry on Boiling Heat Transfer from Silicon Chips with Micro-Pin-Fins Immersed in FC-72," *International Journal of Heat and Mass Transfer*, 46, 4059-4070.
- WEI, J., 2008, "Challenges in Cooling Design of CPU Packages for High Performance Servers," *Heat Transfer Engineering*, 29(2), 178-187.
- Xu, G., Guenin, B., and Vogel, M., 2004, "Extension of Air Cooling for High Power Processors," *Thermal and Thermomechanical Phenomena in Electronic Systems, (ITHERM 2004) and the 9<sup>th</sup> intersociety Conference*, San Diego, CA, USA, 1, 186-193.
- Yang, B., Wang, P., and Bar-Cohen, A., 2007, "Mini-contact enhanced thermoelectric cooling of hot spot in high power devices ," *IEEE Transaction of Component Packaging Technology*, Part A 30, 432-438
- Yang, S.R., and Kim, R.H., 1988, "A mathematical-model of the pool boiling nucleation site density in terms of the surface characteristics," *International Journal of Heat and Mass Transfer*, 31, 1127-1135.
- Ben Yoo, S. J., 2011, "Energy Efficiency in the Future Internet: The Role of Optical Packet Switching and Optical-Label Switching," *IEEE JOURNAL OF SELECTED TOPICS IN QUANTUM ELECTRONICS*, 17(2), 406-418.

and Optical-Label Switching,” *Int. J. Heat Mass Transfer*, 31, 1127-1135.

You, S. M., Simon, T. W., Bar-Cohen, A., and Hong, Y. S., 1995, “Effects of Dissolved Gas Content on Pool Boiling of a Highly Wetting Fluid,” *ASME J. Heat Transfer*, 117, 687-692.

Yu, C. K., Lu, D. C., and Cheng, T. C., 2006, “Pool Boiling Heat Transfer on Artificial Micro-Cavity Surfaces in Dielectric Fluid FC-72,” *Journal of Micromechanics and Microengineering*, 16(10), 2092-2099.

Zuber, N., 1959, “Hydrodynamic Aspects of Boiling Heat Transfer,” Ph.D. Dissertation, University of California, Los Angeles, CA.

Zuber, N., 1963, “Nucleate Boiling. The Region of Isolated Bubbles and the Similarity with Natural Convection,” *International Journal of Heat and Mass Transfer*, 6, 53-76.

## Appendix A: Uncertainty Analysis

This appendix details the methodology used to estimate the uncertainties in the experimental measurements in the performed pool boiling experiments in the course of this research. These include the uncertainties in the measurements of the applied heat flux, temperatures, the heat transfer coefficient and CHF. There are two main kinds of uncertainties, systematic and random. Systematic uncertainties come from the instrument bias or errors in the experimental techniques. Random uncertainties come from the unpredictable variations (human or electronic) in the measurements. The uncertainty of an individual measurement propagates into determine the overall uncertainty. Estimated uncertainties in the experimental measurements are obtained following the method described by Kline and McClintock (1952) using the function:

$$W_G = \left[ \sum_i^n \left( \frac{\partial G}{\partial x_i} \Delta x_i \right)^2 \right]^{1/2} \quad (\text{A.1})$$

where  $G$  is a given function of the independent variables  $x_1, x_2, x_3, \dots, x_n$ , and  $G$  is the variable of interest in the experiments:

$$G = G(x_1, x_2, \dots) \quad (\text{A.2})$$

In Equation (A.1),  $\Delta x_i$  represents the uncertainty in the individual primary measurement or independent variables.

The stated systematic and random uncertainties in the measurements for the power provided to the heating element in the text section by a DC are 0.05% and  $\pm 5\text{mV}$  for the applied voltage and 0.15% and  $\pm 5\text{mA}$  for the supplied electrical current, respectively (Agilent, 2000). The overall uncertainties in the measurements in the applied voltage and current are estimated by the standard deviation of the systematic and random uncertainties,  $\Delta M$ , as:

$$\Delta M = \left[ \Delta M_{\text{systematic}}^2 + \Delta M_{\text{random}}^2 \right]^{1/2} \quad (\text{A.3})$$

where,  $M$  is either the voltage  $V$  or current  $I$ . The calculated overall uncertainties in the supplied current is  $< 1\%$  and very small for the supplied voltage ( $<< 1\%$ ).

The stated uncertainty in the thermocouples temperature measurements is  $\pm 0.2$  K (Omega, 2004) and side heat losses for the assembled test section,  $\varepsilon$ , is less than 3%.

The power removed by the boiling surface is equal to the product of the current through and the voltage drop across the heating element, less the estimated losses:

$$P = IV \quad (\text{A.4})$$

Applying Equation A.1 to Equation A.4 yields an estimate for the uncertainty in the power measurement of

$$\frac{\Delta P}{P} = \left[ \left( \frac{\Delta V}{V} \right)^2 + \left( \frac{\Delta I}{I} \right)^2 \right]^{1/2} \quad (\text{A.5})$$

For example, in saturation boiling experiment of PF-5060 on 80  $\mu\text{m}$ -thick MPC, when the applied surface heat flux is  $10.31 \text{ W/cm}^2$ , the measured input voltage and current are 13.32 V and 0.77 A (Table A.1). The corresponding uncertainty in the power measurement is estimated using Equation A.5 as:

$$\frac{\Delta P}{P} = \left[ \left( \frac{0.012}{13.32} \right)^2 + \left( \frac{0.006}{0.77} \right)^2 \right]^{1/2} = \pm 0.78 \%$$

The heat flux is calculated by the quotient of the power removed to the total surface area through which the power is removed:

$$q = \frac{P^*}{A} \quad (\text{A.6})$$

$$P^* = P(1 - \varepsilon) \quad (\text{A.7})$$

where  $P^*$  is the net input power to the heated surface and  $\varepsilon$  is the estimated sides heat losses (3% , Chapter 4). The uncertainty in the net power is expressed as:

$$\frac{\Delta P^*}{P^*} = \frac{\Delta P}{P} (1 - \varepsilon) = 0.97 * \frac{\Delta P}{P}, \quad (\text{A.8})$$

And the calculated uncertainty in the power dissipation for the MPC surfaces in the experiments is  $\pm 0.76 \%$

The uncertainty in the applied heat flux can be estimated using the following equation:

$$\frac{\Delta q}{q} = \left[ \left( \frac{\Delta P^*}{P^*} \right)^2 + \left( \frac{\Delta A}{A} \right)^2 \right]^{1/2}. \quad (\text{A.9})$$

For 80  $\mu\text{m}$ -thick MPC experiment, the uncertainty in the heat flux is estimated using equation A.7 as:

$$\frac{\Delta q}{q} = \left[ (0.76)^2 + (1)^2 \right]^{1/2} = \pm 1.3\%$$

The heat transfer coefficients in the experiments are calculated from the heat flux divided by the temperature difference between the wall and the bulk liquid:

$$h = \frac{q}{T_w - T_b} \quad (\text{A.10})$$

The associated uncertainty, using Equation A.1, is

$$\frac{\Delta h}{h} = \left[ \left( \frac{\Delta q}{q} \right)^2 + \left( \frac{\Delta(T_w - T_b)}{(T_w - T_b)} \right)^2 \right]^{1/2} \quad (\text{A.11})$$

The uncertainty in the calculated heat transfer coefficient as shown in equation A.9 depends of the surface superheat. For 80  $\mu\text{m}$ -thick MPC at 10.31  $\text{W}/\text{cm}^2$  applied heat flux and 10.2 K corresponding surface superheat, the estimated uncertainty is:

$$\frac{\Delta h}{h} = \left[ (1.3)^2 + (1.9)^2 \right]^{1/2} = \pm 2.3\%$$

The uncertainties in the present experiments for the applied heat flux, surface temperature or superheat, and nucleate boiling heat transfer are estimated at different values of applied heat flux during the experiments and summarized in Table A.1 for plan Cu and 80  $\mu\text{m}$ -thick MPC.



**Table A.1 Selected values and associated uncertainties for test measurements.**

<b>Parameter</b>	<b>80<math>\mu</math>m- MPC</b>		
	<b><math>\sim 10 \text{ W/cm}^2</math></b>	<b><math>\sim 15 \text{ W/cm}^2</math></b>	<b><math>\sim 20 \text{ W/cm}^2</math></b>
Current, $I$ (A)	$0.77 \pm 0.006$ (0.78%)	$0.94 \pm 0.007$ (0.68%)	$1.09 \pm 0.007$ (0.61%)
Voltage, $V$ (V)	$13.32 \pm 0.012$ (0.09%)	$16.1 \pm 0.013$ (0.08%)	$18.43 \pm 0.014$ (0.08%)
Area, $A$ (cm <sup>2</sup> )	$1.0 \pm 0.01$ (1.0%)	$1.0 \pm 0.01$ (2.0%)	$1.0 \pm 0.01$ (1.0%)
Superheat, $\Delta T_{sat}$ (K)	$10.21 \pm 0.2$ (1.96%)	$10.96 \pm 0.2$ (1.82%)	$17.31 \pm 0.084$ (1.16%)
Applied Heat Flux, $q$ (W/cm <sup>2</sup> )	$10.31 \pm 0.13$ (1.3%)	$15.13 \pm 0.2$ (1.3%)	$20.88 \pm 0.27$ (1.3%)
Nucleate Boiling Heat Transfer Coefficient, $h_{NB}$ (W/cm <sup>2</sup> K)	$1.01 \pm 0.023$ (2.3%)	$1.39 \pm 0.03$ (2.2%)	$1.21 \pm 0.021$ (1.7%)

<b>Parameter</b>	<b>Smooth Copper</b>		
	<b><math>\sim 5 \text{ W/cm}^2</math></b>	<b><math>\sim 10 \text{ W/cm}^2</math></b>	<b><math>\sim 15 \text{ W/cm}^2</math></b>
Current, $I$ (A)	$0.53 \pm 0.006$ (1%)	$0.77 \pm 0.007$ (0.80%)	$0.92 \pm 0.007$ (0.7%)
Voltage, $V$ (V)	$9.34 \pm 0.01$ (0.1%)	$13.14 \pm 0.012$ (0.09%)	$16.0 \pm 0.013$ (0.08%)
Area, $A$ (cm <sup>2</sup> )	$1 \pm 0.01$ (2.0%)	$1.0 \pm 0.1$ (2.4%)	$1 \pm 0.1$ (2.0%)
Superheat, $\Delta T_{sat}$ (K)	$14.29 \pm 0.2$ (1.4%)	$16.76 \pm 0.2$ (1.2%)	$19.46 \pm 0.2$ (1%)
Heat Flux, $q$ (W/cm <sup>2</sup> )	$4.96 \pm 0.1$ (1.3%)	$10.3 \pm 0.13$ (1.3%)	$14.95 \pm 0.19$ (1.3%)
Nucleate Boiling Heat Transfer Coefficient, $h_{NB}$ (W/cm <sup>2</sup> K)	$0.35 \pm 0.01$ (1.9%)	$0.62 \pm 0.011$ (1.7%)	$0.77 \pm 0.012$ (1.6%)

## **Appendix B: List of Publications Related to Work**

Ali, A. F., and El-Genk, M. S., 2013, "An Investigation of the Effect of Inclination on Critical Heat Flux of PF-5060 Dielectric Liquid on Microporous Copper Surfaces," ASME IMECE2013, San Diego, California, paper#IMECE2013-65503

El-Genk, M. S., Suszko, A., and Ali, A. F., 2013, "Effects of Surface Roughness and Inclination angle on Nucleate Boiling of PF-5060 Dielectric Liquid on Copper," ASME IMECE2013, San Diego, California.

Ali, A. F., and El-Genk, M. S., 2012a, "Effect of inclination on saturation boiling of PF-5060 dielectric liquid on 80 and 137  $\mu\text{m}$  thick copper micro-porous surfaces," International Journal of Thermal Sciences, 53, 42-48.

Ali, A. F., and El-Genk, M. S., 2012b, "Spreaders for immersion nucleate boiling of a computer chip with a central hot spot," Journal of Energy Conversion and Management, 53(1), 259- 267.

El-Genk, M. S., and Ali, A. F., 2012, "Advanced Spreaders for Enhanced cooling of High Power Chips," Frontiers in Heat and Mass Transfer (FHMT) 3 (4).

Ali, A. F., and El-Genk, M. S., 2012, "Numerical Analysis of Spreaders with an Enhancing Nucleate Boiling Surface for Immersion Cooling of Chips with Central Hot Spots," Proceedings 13th Intersociety Conference on Thermal and Thermomechanical Phenomena in Electronic Systems (ITherm 2012), California, USA, 1106-1113.

El-Genk, M. S., and Ali, A. F., 2011, "Subcooled boiling of PF-5060 dielectric liquid on microporous surfaces," Journal of Heat Transfer, Vol. 133, Issue 8, 081503.

El-Genk, M. S., and Ali, A. F., 2010a, "Enhanced nucleate boiling on copper microporous surfaces," International Journal of Multiphase Flow, Vol. 36, Issue 10, 780-792.

El-Genk, M. S., and Ali, A. F., 2010a, "Enhancement of saturation boiling of PF-5060 on microporous copper Dendrite surfaces," Journal of Heat Transfer, Vol. 132, Issue 7, 071501.

El-Genk, M. S., and Ali, A. F., 2010b, "Saturation and subcooled boiling on copper Nano-Dendrites surfaces," 14th International Heat Transfer Conference, Washington DC, USA, IHTC14-22108.

El-Genk, M. S., and Ali, A. F., 2009, "Saturation boiling of PF-5060 dielectric liquids on micro-porous copper Dendrites surfaces," ASME Heat Transfer Summer Conference, San Francisco, California, USA Vol. 1, pp. 847-855.

El-Genk, M. S., and Ali, A. F., "Methods for Enhanced Cooling of Electronics and Boiling Using Metals Nano-dendrites Surfaces," UNM Ref# 2010-036-02, field 2009, patent pending.